# Synthesis and Characterization of $TiO_2$ Nanostars

## Dissertation

**Zur Erlangung des Grades**
**des Doktors der Ingenieurwissenschaften**
**der Naturwissenschaftlich-Technischen Fakultät III**
**Chemie, Pharmazie und Werkstoffwissenschaften**
**der Universität des Saarlandes**

**von**

**Mehmet Uyanik**

**Saarbrücken**

**2008**

**Tag des Kolloquiums: 21. November 2008**

| | |
|---|---|
| **Dekan:** | **Prof. Dr. Uli Müller** |
| **Vorsitzender:** | **Prof. Dr. Frank Mücklich** |
| **Berichterstatter:** | **Prof. Dr. Helmut Schmidt** |
| | **Prof. Dr. Wilhelm F. Maier** |
| **Akad. Mitarbeiter:** | **Dr. Holger Kohlmann** |

## List of abbreviations

| Abbreviation | Full Name |
|---|---|
| 3-IPTES | 3-Isocyanatopropyltriethoxysilane |
| 2AAEM | 2-Acetoacetoxyethylmethacrylate |
| Ethylenurea | Synthesized from ethylenediamine and 3-IPTES |
| Pentylurea | Synthesized from pentylamine and 3-IPTES |
| Octylurea | Synthesized from octylamine and 3-IPTES |
| Octadecylurea | Synthesized from octadecylamine and 3-IPTES |
| 1Dodecylurea | Synthesized from 1-dodecylamine and 3-IPTES |
| 16Hexylurea | Synthesized from 1,6-diaminohexan and 3-IPTES |
| 112Dodecylurea | Synthesized from 1,12-diaminododecane and 3-IPTES |
| 18Octylurea | Synthesized from 1,8-diaminooctane and 3-IPTES |
| DMSA15urea | Synthesized from DMS-A15 and 3-IPTES |
| DMSA21urea | Synthesized from DMS-A21 and 3-IPTES |
| FT-IR | Fourier transform infrared spectroscopy |
| TEM | Transmission electron microscope |
| XRD | X-ray diffraction |
| DSC | Differential scanning calorimetry |
| TGA | Thermal gravimetric analysis |
| GC/MS | Gas chromatography/mass spectrometry |
| PCS | Photon correlation spectroscopy |
| HTMS | Hexyltrimethoxysilane |
| DTMS | Decyltrimethoxysilane |
| HDTMS | Hexadecyltrimethoxysilane |
| DDTMS | Dodecyltrimethoxysilane |
| AMMO | 3-Aminopropyltrimethoxysilane |
| PMMA | Poly(methyl methacrylate) |
| MMA | Methyl methacrylate |
| AAA | Allyl acetoacetate |
| a.u. | Arbitrary units |
| $\nu$ | Vibration |

## Abstract

In this work, $TiO_2$ nanostars, which have $TiO_2$ nanoparticles in their core and have branches on the surface of $TiO_2$ nanoparticle, were synthesized. Hence, firstly $TiO_2$ nanoparticles were synthesized by hydrothermal method. After that, the nanoparticles were characterized by Photon Correlation Spectroscopy (PCS), Transmission Electron Microscopy (TEM), Energy dispersive X-ray spectroscopy (EDX), X-Ray Diffractometry (XRD), elemental analysis. Thus, it was determined that the size of $TiO_2$ nanoparticles was 6 nm, their particle shape was spherical and the crystalline form of $TiO_2$ was anatase. Moreover, the carbon percentage on the surface of $TiO_2$ nanoparticles was determined to be 8,38 %. Afterwards, so as to synthesize nanostars, $TiO_2$ nanoparticles were modified with five silanes *with different molecular weights*, with three carboxylic acids *with different molecular weights*, with one β-ketoester and also with 10 urea molecules with *different molecular weights* (the urea molecules were synthesized in this work) and also, poly (methyl methacrylate) (PMMA) was grafted onto $TiO_2$ nanoparticles according to "*the combination of both grafting methods"* method. After that, the silane-modified, carboxylic acid-modified, β-ketoester-modified and urea-modified $TiO_2$ nanoparticles were characterized by GC/MS, elemental analysis, FT-IR, EDX and the PMMA-grafted $TiO_2$ nanoparticles were characterized by FT-IR and TGA/DSC.

## Kurzfassung

Ziel dieser Arbeit ist die Herstellung oberflächenfunktionalisierter $TiO_2$-Nanopartikel. Zunächst erfolgte dabei die Synthese der $TiO_2$-Nanopartikel durch Hydrothermalbehandlung. Nach der Synthese wurden Partikelgröße, -morphologie und -zusammensetzung mittels Photonen-Korrelations-Spektroskopie (PCS), Transmissions-Elektronen-Mikroskopie (TEM), Energiedispersive Röntgenspektroskopie (EDRS or EDX) und Elementaranalyse bestimmt. Zur Phasenanalyse wurden Röntgendiffraktogramme angefertigt. Die Teilchen liegen als reine Anatasphase vor, und weisen eine sphärische Morphologie, bei einer durchschnittlichen Größe von 6 nm. auf Der Kohlenstoffgehalt der $TiO_2$-Partikel liegt bei 8,38 %. Nachfolgend wurde die Partikeloberfläche zur Herstellung von core-shell Strukturen mit einer Reihe verschiedener Oberflächenmodifikatoren unterschiedlichen Molekulargewichts (Silane, Carbonsäuren, β-Ketoester, Harnstoffverbindungen) versehen. Die verwendeten Harnstoffverbindungen wurden im Rahmen dieser Arbeit selber synthetisiert. Alternativ wurde die Oberfläche entsprechend der "*the combination of both grafting methods"* Methode mit PMMA funktionalisiert. Schließlich wurden die Silan-, Carboxylsäure-, β-Ketoester- und Harnstoff modifizierten $TiO_2$- Nanopartikel mittels GC/MS, Elementaranalyse, FT-IR und EDX charakterisiert. Die mit PMMA funktionalisierten Partikel wurden mittels FT-IR, TGA/DSC und EDX untersucht.

**Contents**

## 1. Introduction

The research areas of nanoscience, nanotechnology and nanoengineering have developed rapidly recently. The great interest lies in the discovery of new phenomena and applications at the nanoscale in terms of quantum size and shape effects, very high surface areas, molecular manipulation and engineering, and defining the limits of surface chemistries and physics [1, 2]. Hence, nanoparticles have attracted much attention due to their fascinating electronic, optical, magnetic properties, etc. The use of nanoparticles are becoming increasingly important for various applications ranging from biotechnology [3-11] to optic [12-15]. This includes metal (Au, Pt, Pd, Cu, etc.), semiconductor (CdS, CdSe, ZnS, etc.), metal and semiconductor oxide ($Fe_2O_3$, $Al_2O_3$, $TiO_x$, $SiO_x$, etc.) nanoparticles [2]. In spite of their countless using areas, the use of nanoparticles is sometimes restricted because of their incompatibility with organic mediums. To overcome this problem, they need to be chemically modified to change their surface properties, namely their surfaces are functionalized. Of course, providing them compatibility with organic mediums is not unique goal of the surface modifications. Some properties such as hydrophobic/hydrophilic properties, biocompatibility, providing to bonding to an organic matrix via chemical bonds, sensibility to certain substances, corrosion resistance and wettability are gained them by means of the surface modifications [16]. For example; silicate nanoparticles can be modified to make them hydrophobic property. Also, if the nanoparticles have hydrophobic property, they can be modified to increase their hydrophobicity. Thus, their surfaces behave different as compared to their unmodified state.

Organic groups can be linked to inorganic backbone by means of three different ways. One of them is the formation of covalent bonds, for instance; the modification of $SiO_2$ nanoparticles with silanes (for example; 3-methacryloxypropyl trimethoxysilane) to occur covalent bonds (Si-O-Si covalent bonds) on the surface of the nanoparticles. Another one is the formation of complex structures with β-ketoesters, β-diketones or carboxylic acids, for instance; Zr/acetylacetones and the other one is the formation of ionic bond to an organic acid (salt formation) [17, 18]. In the literature, although the modifications of the nanoparticles with modification agents and the grafting of polymers onto the nanoparticles were reported by several researchers, of all nanoparticles, $SiO_2$ nanoparticles were the most commonly reported. However, because $TiO_2$ nanoparticles, which have lots of using areas such as photocatalytic coatings, dyes, etc., were not worked as many as $SiO_2$ nanoparticles and $TiO_2$ nanoparticles worked in the literature did not have –OR groups on their surface (such as -$OC_3H_7$, -$OC_4H_9$, -$OC_5H_{11}$) or it is not mentioned their surface properties, $TiO_2$ nanoparticles were chosen for the modification with modification agents and polymers. Also, all modified $TiO_2$ nanoparticles are named as nanostars in this work. In the Figure 1, general structure of

nanostars is shown. In the Figure 1, a nanoparticle is standing in the core of the structure and surrounded by branches (core-shell structures).

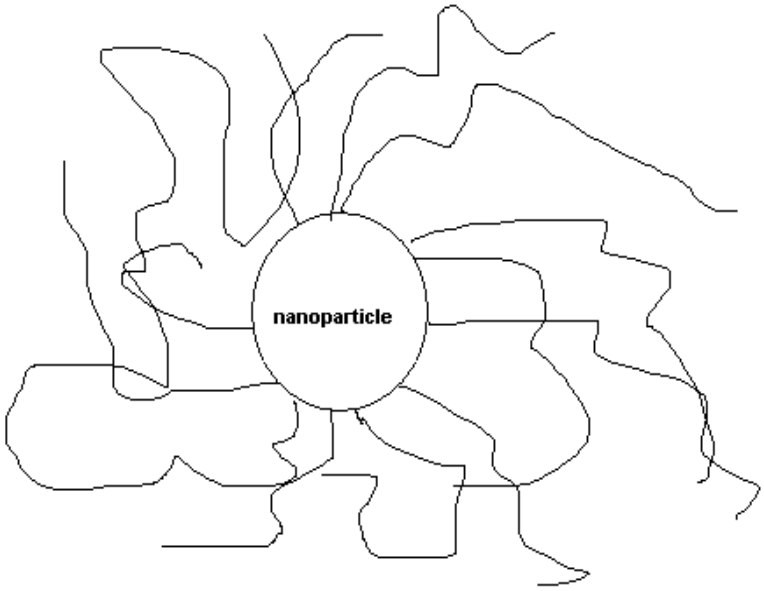


**Figure 1. The general structure of desired nanostars.**

As shown in the Figure 1, nanostars resemble dendrimers which are perfect monodisperse macromolecules with a regular and highly branched three-dimensional architecture. Dendrimers are used in various application areas such as dendritic sensors, crystallisation promoters, dendritic supports, used in medical applications, solubilisation of guest molecules, energy funnels, selective catalysts, and receptors [19]. Their synthesis, characterization, properties and the applications of different types of dendrimers were investigated by several researchers comprehensively [20-34]. Because of this similarity in between nanostars and dendrimers, nanostars may be used in the same applications by having better properties than dendrimers.

## 2. The state of the art

### 2.1. Modification of nanoparticles

Because the nanoparticles have different physical, chemical, biological properties and their smaller particle size, they have been used in countless areas of technology for long time [35]. For example; $SiO_2$ nanoparticles have been used for gene targeting, $FeO_x$ nanoparticles for very stable coatings and in vitro tumour cell penetration and hyperthermal treatment, boehmite nanoparticles for condensation catalyst to prepare very hard transparent coatings for polycarbonate, and an overcoat with polymerizable nanoparticles was used to produce

anti-reflective and ultra hard coatings, in systems with incorporated fluoro silanes, leading to low surface energy coatings nanoparticles were used to synthesize transparent easy-to-clean coatings [36]. But sometimes it is too difficult to control the dispersion of nanoparticles inside an organic medium [37]. To overcome the dispersion problems, nanoparticles need to be chemically modified to change their surface characteristics, namely their surfaces need to be functionalized. Moreover, a lot of properties such as hydrophobic/hydrophilic properties, biocompatibility, providing to bonding to an organic matrix via chemical bonds, sensibility to certain substances, corrosion resistance, wettability, excellent magnetic property, etc. are gained them and the modified nanoparticles also give to coatings excellent scratch performance, abrasion resistance, hydrophobic/oleophobic property and other properties [5, 38-72].

It is known that the surface –OH groups are to be expected on all inorganic particles and they can be modified with modification agents, such as silanes, to gain lots of new properties. For example; a nanoparticle modified with a silane compound, 3-methacryloxypropyl trimethoxysilane, is shown in the Figure 2. As shown in the Figure 2, when the nanoparticle is unmodified, the surrounding of the nanoparticle is only covered with –OH groups. After modification, the surrounding of the nanoparticle is covered with also modified 3-methacryloxypropyl trimethoxysilane molecules and of course the modified nanoparticle behaves different within organic solvents and a matrix as compared to the unmodified nanoparticle. And also, the methacrylate groups on the surface can be polymerized or reacted with some molecules but unmodified nanoparticle does not have these groups. According to the literature, organic groups can be linked to inorganic backbone by means of three different ways. One of them is the formation of covalent bonds, for instance; modification of $SiO_2$ nanoparticles with silanes to occur covalent bonds. Another one is the formation of complex structures with β-ketoesters, β-diketones or carboxylic acids, for instance; Zr/acetylacetones and the other one is the formation of ionic bond to an organic acid (salt formation) [17, 18].

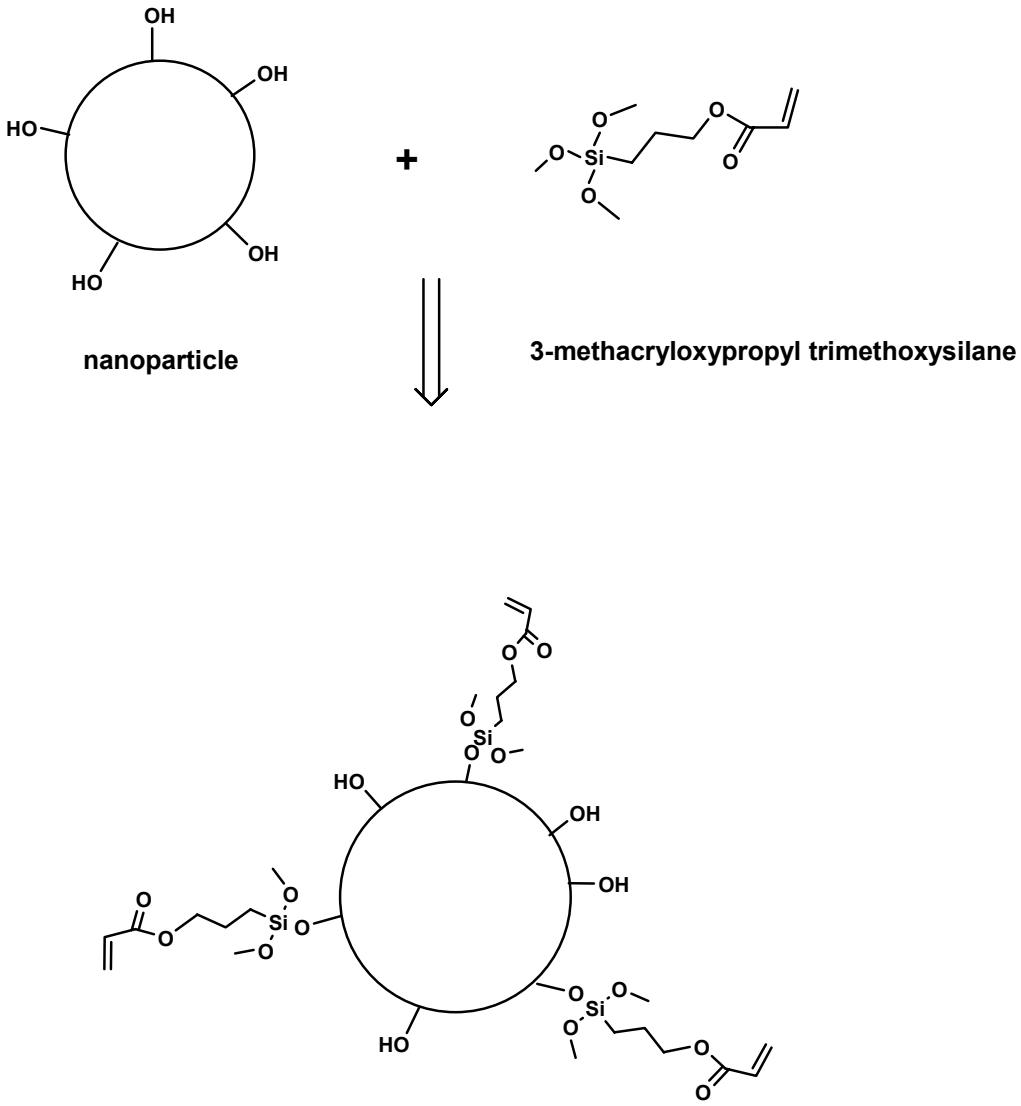


**Figure 2. Modification of a nanoparticle with 3-methacryloxypropyl trimethoxysilane.**

Also, if nanoparticles (such as $TiO_2$, $ZrO_2$) have –OR groups (such as $–OC_3H_7$, $–OC_4H_9$, $–OC_5H_{11}$) on their surface, they can be also modified with carboxylic acids, β-ketoesters or β-diketones. For example; oleic acid-modified $TiO_2$ nanoparticles is shown in the Figure 3. According to the Figure 3, when $TiO_2$ nanoparticle is unmodified, the surrounding of the nanoparticle is only covered with –OH and –OR groups. After modification with oleic acid, the surrounding of the nanoparticle is covered with also oleic acid molecules and of course, the oleic acid-modified nanoparticle behaves different within organic solvents or a matrix as compared to the unmodified nanoparticle. Also, the double bonds on the surface can be polymerized or reacted with some molecules but unmodified nanoparticle does not have these groups. In the literature, it was not found that both –OR and –OH groups bearing nanoparticles were modified with carboxylic acids, β-ketoesters or β-diketones. For this reason, the reactions occurred in these modifications are briefly explained by means of modifications of metal alkoxide compounds with them in the following.

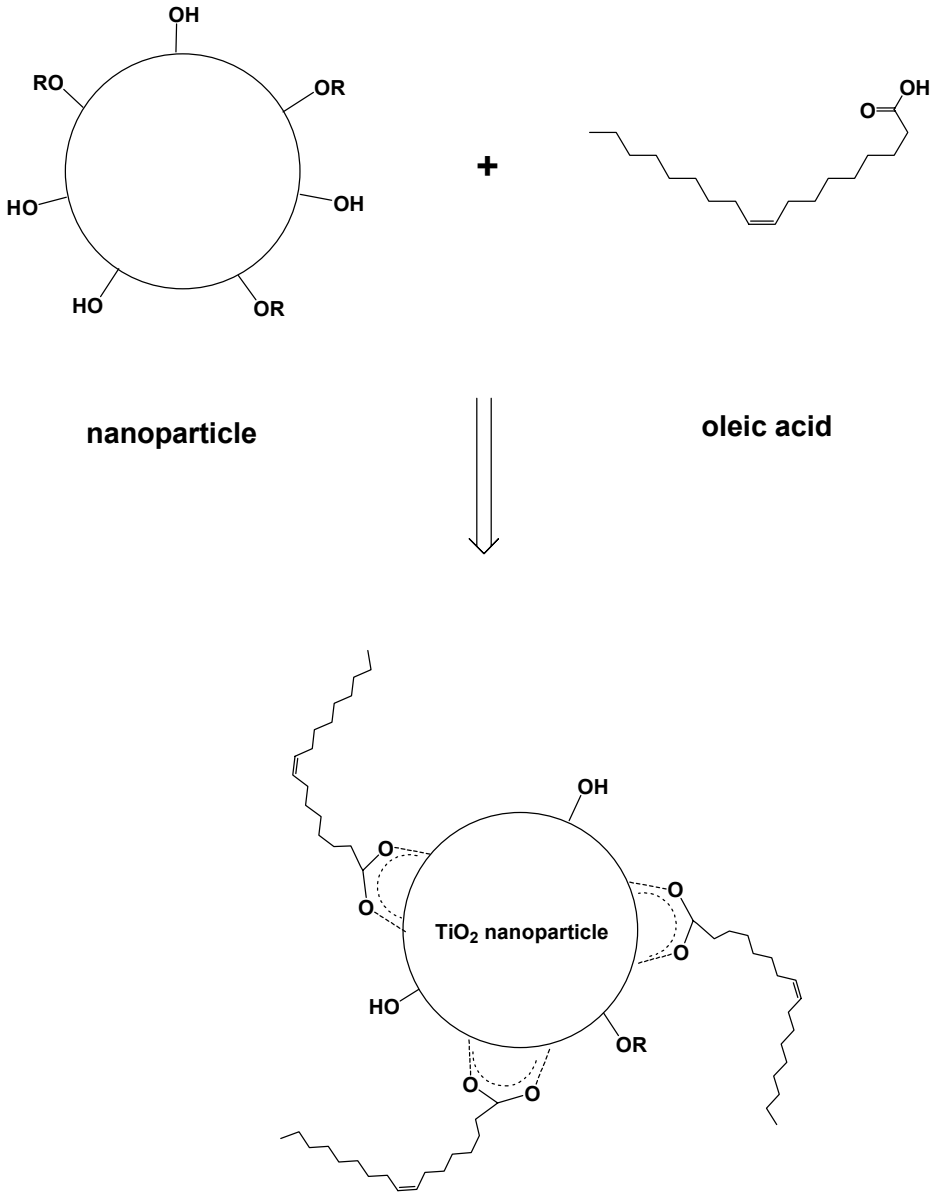


**Figure 3. Modification of $TiO_2$ nanoparticle with oleic acid.**

## 2.2. Complexation reactions of metal alkoxides with carboxylic acids, β-ketoesters and β-diketones

Nanoparticle modifications with carboxylic acids, β-ketoesters and β-diketones resemble the modification of metal alkoxide compounds with carboxylic acid, β-ketoesters or β-diketones. The reason why the chelating of metal alkoxides with these molecules made is to change their characteristics. For example; the direct attachment of organic groups via carbon-metal bonds to other metals such as titanium, zirconium and aluminium is not useful because of the hydrolytic instability of the more ionic Carbon-Metal (C-M) bonds. For this reason, the common way for the organic modification of e.g., Al-, Ti- and Zr- alkoxides is the partial complexation with carboxylic acids, β-ketoesters or β-diketones. These organic ligands of the

metal alkoxide complexes are more stable towards hydrolysis than the ligands with C-M bonds due to the chelate bond formation and sterical hindrance effects. Organic complex ligands act as modifier of the condensation degree of metal alkoxides. If organic ligands with reactive, for example; unsaturated bonds are used, additional organic networks between metal alkoxide complexes can be built up by polymerization or additive reaction. This organic network is linked with the organic one by means of C-O-M-O-M bridges. Unsaturated compounds used as ligands for the metal alkoxide complexes are mostly organic acids such as methacrylic-, acrylic-, or methacrylamidosalicilic acid [49, 73-76] but several β-ketoesters and β-diketones can be also used. The reaction between $Ti(OR)_4$ and Allyl acetoacetate (AAA) is shown in the Figure 4 [76];

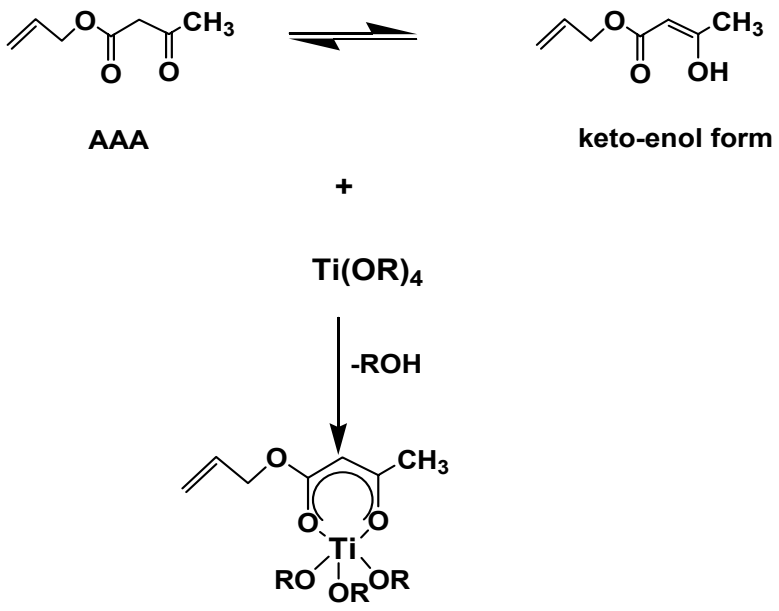


**Figure 4. Modification of $Ti(OR)_4$ with AAA.**

According to the literature, if the reaction shown in the Figure 4 is monitored by FT-IR, the peaks of the stretching vibrations ν(C=O) and ν(C=C) of the enolic forms of the at about 1615 $cm^{-1}$ and 1525 $cm^{-1}$ for β-ketoesters and also the stretching vibrations ν(C=O) of the keto forms of free β-ketoesters at about 1740 $cm^{-1}$ and 1710 $cm^{-1}$ are determined [76]. FT-IR is very important method for the characterization of carboxylic acid, β-ketoester and β-diketone complexation reactions with metal alkoxides. Several works are summarized related to the chelating reactions of metal alkoxides with organic acids, β-diketonates, and β-ketoesters in the following.

Al, Ti-, Zr- alkoxides were used and modified with some β-diketonates, β-ketoesters. It is concluded from that the hydrolytic stability of the ligands of the metal alkoxides complexes during hydrolysis/condensation reactions at the molar ratio h ($H_2O$: OR) = 0,5-2.0 decreases with increasing $H_2O$:complex ratio. And it is understood from this work that after modification of alkoxides with another complex occurring compounds hydrolytic stability is increased to unmodified structures. For the reason, it is contributed more controlled synthesis of sols and of new inorganic-organic polymers by means of the sol-gel process [76].

Acetylacetone modified cerium (IV) isopropoxide precursors have been synthesised and about acac/Ce = x value three different results have been obtained. For $x < 0.15$, hydrolysis leads to precipitation and for $0.15 \leq x < 1$, sols are obtained and for $1 \leq x \leq 1$, small oligomeric species are formed and remain stable without any gelation. This simple model is proposed to account for the size control. Also, it is relied on the variation of the functionality of the precursor, which comes from the fact that acetylacetonato ligands are not removed upon hydrolysis [77]. After modification, generally the bands of the stretching vibrations $\nu$(C=O) and $\nu$(C=C) of the enolic forms of the β-diketones around 1600 $cm^{-1}$ and of the β-ketoesters at about 1615 $cm^{-1}$ and 1525 $cm^{-1}$ were integrated. Additionally, the integrals of the stretching vibrations $\nu$(C=O) of the keto forms of free β-diketones and β-ketoester at about 1740 $cm^{-1}$ and 1700 $cm^{-1}$ were measured [76].

Complexation reactions of alkoxides are limited by conditions such as alkoxide and ligand type and also, alkoxides to ligand ratio chances to precursors and ligands. For instance; when zirconium tetra-n-butylate modified with methacrylic acid, it is provided the maximum combination ratio was found to be 1:2 for $Zr(OBu^n)$ : methacrylic acid and for methacrylic acid-acetic acid mixture and methacrylic acid-propionic acid and methacrylic acid-butyric acid 1:1:1 and they were measured by some instruments [50].

Aluminum sec-butoxide modified with ethylacetoacetote and attractive precursors for the sol-gel synthesis of ceramics were obtained. The modified precursor $Al(OBu^s)_2$(etac) appears quite attractive for the preparation of multicomponent systems. The presence of poorly hydrolysable ligands slows down the hydrolysis-condensation process. Also, several oligomeric species containing 4, 5 or 6 coordinated Al atoms could be present [78].

## 2.3. Polymers

Polymers are chemical substances (chemical compounds) composed of polymer molecules. The term polymer refers to molecules composed of many units (Greek: *poly* = many,

*meros* = parts). Polymer molecules may thus consist of many atoms, usually a thousand or more, thereby having high molar masses ("molecular weights"). Polymers are a group of materials made up of long covalently-bonded molecules, which include plastics and rubbers. They have existed in natural form since life began and those such as DNA, RNA, proteins and polysaccharides play crucial roles in plant and animal life. From the earliest times, man has exploited naturally-occurring polymers as materials for providing clothing, decoration, shelter, tools, weapons, writing materials and other requirements. The use of polymeric materials is increasing rapidly year by year and in many applications they are replacing conventional materials such as metals, wood and natural fibres such as cotton and wool [79, 80].

### 2.3.1. Polymerization mechanisms

Polymerization reactions can be classified as step-growth and chain-growth reactions. Generally polymer physical properties can differ significantly depending on the polymerization mechanism, this is often due to the difference in molecular masses, i.e., polymers synthesized by chain-growth polymerization often have higher molecular masses. With step-growth polymerization, the reactions that link monomers, oligomers, and polymers involve same reaction mechanism, and any two molecular species (monomer, oligomer, or polymer) can be coupled. The growth of a polymer chain proceeds slowly from monomer to dimer, trimer, tetramer, and so on, until full-sized polymer molecules are formed at high monomer conversions. Polymer chains continue to grow from both ends throughout the polymerization and, therefore, both chain lifetimes and polymerization times are usually of the order of hours. On the other hand, in the chain-growth polymerization, polymer molecules generally grow to full size in a time-scale which is much smaller than the time required for high conversion of monomer to polymer. The lifetime of a growing polymer molecule may be less than a few seconds for a free-radical polymerization, which is a typical example of chain-growth polymerization, while a typical polymerization time to obtain high monomer conversion may be several hours. Chain-growth polymerizations require an active center, which may be a free radical, cation, or anion. Once an active center is created, a polymer chain grows extremely rapidly, and when the growing chain is deactivated by a termination reaction, the polymer chain is dead and no longer takes part as a reactant. With free-radical polymerization, however, the so-called dead polymer chain is not always truly dead because under certain circumstances it may itself react with radicals. The active center may initiate the growth of many polymer chains [81].

#### 2.3.1.1. Step-growth polymerization

##### 2.3.1.1.1. Linear polymerization

In this type polymerization, there is generally only one type of chemical reaction which links molecules of all sizes. The number of functional groups present on a molecule of monomer is of crucial importance as can be appreciated by considering the formation of ester linkages from the condensation reactions of carboxylic groups with hydroxyl groups. For instance; acetic acid and ethanol are monofunctional compounds which upon reaction together yield ethyl acetate with elimination of water but ethyl acetate in incapable of further reaction a polymer chain can not form. Hence linear polymerization involves reactions of difunctional monomers. Some of the typical chemical reactions are amidation, esterification, and the formation of urethanes and aromatic substitution [79, 81].

##### 2.3.1.1.2. Interfacial polymerization

Interfacial polymerization can provide a method to produce very high molecular mass polymers by step-growth polymerization. Polymers are formed at or in the vicinity of the phase boundary of two immiscible monomer solutions. This technique requires an extremely fast polymerization. The best reaction type for step-growth polymerization would be Schotten–Baumann reactions involving acid chlorides. For example; polyamidation is performed at room temperature by placing an aqueous solution of diamine over an organic phase containing the diacid chloride. The polymer formed at the interface can be pulled off as a continuous film or filament. The amine–acid chloride reaction rate is so fast that the polymerization becomes diffusion controlled. Once the polymer molecules begin to grow and monomer molecules start to add to polymer chain ends, incoming monomer molecules tend to react with polymer chain ends before they can penetrate through the polymer film to start the growth of new chains. Thus, polymers with much higher molecular masses are formed [81].

##### 2.3.1.1.3. Nonlinear polymerization

Another important class of polymers produced by step-growth polymerization is nonlinear polymers formed by polymerization of monomers with more than two functional groups per molecule. In the early stages of such reactions the polymer has a branched structure and increase in molar mass much more rapidly with the extend of reaction than for a linear step polymerization. As the reaction proceeds, further branching reactions lead to the formation of complex network structures which have properties that are quite different from those of the

corresponding linear polymer. For instance; $R(COOH)_2$ with a triol $R(OH)_3$ would lead to structures of the type [79, 81].

### 2.3.1.2. Chain-growth polymerization

Chain-growth polymerization is initiated by a reactive species, $R_{in}^{*}$ produced from an initiator or catalyst $I$ .

$I \rightarrow nR_{in}^{*}$

Depending on the type of active center, chain-growth polymerization can be divided into free-radical, anionic and cationic polymerization. In these polymerization types, the reactive species $nR_{in}^{*}$ adds to monomer molecules are added to the active center successively [81].

#### 2.3.1.2.1. Free radical polymerization

Free-radicals are independently-existing which possess an unpaired electron and normally are highly reactive with short lifetimes. Free-radical polymerization is chain polymerizations in which each polymer molecule grows by addition of monomer to a terminal free-radical reactive site known as an active centre. Consequent upon every addition of monomer, the active centre in transferred to the newly-created chain end. Free radical polymerization is the most widely practised method of chain polymerization and is used almost exclusively for the preparation of polymers from monomers of the general structure $CH_2=CR_1R_2$. In common with other types of chain polymerization the reaction can be divided into three distinct stages: initiation, propagation and termination. Initiation stage involves creation of the free-radical active centre and usually takes place in two steps. The first is the formation of free radicals from an initiator and the second is the addition of one of these free radicals to a molecule of monomers. Also, there are two principal ways in which free radicals can be formed: homolytic scission of a single bond for instance; homolyis and single electron transfer to or from an ion or molecule, for instance; redox reactions. Homolysis can be affected by the application of heat and there are many compounds, in particular those containing peroxide or azo linkages, which undergo thermolysis. Additionally, homolysis can be brought about by photolysis, for instance; the action of radiation propagation needs growth of the polymer chain by rapid sequential addition of monomer to the active centre. Propagation reaction controls both the rate of growth and the structure of the polymer chain. The time required for each monomer addition typically is of the order of a millisecond and therefore several thousand additions can take place within a few seconds [79]. In termination stage, an active center on a growing polymer radical may be destroyed by a variety of processes, including

termination by added substances. The most common mechanisms of termination involve biomolecular reaction of growing polymer chains.

#### 2.3.1.2.2. Ionic polymerization

Chain polymerization of olefinic monomers can be also affected via active centers. There are two types of ionic polymerization: those in which the active centre is positively charged termed cationic polymerization and those in which it is negatively charged are termed anionic polymerization. Because the active centre has an ionic charge, these polymerizations are more monomer-specific than free-radical polymerization and will proceed only with monomers that have substituent groups which can stabilize the active centre [79].

##### 2.3.1.2.2.1. Cationic polymerization

Cationic polymerization proceeds by means of attack on the monomer by an electrophilic species, resulting in heterolytic splitting of the double bond to produce a carbenium ion. For instance; the most commercial polymers, polyisobutylenes and butyl rubber are produced by this method. In this method, there are three stages: initiation, propagation and termination.

In initiation stage, cationic active centres are created by reaction of monomer with electrophiles and for this generally protonic acid such as sulphiric acid, perchloric acid and also, Lewis acids such as boron trifluoride, aluminium chloride can be used. In propagation stage, after the cationic centre is produced, propagation proceeds predominantly via successive head-to-tail addition of monomer to the active centre. Afterwards, in termination stage, growth of individual chains is terminated most commonly either by unimolecular rearrangement of the ion pair or by means of chain transfer [79, 81].

##### 2.3.1.2.2.2. Anionic polymerization

Anionic polymerization shows many of same characteristics as cationic polymerizations. An important property of anionic polymerization is the absence of inherent termination process. Termination by ion-pair rearrangement does take place as it requires the highly unfavourable elimination of a hydride ion. Also, the alkali metal counter-ions used have no tendency to combine with the carbanionic active centres to form unreactive covalent bonds. Thus, in the absence of chain transfer reactions the propagation polymer chains retain their active carbanionic end-groups. If more monomer is added after complete conversion of the initial quantity, the chains will grow further by polymerization of the additional monomer and will again remain active [79, 81].

## 2.4. Polymer grafting onto nanoparticle surface

A key problem with nanomaterials is the difficulty of controlling the dispersion of nanoparticles inside an organic medium. To overcome this problem, functionalizaton of the nanoparticle surface is required [37]. Nowadays surface modifications with polymers have become important for various applications such as biotechnology, materials having optical, magnetic, mechanical properties, biocompatibility, advanced microelectronic. Surface functionalization of inorganic fillers with a polymer shell is attracting attention because the polymer coating changes the interfacial properties of these modified particles. Furthermore, the thermal and mechanical properties of the matrix polymers in hybrid systems can be improved by the compatibility of the nanoparticles with the matrix, whereas nanoparticle physical properties are governed by both the shape and size of the inorganic core and the surrounding organic layer. The choice of the nanoparticles ranges from reinforcing fillers such as silica, alumina and carbon black to metals such as gold and silver, up to semiconductor quantum dots such as cadmium sulphide and the size of the particles range from 1 nm to several μm [82].

Generally the surfaces of inorganic materials are functionalized with polymer chains either chemically (covalent bonding) or physically (physisorpsion). Physisorpsion involves absorption of block copolymers with sticky segments covalent grafting techniques are preferred to maximize a stable interfacial compatibility between the two phases. For example; the chemical and physical modifications of the surfaces of $SiO_2$ nanoparticles, carbon black and carbon nanotubes were extensively studied by researchers and they concluded that the chemical modification of a surface is permanent, but physical modification is temporary and also, after modifications it was pointed that the dispersibility of $SiO_2$ nanoparticles, carbon black and carbon nanotubes is extremely improved by surface grafting by means of chemical bonding [83]. According to the literature, there are three methods for surface grafting of polymer chains onto nanoparticles. They can be categorized into *"grafting to (onto)", "grafting from"* [16, 37, 82, 84-86] and the other is named as *"the combination of both grafting methods"* in this work because of its similarity with both *"grafting to (onto)"* and *"grafting from"*, but this name is not defined like that in the literature.

### 2.4.1. *Grafting to* method

*Grafting to* method involves the reaction of reactive, preformed macromolecules with compatible surface groups [82]. Namely, the grafting of polymers onto the surface proceeds based on termination of growing polymer radicals, cations, and anions formed during the polymerization [83]. They in particular allow for the facile conversion of the chain ends to any

number of desired functionalities (hydoxyl, carboxyl, amino, thiol, etc.). Also, the substrate surface plays an important role in the synthesis of the polymer brush layers. Silica and gold surfaces possess surface functionalities that can undergo condensation reactions with polymer chains containing thiol, hydroxyl, and carboxyl functionalities [87]. Although the *grafting to* method is experimentally simple, it has not been used frequently because of its limitations. Of all mentioned limitations, the most notably is low grafting densities because of steric crowding of reactive sites by previously attacted polymers. The steric hindrance inhibits diffusion of large free polymer chains to diffuse to open-surface reactive sites and creation of a dense polymer brush layer. It is this low surface density that allowed for small molecules to migrate to the polymer brush anchoring sites and resulted in brush degrafting [82, 87]. In the following, several works concerning the grafting of polymers onto nanoparticles and solid surfaces according to *grafting to* method are summarized.

The surface grafting onto inorganic ultrafine particles, such as silica, titanium oxide, and ferrite, by the reaction of acid anhydride groups on the surfaces with functional polymers having hydroxyl and amino groups was examined. The introduction of acid anhydride groups onto inorganic ultrafine particle was achieved by the reaction of hydroxyl groups on these surfaces with 4-trimethoxysilyltetrahydrophthalic anhydride in toluene. Then, functional polymers having terminal hydroxyl or amino groups, such as diol-type poly (propylene glycol), and diamine-type polydimethylsiloxane, reacted with acid anhydride groups on these ultrafine particles to give polymer-grafted ultrafine particles [88].

Carboxylic acid- and anhydride-terminated polystyrenes of different molecular weights from 4500 to 672 000 were grafted from melt onto silicon substrates modified with epoxysilane monolayer. The grafted chains are densely packed with a density close to the known value for the bulk material. The tethered polymer layers are very smooth, uniform, mechanically stable, and cover homogeneously the modified silicon. At the degree of polymerization close to the critical molecular weight, the grafting process is the most effective, resulting in the grafted unperturbed macromolecules [89].

It was report a simple method to synthesize binary polymer brushes from two incompatible polymers of different polarity. The synthetic route is based on a subsequent step-by-step grafting of carboxyl-terminated polystyrene and poly(2-vinylpyridine) to the surface of a Si wafer functionalized with 3-glycidoxypropyltrimethoxysilane. The end-functional polymers were spin-coated on the substrate, and grafting was carried out at a temperature higher than the glass transition temperature of the polymers. The composition of the binary brushes can be regulated based on grafting kinetics of the first polymer by the change of time or/and

temperature of grafting. This method reveals a smooth and homogeneous polymer film on the macroscopic scale, while at the nanoscopic scale the system undergoes phase segregation effecting switching/adaptive properties of the film. Upon exposure to different solvents, the film morphology reversibly switches from “ripple” to “dimple” structures as well as the surface energetic state switches from hydrophobic to hydrophilic. The same switching of hydrophilic/hydrophobic properties was obtained for the different ratios between two grafted polymers in the binary brush [90].

### 2.4.2. *Grafting from* method

As for *grafting from* method, graft polymerization of various monomers is initiated from radical, cationic, and anionic initiating groups previously introduced onto the nanoparticle surface [16, 83]. Namely, in this process the surface of the particle is modified with an initiator monolayer followed by polymerization under conventional conditions. The *“grafting from”* technique results in significally higher grafting density because the steric barrier to incoming polymers imposed by the in-situ grafted chains does not limit the access of smaller monomer molecules to the active initiation sites [82]. In this method, the free radical polymerization was succeeded for polymer grafting onto nanoparticles or solid surfaces by means of conventional radical polymerization or controlled radical polymerization. Conventional free radical polymerization is one of the most studied systems. According to this method, nanoparticles are firstly modified with some initiators having reactive groups such as azo or peroxyester initiators, then these modified molecules are polymerized from the surface using some monomers such as methyl methacrylate, styrene, vinyl compounds, etc. by thermal or photopolymerization [91-93]. After polymerization is completed, the structures, which have inorganic particle in the core and polymer branches on the surface, are synthesized (core-shell). But, in this method, the introduction of the initiating groups, such as peroxyester groups or azo groups, onto the surface of the inorganic particles usually need multi-step synthesis [94]. In the following, several works from the literature are summarized.

The effect of polymerization conditions on the molecular weight of polystyrene grafted onto silica obtained from the radical graft polymerization initiated by azo and peroxyester groups introduced onto the surface was investigated. The molecular weight of polystyrene grafted onto silica obtained from the radical graft polymerization initiated by surface azo and peroxyester groups decreased with decreasing monomer concentration and polymerization temperature. The molecular weight of polystyrene was found to be controlled to some extent by the addition of a chain transfer agent. The molecular weight of grafted chain on silica surface obtained from the graft polymerization initiated by surface radicals formed by

photodecomposition of azo groups was considerably smaller than that by thermal decomposition. The number of grafted polystyrene in photopolymerization, however, was much larger than that in thermal polymerization. These results are explained by the blocking of surface radicals formed on the silica surface by previously grafted polymer chain. When the decomposition of surface azo and peroxyester groups proceed instantaneously at the initial stage of the polymerization, the number of grafted polymer chains increased [92].

The photografting of polymers onto ultrafine inorganic particles, such as silica and titanium oxide, initiated by azo groups introduced onto these surfaces was investigated. The introduction of azo groups onto the particles was achieved by the reaction of 4,4'-azobis (4-cyanopentanoic acid) with surface isocyanate groups, which were introduced by the treatment with tolylene 2,4-diisocyanate. It was found that the photopolymerization of vinyl monomers, such as methyl methacrylate, styrene, and N-vinylcarbazole, is initiated by ultrafine particles having azo groups. The corresponding polymers were effectively grafted onto these surfaces through the propagation of the polymer from the surface radicals formed by the photodecomposition of the azo groups: e.g., the percentage of grafting of PMMA and polystyrene onto silica was reached to 112 % and 176 % respectively. The percentage of grafting onto silica in the graft polymerization initiated by photodecomposition of surface azo groups was much larger than that initiated by thermal decomposition [93].

The radical graft polymerization of vinyl monomers from inorganic ultrafine particles, such as silica, titanium oxide, and ferrite, by use of azo groups introduced onto their surface was investigated. The introduction of azo groups onto the ultrafine particles was achieved by the reaction of glycidyl groups, which were introduced by the reaction of hydroxyl groups on the surface with 3-glycidoxypropyltrimethoxysilane, with 4,4′-azobis(4-cyanopentanoic acid). The amounts of azo groups introduced onto silica, titanium oxide, and ferrite were determined to be 0.07, 0.05, and 0.03 $mmol.g^{-1}$ respectively. The polymerization of vinyl monomers, such as methyl methacrylate, styrene, and N-vinylcarbazole, was found to be initiated by radicals formed by the decomposition of the azo groups. During the polymerization, the polymer was effectively grafted onto these surfaces through propagation from the surfaces; the percentage of grafting of poly(methyl methacrylate) onto silica, titanium oxide, and ferrite reached to 45,1 %; 42,8 % and 40,5 % respectively [95].

*Grafting from* polymerizations from initiators bound to surfaces are a powerful alternative to control the functionality, density and thickness of polymer brushes with almost molecular precision. But, in order to achieve maximum control over brush density, polydispersity, and composition, plus at the same time allowing the formation of block copolymers on the

surface, a controlled polymerization is highly desirable. In the controlled radical polymerization, polymer brushes on the surfaces are constituted such as by ring-opening polymerization, living ring opening polymerization, living anionic polymerization, living cationic, ring opening metathesis polymerization, nitroxide-mediated polymerization, reversible addition-fragmentation chain transfer polymerization and atom transfer radical polymerization [16, 82].

### 2.4.2.1. Living ring opening polymerization

Several commercially important polymers, such as polycaprolactone and polylactide, are synthesized by ring-opening polymerization (ROP). Thus, surface-initiated ROP is an attractive route to surfaces coated with thin layers of these polymers. First work by Jordan and Ulman used the living cationic ROP of 2-ethyl-2-oxazoline to produce linear poly (N-propionylethylenimine). A self-assembled monolayer presenting trifluoromethane sulfonate groups was prepared on a gold-coated glass slide by the adsorption of 11-hydroxyundecanethiol and subsequent vapour-phase functionalisation. After seven days in refluxing chloroform, a 9 nm thick layer poly (N-propionylethylenimine) and termination for this polymerization was succeeded adding N,N-dioctylamine [16].

### 2.4.2.2. Ring opening metathesis polymerization

Recently polymerization of strained cyclic monomers by this method, especially functionalized norbornenes, has attracted for the synthesis of polymers with useful electrical properties. In a study, brushes were grown using norbornene as a monomer, again from silicon wafer surfaces. In an attempt to eliminate the electrically defective surface $SiO_2$ layer normally present when brushes are grown from silicon, an alternative initiator attachment procedure was developed, allowing brushes with a direct Si–C bond to the surface to be synthesized. Some of the thickest films produced using surface-initiated polymerization were grown in short times using a surface-bound ruthenium catalyst. Brushes anchored to the surface in this way provide a route to very well-defined insulating layers on silicon, with applications in electrical device construction [16].

### 2.4.2.3. Nitroxide-mediated polymerization (NMP)

This method is based on the concept of activation–deactivation equilibrium between dormant species and a small fraction of propagating macro radicals. The reactions are done at elevated temperatures where the initiation is rapid and all the chains are formed at the same time. The initiated polymer chains are reversibly capped by a stable free radical to give a dormant polymer chain. The nitroxides can reversibly react with the growing chain but do not

initiate polymerization. Initiators are usually peroxides, azo compounds and redox systems commonly used in conventional free radical polymerizations. NMP was initially restricted to the high temperature polymerization of styrene [82]. It was reported in a study the use of nitroxide-mediated controlled free radical polymerization directly from the surface of CdSe nanoparticles to prepare polymer-nanoparticle composite materials. While free radicals can quench the fluorescence of CdSe nanoparticles, nitroxide-mediated polymerization allows for the preparation of the desired polymer-nanoparticle composites while maintaining the inherent fluorescence of the nanoparticles. The low concentration of radicals inherent to this controlled free radical polymerization technique contributes to the success of this process. Nitroxide-containing ligand was prepared for this study and used to functionalize 3-4 nm CdSe nanoparticles. Polystyrene and poly(styrene-r-methyl methacrylate) copolymers were grown from the nanoparticle surface by using this method [96].

#### 2.4.2.4. Reversible addition-fragmentation chain transfer (RAFT) polymerization

RAFT polymerization is a controlled polymerization in which chain growth is initiated using a conventional technique (for example; by a free radical initiator such as AIBN) and mediated by a dithioester chain transfer agent. Radical transfer between growing chains, either that in solution or those on a surface, gives good control of the polymerization, and “capping” of growing chains by the dithioester moiety gives the reaction good living characteristics. In a study, a self-assembled monolayer containing an azo initiator group (like that in AIBN) was used to grow polymer brushes from silica surfaces in the presence of a dithiobenzoate chain transfer agent. At temperatures up to 90 °C and times of up to 48 hours, poly(methyl methacrylate) brushes with a thickness of 28 nm and poly(N,N-dimethylacrylamide) and polystyrene brushes up to 11 nm were grown. It was found that small amounts of untethered radical initiator (AIBN) were required in solution for brush growth to proceed [16].

#### 2.4.2.5. Atom transfer radical polymerization (ATRP)

ATRP has been applied to surface-initiated graft polymerization on a variety of materials including flat substrates [97, 98], fine particles [99, 100] and porous materials [101-103]. ATRP is a metal catalyzed polymerization involving the reversible activation–deactivation reaction between a growing polymer chain and a metal-ligand species. The ATRP initiator (typically an α-halo ester or α-benzyl moiety) is activated in the presence of metals such as Cu, Ru, Fe, and others. The solubility and activity of the metal is enhanced by ligation with aliphatic or aromatic amines. ATRP is tolerant to functional groups and impurities and hence wide range of monomers can be polymerized in organic as well as aqueous phases. This facile polymerization and less stringent experimental conditions promoted the application to

brush growth on nanoparticles, especially silica [82]. In a study, several hybrid nanocomposites consisting of a magnesiumdihydroxide core and tethered poly(methyl)acrylate chains were synthesized via ATRP. The hydroxyl groups on the surface of the MDH particles were modified by reaction with 2-bromopropionyl or 2-bromoisobutyryl bromide to attach ATRP initiator moieties to the particle. n-Butyl acrylate, methyl methacrylate, dodecyl methacrylate and octadecyl methacrylate were polymerized from the functionalized MDH particles using the "grafting-from" technique [104].

### 2.4.3. The combination of both grafting methods

Because of some deficiencies of *grafting to* and *grafting from* method such as some limitations and difficulty because of its multi-step synthesis, *the combination of both grafting methods* can be used for grafting of the surfaces according to the literature. Although "*grafting to"* method is experimentally simple, it has not been used frequently because of its limitations. Of all mentioned limitations, the most notably is low grafting densities because of steric crowding of reactive sites by previously attacted polymers. As for *grafting from* method, the introduction of the initiating groups, such as peroxyester groups or azo groups, onto the surface of the inorganic particles usually need multi-step synthesis. Unlike the other methods, in *the combination of both grafting methods,* the nanoparticles are firstly modified with double bond containing modification agents, such as with 3-methacryloxypropyl trimethoxysilane, in an appropriate solvent. After that, polymer chains were grafted onto the surface using monomers, such as MMA, styrene and initiators such as azo or peroxy, by thermal or or photopolymerization [94, 105-110]. Also, the name of this type grafting polymerization was not called as *the combination of both grafting methods* in the literature. This name is given to this method for only the present work. In addition, of all methods, this method is experimentally easiest method. In the following, several works concerning the polymer grafting onto the nanoparticles by means of *the combination of both grafting methods* are summarized.

Polystyrene/$TiO_2$ nanocomposite particles were synthesized in high yield by in situ polymerizing styrene in the presence of 3-(trimethoxysilyl) propylmethacrylate modified nano $TiO_2$ in ethanol media. Polystyrene/$TiO_2$ nanocomposite particles were characterized by means of FTIR spectroscopy, elemental analysis, gel permeation chromatography, and thermogravimetric analysis. FTIR investigation provided direct and clear evidence for the presence of polystyrene shell on nano $TiO_2$ core particles, and TGA showed quantitative evidence of the presence of polystyrene shell on nano $TiO_2$ core particles [105].

A new procedure for the preparation of polymer/magnetic nanoparticle composites is described. Magnetite nanoparticles capped with methacrylate units were dispersed in a toluene solution of the monomer, and polymerization occurred after the addition of the initiator a'-a-azo-iso-butyronitrile at reflux temperature. The structural properties were determined by infrared spectroscopy, X-ray diffractometry and transmission electron microscopy. The thermal properties of the resulting nanocomposite were studied extensively with modulated differential scanning calorimetry. An increase in the glass transition temperature was observed after the incorporation of the nanoparticles [108].

To overcome the disadvantages generated by the loosened nanoparticle agglomerates dispersed in polymer composites, a chemical grafting method was applied to modify nano-alumina, silicon carbide and silicon nitride through covalently introducing polyacrylamide onto the particles. Sliding wear tests demonstrated that the frictional coefficient and specific wear rate of the nanoparticles/epoxy composites are lower than those of unfilled epoxy. Grafted nanoparticles reinforced composites have the lowest frictional property and the highest wear resistance due to the strengthening of the nanoparticle agglomerates and the enhancement of filler/matrix interfacial interaction resulting from the grafting polymers. Comparatively, graft treatment of nanoparticles is more beneficial to the improvement of the tribological features of the composites than the silane treatment that is used conventionally [107] .

How PMMA molecules grafted onto the nanoparticles by means of *the combination of both grafting methods* is shown in the Figure 5. According to the Figure 5, a nanoparticle is firstly modified with a double bond bearing silane molecule. After that, PMMA chains are grafted onto the surface using monomers such as MMA, styrene and an initiator such as azo or peroxy intiators and by thermal- or photopolymerization.

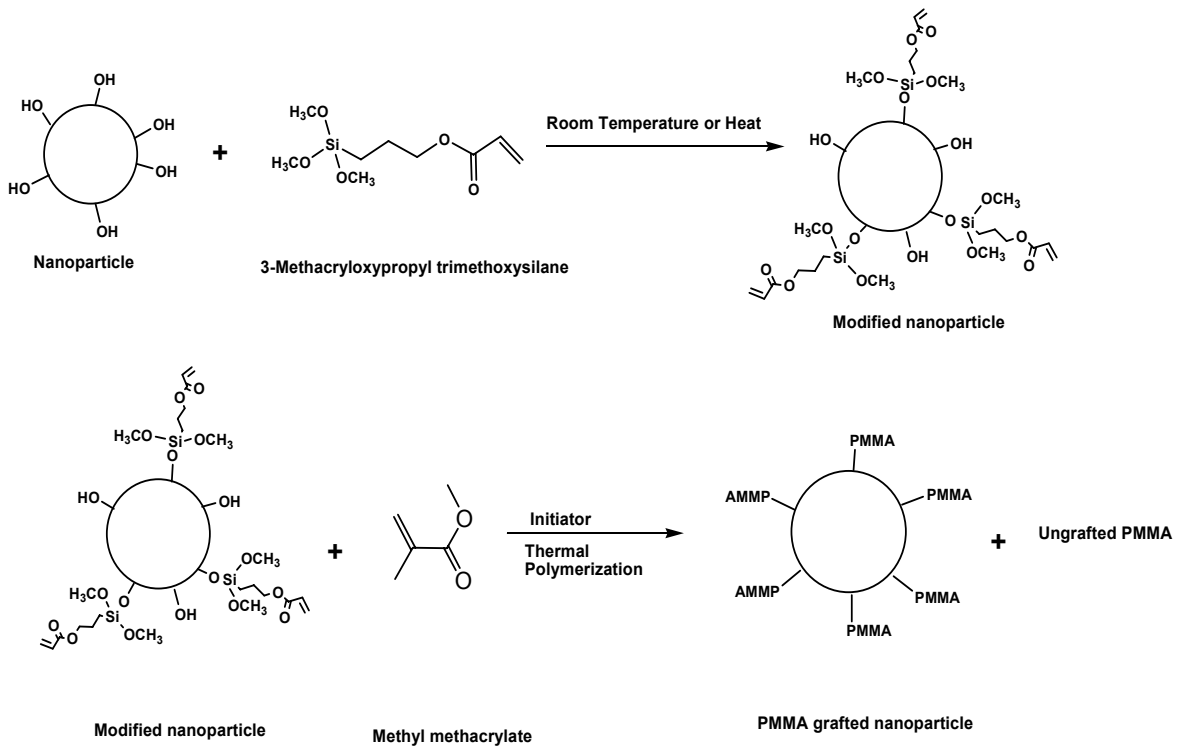


**Figure 5. PMMA grafting onto the nanoparticle by means of *the combination of both grafting methods.***

### 2.4.4. Characterization of polymer-grafted nanoparticles

Nowadays polymer grafting onto the nanoparticles has become a subject of extensive research. Namely, it is attributed to the fact that modification of the surface of the inorganic particles with a well defined polymer improves the processing properties of the colloidal dispersions. It prevents flocculation and improves thermal and mechanical properties of the polymer itself. Polymer grafted nanoparticles (such as silica nanoparticles) are characterized by several characterization methods. Spectroscopic techniques such as NMR, IR, X-ray photoelectron microscopy (XPS) are used for characterization after and before modifications, gravimetric methods are used to determine the changes in weight before and after modification of the surface, thermal analysis methods such as TGA and DSC are used for a bulk compositional property of the hybrid material, provide, microscobic techniques such as TEM, SEM are used to determine the size and nature of the nanoparticles after and before each stage of modifications [82]. For example; FT-IR is used to observe the characteristic peaks for the initiator and polymer bound to the surface. Consequently, FT-IR measurements are preformed after and before modifications. Also, sometimes elemental analysis results are very important for the quantitative amount of modification agents on the nanoparticle [105, 109]. Elemental analysis measurements are generally performed to observe the modification amount on the surface after and before modifications. Also

according to the literature, the percentage of polymer grafting onto the surfaces is calculated by the following equation. Where A is weight of grafted polymer, B is weight of silica charged [88, 92, 93, 95, 111].

$$\text{Percentage of Grafting}\,(\%) = \frac{A}{B}\,x\,100$$

In addition, after polymer grafting onto the surface is succeeded by the mentioned methods above, they have some different and new properties. In the grafted nanoparticle systems, tethered polymers do not have good mobility as compared to pure polymer and these results in the increasing of glass transition temperature, "$T_g$". For example; $Fe_3O_4$ particles were modified with methacrylic acid and these modified particles are subsequently polymerized using MMA and styrene monomers by means of an initiator and then, $T_g$ measurements were performed by DSC. $T_g$ result for pure PMMA was 99,59 °C. After the addition of 2; 6; 32; 32 % $Fe_3O_4$ particles into PMMA, $T_g$ values increased to 112,85 °C ; 114,13 °C and 118,98 °C respectively in comparison with 99,5 °C of the pure polymer [108]. In addition, $SiO_2$ particles were grafted with polystyrene and $T_g$ was measured by DSC. For pure polystyrene $T_g$ was determined to be 81 °C and for polystyrene grafted $SiO_2$ it was determined to be 94 °C [112].

## 2.5. Sol-gel process

### 2.5.1. The history and applications of sol-gel process

The combination of different types of materials for achieving novel properties has always been of high interest in technology, because in many cases the properties of the basic materials do not meet special requirements for application. The combination between inorganic and organic polymeric materials on nanometer scale depends strongly on methods for synthesizing inorganic polymeric networks suitable to thermal stability of organic materials. The sol-gel process as a "soft chemistry" method has been proved to be a proper tool for building up inorganic network with incorporated organic components [17]. The sol-gel process is a process for making glass/ceramic materials. This method involves the transition of a system from a liquid (the colloidal "sol") into a solid (the "gel") phase. The sol-gel process allows the fabrication of materials with a large variety of properties: ultra-fine powders [10, 113-118], monolithic ceramics [119, 120] and glasses, ceramic fibers [121, 122], inorganic membranes [123-126], thin film coatings [127-158] and aerogels [62, 159-162]. Starting from molecular precursors, an oxide network is obtained via inorganic polymerization reactions. These reactions occur in solutions and the term "sol-gel

processing" is often broadly used to describe inorganic synthesis by "wet chemistry" methods. These processes offer many advantages as compared to the conventional "powder" route [163-165].

The sol-gel process has become a wide and increasing research area day by day in the technologic field during the last two decades. Interest in the sol-gel processing of inorganic ceramic and glass materials began as early as the mid-1800s with Ebelman and Graham's studies on silica gels. These early investigators observed that the hydrolysis of tetraethyl orthosilicate (TEOS) under acidic conditions produced $SiO_2$ in the form of a "glass-like material". However, exceedingly long drying times of 1 year or more were necessary to avoid the silica gels fracturing into a fine powder, and consequently there was little technological interest. After some experiments, Roy and co-workers recognized the potential for achieving very high levels of chemical homogeneity in colloidal gels and used the sol-gel method in the 1950s and 1960s to synthesise a large number of novel ceramic oxide compositions, involving Al, Ti, Zr, etc. that could not be made using traditional ceramic powder methods. After this investigation, especially at the producing ceramic powder enormous and very important proceedings were achieved by chemists [165].

Basically the sol-gel process means the synthesis of an inorganic network by a chemical reaction in solution at low temperature and this inorganic network can be built up by other chemical reactions, for instance; from the vapour phase or by high temperature process like melting. Firstly in the sol-gel process, amorphous network occurs in opposition to crystallization process from solution. As precursors most work in the sol-gel process has been performed by the use of alkoxides. Alkoxides provide a convenient source for "inorganic" monomers which in most cases are soluble in common solvents. Another advantage of the alkoxide route is the possibility to control rates by controlling hydrolysis (a) and condensation by chemical means and not by surface or colloid chemistry (b) shows the most important condensation reactions: The condensation of two M-OH groups or the reaction of an M-X with an M-OH group [166].

$$M\text{-}X + H_2O \longrightarrow M\text{-}OH + HX, \qquad (a)$$

Here, M = Metal or Si; X = reactive ligand like halogen, OR, acrylate;

$$M\text{-}OH + X\text{-}M \longrightarrow M\text{-}O\text{-}M + HX$$

$$M\text{-}OH + HO\text{-}M \longrightarrow M\text{-}O\text{-}M + H_2O \qquad (b)$$

Nevertheless, sol-gel process has lots of advantages as compared to the conventional methods. Potential advantages of the sol-gel process can be summarized: sol-gel process a) provides an easy way to purify precursors; b) provides an easy way to get homogenous distributions of precursors; c) provides an easy way to introduce trace elements; d) allows the use of chemistry to control reactions; e) allows the formation of a "pre"–inorganic network in solution; f) allows the adjustment of appropriate viscosities for coatings; g) allows the preparation of new glass compositions; h) allows the densification to organic solids at comparatively low temperatures ; i) allows the synthesis of active ceramic powders [167]. And, sol-gel process doesn't allow only for materials to have any composition, but it also permits the production of new hybrid organic-inorganic materials which do not exist naturally [168]. This explains why the sol-gel process has received so much scientific and technological attention during the last decade. Moreover, the structure of sol-gel ceramics can be easily controlled as the size of the particles. But the greatest limitation of sol-gel processing for synthesizing of ceramic is still the cost of precursors and these are especially alkoxides. Most of these alkoxides are nonetheless quite easy to make; especially if they do not tend to polymerize. A few of them such as Ti and Zr are even used industrially by the Schott Company for coating applications [169].

With sol-gel method, it is possible to produce countless materials such as monoliths, powders, films and coatings, nanocomposite/nanoparticles. In this connection, sol-gel method opened new research area for improving properties of materials such as in optic (for example; transparent hard coatings, LC displays, colored coatings, reflecting coatings, antireflective coatings, etc), electrical coatings ( for example; dielectric, electrochromic, etc.), thermal (for example; thermally resistant coatings, IR reflective glazing, thermally resistant paints, etc.), passivation (for example; passivation of semiconductors, protective coatings on polymer and metals), release/wetting (for example; biomedical applications, slow release of materials/drugs, antistick coatings, easy-to-clean coatings, antigraffiti coatings, antifouling coatings, etc.), sensors (for example; pH sensors, gas sensors, fiber sensors, etc), catalyst (aerogel catalyst, catalyst supports, microfilters, controlled pore materials, liquid chromatographic elements, etc.), membranes, filters, selective adsorbents, coloured thin coatings, etc [64, 154, 170-182].

### 2.5.2. Hydrothermal method

The term "hydrothermal" came from the earth sciences, where it implied a regime of high temperatures and water pressures. Hydrothermal processing is one of the processing in

fields of materials science and engineering and comes from geology since 1850. Nowadays this method has been used to synthesize fine oxide powders. Hydrothermal method has lots of advantages as compared to other methods. These advantages are a) powders are formed directly from solution, b) powders are anhydrous, crystalline or amorphous depending on producing of hydrothermal powder temperature, c) the size of particles synthesized can be controlled by hydrothermal method, d) it is able to control particle shape by starting materials, e) it is able to control chemical, composition, stochiometry, etc, f) powders are highly reactive in sintering, g) many cases, powders do not need calcinations, h) many cases, powders do not need milling process, i) the purity of product prepared in appropriate conditions could be high owing to recrystallization in hydrothermal solution, j) the equipment and processing required are simpler and the control of reaction conditions is easier, k) if hydrothermal conditions are changed, for example; pH, temperature or reactant concentration, crystalline product having different compositions, structures and morphology might be formed, l) a crystalline product can be obtained directly at relatively lower reaction temperatures. Because of that, the sintering process can be avoided [183-185]. Consequently, lots of fine nanoparticles can be synthesized such as titan dioxide, zirconium dioxide, iron oxide, etc [25, 186-197].

### 2.5.3. Synthesis of $TiO_2$ nanoparticles by hydrothermal method

Titanium dioxide is very important as a white pigment commercially because of its maximum light scattering with virtually no absorption and it is non-toxic, inert to chemicals and a dielectric ceramic material for its higher dielectric constant. $TiO_2$ can be used in gas sensors, dielectric ceramics, catalyst for thermal or photoinduced processes, photovoltaic solar cells, pigments. Titanium dioxide has three crystalline forms: rutile, anatase and brookide. Brokide and anatase are metastable and transform exothermally and irreversibly to the rutile over a range of temperatures but usually 750 and 1000 °C respectively [183-185].

Titanium dioxide has been synthesized by sulphate and chloride processes in the industry but these methods need very complication conditions, very harsh materials and more requirements for equipment, high reaction temperature (>1400 °C) and because of strong corrosiveness of $Cl_2$ at high temperature. Because of these disadvantages of the other methods, nowadays hydrothermal method has been used to synthesize $TiO_2$ particles.

To synthesize $TiO_2$ nanoparticles by sol-gel process, there are some important conditions such as types of precursors. A lot of titan-compounds can be used as precursors such as $TiCl_4$ [198-200], titanic acid [63, 201], titanium (IV) isopropoxide [202-204], titanium (IV) ethoxide [205, 206], titanium (IV) butoxide [207], etc. The particles are synthesized via

hydrolysis and condensation of the titan-compounds. Also, hydrolysis and condensation of the compounds are affected by some parameters such as water amount [208], pH-value [209], concentration of titanium-compound [210, 211], catalyst [212, 213], salt ions [183, 214] or surfactants [215, 216] and if these parameters are changed, the morphology and crystalline structure of $TiO_2$ nanoparticles can be changed. After an amorphous $TiO_2$ particle containing sol or gel is prepared, it is treated with hydrothermal method and then the nanoparticles are obtained according to precursors and conditions. In the following, several studies are summarized related to the synthesizing of nanoparticles by using hydrothermal method.

Uniform nanosize rutile and anatase particles were prepared by a hydrothermal method using $TiCl_4$ as starting material. The influences of various hydrothermal conditions on the formation, phase, morphology, and grain size of products were investigated. Increasing the acidity in reaction medium and the concentration of $TiCl_4$ aqueous solution favoured of the formation of rutile type $TiO_2$. Raising the temperature (>200 °C) can decrease the agglomeration among $TiO_2$ grains. The mineralizers, $SnCl_4$ and NaCl reduce very much the grain size and favour the formation of rutile type $TiO_2$. Another mineralizer, $NH_4Cl_4$ will increase greatly agglomeration among grains. The optimum conditions for preparing rutile-type $TiO_2$ were that $[TiCl_4] > 0.5$ mol/dm$^{-3}$, 200 °C for 2 h and using $SnCl_4$ or NaCl as mineralizer. The average particle size of rutile $TiO_2$ was 20 nm by 8 nm [183].

Nanocrystalline $ZrO_2$ and $TiO_2$ were synthesized by hydrothermal treatment of $ZrO(NO_3)_2$ and $TiO(NO_3)_2$ nitrates aqueous solutions and amorphous gels of the corresponding hydroxides. The hydrothermal synthesis was performed in a wide range of temperatures (150–250 °C), concentration of starting solutions (0.25–0.5 M) and duration of the process (from 10 min up to 24 h). The hydrothermal treatment at high pressure about 2.0–4.0 GPa was also made. The products were characterized by XRD, TEM and BET. Particle sizes, morphology and properties of the products were investigated. Significant divergences of the phase composition, morphology, and particles size and their variations in response to external factors (temperature, process duration, solution concentration, pressure) were found [188].

Well-dispersed anatase and rutile nano-particles were prepared via hydrothermal treatment of tetrabutylammonium hydroxide-peptized and $HNO_3$-peptized sols at 240 °C. A broad particle size distribution of anatase crystals was observed in the nonpeptized $TiO_2$ species hydrothermally treated at 240 °C. X-ray diffraction and transmission electron microscopy, as well as zeta potential measurement, were used to characterize the particles. The formation of

the well-dispersed anatase and rutile particles from the peptized samples could be attributed to (i) homogeneous distribution of the component in the peptized sols, and (ii) the high long-range electrostatic forces between particles in the presence of both peptizers, which were not present in the nonpeptized samples [190].

Well-shaped pure rutile $TiO_2$ nanocrystals by hydrothermal synthesis are synthesized. The synthesis of the 20 nm rutile particles from titanium isopropoxide and pH 0.5 $HNO_3$ is achieved by vigorous stirring of the solution during the hydrothermal treatment. The significant effect of the stirring and long aging control experiments suggests that, at this composition, most of the condensation to $TiO_2$ occurs during the autoclaving step. The large colloid size distribution and the formation of the anatase structure in the absence of stirring are attributed to the inhomogenity developed in the solution under the extreme conditions of the hydrothermal process. The significance of the work is the elimination of the commonly used mineralizers that can induce impurities into the nanocrystals, in addition to the improved colloid shape in comparison with standard procedures [191].

## 3. The objectives of the present work

Because nanoparticles have different physical, chemical, biological properties as explained above, they have been used in countless areas of technology for long time. But a key problem with nanomaterials is the difficulty of controlling the dispersion of nanoparticles inside an organic medium [35, 37]. To overcome this problem, functionalization of the nanoparticle surface is required. Of course, the main reason of the particle surface modifications is not only their dispersion in a desired medium but also giving them other properties such as hydrophobic/hydrophilic properties, biocompatibility, direct chemical bonding to an organic matrix via nanoparticles, providing sensibility against certain substances, etc. For these reasons, because the functionalization of nanoparticles opens new countless probabilities for nanoparticles in industry and academic areas, interest to the synthesis and characterization of the functionalized nanoparticles is also increasing day by day. The functionalization of the nanoparticles is various such as with silanes, carboxylic acids, β-ketoesters, β-diketones, the grafting of lots of polymers onto nanoparticles, etc. Also, the functionalization of the nanoparticles is generally achieved by forming covalent bonds, complex structures or ionic bonds on their surfaces.

In this work, nanostars named for all of modification types of $TiO_2$ nanoparticles will be synthesized and characterized. The described nanostars will have $TiO_2$ nanoparticles in the centre of structures as core and some branches on the nanoparticle surface as shell (core-shell structures). Furthermore, the planned $TiO_2$ particles will be agglomerate-free, uniform,

and crystalline and they will have a high surface area. They will also have a narrow particle size distribution, a round-like shape and they will possess both $–OC_3H_7$ groups and –OH groups on the surface unlike conventional nanoparticles mentioned in the literature. It is expected that both –OH groups and $–OC_3H_7$ groups bearing nanoparticles will gain more modification possibilities than only –OH groups bearing ones. Namely, $TiO_2$ nanoparticles will be also modified to form covalent bonds, complex structures on the surfaces. $TiO_2$ nanoparticles were chosen for the cores of nanostars because of lots of very good properties of $TiO_2$. Titanium dioxide is very important as a white pigment commercially because of its maximum light scattering with virtually no absorption and it is non-toxic, inert to chemicals and a dielectric ceramic material for its higher dielectric constant. Also, $TiO_2$ is used in gas sensors, dielectric ceramics, catalyst for thermal or photoinduced processes, photovoltaic solar cells, pigments. Furthermore, after the use of $TiO_2$ nanoparticles in this work, another important point is associated with the synthesis of $TiO_2$ nanoparticles. Although $TiO_2$ particles are synthesized by several methods, such as sulphate and chloride methods, a hydrothermal method will be used for the synthesis because of lots of advantages as compared to other methods (see section 2.5.2. and 2.5.3., page 31-32).

In this work, $TiO_2$ nanoparticles will be synthesized by hydrothermal method and characterized by PCS, TEM, XRD, elemental analysis and EDX. After that, they will be modified with several alkylsilanes with different molecular weights and one aminosilane by forming Ti-O-Si covalent bonds on the surface, with carboxylic acids and one β-ketoester by forming complex structures on the surface, with some urea molecules with different molecular weights by forming Ti-O-Si covalent bonds on the surface. The modifications of $TiO_2$ nanoparticles with silanes, carboxylic acids and β-ketoester will be different from the literature because of the surface characteristics of $TiO_2$ nanoparticles. Namely, $TiO_2$ nanoparticles will have both -OR and -OH groups on their surfaces. As for the modifications of $TiO_2$ nanoparticles with urea group containing modification agents with different molecular weights, the reasons why urea molecules chosen for the modifications of $TiO_2$ nanoparticles are that 1) It wasn't found any work about the modifications of $TiO_2$ nanoparticles with the urea group containing modification agents, 2) the coupling reaction between an isocyanate compound and amine compounds is so fast and the characterization of products was easy, 3) to form Ti-O-Si covalent bonds by different modification agents. Thus, the modifications of $TiO_2$ nanoparticles with lots of molecules will have been achieved and then they will be characterized by FT-IR, elemental analysis, GC/MS and EDX.

Also, $TiO_2$ nanoparticles will be modified with different amount of β-ketoester molecule to propoxy groups on the surface *(2AAEM:-$OC_3H_7$)* and then the 2AAEM-modified $TiO_2$

nanoparticles containing dispersion will be dispersed in different amount of MMA to 2AAEM introduced to the surface and subsequently polymerized by free radical polymerization by means of *"the combination of both grafting methods"*. In this work, the PMMA-grafted $TiO_2$ nanoparticles will be different from those synthesized in the literature because of some reasons. Polymer grafting onto nanoparticle works in the literature are generally carried out by means of covalent bonding on the nanoparticles such as Ti-O-Si or Si-O-Si, etc [94, 95, 105, 106, 217-220]. But in this work, polymer grafting onto surface will be carried out by means of the formation of complex structure on the surface of $TiO_2$ nanoparticles. Secondly, polymer grafting onto nanoparticles works is generally carried out via "*grafting to"* or "*grafting from"* methods in the literature. Although "*grafting to"* method is experimentally simple, it has not been used frequently because of its limitations. Of all mentioned limitations, the most notably is low grafting densities because of steric crowding of reactive sites by previously attacted polymers (see section 2.4.1., page 20). As for *grafting from* method, the introduction of the initiating groups, such as peroxyester groups or azo groups, onto the surface of the inorganic particles usually need multi-step synthesis (see section 2.4.2., page 22). However, the introduction of the double bonds can be succeeded by one-step synthesis using β-ketoester compound or silane coupling agent containing double bonds to modify the surface of the inorganic nanoparticles. In this work, this method will be employed and called as "*the combination of both grafting methods"* (see section 2.4.3., page 26). After the PMMA-grafted $TiO_2$ nanoparticles are synthesized, they will be characterized by FT-IR and TGA/DSC. Also, one sample of the PMMA-grafted $TiO_2$ nanoparticles will be investigated by TEM. Consequently, organic-inorganic $TiO_2$ nanostars will have been synthesized in this work.

# 4. Experimental Part

## 4.1. Chemicals used in the research

The name, formula, molecular weight (M. W.), purity, supplier of the chemicals used and molecular structures of some of these molecules used throughout the research work are given in Table 1, 2 and Figure 6.

**Table 1. Chemicals used in the research.**

| **Name** | **M. W. (g. mole$^{-1}$)** | **Purity** | **Supplier** |
|---|---|---|---|
| Titanium (IV) isopropoxide | 284,26 | 100 % | Fluka |
| 2-(Methacryloyloxy) ethylacetoacetate | 214,22 | 95 % | Aldrich |
| (3-isocyanatopropyl)triethoxysilane | 247,36 | 95 % | Aldrich |
| Molecular Sieves | 3 Å, beads, 4-8 Mesh | | Sigma-Aldrich |
| Calcium Hydride ($CaH_2$) | 42,10 | ≥ 97.0 % | Fluka |
| Methyl methacrylate, ~ 0,004 % hydroquinone | 100,12 | ≥ 99 % | Fluka |
| Trigonox EHPS (Di(2-ethylhexyl) peroxydicarbonate, initiator, $t_{1/2}$= 64 °C / 1hour) | 346,5 | 98 % | Akzo Nobel |
| **Amines** | | | |
| Ethylenediamine | 60,10 | > 99,5 % | Fluka |
| 1,6-Diaminohexane | 116,20 | 98 % | Aldrich |
| 1,8-Diaminooctane | 144,26 | ≥ 98 % | Fluka |
| 1,12-Diaminododecane | 200,37 | 98 % | Aldrich |
| Aminopropylterminated PolyDimethylsiloxane (DMS-A15) | 3000 | 100 % | ABCR |
| Aminopropylterminated PolyDimethylsiloxane (DMS-A21) | 5000 | 100 % | ABCR |
| Pentylamine | 87,17 | ≥ 98,5 % | Fluka |
| Octylamine | 129,25 | ≥ 99 % | Fluka |
| 1-Dodecylamine | 185,36 | 98 % | Aldrich |
| Octadecylamine | 269,52 | ≥ 99 % | Fluka |

**Table 2. Chemicals used in the research (continuation)**

| | | | |
|---|---|---|---|
| **Carboxylic Acids** | | | |
| 10-Undecylenic Acid | 184,28 | 99 % | Riedel-dë Haën |
| Oleic Acid | 282,46 | 90-95 % | ABCR |
| Stearic Acid | 284,49 | ≥ 97,0 % | Fluka |
| **β-ketoester** | | | |
| Allyl acetoacetate | 142,15 | ≥ 98,5 % | Fluka |
| **Silanes** | | | |
| 3-Aminopropyltrimethoxysilane | 179,29 | ≥ 97.0 % | Fluka |
| Hexyltrimethoxysilane | 206,35 | 97 % | ABCR |
| Decyltrimethoxysilane | 262,46 | 100 % | ABCR |
| Dodecyltrimethoxysilane | 290,52 | 95 % | ABCR |
| Hexadecyltrimethoxysilane | 346,63 | 90 % | ABCR |
| **Solvents** | | | |
| Methanol | 32,04 | ≥ 99,5 % | Fluka |
| 1-Butanol | 74,12 | ≥ 99,5 % | SDS |
| Ethanol | 46,07 | ≥ 99,8 % | VWR |
| Toluene | 92,14 | 99,9 % | Sigma-Aldrich |
| Tetrahydrofurane | 72,11 | 99,9 % | Sigma-Aldrich |
| 2-Propanol | 60,10 | 99,7 % | SDS |
| 1-Propanol | 60,10 | 100 % | VWR |
| Acetone | 58,1 | 99,8 % | VWR |

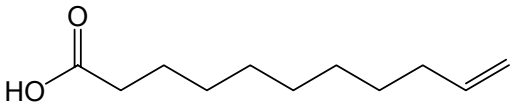


10-Undecylenic Acid

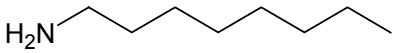


Octylamine

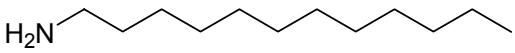


1-Dodecylamine

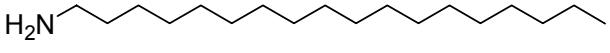


Octadecylamine

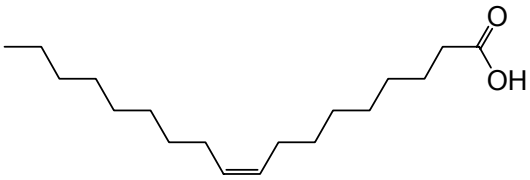


Oleic Acid

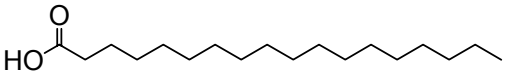


Stearic Acid

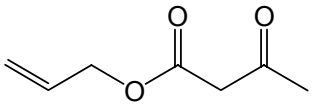


Allyl acetoacetate

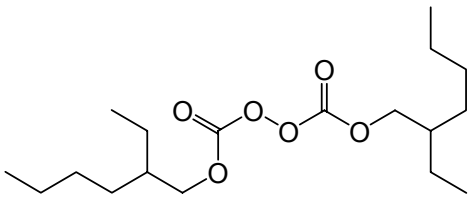


Trigonox EHPS

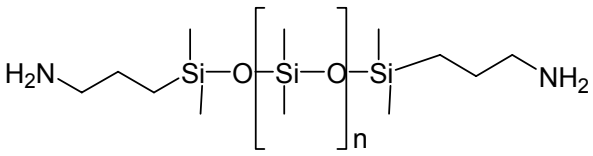


General structures of DMS-A15 and DMS-A21

**Figure 6. The structures of some chemicals used in the research.**

## 4.2. Instruments used in this research

### 4.2.1. Autoclave instrument

Autoclave instrument was used to synthesize anatase $TiO_2$ nanoparticles in this work. The instrument was equipped with a heating block 1000 Watt heat output Type DAH-904, and a temperature controller Type BTU 942, Berghof Gruppe GmbH, 250 ml teflon with cap, V-sealing and pressure digestion vessel with bayonet quick closure. The apparatus of the instrument are shown in the Figure 7.

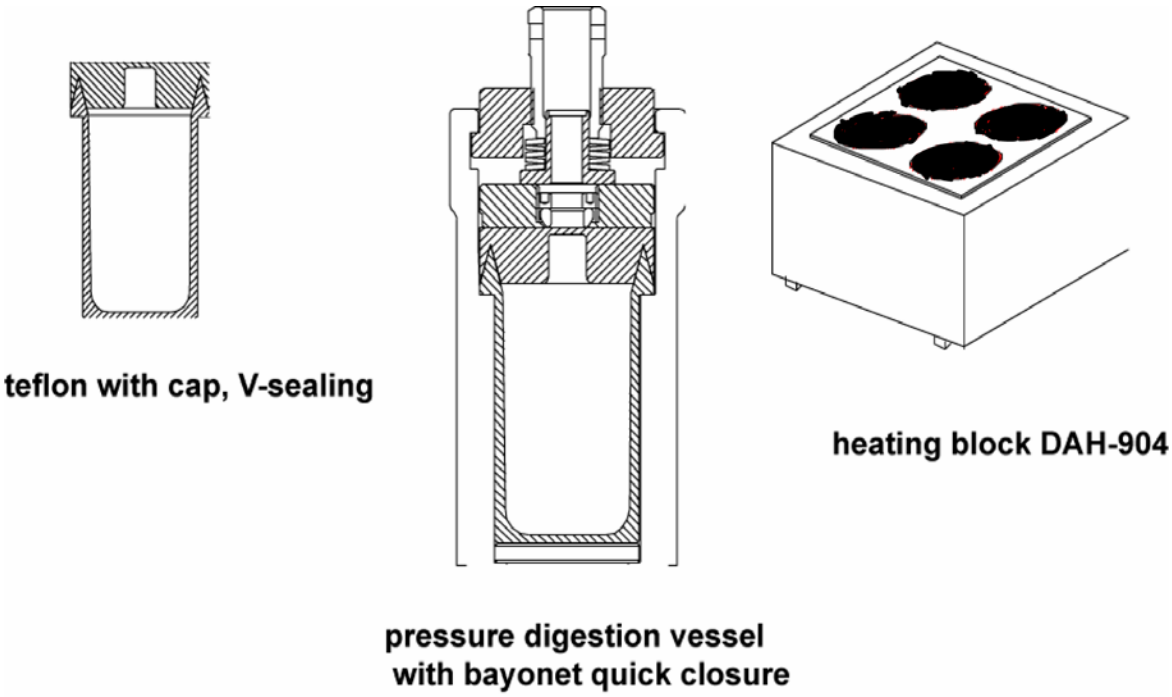


**Figure 7. The apparatus of autoclave instrument used in this research.**

### 4.2.2. Photon correlation spectroscopy (or dynamic light scattering)

Photon correlation spectroscopy (PCS) is used to determine the radius of small beads in Brownian motion in a solution. This technique is one of the most popular methods used to determine the size of particles. Shining a monochromatic light beam, such as a laser, onto a solution with spherical particles in Brownian motion causes a Doppler Shift when the light hits the moving particle, changing the wavelength of the incoming light. Thus, this change is related to the size of the particle. It is possible to compute the sphere size distribution and give a description of the particle's motion in the medium, measuring the diffusion coefficient of the particle and using the autocorrelation function. This method has several advantages: first of all the experiment duration is short and it is almost all automatized so that for routine measurements an extensive experience is not required. Moreover, this method has modest development costs. Commercial "particle sizing" systems mostly operate at only one angle

(90°) and use red light (675 nm). Usually in these systems the dependence on concentration is neglected. Using more sophisticated experimental equipment (projector, short wavelength light source); the methods can be not only considerably extended, but also more complicated and expensive [221]. PCS instrument used in this work is ALV Laser GONIOMETER, Model: ALV/SP-125 # 010.

### 4.2.3. Elemental analysis

Elemental analysis in the classical sense refers to quantitative determination of the constituent elements in an organic compound, especially carbon, hydrogen, nitrogen, oxygen, sulphur, the halogens, phosphorous although the definition would today be expanded to cover determination of any element present in an organic structure [222].

After the samples are dried, they are put into Tin Boats and weighted without air. The weights of the samples are about 5 mg. Then, they are measured by using “Vario EL III” instrument directly and automatically. The firing temperature of the instrument is adjusted to 950 °C; the reduction temperature is adjusted to 500 °C, the temperature of $CO_2$ column is adjusted to 100 °C and the temperature of $H_2O$ column is adjusted to 150 °C. The calibration of the instrument is made by using three samples of acetanilide. Theoretically, the percentages of carbon, nitrogen and hydrogen in the acetanilide are 71,09 ;10,36; 6,71 respectively.

### 4.2.4. X-ray diffraction instrument

Following the discovery of X-rays by W. C. Röntgen in 1895, three major branches of science have developed from the use of this radiation. The first and oldest of these is X-ray radiography, which makes use of the fact that the relative absorption of X-rays by matter is a function of the average atomic number and density of the matter concerned [223]. Solid matter can be described as amorphous and crystalline. In amorphous, the atoms are arranged in a random way similar to the disorder we find in a liquid. Glasses are amorphous materials. About 95 % of all solids can be described as crystalline. In crystalline, the atoms are arranged in a regular pattern, and there is as smallest volume element that by repetition in three dimensions describes the crystal. X-rays, as an electromagnetic wave with high energy and useful penetrability, have been put to good use in modern medicine and structure analysis of materials. Due to the correlation of the structure of a material with its physical properties, X-rays have been used in determining the microstructure of materials and related methods have been developed technically in many diverse applications [224]. If X-Ray hits ordered atoms periodically, the scattered waves are accentuated in certain directions

(diffraction maximum) and extinguished in other directions (diffraction minimum). The distance between network levels and wavelengths of X-rays used can be calculated by means of so-called Braggsche Law, nλ = 2dsinθ. Bragg developed a relationship in 1913 to explain why the cleavage faces of crystals appear to reflect X-ray beams at certain angles of incidence (theta, θ). In this equation, d indicates the distance between atomic layers in a crystal, and lambda λ indicates the wavelength of the incident X-ray beam, n indicates an integer. This observation is an example of X-ray wave interference. X-ray was evidence for the periodic atomic structure of crystals postulated for several centuries [225, 226]. The size of crystal particles is calculated according to *"Scherrer-equation"* in the following [227].

$$D = \frac{0{,}89 \cdot \lambda}{\beta \cdot \cos\theta}$$

Where "D" indicates crystal size, "λ" indicates wavelength of X-ray, "θ" indicates diffraction angle of reflexes, "β" indicates physical line width. Crystalline structure of sample can be compared with a known structure.

In this research, the phase and size of crystalline $TiO_2$ nanoparticles were determined by X-ray measurement. The measurement was performed by Typ X'Pert with copper tube and nickel filter, a product of PANalytical Company and the measurement parameters are shown in the Table 3.

**Table 3. Measurement parameters for XRD instrument.**

| | | | |
|---|---|---|---|
| Start position [2θ] | 20 | Character of Divergence Slit | fest |
| End position [2θ] | 120 | Size of Divergence Slit [°] | 0,4785 |
| Step Size [2θ] | 0,017 | Irradiating Length [mm] | 20,00 |
| Step Time [s] | 150 | Voltage | 40 kV |
| Scan Mode | Continuous | Current | 30 mA |
| X'Celerator Mode | Scanning | Goniometer Radius [mm] | 240,00 |
| X'Celerator Length [2θ] | 2,13 | Distance Focus- Divergence Slit [mm] | 91,00 |
| Offset [2θ] | 0,0 | | |

### 4.2.5. Transmission electron microscopy (TEM)

Transmission Electron Microscopy (TEM) is an imaging technique by means of a beam of electrons is transmitted through a sample, then an image is formed, magnified and directed to appear either on a fluorescent screen or layer of photographic film, or to be detected by a CCD camera. TEM operates on the same basic principles as the light microscope but uses electrons instead of light. What you can see with a light microscope is limited by the wavelength of light. Because of using the electrons as “light source” and their much lower wavelength makes it possible to get a resolution a thousand times better than with a light microscope. The first practical TEM was built in 1938 using concepts developed earlier by Max Knoll and Ernst Ruska [228]. In this research, the morphology and size of $TiO_2$ nanoparticles were determined by a kind of TEM instrument, “Philips CM200 FEG”.

### 4.2.6. Energy dispersive X-ray spectroscopy (EDX)

Energy dispersive X-ray spectroscopy (EDX, EDS or EDXS) is an analytical technique used for the elemental analysis of samples. This method is the most standard and reliable one in the field of analytical electron microscopy and it is widely used. EDX relies on the investigation of a sample through interactions between charged particles (especially electrons) and matter, analyzing X-rays emitted by the matter in this particular case. In this method, when an inner shell electron transits to a higher-energy level, the hole in the inner shell is filled by an electron from a high level, resulting in emission of a characteristic X-ray with energy between those two energy levels. When the electron in the higher-energy level transits into the lower energy level, only the transition, which corresponds to the difference of the quantum number of the orbital angular momentum, $\Delta l = \pm 1$, due to the selection rule may occur. The characterization capabilities of EDX are mainly due to the fundamental principle that each element of the periodic table has a unique atomic structure allowing X-rays that are characteristic of an element's atomic structure to be uniquely distinguished from each other. Namely, because characteristic X-rays have specific energy corresponds to each element, the element can be identified from the peak energy; and the content of the element in the compound can be analysed from the integrated intensity of the peak. It should be noted that when the excited state of the atom with a hole changes to the ground state, an Auger electron may be emitted instead of the characteristic X-ray emission. In general, the emission probability of characteristic X-rays increases with the increase in atomic number, whereas the emission probability of Auger electrons decreases complementarily. Thus, EDX is more useful for heavy elements, especially when the content of the element is small [229-231]. In this work, a type of EDX instrument, “Firma EDAX Typ Genesis” was used to determine the elemental composition of the specimen.

### 4.2.7. GC/MS instruments

Gas chromatography (GC) is the separation technique that is based on the multiplicative distribution of the compounds to be separated between the two-phase system solid or liquid (stationary phase) and gas (mobile phase). On the contrary to the other chromatographic techniques, the role of the gaseous mobile phase-quasi-ideal inert gases such as helium, nitrogen, is purely mechanical. They serve for the transport of solutes along the column axis. The retention time of solutes is affected only by their vapour pressure, which depends on the temperature and on the intermolecular interaction between the solutes and the stationary phase. The GC method is one of the most important and definitely the most economic of all separation methods. Moreover, as far as chromatographic efficiency and GC system selectivity is concerned, no other separation technique can compete with gas chromatography [232]. In the Mass Spectrometry (MS), molecules exit the chromatographic column and then they are introduced in the ion source of the mass spectrometer and ionized. Depending on the ionization method, molecular ions or fragment ions are formed, which are accelerated and separated from each other according to their mass-to-charge ratios (m/z) by a mass analyzer such as a quadrupole. Generally GC and MS are used together to detect molecules [233].

In this work, a kind of GC/MS instrument, GCMS-QP5050 Schimadzu, as a headspace Turbomatrix 40 Perkin Elmer and as a Column ZB-WAXplus, length 30 m, Thickness 0,2 µm, diameter 0,25 mm were used. As for the preparation of samples for measurement, 1 g of each sample was added into a headspace vial and it was closed without air. The oven was arranged to 100 °C, the transfer line was arranged to 180 °C and the injection needle was arranged to 180 °C. Furthermore, after the sample was heated, the used volume of the samples was 0,04 ml. The measurement parameters for methanol and ethanol are shown in the Table 4.

**Table 4. GC/MS measurement parameters for methanol and ethanol.**

| Heating Rate | Temperature | Hold Time |
|---|---|---|
| ------ | 40 °C | 1 minute |
| 10 °C/min. | 150 °C | 1 minute<br>(Total = 13 minutes) |

### 4.2.8. Fourier transform infrared (FT-IR) spectroscopy

Absorption in the infrared region results in changes in vibrational and rotational status of the molecules. The absorption frequency depends on the vibrational frequency of the molecules,

whereas the absorption intensity depends on how effectively the infrared photon energy can be transferred to the molecule, and this depends on the change in the dipole moment that occurs as a result of molecular vibration. As a consequence, a molecule will absorb infrared light only if the absorption causes a change in the dipole moment. Thus, all compounds except for elemental diatomic gases such as $N_2$, $H_2$ and $O_2$, have infrared spectra and most components present in a flue gas can be analysed by their characteristic infrared absorption. If only one species is to be analysed, a species-specific instrument can be used. In this case analysis is carried out in a narrow wavelength interval, where the species of interest has a characteristic absorption. However, other components present in the sample may also absorb at the analytical wavelength, and for this case the spectrometer should be calibrated for cross sensitivities. For quantification of several components absorbing in the mid-infrared region (400-5000 $cm^{-1}$), either conventional dispersive infrared analysis or Fourier Transform Infrared (FTIR) spectroscopy can be used. Compared to dispersive IR analysis, FT-IR analysis is faster and has a better signal-to-noise ratio [234].

In this research, a kind of FT-IR instrument, “Bruker IFS 66V”, was used (optical part and sample part can be evacuated until 5 mbar) for characterization of unmodified $TiO_2$ nanoparticles, the PMMA-grafted $TiO_2$ nanoparticles; the synthesis of the urea molecules and the urea-modified $TiO_2$ nanoparticles; silane, β-ketoester, β-diketone, carboxylic acid-modified $TiO_2$ nanoparticles. The liquid samples by using KBr-Discs and the solid samples by preparing their pellets with KBr were monitored by recording 150 scans in the wavenumber range 400-4000 $cm^{-1}$.

### 4.2.9. TGA/DSC instrument

Thermal analysis has been defined as “a group of techniques in which a physical property of a substance and/or its reaction products is measured a function of temperature while the substance is subjected to a controlled temperature programme” [235]. Thermal Gravimetric Analysis (TGA) is a simple analytical technique that measures the weight loss (or gain) of a material as a function of temperature. When materials are heated to determined temperature, they can loose weight from a simple process such as drying, or from chemical reactions that liberate gasses. The weights of some materials can increase by reacting with the atmosphere in the testing environment. In this process, a material is put into an alumina cup that is suspended from an analytical balance located outside the furnace chamber. The balance is zeroed, and the sample cup is heated according to a determined thermal cycle. The balance sends the weight signal to the computer for storage, along with the sample temperature and the elapsed time. The TGA curve plots the TGA signal, converted to percent weight change on the Y-axis against the reference material temperature on the X-

axis. Differential scanning calorimetry (DSC) is a technique for measuring the energy necessary to establish a nearly zero temperature difference between a substance and an inert reference material, as the two specimens are subjected to identical temperature regimes in an environment heated or cooled at a controlled rate and also there are two types of DSC systems in common use. They are power-compensation DSC and heat-flux DCS [236].

In this research, the PMMA-grafted and unmodified $TiO_2$ nanoparticles were investigated to determine their thermal behaviour by a kind of TGA/DSC instrument, Netzsch STA 449 C Jupiter and all TG/DSC measurements were performed under air atmosphere between 50-800 °C with heating rates 10 K/min.

## 4.3. Synthesis and characterization of anatase $TiO_2$ nanoparticles

### 4.3.1. Synthesis of $TiO_2$-sol at room temperature

$TiO_2$ nanoparticles were synthesized by hydrothermal method in the present work. Before hydrothermal treatment, how $TiO_2$-sol prepared is shown in the Figure 8.

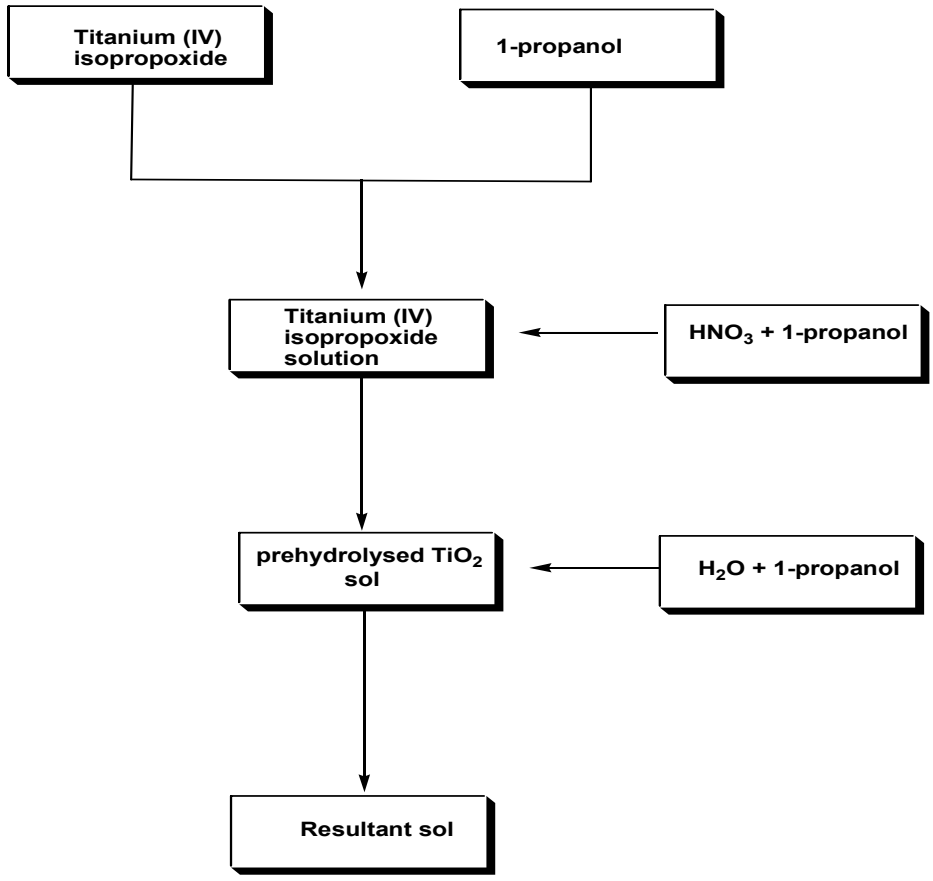


**Figure 8. The schema of the preparation of $TiO_2$-sol before hydrothermal process.**

293,54 g 1-Propanol and 73,84 g Titanium (IV) isopropoxide (0,2598 mole) were added into a 1000 ml flask and then it was stirred using a magnetic stirrer for 10 minutes. After that, a solution mixture of 5,036 g $HNO_3$ (0,05195 mole) in 60 g 1-propanol was added into the Titanium (IV) isopropoxide solution by dropping slowly. After it was stirred for 10 minutes, "prehydrolysed $TiO_2$-sol" was obtained. Then, a solution of 7,588 g water (0, 4216 mol) in 80 g 1-propanol was added into the prehydrolysed $TiO_2$-sol and it was stirred for 20 minutes at room temperature.

### 4.3.2. Synthesis of anatase $TiO_2$ nanoparticles by hydrothermal method

Approximately 160 ml of $TiO_2$-sol synthesized in the section 4.3.1 was added into the Teflon caps (V-sealing) of autoclave instrument and they were closed with their lids. The vessels were inserted into other steel vessels (pressure digestion vessel with bayonet quick closure) and their lids were tightened until 35 Nm rotary forces by means of a type of wrench. After that, these vessels were inserted into preheated heating blocks at 180 °C and they were treated for 85 minutes. Then, these steel vessels were taken out and cooled down to the room temperature. The precipitate, which is $TiO_2$ powder, was separated from the liquid part by decanting. After that, $TiO_2$ powder was put into a round glass flask and dried at 40-45 °C by a rotation evaporator.

### 4.3.3. Elemental analysis of $TiO_2$ nanoparticles

After $TiO_2$ powder was synthesized and dried by a rotation evaporator, the powder was grinded and dried under vacuum at 100 °C for 2 hours. After that, elemental analysis measurements were performed three times and their average C %, H % and N % were calculated.

### 4.3.4. TEM and EDX analysis of $TiO_2$ nanoparticles

0,1 g $TiO_2$ powder and 9,8 g toluene was added into a glass vessel and it was treated in an ultrasonic bath for 2 minutes. The appearance of the mixture was turbid firstly. After 0,1 g of stearic acid was added into the suspension, it became yellow-transparent. The dispersion was filtered by using 0,2 µm-PTFE filter and a little dispersion was dropped on a TEM-Grid (amorphous carbon film on a copper grid) and measured. Also, the elemental compositions of the unmodified-$TiO_2$ nanoparticles, the AMMO-modified $TiO_2$ nanoparticles and the HDTMS-modified $TiO_2$ nanoparticles were also determined by EDX.

## 4.4. Synthesis of $TiO_2$ nanostars

In the following, three ways, which were used to synthesize nanostars, are summarized.

a) One of them is the modification of $TiO_2$ nanoparticles with silanes with different molecular weights by forming Ti-O-Si covalent bonds on the surface, one β-ketoester molecule and three carboxylic acids by forming complex structures on the surface.
b) Another one is the modification of $TiO_2$ nanoparticles with urea molecules with different molecular weights by forming Ti-O-Si covalent bonds on the surface. After the urea molecules are synthesized, $TiO_2$ nanoparticles are modified with them.
d) The other one is the grafting of PMMA molecules onto $TiO_2$ nanoparticle surface via *"the combination of both grafting methods".*

### 4.4.1. Modification of $TiO_2$ nanoparticles with silanes, carboxylic acids and β-ketoester

For the purpose of synthesizing of $TiO_2$ nanostars, $TiO_2$ nanoparticles were modified with four alkylmethoxysilanes with different molecular weights, with an aminosilane, with a β-ketoester and with three carboxylic acids. Two of the carboxylic acids have double bond on their structures but one of them has not double bond. They are summarized in the Table 5. Also, in these modification reactions, it is expected that the silanes will react with –OH groups on the $TiO_2$ nanoparticles and the β-ketoester and the carboxylic acids will react $–OC_3H_7$ groups on the $TiO_2$ nanoparticles. Furthermore, because of sensitivity of $–OC_3H_7$ groups on the $TiO_2$ nanoparticles against to water; water-free toluene was used throughout this work.

**Table 5. The silanes, carboxylic acids and β-ketoester used in the modifications.**

| | |
|---|---|
| **Silanes** | Hexyltrimethoxysilane (HTMS) |
| | Decyltrimethoxysilane (DTMS) |
| | Dodecyltrimethoxysilane (DDTMS) |
| | Hexadecyltrimethoxysilane (HDTMS) |
| | 3-Aminopropyltrimethoxysilane (AMMO) |
| **Carboxylic Acids** | 10-Undecylenic acid |
| | Stearic acid |
| | Oleic acid |
| **β-ketoester** | Allyl acetoacetate (AAA) |

#### 4.4.1.1. Modification of $TiO_2$ nanoparticles with HTMS

2 g $TiO_2$ powder and 40 g toluene were added into a glass flask and stirred at room temperature using a magnetic stirrer. After 2 minutes, the suspension was treated in an ultrasonic bath for 2 minutes. 0,537 g (0,0025 mole) HTMS was added into the suspension and it was stirred at room temperature. After a yellow-transparent dispersion was obtained, it was continued to be stirred for further 2 hours. Then, 1 g of the dispersion was added into a headspace vial to detect the liberated molecules by GC/MS (see section 4.2.6, page 43). The solvents in the dispersion were evaporated to dryness at 40 °C by using a rotation evaporator. After that, the HTMS-modified $TiO_2$ powder was washed to remove unreacted HTMS molecules with 300 g methanol (three times, 100 g x 3). The powder was dried at 50 °C under at 10 mbar for 1 hour. After the powder was grinded, it was dried under vacuum at 100 °C for 2 hours. Afterwards, a pellet from the HTMS-modified $TiO_2$ powder and KBr was prepared and then, FT-IR measurements were performed by recording 150 scans in the wavenumber range 400-4000 $cm^{-1}$ by FT-IR.

#### 4.4.1.2. Modification of $TiO_2$ nanoparticles with DTMS

2 g $TiO_2$ powder and 40 g toluene were added into a glass flask and stirred at room temperature using a magnetic stirrer. After 2 minutes, the suspension was treated in an ultrasonic bath for 2 minutes. 0,663 g (0,0025 mole) DTMS was added into the suspension and it was stirred at room temperature. After a yellow-transparent dispersion was obtained, it was continued to be stirred for further 2 hours. Then, 1 g of the dispersion was added into a headspace vial to detect the liberated molecules by GC/MS. The solvents in the dispersion were evaporated to dryness at 40 °C by using a rotation evaporator. After that, the DTMS-modified $TiO_2$ powder was washed to remove unreacted DTMS molecules with 300 g methanol (three times, 100 g x 3). The powder was dried at 50 °C at 10 mbar for 1 hour. After the powder was grinded, it was dried 100 °C at 10 mbar for 2 hours. Afterwards, a pellet from the DTMS-modified $TiO_2$ powder and KBr was prepared and then, FT-IR measurements were performed by recording 150 scans in the wavenumber range 400-4000 $cm^{-1}$ by FT-IR.

#### 4.4.1.3. Modification of $TiO_2$ nanoparticles with DDTMS

2 g $TiO_2$ powder and 40 g toluene were added into a glass flask and stirred at room temperature using a magnetic stirrer. After 2 minutes, the suspension was treated in an ultrasonic bath for 2 minutes. 0,773 g (0,0025 mole) DDTMS was added into the suspension and it was stirred at room temperature. After a yellow-transparent dispersion was obtained, it was continued to be stirred for further 2 hours. Then, 1 g of the dispersion was added into a headspace vial to detect the liberated molecules by GC/MS. The solvents in the dispersion

were evaporated to dryness at 40 °C by using a rotation evaporator. After that, the DDTMS-modified $TiO_2$ powder was washed to remove unreacted DDTMS molecules with 300 g methanol (three times, 100 g x 3). The powder was dried at 50 °C at 10 mbar for 1 hour. After the powder was grinded, it was dried at 100 °C at 10 mbar for 2 hours. Afterwards, a pellet from the DDTMS-modified $TiO_2$ powder and KBr was prepared and then, FT-IR measurements were performed by recording 150 scans in the wavenumber range 400-4000 $cm^{-1}$ by FT-IR.

#### 4.4.1.4. Modification of $TiO_2$ nanoparticles with HDTMS

2 g $TiO_2$ powder and 40 g toluene were added into a glass flask and stirred at room temperature using a magnetic stirrer. After 2 minutes, the suspension was treated in an ultrasonic bath for 2 minutes. 0,973 g (0, 0025 mole) HDTMS was added into the suspension and it was stirred at room temperature. After a yellow-transparent dispersion was obtained, it was continued to be stirred for further 2 hours. 1 g of the dispersion was added into a headspace vial to detect the liberated molecules by GC/MS. The solvents in the dispersion were evaporated to dryness at 40 °C by using a rotation evaporator. After that, the HDTMS-modified $TiO_2$ powder was washed to remove unreacted HDTMS molecules with 300 g methanol (three times, 100 g x 3). The powder was dried at 50 °C at 10 mbar for 1 hour. After the powder was grinded, it was dried at 100 °C at 10 mbar for 2 hours. Afterwards, a pellet from the HDTMS-modified $TiO_2$ powder and KBr was prepared and FT-IR measurements were performed by recording 150 scans in the wavenumber range 400-4000 $cm^{-1}$ by FT-IR. Also, after modification of $TiO_2$ nanoparticles with HDTMS molecules, the elemental composition of the HDTMS-modified $TiO_2$ nanoparticles was determined by EDX and also, the appearance of the HDTMS-modified $TiO_2$ nanoparticles was investigated by TEM.

#### 4.4.1.5. Modification of $TiO_2$ nanoparticles with AMMO

2 g $TiO_2$ powder and 40 g toluene were added into a glass flask and stirred at room temperature using a magnetic stirrer. After 2 minutes, the suspension was treated in an ultrasonic bath for 2 minutes. 0,467 g (0,0025 mole) AMMO was added into the suspension and it was stirred at room temperature. After a yellow-transparent dispersion was obtained, it was continued to be stirred for further 2 hours. Then, 1 g of the dispersion was added into a headspace vial to detect the liberated molecules by GC/MS. The solvents in the dispersion were evaporated to dryness at 40 °C by using a rotation evaporator. After that, AMMO-modified $TiO_2$ powder was washed to remove unreacted AMMO molecules with 300 g methanol (three times, 100 g x 3). The powder was dried at 50 °C at 10 mbar for 1 hour.

After the powder was grinded, it was dried at 100 °C at 10 mbar for 2 hours. Afterwards, a pellet from the AMMO-modified $TiO_2$ powder and KBr was prepared and FT-IR measurements were performed by recording 150 scans in the wavenumber range 400-4000 $cm^{-1}$ by FT-IR. Also, after modification of $TiO_2$ nanoparticles with AMMO molecules, the elemental composition of the AMMO-modified $TiO_2$ nanoparticles was determined by EDX and also, the appearance of the AMMO-modified $TiO_2$ nanoparticles was investigated by TEM.

#### 4.4.1.6. Modification of $TiO_2$ nanoparticles with 10-undecylenic acid

2 g $TiO_2$ powder and 40 g toluene were added into a glass flask and stirred at room temperature using a magnetic stirrer. After 2 minutes, the suspension was treated in an ultrasonic bath for 2 minutes. 0,867 g (0, 0047 mole) 10-undecylenic acid was added into the suspension and it was stirred at room temperature. After a yellow-transparent dispersion was obtained, it was continued to be stirred for further 2 hours. The solvents in the dispersion were evaporated to dryness at 40 °C by using a rotation evaporator. After that, the 10-undecylenic acid-modified-$TiO_2$ powder was washed to remove unreacted 10-undecylenic acid molecules with 300 g methanol (three times, 100 g x 3). The powder was dried at 50 °C at 10 mbar for 1 hour. After the powder was grinded, it was dried at 100 °C at 10 mbar for 2 hours. Afterwards, a pellet from the 10-undecylenic acid-modified $TiO_2$ powder and KBr was prepared and FT-IR measurements were performed by recording 150 scans in the wavenumber range 400-4000 $cm^{-1}$ by FT-IR.

#### 4.4.1.7. Modification of $TiO_2$ nanoparticles with stearic acid

2 g $TiO_2$ powder and 40 g toluene were added into a glass flask and stirred at room temperature using a magnetic stirrer. After 2 minutes, the suspension was treated in an ultrasonic bath for 2 minutes. 1,37 g (0,0047 mole) stearic acid was added into the suspension and it was stirred at room temperature. After a yellow-transparent dispersion was obtained, it was continued to be stirred for further 2 hours. Then, the solvents in the dispersion were evaporated to dryness at 40 °C by using a rotation evaporator. After that, the stearic acid-modified $TiO_2$ powder was washed to remove unreacted stearic acid molecules with 300 g methanol (three times, 100 g x 3). The powder was dried at 50 °C at 10 mbar for 1 hour. After the powder was grinded, it was dried at 100 °C at 10 mbar for 2 hours. Afterwards, a pellet from the stearic acid-modified $TiO_2$ powder and KBr was prepared and FT-IR measurements were performed by recording 150 scans in the wavenumber range 400-4000 $cm^{-1}$ by FT-IR.

#### 4.4.1.8. Modification of $TiO_2$ nanoparticles with oleic acid

2 g $TiO_2$ powder and 40 g toluene were added into a glass flask and stirred at room temperature using a magnetic stirrer. After 2 minutes, the suspension was treated in an ultrasonic bath for 2 minutes. 1,42 g (0,0047 mole) oleic acid was added into the suspension and it was stirred at room temperature. After a yellow-transparent was obtained, it was continued to be stirred for further 2 hours. The solvents in the dispersion were evaporated to dryness at 40 °C by using a rotation evaporator. After that, the oleic acid-modified $TiO_2$ powder was washed to remove unreacted oleic acid molecules with 300 g methanol (three times, 100 g x 3). The powder was dried at 50 °C at 10 mbar for 1 hour. After the powder was grinded, it was dried at 100 °C at 10 mbar for 2 hours. Afterwards, a pellet from the oleic acid-modified $TiO_2$ powder and KBr was prepared and FT-IR measurements were performed by recording 150 scans in the wavenumber range 400-4000 $cm^{-1}$ by FT-IR.

#### 4.4.1.9. Modification of $TiO_2$ nanoparticles with AAA

2 g $TiO_2$ powder and 40 g toluene were added into a glass flask and stirred at room temperature using a magnetic stirrer. After 2 minutes, the suspension was treated in an ultrasonic bath for 2 minutes. 0,672 g (0, 0047 mole) AAA was added into the suspension and it was stirred at room temperature for 2 hours. After 2 hours, the mixture was not still become transparent. The solvents in the mixture were evaporated to dryness at 40 °C by using a rotation evaporator. After that, the AAA-modified-$TiO_2$ powder was washed to remove unreacted AAA molecules with 300 g acetone (three times, 100 g x 3). The powder was dried at 50 °C at 10 mbar for 1 hour. After the powder was grinded, it was dried at 100 °C at 10 mbar for 2 hours. Afterwards, a pellet from the AAA-modified $TiO_2$ powder and KBr was prepared and FT-IR measurements were performed by recording 150 scans in the wavenumber range 400-4000 $cm^{-1}$ by FT-IR.

### 4.5. Synthesises of urea molecules and modifications of $TiO_2$ nanoparticles with these molecules

As explained in the section 4.4. (page 48), $TiO_2$ nanoparticles were also modified with the urea molecules with different molecular weights. For this reason, a coupling reaction between an isocyanate compound and 10 amine compounds was performed under suitable conditions to synthesize the urea compounds with different molecular weights. This typical coupling reaction has been already known in the literature [237-245]. 3-isocyanatopropyl triethoxysilane (3-IPTES) and also 10 amine molecules with different molecular weights were used in the reactions. The amine molecules containing two amine groups in their molecules:

ethylenediamine, 1,6-diaminohexane, 1,8-diaminooctane, 1,12-diaminododecane, DMS-A15, DMS-A21 and the amine molecules containing one amine group in their molecules: pentylamine, octylamine, 1-dodecylamine, octadecylamine. Also, the amount of the amines used in the reactions was a little more than their necessary amount to guarantee the formation of the urea molecules.

### 4.5.1. Reaction between ethylenediamine and 3-IPTES

13,02 g (0,05 mole) 3-IPTES and 16,04 g toluene were added into a 100 ml round glass flask and then 3,04 g (0,0503 mole) ethylenediamine was added into this solution. It was refluxed at 50 °C under $N_2$ atmosphere for 1 hour. After that, the formation of urea molecule was monitored by FT-IR using KBr discs by recording 150 scans in the wavenumber range 400-4000 $cm^{-1}$. The product was marked as “Ethylenurea” in the present work.

### 4.5.2. Reaction between 1,6-diaminohexane and 3-IPTES

7,81 g (0,03 mole) 3-IPTES and 26,38 g toluene were added into a 100 ml round glass flask and then 3,51 g (0,0302 mole) 1,6-diaminohexane was added into the solution. They were refluxed at 50 °C under $N_2$ atmosphere for 1 hour. After that, the formation of urea molecule was monitored by FT-IR using KBr discs by recording 150 scans in the wavenumber range 400-4000 $cm^{-1}$. The product was marked as “16Hexylurea” in the present work.

### 4.5.3. Reaction between 1,8-diaminooctane and 3-IPTES

7,81 g (0, 03 mole) 3-IPTES and 24,50 g toluene were added into a 100 ml round glass flask and then 4,44 g (0,0302 mole) 1,8-Diaminooctane was added into the solution. It was refluxed at 50 °C under $N_2$ atmosphere for 1 hour. After that, the formation of the urea molecule was monitored by FT-IR using KBr discs by recording 150 scans in the wavenumber range 400-4000 $cm^{-1}$ by FT-IR. The product was marked as “18Octylurea” in the present work.

### 4.5.4. Reaction between 1,12-diaminododecane and 3-IPTES

7,81 g (0,03 mole) 3-IPTES and 27,97 g toluene were added into a 100 ml round glass flask and then 6,18 g (0,0302 mole) 1,12-diaminododecane was added into the solution. It was refluxed at 50 °C under $N_2$ atmosphere for 1 hour. After that, the formation of urea molecule was monitored by FT-IR using KBr discs by recording 150 scans in the wavenumber range 400-4000 $cm^{-1}$. The product was marked as “112Dodecylurea” in the present work.

### 4.5.5. Reaction between DMS-A15 and 3-IPTES

1,56 g (0,006 mole) 3-IPTES and 20,76 g toluene were added into a 100 ml round glass flask and then 19,2 g (0,0064 mole) DMS-A15 was added into the solution. It was refluxed at 50 °C under $N_2$ atmosphere for 1 hour. After that, the formation of urea molecule was monitored by FT-IR using KBr discs by recording 150 scans in the wavenumber range 400-4000 $cm^{-1}$. The product was marked as “DMSA15urea” in the present work.

### 4.5.6. Reaction between DMS-A21 and 3-IPTES

1,04 g (0,004 mole) 3-IPTES and 22,04 g toluene were added into a 100 ml round glass flask and then 21 g (0,0042 mole) DMS-A21 was added into the solution. It was refluxed at 50 °C under $N_2$ atmosphere for 1 hour. After that, the formation of urea molecule was monitored by FT-IR using KBr discs by recording 150 scans in the wavenumber range 400-4000 $cm^{-1}$. The product was marked as “DMSA21urea” in the present work.

### 4.5.7. Reaction between pentylamine and 3-IPTES

13,02 g (0,05 mole) 3-IPTES and 26,04 g toluene were added into a 100 ml round glass flask and 4,44 g (0,0501 mole) pentylamine was added into the solution. It was refluxed at 50 °C under $N_2$ atmosphere for 1 hour. After that, the formation of urea molecule was monitored by FT-IR using KBr discs by recording 150 scans in the wavenumber range 400-4000 $cm^{-1}$. The product was marked as “Pentylurea” in the present work.

### 4.5.8. Reaction between octylamine and 3-IPTES

7,81 g (0,03 mole) 3-IPTES and 11,76 g toluene were added into a 100 ml round glass flask and then 3,95 g (0,0302 mole) octylamine was added into the solution. It was refluxed under $N_2$ atmosphere at 50 °C for 1 hour. After that, the formation of urea molecule was monitored by FT-IR using KBr discs by recording 150 scans in the wavenumber range 400-4000 $cm^{-1}$. The product was marked as “Octylurea” in the present work.

### 4.5.9. Reaction between 1-dodecylamine and 3-IPTES

7,81 g (0,03 mole) 3-IPTES and 23,53 g toluene were added into a 100 ml round glass flask. It was refluxed at 50 °C under $N_2$ atmosphere for 1 hour. After 1 hour, the formation of the urea molecules was monitored by FT-IR using KBr discs by recording 150 scans in the wavenumber range 400-4000 $cm^{-1}$. The product was marked as “1Dodecylurea” in the present work.

### 4.5.10. Reaction between octadecylamine and 3-IPTES

7,81 g (0,03 mole) 3-IPTES and 26,03 g toluene were added into a 100 ml round glass flask and 8,22 g (0,0302 mole) octadecylamine was added into the solution. It was refluxed at 50 °C under $N_2$ atmosphere for 1 hour. After that, the formation of urea molecule was monitored by FT-IR using KBr discs by recording 150 scans in the wavenumber range 400-4000 $cm^{-1}$. The product was marked as “Octadecylurea” in the present work.

## 4.6. Modification of $TiO_2$ nanoparticles with the urea molecules

After the urea molecules were synthesized, $TiO_2$ nanoparticles were modified with them. It is expected that –OH groups on $TiO_2$ nanoparticles will react with ethoxy silane functional groups in the urea molecules and thus, the formation of Ti-O-Si covalent bonds will be observed.

### 4.6.1. Modification of $TiO_2$ nanoparticles with Ethylenurea

3 g $TiO_2$ powder and 94,57 g toluene were added into a 250 ml round glass flask and the suspension was treated in an ultrasonic bath for 2 minutes. The appearance of the mixture was turbid firstly. After that, 2,43 g Ethylenurea mixture (0,00379 mole Ethylenurea) was added into the flask and it was stirred using a magnetic stirrer for 5 minutes at room temperature. The appearance of the suspension changed to semi-turbid; namely its appearance became less turbid than before. Afterwards, the suspension was refluxed at 60 °C under $N_2$ atmosphere for 1 hour. After the refluxing was completed, the appearance was still semi-turbid. 1 g of the suspension was added into a headspace vial to detect the liberated molecules by GC/MS (see section 4.2.6., page 43). The solvents in the suspension were evaporated to dryness at 40 °C by using a rotation evaporator. The Ethylenurea-modified $TiO_2$ powder was washed to remove unreacted Ethylenurea molecules with 300 g methanol (three times, 100 g x 3). The powder was dried at 50 °C at 10 mbar for 1 hour. After the powder was grinded, it was dried at 100 °C at 10 mbar for 2 hours. Afterwards, a pellet from the Ethylenurea-modified $TiO_2$ powder and KBr was prepared and FT-IR measurements were performed by recording 150 scans in the wavenumber range 400-4000 $cm^{-1}$ by FT-IR.

### 4.6.2. Modification of $TiO_2$ nanoparticles with 16Hexylurea

3 g $TiO_2$ powder and 93,0 g toluene were added into a 250 ml round glass flask and it was treated in an ultrasonic bath for 2 minutes. The appearance of the mixture was turbid firstly. After that, 4,76 g 16Hexylurea mixture (0,00379 mole 16Hexylurea) was added into the flask

and it was stirred using a magnetic stirrer at room temperature for 5 minutes. The appearance of the suspension changed to semi-turbid. Then, the suspension was refluxed at 60 °C under $N_2$ atmosphere for 1 hour. After the refluxing was completed, the appearance of the mixture didn't become transparent. 1 g of the suspension was added into a headspace vial to detect the liberated molecules by GC/MS. The solvents in the mixture were evaporated to dryness at 40 °C by using a rotation evaporator. 16Hexylurea-modified $TiO_2$ powder was washed to remove unreacted 16Hexylurea molecules with 300 g methanol (three times, 100 g x 3). The powder was dried at 50 °C at 10 mbar for 1 hour. After the powder was grinded, it was dried at 100 °C at 10 mbar for 2 hours. Afterwards, a pellet from the 16Hexylurea-modified $TiO_2$ powder and KBr was prepared and FT-IR measurements were performed by recording 150 scans in the wavenumber range 400-4000 $cm^{-1}$ by FT-IR.

### 4.6.3. Modification of $TiO_2$ nanoparticles with 18Octylurea

3 g $TiO_2$ powder and 100,0 g toluene were added into a 250 ml round glass flask and it was treated in an ultrasonic bath for 2 minutes. The appearance of the mixture was turbid firstly. After that, 4,64 g 18Octylurea mixture (0,00379 mole 18Octylurea) was added into the flask and it was stirred using a magnetic stirrer at room temperature for 5 minutes. The appearance of suspension didn't change. Then, the suspension was refluxed at 60 °C under $N_2$ atmosphere for 1 hour. After the refluxing was completed, the appearance of the mixture didn't become transparent. 1 g of the suspension was added into a headspace vial to detect the liberated molecules by GC/MS. The solvents in the suspension were evaporated to dryness at 40 °C by using a rotation evaporator. The 18Octylurea-modified $TiO_2$ powder was washed to remove unreacted 18Ocytlurea molecules with 300 g methanol (three times, 100 g x 3). The powder was dried at 50 °C at 10 mbar for 1 hour. After the powder was grinded, it was dried at 100 °C at 10 mbar for 2 hours. Afterwards, a pellet from the 18Octylurea-modified $TiO_2$ powder and KBr was prepared and FT-IR measurements were performed by recording 150 scans in the wavenumber range 400-4000 $cm^{-1}$ by FT-IR.

### 4.6.4. Modification of $TiO_2$ nanoparticles with 112Dodecylurea

3 g $TiO_2$ powder and 92,60 g toluene were added into a 250 ml round glass flask and it was treated in an ultrasonic bath for 2 minutes. The appearance of the mixture was turbid firstly. After that, 5,30 g 112Dodecylurea mixture (0,00379 mole 112Dodecylurea) was added into the flask and it was stirred by a magnetic stirrer at room temperature for 5 minutes. The appearance of the suspension didn't change. Then, the suspension was refluxed at 60 °C under $N_2$ atmosphere for 1 hour. After the refluxing was completed, the appearance of the suspension didn't become transparent. 1 g of the suspension was added into a headspace

vial to detect the liberated molecules by GC/MS. The solvents in the suspension were evaporated to dryness at 40 °C by using a rotation evaporator. 112Dodecylurea-modified $TiO_2$ powder was washed to remove unreacted 112Dodecylurea molecules with 300 g 1-propanol (three times, 100 g x 3). The powder was dried at 50 °C at 10 mbar for 1 hour. After the powder was grinded, it was dried at 100 °C at 10 mbar for 2 hours. Afterwards, a pellet from the 112Dodecylurea-modified $TiO_2$ powder and KBr was prepared and FT-IR measurements were performed by recording 150 scans in the wavenumber range 400-4000 $cm^{-1}$ by FT-IR.

### 4.6.5. Modification of $TiO_2$ nanoparticles with DMSA15urea

2 g $TiO_2$ powder and 47,19 g toluene were added into a 250 ml round glass flask and it was treated in an ultrasonic bath for 2 minutes. The appearance of the mixture was turbid firstly. After that, 17,48 g DMSA15urea mixture (0,0025 mole DMSA15urea) was added into the flask and it was stirred using a magnetic stirrer at room temperature for 5 minutes. The appearance of the suspension changed to semi-turbid. Then, the suspension was refluxed at 60 °C under $N_2$ atmosphere for 1 hour. After the refluxing was completed, the appearance of the mixture became transparent. 1 g of the dispersion was added into a headspace vial to detect the liberated molecules by GC/MS. The solvents in the dispersion were evaporated to dryness at 40 °C by using a rotation evaporator. DMSA15urea-modified $TiO_2$ powder was washed to remove unreacted DMSA15urea molecules with 300 g ethanol (three times, 100 g x 3). The powder was dried at 50 °C at 10 mbar for 1 hour. After the powder was grinded, it was dried at 100 °C at 10 mbar for 2 hours. Afterwards, a pellet from the DMSA15urea-modified $TiO_2$ powder and KBr was prepared and FT-IR measurements were performed by recording 150 scans in the wavenumber range 400-4000 $cm^{-1}$ by FT-IR.

### 4.6.6. Modification of $TiO_2$ nanoparticles with DMSA21urea

1,5 g $TiO_2$ powder and 27,62 g toluene were added into a 250 ml round glass flask and it was treated in an ultrasonic bath for 2 minutes. The appearance of the mixture was turbid firstly. After that, 20,88 g DMSA21urea mixture (0,0019 mole DMSA21urea) was added into the flask and it was stirred using a magnetic stirrer at room temperature for 5 minutes. The appearance of the suspension changed to semi-turbid. Then, the suspension was refluxed at 60 °C under $N_2$ atmosphere for 1 hour. After the refluxing was completed, the appearance of the mixture became transparent. 1 g of the dispersion was added into a headspace vial to detect the liberated molecules by GC/MS. The solvents in the dispersion were evaporated to dryness at 40 °C by using a rotation evaporator. The DMSA21urea-modified $TiO_2$ powder was washed to remove unreacted DMSA21urea molecules with 300 g 2-isopropoxyethanol

(2-IPE) (three times, 100 g x 3). The powder was dried at 50 °C at 10 mbar for 1 hour. After the powder was grinded, it was dried at 100 °C at 10 mbar for 2 hours. Afterwards, a pellet from the DMSA21urea-modified $TiO_2$ powder and KBr was prepared and FT-IR measurements were performed by recording 150 scans in the wavenumber range 400-4000 $cm^{-1}$ by FT-IR.

### 4.6.7. Modification of $TiO_2$ nanoparticles with Pentylurea

3 g $TiO_2$ powder and 93,70 g toluene were added into a 250 ml round glass flask and it was treated in an ultrasonic bath for 2 minutes. The appearance of the mixture was turbid firstly. After that, 3,30 g Pentylurea mixture (0,00379 mole Pentylurea) was added into the flask and it was stirred using a magnetic stirrer for 5 minutes at room temperature. The appearance of the suspension didn't change, namely it was still turbid. The suspension was refluxed at 60 °C under $N_2$ atmosphere for 1 hour. After the refluxing was completed, the appearance of the mixture was still turbid. 1 g of the suspension was added into a headspace vial to detect the liberated molecules by GC/MS. The solvents in the suspension were evaporated to dryness at 40 °C by using a rotation evaporator. The Pentylurea-modified $TiO_2$ powder was washed to remove unreacted Pentylurea molecules with 300 g methanol (three times, 100 g x 3). The powder was dried at 50 °C at 10 mbar for 1 hour. After the powder was grinded, it was dried at 50 °C at 10 mbar for 3 hours. Afterwards, a pellet from the Penytlurea-modified $TiO_2$ powder and KBr was prepared and FT-IR measurements were performed by recording 150 scans in the wavenumber range 400-4000 $cm^{-1}$ by FT-IR.

### 4.6.8. Modification of $TiO_2$ nanoparticles with Octylurea

3 g $TiO_2$ powder and 94,03 g toluene were added into a 250 ml round glass flask and it was treated in an ultrasonic bath for 2 minutes. The appearance of the mixture was turbid firstly. After that, 2,97 g from Octylurea mixture (0,00379 mole Octylurea) was added into the flask and it was stirred using a magnetic stirrer at room temperature for 5 minutes. The appearance of suspension changed to semi-turbid. The suspension was refluxed at 60 °C under $N_2$ atmosphere for 1 hour. After the refluxing was completed, the appearance of the mixture became yellow-transparent. 1 g of the dispersion was added into a headspace vial to detect the liberated molecules by GC/MS. The solvents in the dispersion were evaporated to dryness at 40 °C by using a rotation evaporator. The Octylurea-modified $TiO_2$ powder was washed to remove unreacted Octylurea molecules with 300 g methanol (three times, 100 g x 3). The powder was dried at 50 °C at 10 mbar for 1 hour. After the powder was grinded, it was dried at 100 °C at 10 mbar for 2 hours. Afterwards, a pellet from the Octylurea-modified

$TiO_2$ powder and KBr was prepared and FT-IR measurements were performed by recording 150 scans in the wavenumber range 400-4000 $cm^{-1}$ by FT-IR.

### 4.6.9. Modification of $TiO_2$ nanoparticles with 1Dodecylurea

3 g $TiO_2$ powder and 92,32 g toluene were added into a 250 ml round glass flask and it was treated in an ultrasonic bath for 2 minutes. The appearance of the mixture was turbid firstly. After that, 4,68 g 1Dodecylurea mixture (0,00379 mole 1Dodecylurea) was added into the flask and it was stirred using a magnetic stirrer at room temperature for 5 minutes. The appearance of this suspension changed to semi-turbid. Then, the suspension was refluxed at 60 °C under $N_2$ atmosphere for 1 hour. After the refluxing was completed, the appearance of the mixture became yellow-transparent. 1 g of the dispersion was added into a headspace vial to detect the liberated molecules by GC/MS. The solvents in the dispersion were evaporated to dryness at 40 °C by using a rotation evaporator. The 1Dodecylurea-modified $TiO_2$ powder was washed to remove unreacted 1Dodecylurea molecules with 300 g methanol (three times, 100 g x 3). The powder was dried at 50 °C at 10 mbar for 1 hour. After the powder was grinded, it was dried at 100 °C at 10 mbar for 2 hours. Afterwards, a pellet from the 1Dodecylurea-modified $TiO_2$ powder and KBr was prepared and FT-IR measurements were performed by recording 150 scans in the wavenumber range 400-4000 $cm^{-1}$ by FT-IR.

### 4.6.10. Modification of $TiO_2$ nanoparticles with Octadecylurea

3 g $TiO_2$ powder and 91,69 g toluene were added into a 250 ml round glass flask and it was treated in an ultrasonic bath for 2 minutes. The appearance of the mixture was turbid firstly. After that, 5,31 g Octadecylurea mixture (0,00379 mole Octadecylurea) was added into the flask and it was stirred using a magnetic stirrer at room temperature for 5 minutes. The appearance of the suspension changed to semi-turbid. The suspension was refluxed at 60 °C under $N_2$ atmosphere for 1 hour. After the refluxing was completed, the appearance of the mixture became yellow-transparent. 1 g of the dispersion was added into a headspace vial to detect the liberated molecules by GC/MS. The solvents in the dispersion were evaporated to dryness at 40 °C by using a rotation evaporator. The Octadecylurea-modified $TiO_2$ powder was washed to remove unreacted Octadecylurea molecules with 300 g 2-propanol (three times, 100 g x 3). The powder was dried at 50 °C at 10 mbar for 1 hour. After the powder was grinded, it was dried at 100 °C at 10 mbar for 2 hours. Afterwards, a pellet from the Octadecylurea-modified $TiO_2$ powder and KBr was prepared and FT-IR measurements were performed by recording 150 scans in the wavenumber range 400-4000 $cm^{-1}$ by FT-IR.

## 4.7. PMMA grafting onto $TiO_2$ nanoparticles via the combination of both grafting methods

The other planned experiments to synthesize nanostars were the grafting of PMMA molecules onto $TiO_2$ nanoparticle by means of *"the combination of both grafting methods".* For this reason, firstly $TiO_2$ nanoparticles were modified with different amounts of 2AAEM to $–OC_3H_7$ groups on $TiO_2$ surface to observe the effect of the modification amount of 2AAEM onto the grafting amount, namely to 30 %; 50 % and 80 % of $–OC_3H_7$ groups on the surface. Then, double bonds containing 2AAEM molecules on $TiO_2$ nanoparticles were dispersed into the different amounts of MMA to investigate the effect of the concentration of MMA on the grafting (20 % and 40 % MMA by weight with respect to the total weight). Furthermore, the molar ratio of 2AAEM:MMA was changed from 1:100 to 1:1000. It is expected that the percentage of PMMA grafting onto $TiO_2$ nanoparticles will increase with the increase of the molar ratio of 2AAEM:MMA from 1:100 to 1:1000 and will increase with the increase of MMA concentration from 20 % to 40 % and will increase directly proportional to the amount of $–OC_3H_7$ groups with 2AAEM, namely with 30 %, 50 % and 80 % of $–OC_3H_7$ groups on $TiO_2$ surface. Also, the appearance of the PMMA-grafted $TiO_2$ nanoparticles was investigated by TEM for a sample.

### 4.7.1. Purification of MMA

MMA was washed twice with aqueous 5 % NaOH (MMA contains 0,004 % hydroquinone) and then, it was washed twice with water and distilled with $CaH_2$ under $N_2$ atmosphere at reduced pressure. After that, the distillate was stored at low temperature [246]. In this work, MMA was stored at -20 °C.

### 4.7.2. The modification of 30 % of $–OC_3H_7$ groups on $TiO_2$ nanoparticles with 2AAEM

10 g $TiO_2$ and 88,42 g toluene were added into a flask and the suspension was treated in an ultrasonic bath for 2 minutes. Then, 1,58 g 2AAEM (0,007 mole) was added into the suspension. After it was stirred using a magnetic stirrer for 3 hours, its appearance became yellow-transparent. This dispersion was marked as "2AAEM-30".

#### 4.7.2.1. PMMA grafting onto $TiO_2$ surface with the modification of 30 % of $–OC_3H_7$ groups with 2AAEM, with a molar ratio of 2AAEM:MMA = 1:100 and 20 % MMA by weight with respect to the total weight

15,05 g 2AAEM-30 dispersion and 26,78 g toluene were added into a 250 ml round glass flask. Then, 10,55 g (0,1054 mole) MMA and 0,365 g initiator Trigonox EHPS (1 % mole of MMA used) were added into the flask. This mixture was yellow-transparent in the beginning. After it was refluxed at 65 °C under $N_2$ atmosphere for 2 hours, it was precipitated. After the solvents in the mixture were evaporated at 50 °C by using a rotation evaporator, the obtained powder was washed with 600 g toluene first (three times, 200 g x 3) and afterwards with 200 g tetrahydrofurane (twice, 100 g x 2). The obtained powder was then dried at 50 °C at 10 mbar for 3 hours. After grinding, it was dried at 100 °C at 10 mbar for 2 hours and characterized by FT-IR and TGA/DSC. The synthesized powder was marked as "$TiO_2$-2AAEM-30-1:100-20".

#### 4.7.2.2. PMMA grafting onto $TiO_2$ surface with the modification of 30 % of $–OC_3H_7$ groups with 2AAEM, with a molar ratio of 2AAEM:MMA= 1:1000 and 20 % MMA by weight with respect to the total weight

1,505 g 2AAEM-30 dispersion and 40,33 g toluene were added into a 250 ml round glass flask. Then, 10,55 g (0,1054 mole) MMA and 0,365 g initiator Trigonox EHPS (1 % mole of MMA) were also added into the flask. This mixture was yellow-transparent in the beginning. After it was refluxed at 65 °C under $N_2$ for 2 hours, it was precipitated. After the solvents in the mixture were evaporated at 50 °C by using a rotation evaporator, the obtained powder was washed with 600 g toluene first (three times, 200 g x 3) and afterwards with 200 g tetrahydrofurane (twice, 100 g x 2). The obtained powder was then dried at 50 °C at 10 mbar for 3 hours. After grinding, it was dried at 100 °C at 10 mbar for 2 hours and characterized by TGA/DSC. The synthesized powder was marked as "$TiO_2$-2AAEM-30-1:1000-20".

#### 4.7.2.3. PMMA grafting onto $TiO_2$ surface with the modification of 30 % of $–OC_3H_7$ groups with 2AAEM, with a molar ratio of 2AAEM:MMA= 1:100 and 40 % MMA by weight with respect to the total weight

15,05 g of 2AAEM-30 dispersion and 0,41 g toluene were added into a 250 ml round glass flask. Then, 10,55 g (0,1054 mole) MMA and 0,365 g initiator Trigonox EHPS (1% mole of MMA) were also added into the flask. This mixture was yellow-transparent in the beginning. It was refluxed at 65 °C under $N_2$ for 2 hours. After refluxing, it was precipitated. After the solvents in the mixture were evaporated at 50 °C by using a rotation evaporator, the obtained

powder was washed with 600 g toluene first (three times, 200 g x 3) and afterwards with 200 g tetrahydrofurane (twice, 100 g x 2). The obtained powder was dried at 50 °C at 10 mbar for 3 hours. After grinding, it was dried at 100 °C at 10 mbar for 2 hours and characterized by FT-IR and TGA/DSC. The synthesized powder was marked as "$TiO_2$-2AAEM-30-1:100-40". Also, for this experiment, the monomer conversion was determined by FT-IR by calculating the peak areas of double bonds at the same monomer concentration after and before polymerization.

#### 4.7.2.4. PMMA grafting onto $TiO_2$ surface with the modification of 30 % of $–OC_3H_7$ groups with 2AAEM, with a molar ratio of 2AAEM:MMA= 1:1000 and 40 % MMA by weight with respect to the total weight

1,505 g of 2AAEM-30 dispersion and 13,96 g toluene were added into a 250 ml round glass flask. Then, 10,55 g (0,1054 mole) MMA and 0,365 g initiator Trigonox EHPS (1 % mole of MMA) were added into the flask. This mixture was yellow-transparent in the beginning. After it was refluxed at 65 °C under $N_2$ for 2 hours, it was precipitated. After the solvents in the mixture were evaporated at 50 °C by using a rotation evaporator, the obtained powder was washed with 600 g toluene first (three times, 200 g x 3) and afterwards with 200 g tetrahydrofurane (twice, 100 g x 2) again. The obtained powder was dried at 50 °C at 10 mbar for 3 hours. After grinding, it was dried at 100 °C at 10 mbar for 2 hours and characterized by TGA/DSC. The synthesized powder was marked as "$TiO_2$-2AAEM-30-1:1000-40". Also, the monomer conversion was determined by FT-IR by calculating the peak areas of double bonds at the same monomer concentration after and before polymerization.

### 4.7.3. The modification of 50 % of $–OC_3H_7$ groups on $TiO_2$ nanoparticles with 2AAEM

10 g $TiO_2$ and 87,37 g toluene were added into a flask and the suspension was treated in an ultrasonic bath for 2 minutes. Then, 2,63 g 2AAEM (0,0116 mole) was added into the suspension. After it was stirred using a magnetic stirrer for 3 hours, its appearance became yellow-transparent. This dispersion was marked as "2AAEM-50".

#### 4.7.3.1. PMMA grafting onto $TiO_2$ surface with the modification of 50 % of $–OC_3H_7$ groups with 2AAEM, with a molar ratio of 2AAEM:MMA= 1:100 and 20 % MMA by weight with respect to the total weight

9,03 g 2AAEM-50 dispersion and 32,61 g toluene were added into a 250 ml round glass flask. Then, 10,50 g (0,1048 mole) MMA and 0,363 g initiator Trigonox EHPS (1 % mole of MMA used) were added into the flask. This mixture was yellow-transparent in the beginning. After it was refluxed at 65 °C under $N_2$ for 2 hours, it was precipitated. After the solvents in the mixture were evaporated at 50 °C by using a rotation evaporator, the obtained powder was washed with 600 g toluene first (three times, 200 g x 3) and afterwards with 200 g tetrahydrofurane (twice, 100 g x 2). The obtained powder was dried at 50 °C at 10 mbar for 3 hours. After grinding, it was dried at 100 °C at 10 mbar for 2 hours and characterized by FT-IR and TGA/DSC. The synthesized powder was marked as "$TiO_2$-2AAEM-50-1:100-20".

#### 4.7.3.2. PMMA grafting onto $TiO_2$ surface with the modification of 50 % of $–OC_3H_7$ groups with 2AAEM, with a molar ratio of 2AAEM:MMA= 1:1000 and 20 % MMA by weight with respect to the total weight

0,903 g 2AAEM-50 dispersion and 40,73 g toluene were added into a 250 ml round glass flask. Then, 10,50 g (0,1048 mole) MMA and 0,363 g initiator Trigonox EHPS (1 % mole of MMA used) were added into the flask. This mixture was yellow transparent in the beginning. After it was refluxed at 65 °C under $N_2$ for 2 hours, it was precipitated. After the solvents in the mixture were evaporated at 50 °C by using a rotation evaporator, the obtained powder was washed with 600 g toluene first (three times, 200 g x 3) and afterwards with 200 g tetrahydrofurane (twice, 100 g x 2). The obtained powder was dried at 50 °C at 10 mbar for 3 hours. After grinding, it was dried at 100 °C at 10 mbar for 2 hours and characterized by TGA/DSC. The synthesized powder was marked as "$TiO_2$-2AAEM-50-1:1000-20".

#### 4.7.3.3. PMMA grafting onto $TiO_2$ surface with the modification of 50 % of $–OC_3H_7$ groups with 2AAEM, with a molar ratio of 2AAEM:MMA= 1:100 and 40 % MMA by weight with respect to the total weight

9,03 g 2AAEM-50 dispersion and 6,36 g toluene were added into a 250 ml round glass flask. Then, 10,50 g (0,1048 mole) MMA and 0,363 g initiator Trigonox EHPS (1 % mole of MMA used) were also added into the flask. This mixture was yellow transparent in the beginning. After it was refluxed at 65 °C under $N_2$ for 2 hours, it was precipitated. After the solvents in the mixture were evaporated at 50 °C by using a rotation evaporator, the obtained powder was washed with 600 g toluene first (three times, 200 g x 3) and afterwards with 200 g

tetrahydrofurane (twice, 100 g x 2). The obtained powder was dried at 50 °C at 10 mbar for 3 hours. After grinding, it was dried at 100 °C at 10 mbar for 2 hours again and characterized by FT-IR and TGA/DSC. The synthesized powder was marked as "$TiO_2$-2AAEM-50-1:100-40".

#### 4.7.3.4. PMMA grafting onto $TiO_2$ surface with the modification of 50 % of $–OC_3H_7$ groups with 2AAEM, with a molar ratio of 2AAEM:MMA= 1:1000 and 40 % MMA by weight with respect to the total weight

0,903 g 2AAEM-50 dispersion and 14,48 g toluene were added into a 250 ml round glass flask. Then, 10,50 g (0,1048 mole) MMA and 0,363 g initiator Trigonox EHPS (1 % mole of MMA used) were also added into the flask. This mixture was yellow transparent in the beginning. After it was refluxed at 65 °C under $N_2$ for 2 hours, it was precipitated. After the solvents in the mixture were evaporated at 50 °C by using a rotation evaporator, the obtained powder was washed with 600 g toluene first (three times, 200 g x 3) and afterwards with 200 g tetrahydrofurane (twice, 100 g x 2). The obtained powder was dried at 50 °C at 10 mbar for 3 hours. After grinding, it was dried at 100 °C at 10 mbar for 2 hours and characterized by TGA/DSC. The synthesized powder was marked as "$TiO_2$-2AAEM-50-1:1000-40".

### 4.7.4. The modification of 80 % of $–OC_3H_7$ groups on $TiO_2$ nanoparticles with 2AAEM

12 g $TiO_2$ and 102,96 g toluene were added into a flask and the suspension was treated in an ultrasonic bath for 2 minutes. Then, 5,04 g 2AAEM (0,0224 mole) was also added into the suspension. After it was stirred using a magnetic stirrer for 3 hours, its appearance became yellow-transparent. This dispersion was marked as "2AAEM-80".

#### 4.7.4.1. PMMA grafting onto $TiO_2$ surface with the modification of 80 % of $–OC_3H_7$ groups with 2AAEM, with a molar ratio of 2AAEM:MMA= 1:100 and 20 % MMA by weight with respect to the total weight

5,95 g 2AAEM-80 dispersion and 38,18 g toluene were added into a 250 ml round glass flask. Then, 11,13 g (0,111 mole) MMA and 0,385 g initiator Trigonox EHPS (1 % mole of MMA used) were also added into the flask. This mixture was yellow transparent in the beginning. After it was refluxed at 65 °C under $N_2$ for 2 hours, it was precipitated. After the solvents in the mixture were evaporated at 50 °C by using a rotation evaporator, the obtained

powder was washed with 600 g toluene first (three times, 200 g x 3) and afterwards with 200 g tetrahydrofurane (twice, 100 g x 2). The obtained powder was dried at 50 °C at 10 mbar for 3 hours. After grinding, it was dried at 100 °C at 10 mbar for 2 hours and characterized by FT-IR and TGA/DSC. The synthesized powder was marked as "$TiO_2$-2AAEM-80-1:100-20".

#### 4.7.4.2. PMMA grafting onto $TiO_2$ surface with the modification of 80 % of $–OC_3H_7$ groups with 2AAEM, with a molar ratio of 2AAEM:MMA= 1:1000 and 20 % MMA by weight with respect to the total weight

0,595 g 2AAEM-80 dispersion and 43,54 g toluene were added into a 250 ml round glass flask. Then, 11,13 g (0,111 mole) MMA and 0,385 g initiator Trigonox EHPS (1 % mole of MMA used) were also added into the flask. This mixture was yellow transparent in the beginning. After it was refluxed at 65 °C under $N_2$ for 2 hours, it was precipitated. After the solvents in the mixture were evaporated at 50 °C by using a rotation evaporator, the obtained powder was washed with 600 g toluene first (three times, 200gx3) and afterwards with 200 g tetrahydrofurane (twice, 100 g x 2). The obtained powder was dried at 50 °C at 10 mbar for 3 hours. After grinding, it was dried at 100 °C at 10 mbar for 2 hours and characterized by TGA/DSC. The synthesized powder was marked as "$TiO_2$-2AAEM-80-1:1000-20".

#### 4.7.4.3. PMMA grafting onto $TiO_2$ surface with the modification of 80 % of $–OC_3H_7$ groups with 2AAEM, with a molar ratio of 2AAEM:MMA= 1:100 and 40 % MMA by weight with respect to the total weight

5,95 g 2AAEM-80 dispersion and 10,36 g toluene were added into a 250 ml round glass flask. Then, 11,13 g (0,111 mole) MMA and 0,385 g initiator Trigonox EHPS (1 % mole of MMA used) were also added into the flask. This mixture was yellow transparent in the beginning. After it was refluxed at 65 °C under $N_2$ for 2 hours, it was precipitated. After the solvents in the mixture were evaporated at 50 °C by using a rotation evaporator, the obtained powder was washed with 600 g toluene first (three times, 200 g x 3) and afterwards with 200 g tetrahydrofurane (twice, 100 g x 2). The obtained powder was dried at 50 °C at 10 mbar for 3 hours. After grinding, it was dried at 100 °C at 10 mbar for 2 hours and characterized by FT-IR and TGA/DSC. Also, the appearance of the PMMA-modified $TiO_2$ nanoparticles is investigated by TEM analysis. Also, the synthesized powder was marked as "$TiO_2$-2AAEM-80-1:100-40".

#### 4.7.4.4. PMMA grafting onto $TiO_2$ surface with the modification of 80 % of $–OC_3H_7$ groups with 2AAEM, with a molar ratio of 2AAEM:MMA= 1:1000 and 40 % MMA by weight with respect to the total weight

0,595 g 2AAEM-80 and 15,72 g toluene were added into a 250 ml round glass flask. Then, 11,13 g (0,111 mole) MMA and 0,385 g initiator Trigonox EHPS (1 % mole of MMA used) were also added into the flask. This mixture was yellow transparent in the beginning. After it was refluxed at 65 °C under $N_2$ for 2 hours, it was precipitated. After the solvents in the mixture were evaporated at 50 °C by using a rotation evaporator, the obtained powder was washed with 600 g toluene first (three times, 200 g x 3) and afterwards with 200 g tetrahydrofurane (twice, 100 g x 2). The obtained powder was dried at 50 °C at 10 mbar for 3 hours. After grinding, it was dried at 100 °C at 10 mbar for 2 hours and characterized by TGA/DSC. The synthesized powder was marked as "$TiO_2$-2AAEM-80-1:1000-40".

## 5. Results and discussions

### 5.1. Characterization of $TiO_2$ nanoparticles

#### 5.1.1. PCS results

PCS is one of the most commonly used methods for measuring size of submicron particles in liquid dispersions and also, the measurements are performed very fast by this technique. In this work, after $TiO_2$ nanoparticles were synthesized by hydrothermal method, the particle size of nanoparticles was determined by PCS. Particle size distribution for $TiO_2$ nanoparticles is shown in Figure 9.

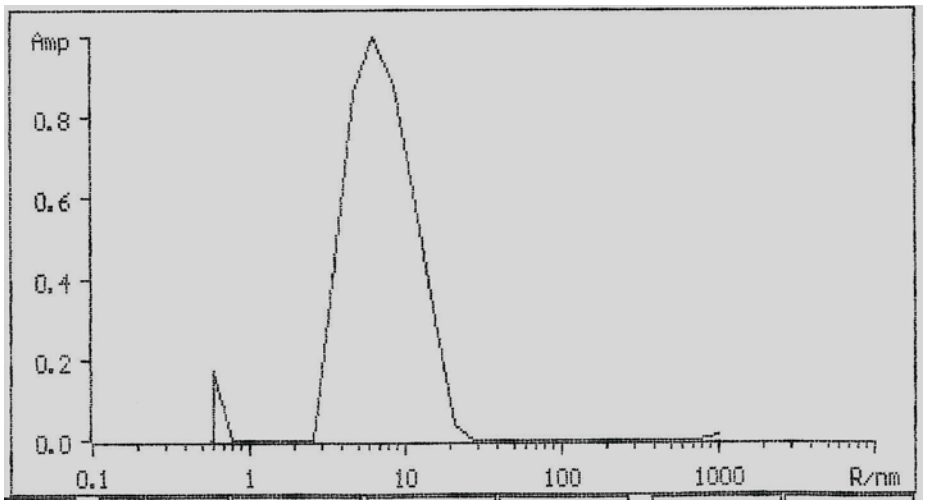


**Figure 9. Particle size distribution for $TiO_2$ nanoparticles.**

According to the PCS measurement, it is shown two different peaks in the particle range 0,1-1000 nm. Because PCS instrument measures in the particle size range between 1 nm and 1 μm, the size at nearly 0,7 nm is not taken into account. Consequently, the particle size varies between 2,5-11,5 nm with an average particle size of 7,1 nm.

#### 5.1.2. TEM results

The shape and size of $TiO_2$ nanoparticles synthesized in this work were characterized by TEM. Firstly unmodified $TiO_2$ nanoparticles were investigated to see by TEM how $TiO_2$ nanoparticles were seen without any modification with modification agent. The results are shown in the Figure 10, 11, 12.

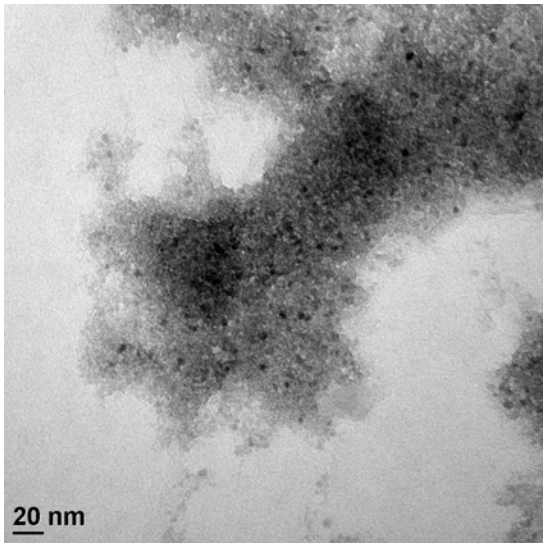


**Figure 10. TEM picture of unmodified $TiO_2$ nanoparticles.**

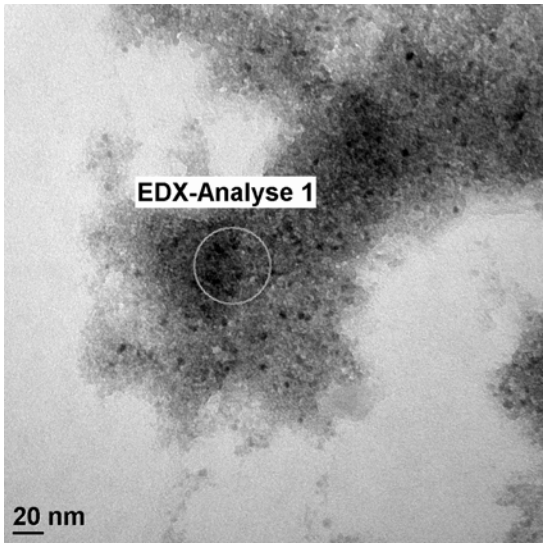


**Figure 11. TEM picture of unmodified $TiO_2$ nanoparticles.**

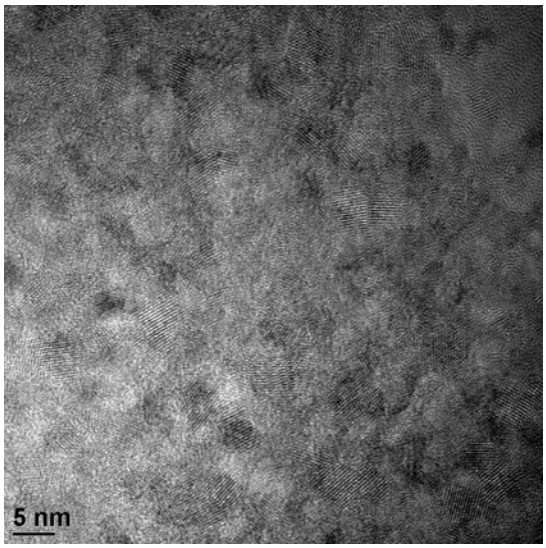


**Figure 12. TEM picture of unmodified $TiO_2$ nanoparticles.**

According to the pictures of the unmodified-$TiO_2$ nanoparticles shown above, $TiO_2$ nanoparticles were much agglomerated in toluene, it is difficult to see single particles and difficult to calculate the size of particles and difficult to speak about their shapes. For this reason, $TiO_2$ nanoparticles were modified with stearic acid molecules to see single particles. In the following, the pictures of the stearic acid-modified $TiO_2$ nanoparticles were shown in the Figure 13, 14, 15, 16.


**Figure 13. TEM picture of the stearic acid-modified $TiO_2$ nanoparticles.**

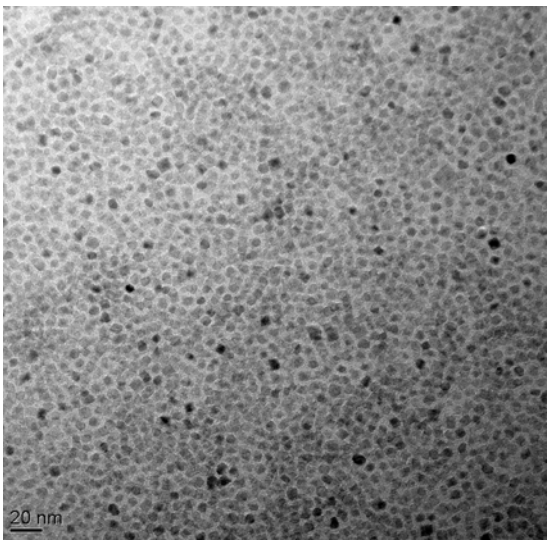


**Figure 14. TEM picture of the stearic acid-modified $TiO_2$ nanoparticles.**

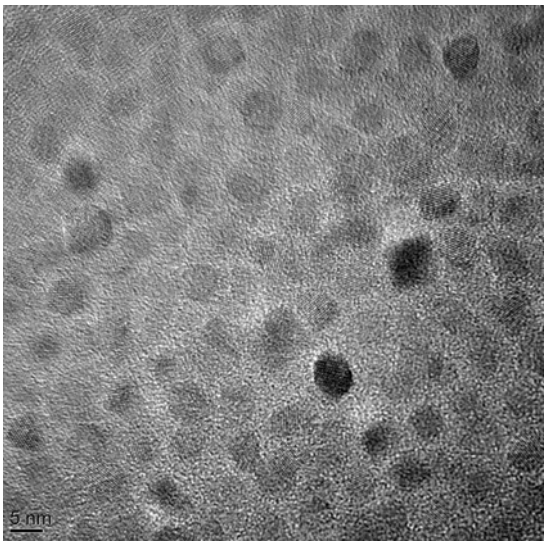


**Figure 15. TEM picture of the stearic acid-modified $TiO_2$ nanoparticles.**

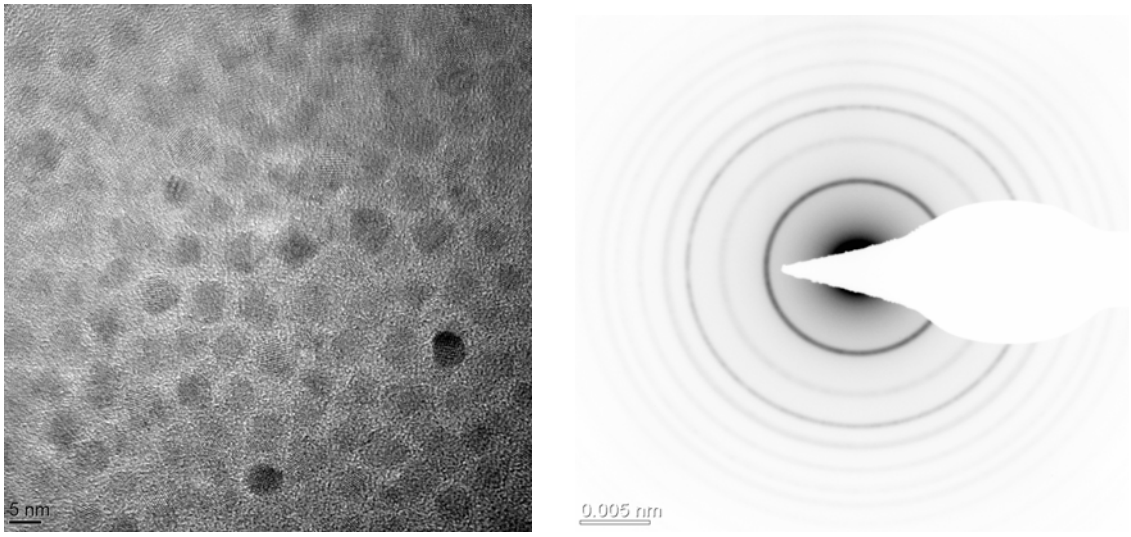


**Figure 16. TEM picture of the stearic acid-modified $TiO_2$ nanoparticles with high resolution and the negative diagram of electron diffraction.**

The TEM pictures of the stearic acid modified-$TiO_2$ nanoparticles show that $TiO_2$ nanoparticles were dispersed in toleuene very well, namely there is no agglomeration and the diagram of electron diffraction shows that $TiO_2$ nanoparticles are crystalline. The shape of nanoparticles is nearly spherical and their size is 6 nm. The average size of particles was approximately same as PCS results (7,1 nm). It is likely that a little difference between PCS result and TEM results might be because of the modification of $TiO_2$ nanoparticles with stearic acid. Namely, after $TiO_2$ nanoparticles were modified with stearic acid, stearic acid molecules on $TiO_2$ nanoparticles increased their size from 6 nm to 7,1 nm. Eventually, nearly monodisperse $TiO_2$ nanoparticles with a diameter of 6 nm and with agglomeration-free were prepared by hydrothermal method. But the shape and size of $TiO_2$ nanoparticles were not detected without modification of the stearic acid molecules. Also, the unmodified-$TiO_2$ nanoparticles were much agglomerated.

### 5.1.3 EDX result of the unmodified $TiO_2$ nanoparticles

After $TiO_2$ nanoparticles were synthesized, the elemental combination of the unmodified $TiO_2$ nanoparticles were detected by means of EDX from the place of having a lot of $TiO_2$ nanoparticles in the Figure 17. This place is signed as a circle in this picture. This result is shown in the following. According to the result, the peaks of belonging to the ***Ti, O***, ***C and Cu*** were exactly determined by EDX. Also as further information, the peaks of belonging to the Cu are come from the grating of the instrument.

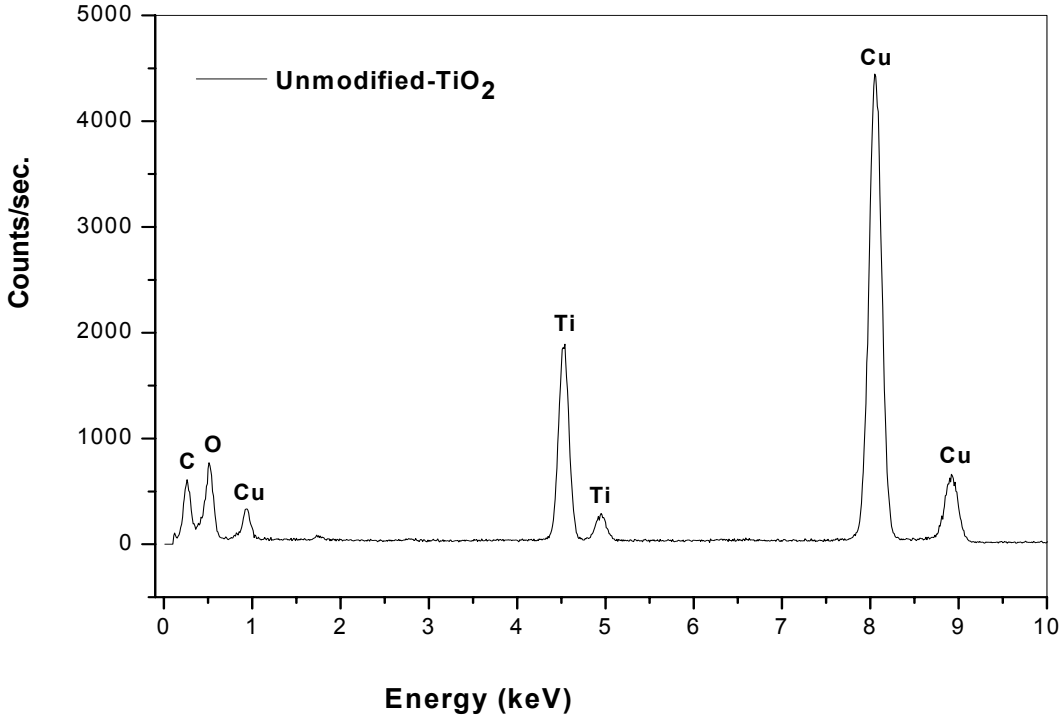


**Figure 17. The EDX result of the unmodified $TiO_2$ nanoparticles.**

### 5.1.4 XRD results

The crystalline phase and the size of $TiO_2$ nanoparticles were investigated by X-ray. X-ray diffraction of $TiO_2$ powder and the reflex of anatase $TiO_2$ powder are shown in the Figure 18.

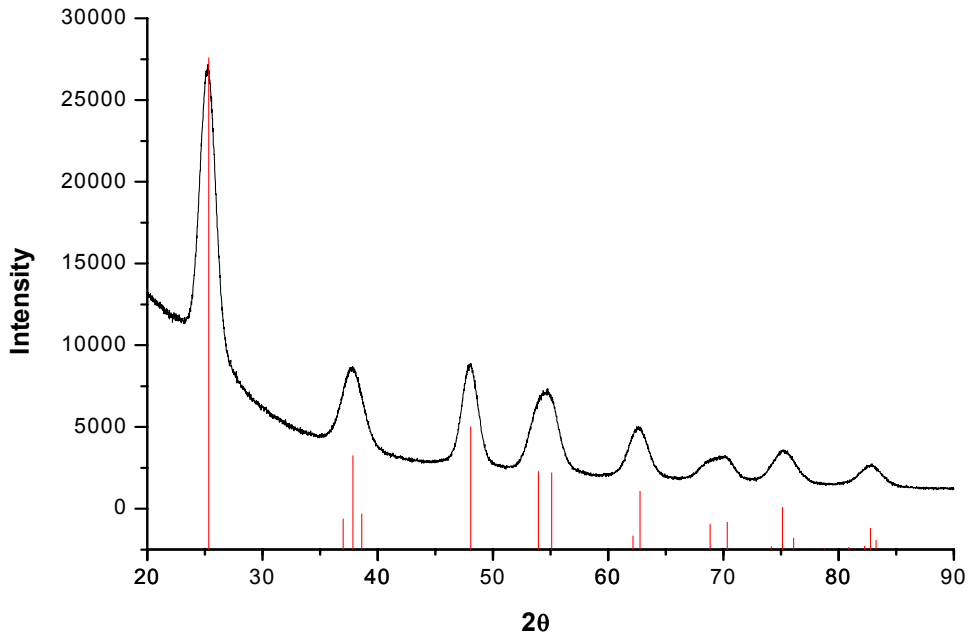


**Figure 18. X-ray diffraction of $TiO_2$ synthesized by hydrothermal process (black line) and the reflex of anatase $TiO_2$ (red line) according to JCPDS-Nr. 84-1286 (Anatase).**

By means of XRD measurement, it is determined that $TiO_2$ was anatase, the density of $TiO_2$ nanoparticles was 3,88 g/cm$^3$ and it crystallized in tetragonal system according to JCPDS-Nr. 84-1286**.** Furthermore, the particle size of nanoparticles was calculated 6,3 nm through *"Scherrer Equation"* and this result was same as TEM results (6 nm).

### 5.1.5 Elemental analysis result

The amount of C, H and N on the surface of $TiO_2$ nanoparticles was determined by elemental analysis. According to the elemental analysis results, the amount of the carbon, hydrogen and nitrogen were 8,38 %; 2,13 % and 0,0 % respectively. These elemental analysis results will be used to calculate the amount of the $–OC_3H_7$ and –OH on $TiO_2$ nanoparticle later on.

### 5.1.6 The evaluation of synthesis and characterization of $TiO_2$ nanoparticles

In this work, $TiO_2$ nanoparticles are synthesized as shown in the Figure 19. After hydrolyse and condensation reactions of Titanium (IV) isopropoxide molecules using $H_2O/HNO_3$, amorphous $TiO_2$ particles are obtained. After that, isopropoxy groups on the particle surfaces are exchanged with 1-propanol molecules by alcohol interchange reaction and finally crystalline $TiO_2$ nanoparticles are synthesized.

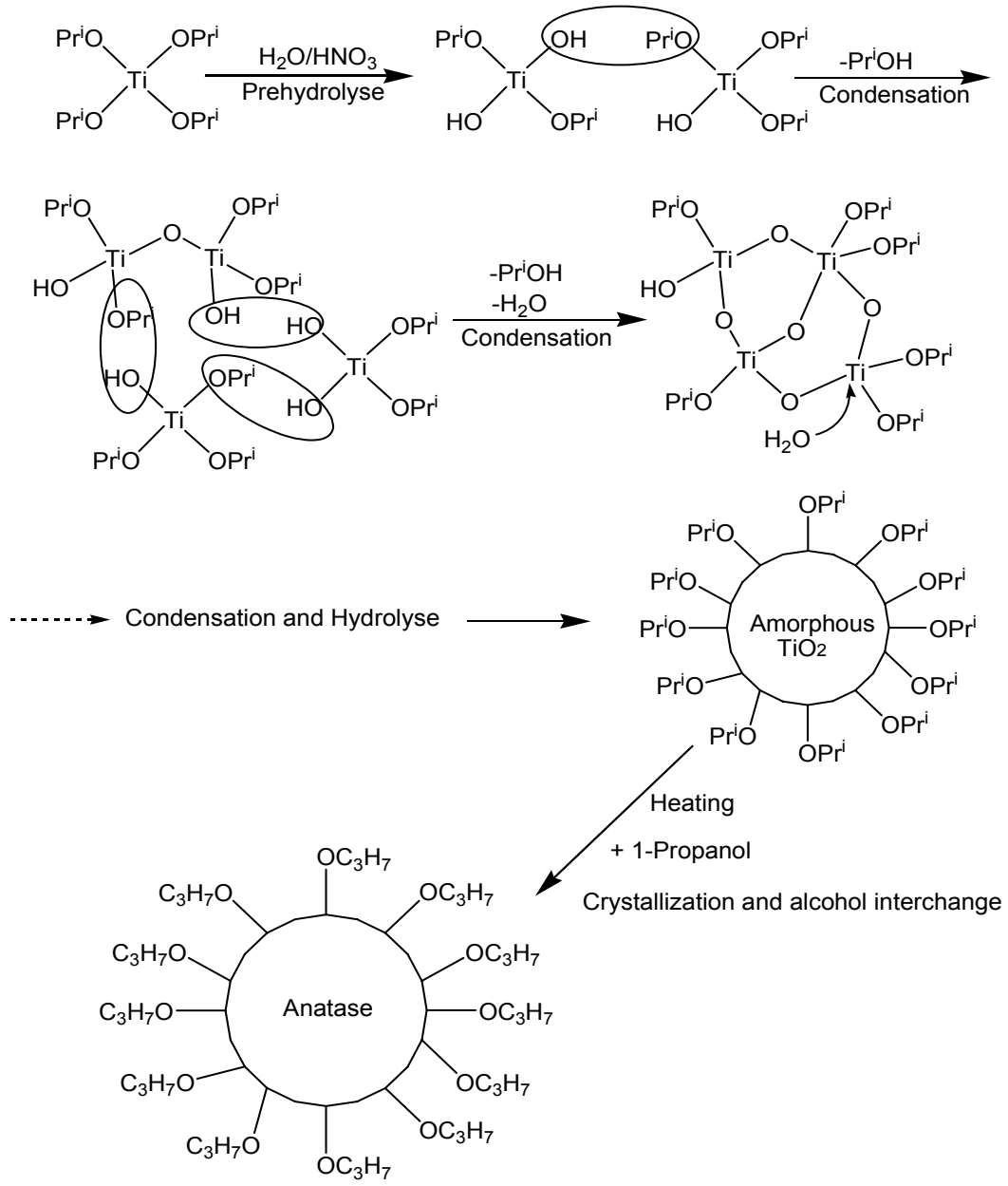


**Figure 19. Synthesis of crystalline anatase $TiO_2$ nanoparticles by hydrothermal method.**

## 5.2. Characterization of the silanes, carboxylic acids and β-ketoester-modified $TiO_2$ nanoparticles

The percentage of carbon on the surface of $TiO_2$ nanoparticles was determined to be 8,38 % by elemental analysis (see section 5.1.5., page 72), the density of anatase particles was 3,88 x $10^6$ g/$m^3$ according to JCPDS-Nr. 84-1286 (see section 5.1.4., page 71) and the size of $TiO_2$ nanoparticles was determined to be nearly 6 nm (see section 5.1.1. and 5.1.2., page 67-70) and their shape is nearly spherical (see section 5.1.2., page 70). By means of these results, the surface area of anatase $TiO_2$ nanoparticles was calculated using the following

equation. Where A is specific surface area ($m^2/g$), r is radius of the particle (m) and d is density of the particle ($g/m^3$). In the calculation, it is assumed that $TiO_2$ nanoparticles are spherical.

$$A = \frac{3}{r \cdot d}$$

The specific surface area of $TiO_2$ nanoparticles was calculated to be 258 $g/m^2$. Furthermore, the amount of $–OC_3H_7$ groups in 1 gram $TiO_2$ powder is $2{,}33.10^{-3}$ mole and the amount of –OH groups in 1 g $TiO_2$ powder is $3{,}79.10^{-3}$ mole were calculated. In this calculation, it is assumed that the surface density for fully hydroxylated anatase $TiO_2$ nanoparticles are 14 -OH groups/100 $Å^2$ [247, 248]. Namely, 38 % of the surface area of $TiO_2$ nanoparticles was covered with $–OC_3H_7$ groups and 62 % of the surface area of $TiO_2$ nanoparticles was covered with –OH groups. Thus, it is concluded that the synthesized $TiO_2$ nanoparticles have both –OH groups and $–OC_3H_7$ groups on their surface. From that angle, $TiO_2$ nanoparticles synthesized in this work are different from the literature. As for the modifications of these $TiO_2$ nanoparticles, if the –OH groups on their surfaces are modified with silanes (for example; methoxysilanes, ethoxysilanes, etc.), the Si-O-Ti covalent bonds formed on the surface and alcohol molecules (for example; methanol, ethanol, etc.) are liberated from the surface. In addition, the $–OC_3H_7$ groups on $TiO_2$ surface can react with carboxylic acids, β-ketoesters and β-diketones for the formation of complex structures on their surface and 1-propanol molecules are liberated from the surfaces.

As explained before (see section 4.4.1, page 48), toluene used in the experiments as solvent was water-free because $–OC_3H_7$ groups on the $TiO_2$ nanoparticles are very sensitive against water. Namely, in the presence of water, $–OC_3H_7$ groups on the surface are hydrolysed immediately. For this reason, the mentioned effect was investigated by an experiment. 1 g $TiO_2$ powder, 8 g toluene and 1 g water which is enough to hydrolyse $–OC_3H_7$ groups on $TiO_2$ nanoparticles were added into a glass vessel. Although the whole $–OC_3H_7$ groups on $TiO_2$ nanoparticles should have been disappeared by 1 g water, the carbon amount on the surface was decreased from 8,38 % to 2,53 %. Consequently, it is understood that even if a solvent contains only a little water, the $–OC_3H_7$ groups on $TiO_2$ nanoparticles are hydrolyzed. For this reason, the solvent used throughout this work was water-free toluene.

### 5.2.1. Modification with HTMS

After $TiO_2$ nanoparticles were modified with HTMS (according to section 4.4.1.1., page 49), this modification was characterized by GC/MS, elemental analysis and FT-IR measurements. The results are shown in the following.

#### 5.2.1.1. GC/MS result

After $TiO_2$ nanoparticles were modified with HTMS, the liberated methanol was detected by GC/MS and it was compared with standard methanol solution.

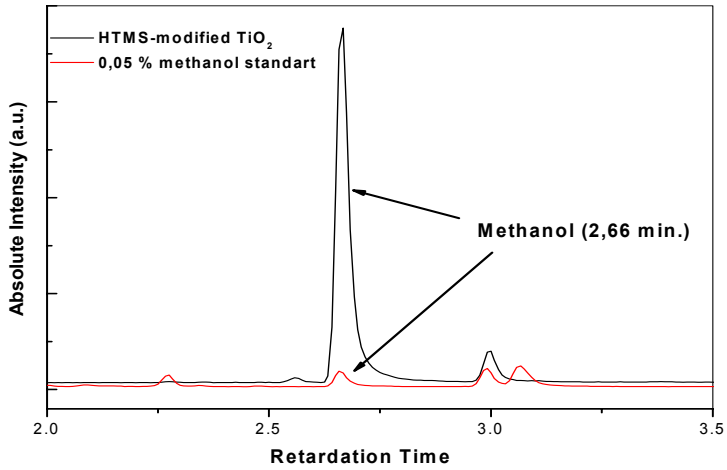


**Figure 20. GC/MS result of the HTMS-modified $TiO_2$ nanoparticles.**

According to the Figure 20, the liberated methanol molecules in this measurement resulted from the reaction of –OH groups on $TiO_2$ nanoparticles with Si-O-$CH_3$ groups of HTMS for the formation of Si-O-Ti covalent bond on the surface.

#### 5.2.1.2. Elemental analysis result

After the HTMS-modified $TiO_2$ particles were dried, it was also characterized by elemental analysis. The result of this measurement is shown in the following.

| Powder | C% | H% | N% |
|---|---|---|---|
| HTMS-modified $TiO_2$ powder | 10,7 | 2,48 | 0,0 |
| Unmodified $TiO_2$ powder | 8,38 | 2,13 | 0,0 |

According to this result, the increase in the carbon and hydrogen percentages indicates that $TiO_2$ nanoparticles were modified with HTMS.

### 5.2.1.3. FT-IR analysis result

After the HTMS-modified $TiO_2$ powder was dried, it was also characterized by FT-IR. The result is shown in the Figure 21.

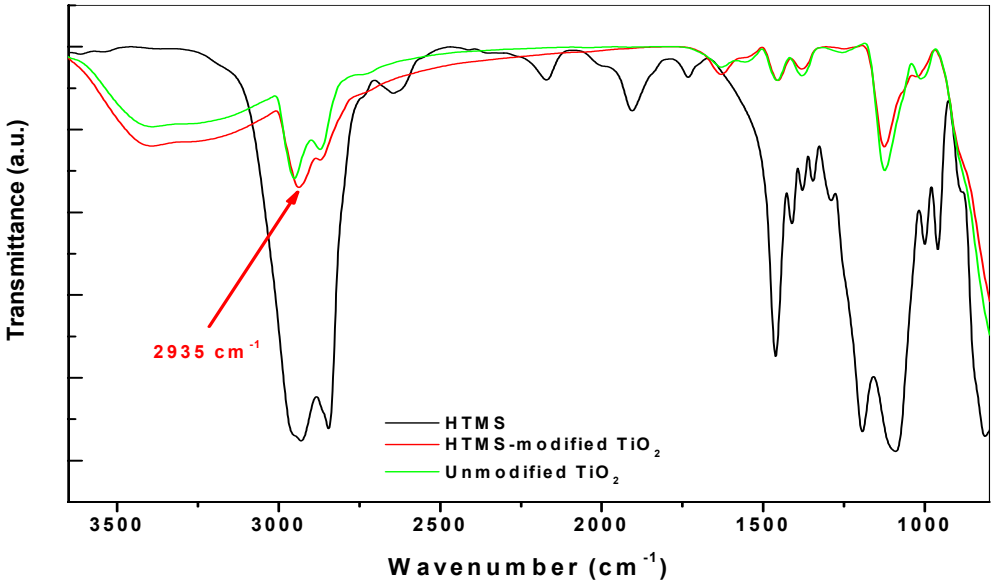


**Figure 21. FT-IR spectrums of the HTMS-modified $TiO_2$ powder, HTMS and unmodified $TiO_2$ powder.**

In the Figure 21, it is difficult to characterize whether $TiO_2$ nanoparticles were modified with HTMS or not. Generally after $TiO_2$ nanoparticles are modified with silanes, Ti-O-Si bonds occur and these bonds appear at around 920-950 $cm^{-1}$ in the FT-IR spectrums [249-251]. But this peak can't be detected in this area. But also, one possibility to prove this bonding is the increase in the intensity of $-CH_2-$ and $-CH_3$ absorption bands at around 2800-3000 $cm^{-1}$ as compared to the unmodified $TiO_2$ powder. Unfortunately, the HTMS-modified $TiO_2$ powder doesn't show any increase at this area. Namely, the modification of $TiO_2$ nanoparticles with HTMS can't be proved by FT-IR measurement. Of course, this modification was proved by GC/MS measurement, elemental analysis.

### 5.2.2. Modification with DTMS

After the modifications of $TiO_2$ nanoparticles with HTMS, $TiO_2$ nanoparticles were modified with another silane molecule with higher molecular weight, with DTMS. After $TiO_2$ nanoparticles were modified with DTMS (according to section 4.4.1.2., page 49), it was

characterized by GC/MS, elemental analysis and FT-IR measurements. The results are shown in the following.

### 5.2.2.1. GC/MS result

After $TiO_2$ nanoparticles were modified with DTMS, the liberated methanol molecules were detected by GC/MS and it was compared with standart methanol solution.

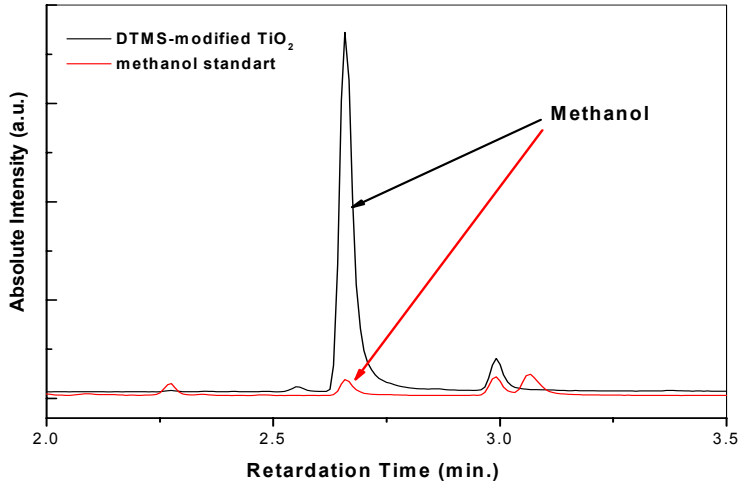


**Figure 22. GC/MS result of the DTMS-modified $TiO_2$ nanoparticles.**

According to the Figure 22, the liberated methanol molecules resulted from the reaction of –OH groups on $TiO_2$ nanoparticles with Si-O-$CH_3$ groups of DTMS for the formation of Si-O-Ti covalent bond on the surface.

### 5.2.2.2. Elemental analysis result

After the DTMS-modified $TiO_2$ particles were dried, it was characterized by elemental analysis. The result of this measurement is shown in the following.

| Powder | C% | H% | N% |
|---|---|---|---|
| DTMS-modified $TiO_2$ powder | 13,14 | 2,94 | 0,0 |
| Unmodified $TiO_2$ powder | 8,38 | 2,13 | 0,0 |

According to this result, the increase in the carbon and hydrogen percentages of the DTMS-modified $TiO_2$ powder indicates that $TiO_2$ nanoparticles were modified with DTMS. Furthermore, the increase in the carbon amount of the DTMS-modified $TiO_2$ particles is more than that of the HTMS-modified $TiO_2$ nanoparticles. Its reason might be difference in the

number of carbon atoms in DTMS and HTMS molecules. Namely, although DTMS molecule has 10 carbon atoms, HTMS molecule has 6 carbon atoms in their molecules.

### 5.2.2.3. FT-IR analysis result

After the DTMS-modified $TiO_2$ powder was dried, it was characterized by FT-IR. The result of this measurement is shown in the Figure 23.

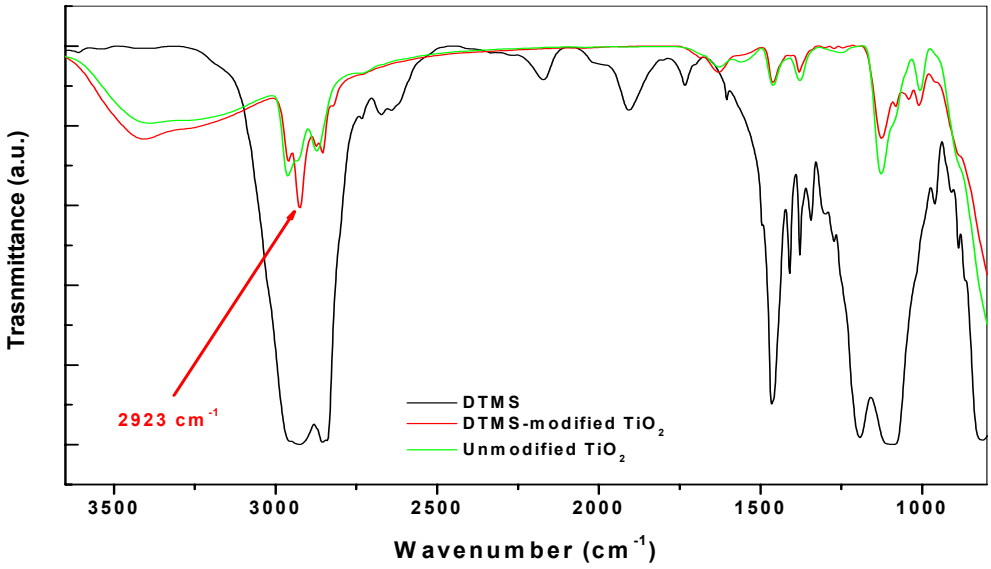


**Figure 23. FT-IR spectrums of the DTMS-modified $TiO_2$ powder, DTMS and unmodified $TiO_2$ powder.**

In the Figure 23, it is difficult to characterize whether $TiO_2$ nanoparticles were modified with DTMS. Generally, after $TiO_2$ nanoparticles were modified with silanes, normally Ti-O-Si bonds occur and these bonds in the FT-IR spectrums appear at around 920-950 $cm^{-1}$. But it can't be detected in this area. But after modification, one possibility to prove this modification is the increase in the intensity of $-CH_2-$ and $-CH_3$ absorption bands at around 2800-3000 $cm^{-1}$. Fortunately, the peak intensity at 2923 $cm^{-1}$ in the spectrum of the DTMS-modified $TiO_2$ nanoparticles increased as compared to that of the unmodified $TiO_2$ nanoparticles. Thus, it is concluded that $TiO_2$ nanoparticles were modified with DTMS molecules. Of course, this modification was also proved by GC/MS measurement, elemental analysis.

### 5.2.3. Modification with DDTMS

After the modifications of $TiO_2$ nanoparticles with HTMS and DTMS, $TiO_2$ nanoparticles were modified with another silane molecule with higher molecular weight, namely with DDTMS. After $TiO_2$ nanoparticles were modified with DDTMS (according to section 4.4.1.3., page 49), the modification was characterized by GC/MS, elemental analysis and FT-IR measurements. The results are shown in the following.

#### 5.2.3.1. GC/MS result

In the Figure 24 and 25, after $TiO_2$ nanoparticles were modified with DDTMS, the liberated methanol molecule was detected and compared with standart methanol solution. Furthermore, a solution of DDTMS in toluene was also measured by GC/MS.

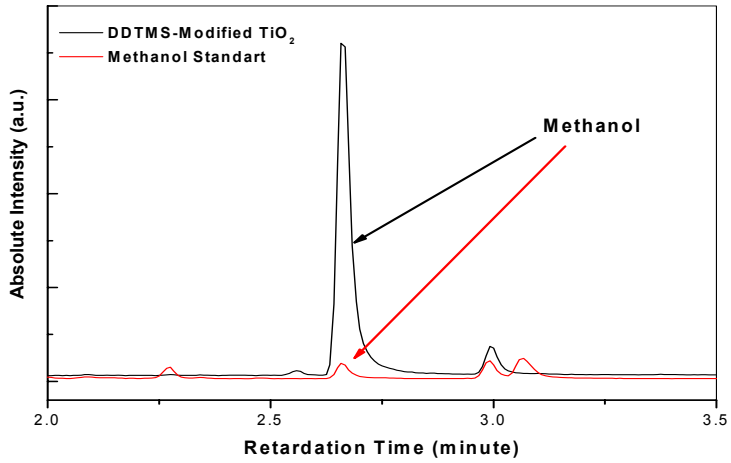


**Figure 24. GC/MS result of the DDTMS-modified $TiO_2$ nanoparticles.**

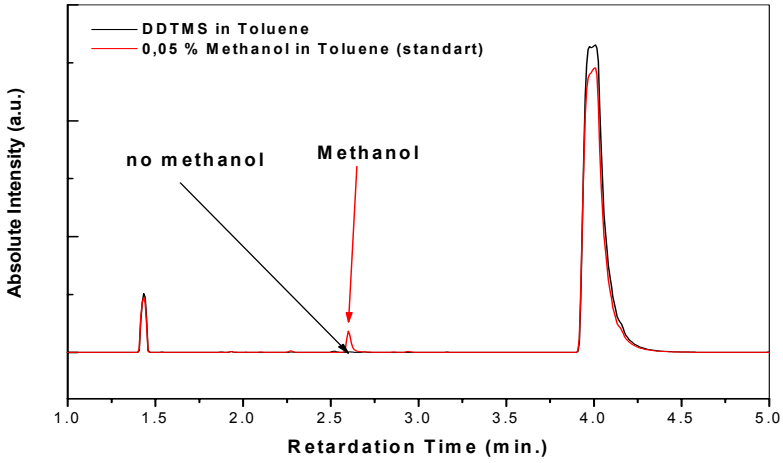


**Figure 25. GC/MS result of a solution of DDTMS in toluene and methanol in toluene (standart).**

According to the Figure 24, the liberated methanol molecules in this measurement resulted from the reaction of –OH groups on $TiO_2$ nanoparticles with Si-O-$CH_3$ groups of DDTMS. Furthermore, according to the Figure 25, a solution of DDTMS in toluene was measured by GC/MS and no methanol was detected. It means that all methanol detected by GC/MS resulted from the DDTMS modification.

### 5.2.3.2. Elemental analysis result

After the DDTMS-modified $TiO_2$ powder was dried, it was characterized by elemental analysis. The result is shown in the following.

| Powder | C% | H% | N% |
|---|---|---|---|
| DDTMS-modified $TiO_2$ powder | 13,21 | 2,90 | 0,0 |
| Unmodified $TiO_2$ powder | 8,38 | 2,13 | 0,0 |

According to this result, the increase in the carbon and hydrogen amount indicates that $TiO_2$ nanoparticles were modified with DDTMS. Furthermore, the increase in the amount of carbon of the DDTMS-modified $TiO_2$ particles is little more than that of the DTMS-modified $TiO_2$ nanoparticles. Namely, the increase in the carbon amount is not enough. Its reason might be sterical hindrance effects by previously attached silanes.

### 5.2.3.3. FT-IR analysis result

After the DDTMS-modified $TiO_2$ powder was dried, it was characterized by FT-IR. The result is shown in the Figure 26.

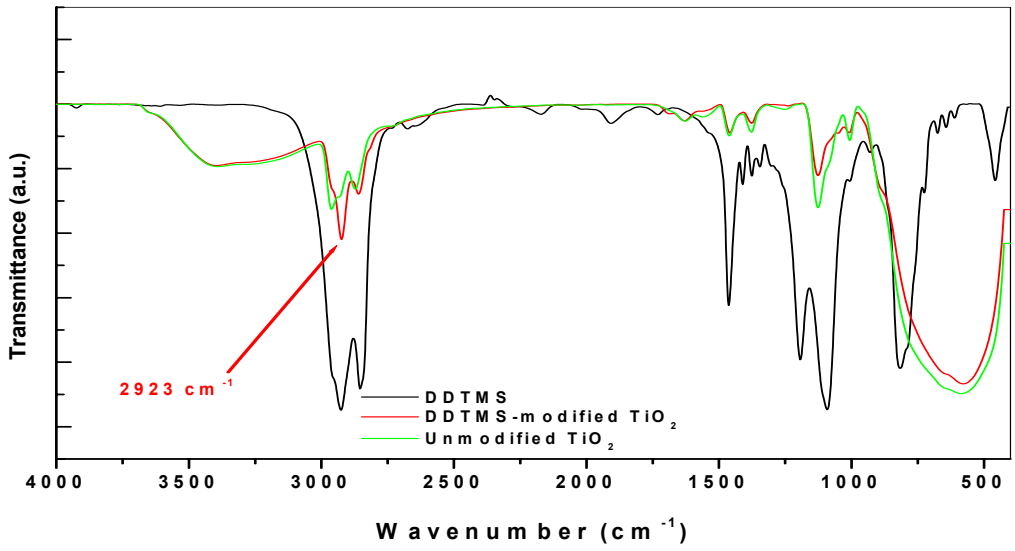

**Figure 26. FT-IR spectrums of the DDTMS-modified $TiO_2$ Powder, DDTMS and unmodified $TiO_2$ Powder.**

In the Figure 26, it is difficult to characterize whether $TiO_2$ nanoparticles were modified with DDTMS. Generally after $TiO_2$ nanoparticles were modified with silanes, normally Ti-O-Si bonds occur and this bond in the FT-IR spectrums appears at around 920-950 $cm^{-1}$. But it can't be detected in this area of the spectrum. But after modification, another possibility to prove is the increase in the intensity of $-CH_2-$ and $-CH_3$ absorption bonds at around 2800-3000 $cm^{-1}$. Fortunately, the peak intensity at 2923 $cm^{-1}$ in the spectrum of the DDTMS-modified $TiO_2$ nanoparticles increased as compared to that of the unmodified $TiO_2$ nanoparticles. Thus, it is concluded that $TiO_2$ nanoparticles were modified with DDTMS molecules. Of course, this modification was also proved by GC/MS measurement, elemental analysis.

### 5.2.4. Modification with HDTMS

After $TiO_2$ nanoparticles were modified with HTMS, DTMS and DDTMS, $TiO_2$ nanoparticles were modified with another silane molecule with higher molecular weight, namely with HDTMS (according to section 4.4.1.4., page 50). After modification, it was characterized by GC/MS, elemental analysis, FT-IR and EDX. The results are shown in the following.

#### 5.2.4.1. GC/MS result

After $TiO_2$ nanoparticles were modified with HDTMS, the liberated methanol molecule was detected and compared with standart methanol solution. The results are shown in the following.

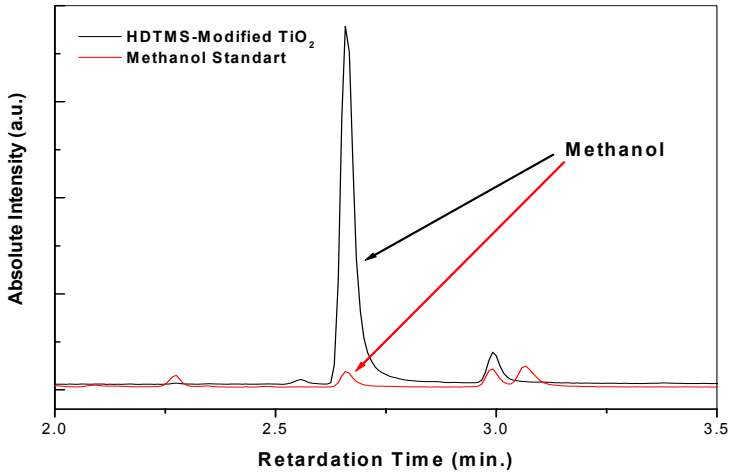


**Figure 27. GC/MS result of the HDTMS-modified $TiO_2$ nanoparticles.**

According to the Figure 27, the liberated methanol molecules in this measurement resulted from the reaction of –OH groups on $TiO_2$ nanoparticles with Si-O-$CH_3$ groups of HDTMS for the formation of Si-O-Ti covalent bonds on the surface.

### 5.2.4.2. Elemental analysis result

After the HDTMS-modified $TiO_2$ powder was dried, it was characterized by elemental analysis. The result of this measurement is shown in the following.

| Powder | C% | H% | N% |
|---|---|---|---|
| HDTMS-modified $TiO_2$ powder | 14,73 | 3,07 | 0 |
| Unmodified $TiO_2$ powder | 8,38 | 2,13 | 0,0 |

According to this result, the increase in the carbon and hydrogen percent indicates that $TiO_2$ nanoparticles were modified with HDTMS molecules. Furthermore, the increase in the amount of the carbon of the HDTMS-modified $TiO_2$ particles is little more than that of DDTMS-modified $TiO_2$ nanoparticles. Namely, the increase in the carbon amount is not enough. Its reason might be sterical effects by previously attacted silanes.

### 5.2.4.3. FT-IR analysis result

After the HDTMS-modified $TiO_2$ nanoparticles were dried, it was characterized by FT-IR. The result is shown in the Figure 24.

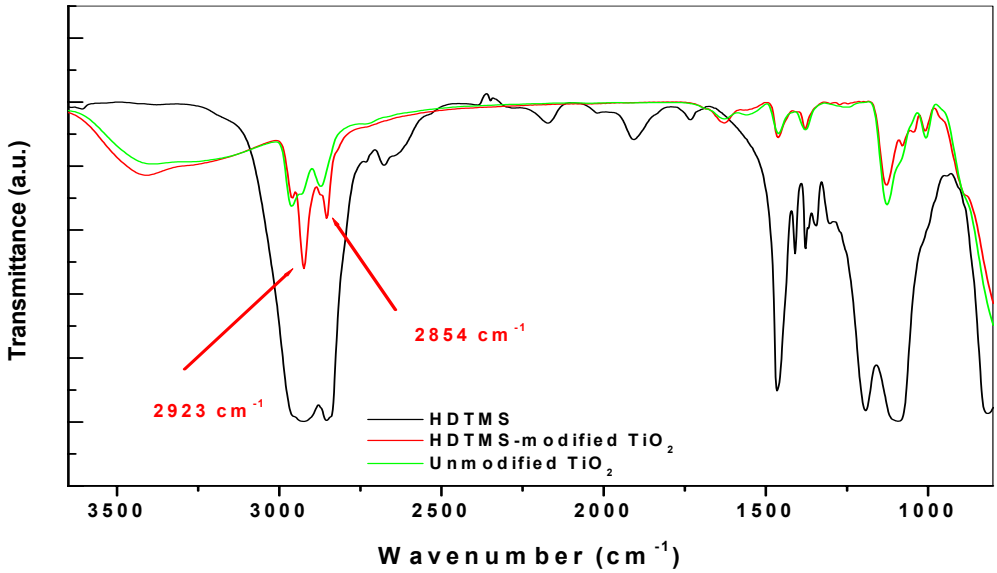


**Figure 28. FT-IR spectrums of the HDTMS-modified $TiO_2$ powder, HDTMS and unmodified $TiO_2$ Powder.**

In the Figure 28, it is difficult to characterize whether $TiO_2$ nanoparticles were modified with HDTMS or not. Generally, after $TiO_2$ nanoparticles are modified with silanes, normally Ti-O-Si bonds occur and this bond appears at around 920-950 $cm^{-1}$. But it can't be detected in this area of the spectrum. But after modification, one possibility to prove this modification is the increase in the intensity of $-CH_2-$ and $-CH_3$ absorption bands at around 2800-3000 $cm^{-1}$. Fortunately, the peak intensity at 2923 $cm^{-1}$ and 2854 $cm^{-1}$ in the spectrum of the HDTMS-modified $TiO_2$ nanoparticles increased as compared to that of the unmodified $TiO_2$ nanoparticles. Thus, it is concluded that $TiO_2$ nanoparticles were modified with HDTMS. Of course, this modification was also proved by GC/MS and elemental analysis.

### 5.2.4.4. TEM and EDX results of the HDTMS-modified $TiO_2$ nanoparticles

After $TiO_2$ nanoparticles were modified with HDTMS molecules, the appearance of the HDTMS-modified $TiO_2$ nanoparticles was investigated by TEM and elemental composition of the HDTMS-modified $TiO_2$ nanoparticles was determined by EDX. The results are shown in the following Figure 29, 30, 31, 32, 33.

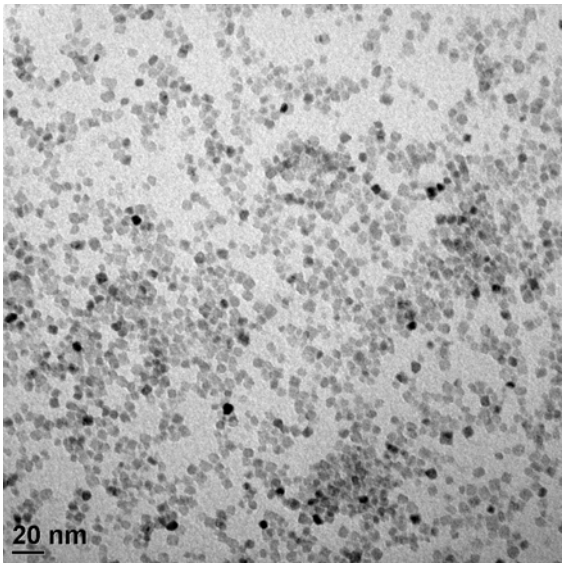


**Figure 29. TEM picture of the HDTMS-modified $TiO_2$ nanoparticles.**

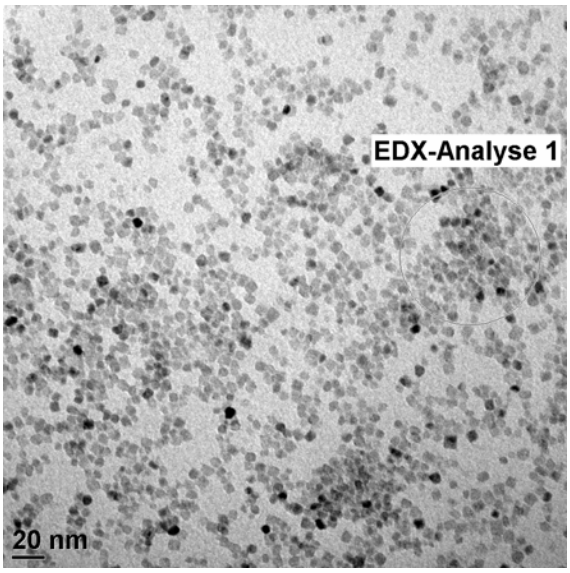


**Figure 30. TEM picture of the HDTMS-modified $TiO_2$ nanoparticles.**

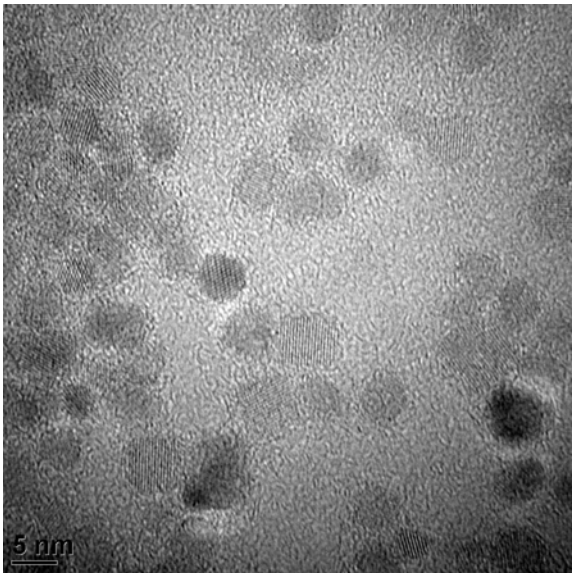


**Figure 31. TEM picture of the HDTMS-modified $TiO_2$ nanoparticles.**

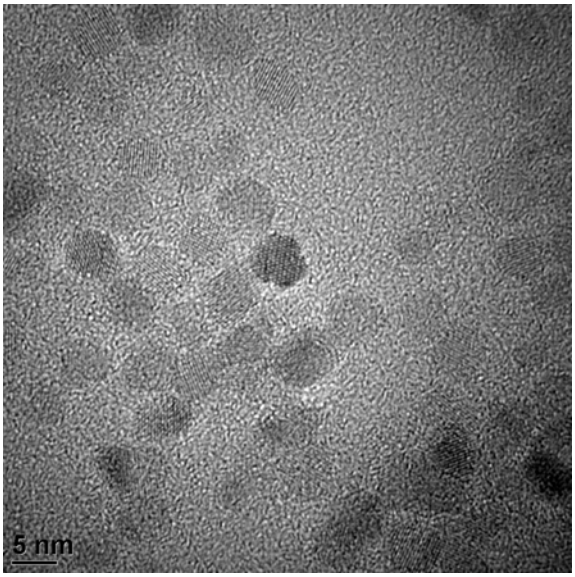


**Figure 32. TEM picture of the HDTMS-modified $TiO_2$ nanoparticles.**

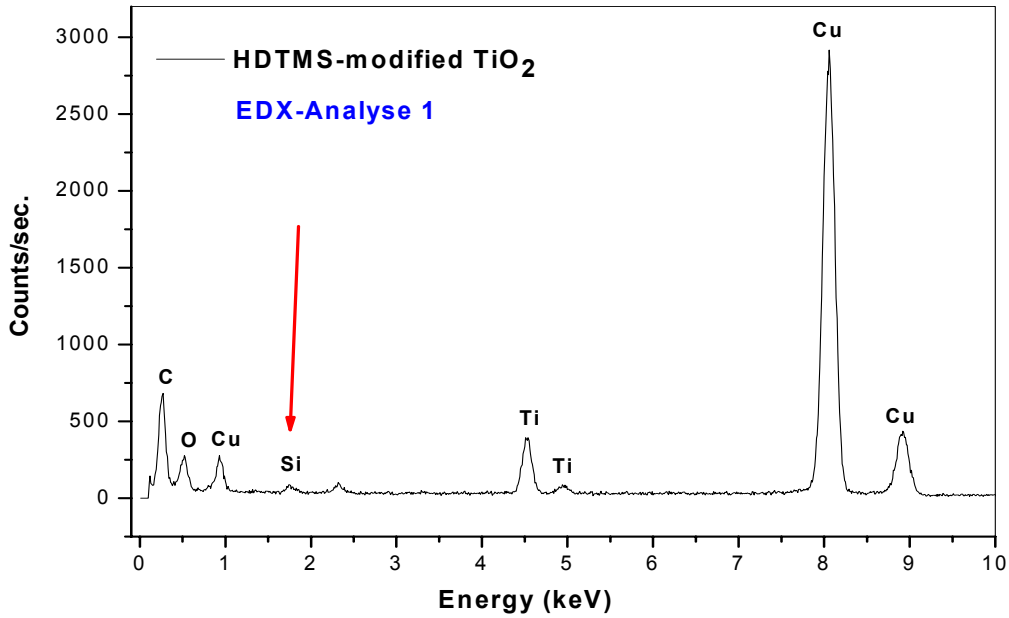


**Figure 33. EDX result of the HDTMS-modified $TiO_2$ nanoparticles.**

According to the TEM results, it seems that after modification of $TiO_2$ nanoparticles with HDTMS molecules, the particles are very good separated, dispersed. Namely, it is observed agglomeration-free $TiO_2$ nanoparticles. After modification with HDTMS molecules, HDTMS molecules form an apolar layer on the surface and this provides the separation of the nanoparticles. Also, according to the result of EDX, elemental composition of the HDTMS-modified $TiO_2$ nanoparticles was determined (Figure 30). The peaks of belonging to the ***Ti, O, C, Cu and Si*** were exactly determined by EDX. Also as further information, the peaks of belonging to the Cu are come from the grating of the instrument. The peak belongs to the Silicon is resulted from the silane molecules (HDTMS) on the surface of the $TiO_2$ nanoparticles. But, the peak intensity belongs to the Silicon is not much because the HDTMS molecules are big molecules and the previously reacted HDTMS molecules hindered the reaction of more HDTMS molecules with the surface of the $TiO_2$ nanoparticles. So the amount of the reacted HDTMS molecules is less. It is also proved by elemental analysis.

### 5.2.5. Modification with AMMO

After the modifications of $TiO_2$ nanoparticles with HTMS, DTMS, DDTMS and HDTMS, they were also modified with amine group containing silane molecule, with AMMO (according to section 4.4.1.5., page 50). After modification, it was characterized by GC/MS, elemental analysis, FT-IR, TEM and EDX. The results are shown in the following.

### 5.2.5.1. GC/MS result

After $TiO_2$ nanoparticles were modified with AMMO, the liberated methanol molecules were detected and compared with standart methanol solution. The results are shown in the following.

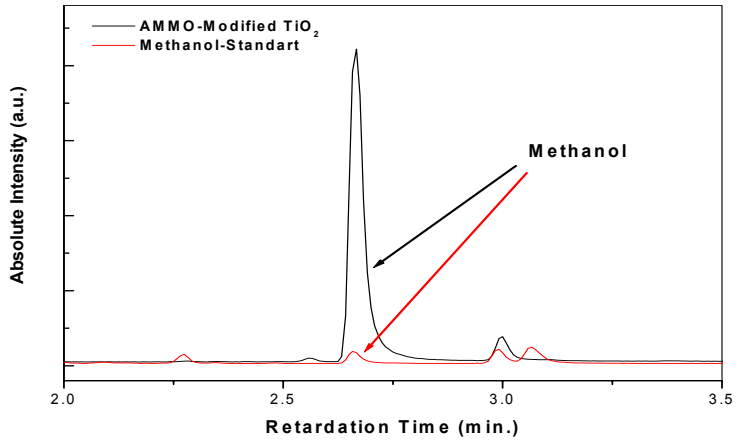


**Figure 34. GC/MS result of the AMMO-modified $TiO_2$ nanoparticles.**

According to the Figure 34, the liberated methanol molecules resulted from the reaction of –OH groups on $TiO_2$ nanoparticles with Si-O-$CH_3$ groups of AMMO molecules for the formation of Si-O-Ti covalent bonds on the surface.

### 5.2.5.2. Elemental analysis result

After the AMMO-modified $TiO_2$ powder was dried, it was characterized by elemental analysis. The result is shown in the following.

| Powder | C% | H% | N% |
|---|---|---|---|
| AMMO-modified $TiO_2$ powder | 11,24 | 2,69 | 1,24 |
| Unmodified $TiO_2$ powder | 8,38 | 2,13 | 0,0 |

According to this result, the increase in the carbon and hydrogen percent indicates that $TiO_2$ nanoparticles were modified with AMMO molecules. Furthermore, it is interesting that the increase in the amount of carbon of the AMMO-modified $TiO_2$ nanoparticles is more than that of the HTMS-modified $TiO_2$ nanoparticles. The reason for that finding might be various interaction types between AMMO molecules and $TiO_2$ surfaces. According to the literature, there are some various interaction types between amino groups and inorganic surfaces: 1) the amine may enter into hydrogen bonding interaction with surface hydroxyl group, 2) the

basic amine function may form and ionic bonding with a surface hydroxyl group. This type of interaction is more stable than the former interaction, 3) the hydrogen-bonded molecules may self-catalyze the condensation of the silanol with a surface hydroxyl group, and covalent siloxane bond is formed [252-256]. Because of the mentioned interactions, in this experiment, much more AMMO molecules might interact with $TiO_2$ surface besides covalent bonding to the surface. Thus, the increase in the carbon amount of the AMMO-modified $TiO_2$ nanoparticles is more than that of the HTMS-modified $TiO_2$ nanoparticles although the number of carbon atoms in HTMS molecule is twice more than that in AMMO molecule.

### 5.2.5.3. FT-IR analysis result

After the AMMO-modified $TiO_2$ powder was dried, it was characterized by FT-IR. The result is shown in the Figure 35.

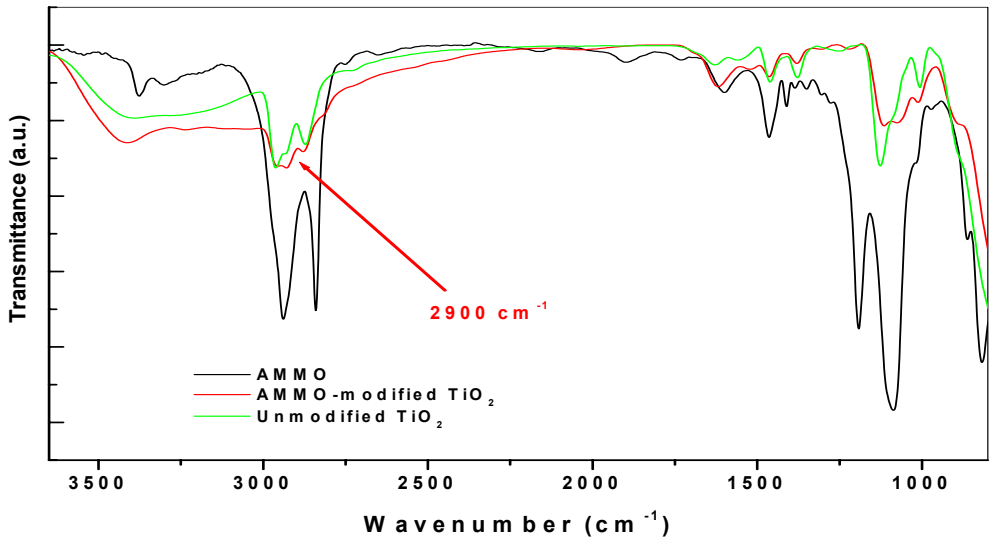


**Figure 35. FT-IR spectrums of the AMMO-modified $TiO_2$ powder, AMMO and unmodified $TiO_2$ powder.**

In the Figure 35, it is too difficult to characterize whether $TiO_2$ nanoparticles were modified with AMMO or not. Generally, after $TiO_2$ nanoparticles were modified with silanes, normally Ti-O-Si bonds occur and this bond appears at around 920-950 $cm^{-1}$ in the FT-IR spectrums. But it can't be detected in this area of the spectrum. But after modification, another possibility to prove this modification is the increase in the intensity of $-CH_2-$ and $-CH_3$ absorption bands at around 2800-3000 $cm^{-1}$. Unfortunately, the AMMO-modified $TiO_2$ powder does not show any increase at this area. Namely, the modification of $TiO_2$ nanoparticles with AMMO can't be

proved by FT-IR measurement. Of course, this modification was proved by GC/MS measurement and elemental analysis.

### 5.2.5.4. TEM and EDX results of the AMMO-modified $TiO_2$ nanoparticles

After $TiO_2$ nanoparticles were modified with AMMO molecules, the appearance of the AMMO-modified $TiO_2$ nanoparticles was investigated by TEM and elemental composition of the AMMO-modified $TiO_2$ nanoparticles was determined by EDX. The results are shown in the following Figure 36, 37, 38, 39, 40, 41.

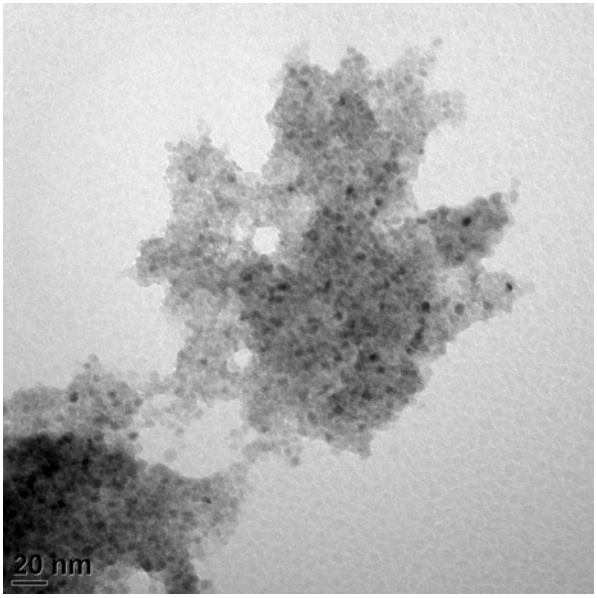


**Figure 36. TEM picture of the AMMO-modified $TiO_2$ nanoparticles.**

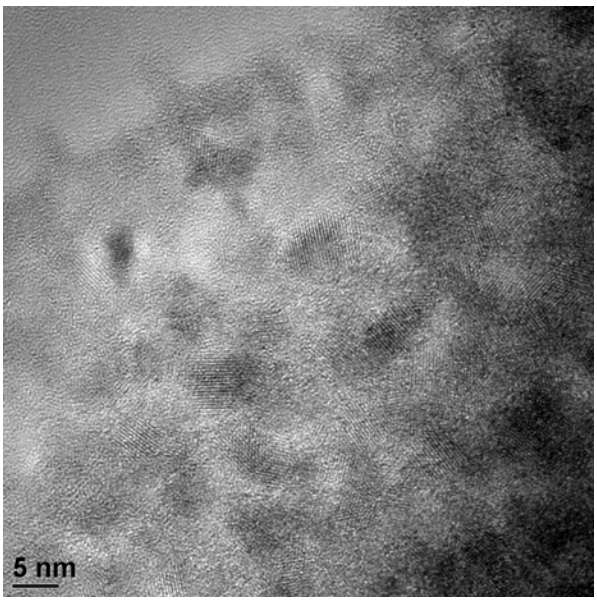


**Figure 37. TEM picture of the AMMO-modified $TiO_2$ nanoparticles.**

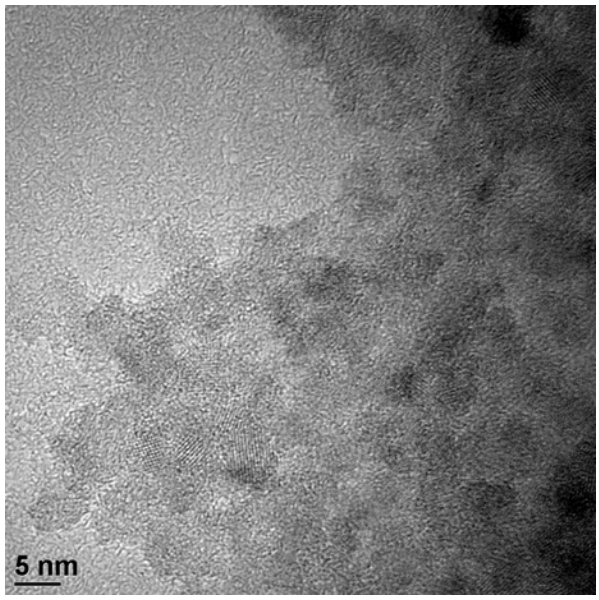


**Figure 38. TEM picture of the AMMO-modified $TiO_2$ nanoparticles.**

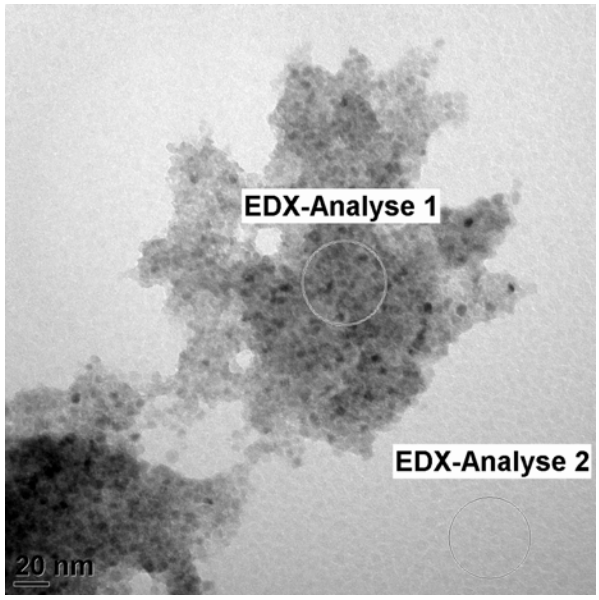


**Figure 39. TEM picture of the AMMO-modified $TiO_2$ nanoparticles.**

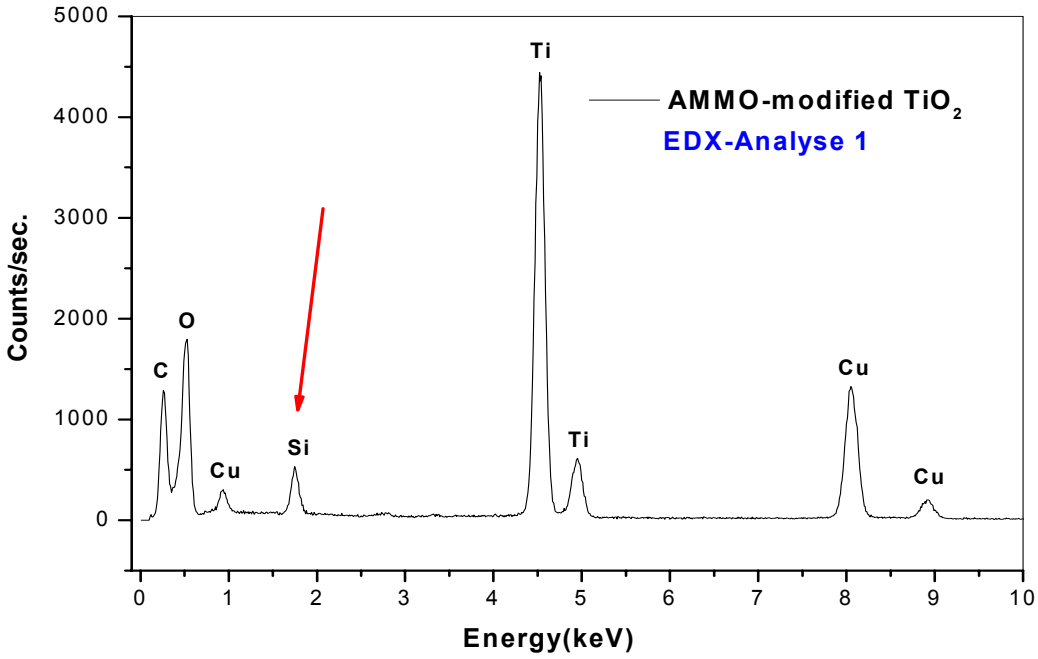


**Figure 40. EDX result of the AMMO-modified $TiO_2$ nanoparticles.**

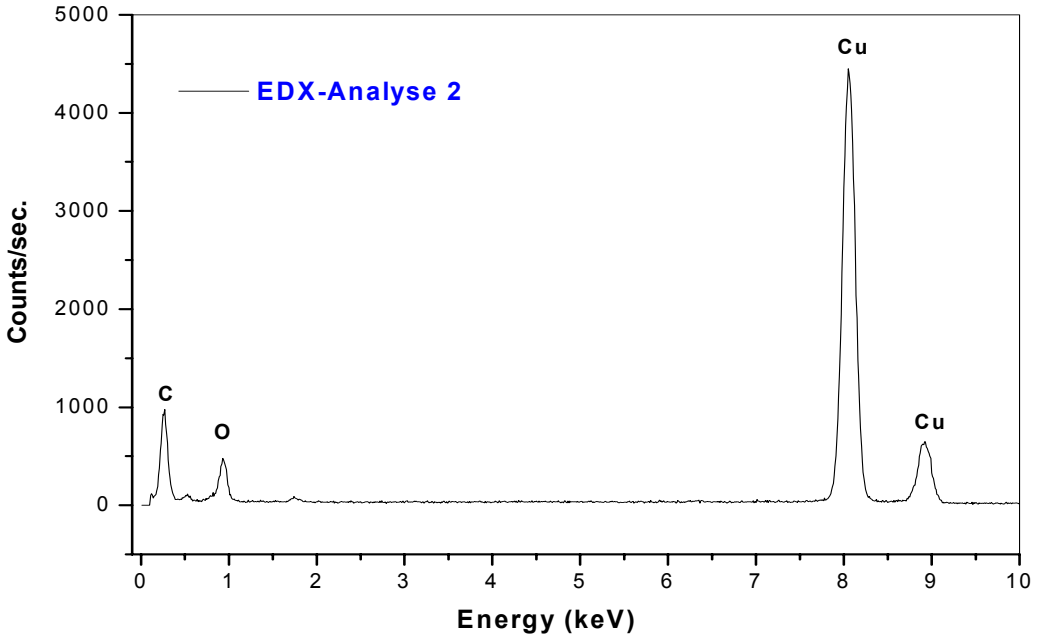


**Figure 41. EDX result of the AMMO-modified $TiO_2$ nanoparticles.**

According to the TEM results, it seems that after modification of $TiO_2$ nanoparticles with AMMO molecules, the particles are not separated, namely $TiO_2$ nanoparticles are agglomerated. After modification with AMMO molecules, because AMMO molecules are small molecules and they formed a polar layer on the surface, the AMMO-modified $TiO_2$

interacted among themselves. These reasons provided the agglomeration of the nanoparticles. Also, according to the result of EDX, elemental composition of the AMMO-modified $TiO_2$ nanoparticles was determined. For this reason, two circles in the Figure 39 were signed for EDX analysis (EDX-Analyse 1 and EDX-Analyse 2). The circle belongs to the EDX-Analyse 1 related to the place having much $TiO_2$ nanoparticles and the circle belongs to the EDX-Analyse 2 related to the place not having $TiO_2$ nanoparticles. It seems that although ***C, O, Cu and Si*** were detected by EDX-Analyse 1 (the place having much $TiO_2$ nanoparticles), only ***C, O and Cu*** were detected by EDX-Analyse 2 (the place not having $TiO_2$ nanoparticles). Also as further information, the peaks of belonging to the Cu are come from the grating of the instrument. It is concluded from these results that $TiO_2$ nanoparticles were really modified with AMMO molecules and this modification is proved by EDX. Furthermore, by the comparison of the results of the AMMO-modified $TiO_2$ nanoparticles and the HDTMS-modified $TiO_2$ nanoparticles, it is concluded that the peak intensity belongs the **silicon** in the AMMO-modified $TiO_2$ nanoparticles is much more than that in the HDTMS-modified $TiO_2$ nanoparticles. Its reason is resulted from the difference in the structures of the modification agents. Because AMMO molecules are small molecules with respect to the HDTMS molecules, the sterical effect of AMMO molecules on the surface of $TiO_2$ nanoparticles is less than that of the HDTMS molecules. Consequently, much more AMMO molecules reacted and interacted with the surface of $TiO_2$ nanoparticles. Because of these reasons, the peak intensity of the **silicon** in the AMMO-modified $TiO_2$ nanoparticles is much more than that in the HDTMS-modified $TiO_2$ nanoparticles (Figure 33 and 40). These results are exactly compatible with the elemental results of the AMMO- and HDTMS-modified $TiO_2$ nanoparticles.

#### 5.2.5.5. Short evaluation on the modification of $TiO_2$ nanoparticles with silanes

According to above results, after $TiO_2$ nanoparticles were modified with silanes with different molecular weights, methanol molecules were liberated from the surfaces of $TiO_2$ nanoparticles by means of the reaction of –OH groups on the surface with methoxy groups of silanes as expected and methanol molecules, which are liberated from the nanoparticle surfaces, were detected by GC/MS and it is also understood that methanol molecules in the measurements were only resulted from the nanoparticle modifications. Thus, the formation of Ti-O-Si covalent bonds was confirmed by GC/MS. It is also known that covalent bond formation on the surface is one possibility of the linking organic groups to inorganic backbones (others; complex formation and ionic bond formation) [17, 18].

According to the elemental analysis results, the amount of carbon and hydrogen on the surface increased after modifications. As the number of carbon atoms in the HDTMS

molecule is more than that in the other alkylsilanes, the amount of carbon of the HDTMS-modified $TiO_2$ nanoparticles increased more than that of the other silanes-modified $TiO_2$ nanoparticles. As for the modification with AMMO, the increase in the amount of carbon is more than that with HTMS. Its reasons might be various interaction types between AMMO and $TiO_2$ surfaces. Namely, because of the mentioned interactions, much more AMMO molecules might interact with $TiO_2$ surface besides covalent bonding to the surface. For this reason, the increase in the amount of carbon of the AMMO-modified $TiO_2$ nanoparticles is more than that of the HTMS-modified $TiO_2$ nanoparticles although the number of carbon atoms in the HTMS molecule is twice more than that in the AMMO molecule. As for FT-IR results, all modifications weren't proved by FT-IR measurements, for example; AMMO and HTMS modifications. It might be low concentration of modification agents in the modified-$TiO_2$ nanoparticles.

Also, after $TiO_2$ nanoparticles were modified with AMMO molecules and also with HDTMS molecules, the appearance of the AMMO-modified $TiO_2$ nanoparticles and the HDTMS-modified $TiO_2$ nanoparticles was investigated by TEM and elemental compositions of the AMMO-modified $TiO_2$ nanoparticles and the HDTMS-modified $TiO_2$ nanopartcles were determined by EDX. According to the results, **silicon** is detected after both modifications. The amount of the Si on the surface of the nanoparticle with respect to the intensities of the peaks was detected and it is concluded that Si amount is related to the structure of the modification agent. Also, according to the TEM results of the AMMO-modified $TiO_2$ nanoparticles and the HDTMS-modified $TiO_2$ nanoparticles, it is concluded that the dispersations of the modified-$TiO_2$ nanoparticles are also related to the structures of the modification agents (see 5.2.4. and 5.2.5).

Furthermore, according to the literature the surface areas of $TiO_2$ nanoparticles used or produced in the literature are less than those in the present work, the sizes of $TiO_2$ nanoparticles were bigger than 6 nm ($TiO_2$ nanoparticles with a diameter of 6 nm in this work) and it is very important point that $TiO_2$ nanoparticles used in the present work were agglomeration-free. Also, of all silanes, aminosilanes were chiefly used in the surface modifications and of all nanoparticles, $SiO_2$ nanoparticles were chiefly used in the surface modifications [255-257]. The other silanes used in this work were not worked. In addition, $TiO_2$ nanoparticles produced or worked in the literature didn't have –OR groups on their surfaces.

### 5.2.6. Modification with 10-undecylenic acid

After the modifications of $TiO_2$ nanoparticles with silanes with different molecular weights by forming Si-O-Ti covalent bonds on their surface, the complexation reaction on $TiO_2$

nanoparticles was carried out as another possibility for the linking of organic groups to inorganic backbones. $TiO_2$ nanoparticles were modified with 10-undecylenic acid containing double bond (according to section 4.4.1.6., page 51) and then, the 10-undecylenic acid-modified $TiO_2$ nanoparticles were characterized by elemental analysis and FT-IR. Also, conversion of 10-undecylenic acid was determined by FT-IR measurements. The results are shown in the following.

### 5.2.6.1. Elemental analysis result

After the 10-undecylenic acid-modified $TiO_2$ powder was dried, it was characterized by elemental analysis. The result is shown in the following.

| Powder | C% | H% | N% |
|---|---|---|---|
| 10-Undecylenic acid-modified $TiO_2$ powder | 17,61 | 3,23 | 0,0 |
| Unmodified $TiO_2$ powder | 8,38 | 2,13 | 0,0 |

According to this result, the increase in the carbon and hydrogen percentages as compared to the unmodified nanoparticles indicates that $TiO_2$ nanoparticles were modified with 10-undecylenic acid.

### 5.2.6.2. FT-IR analysis result

After the 10-undecylenic acid-modified $TiO_2$ powder was dried, it was characterized by FT-IR. The result is shown in the following.

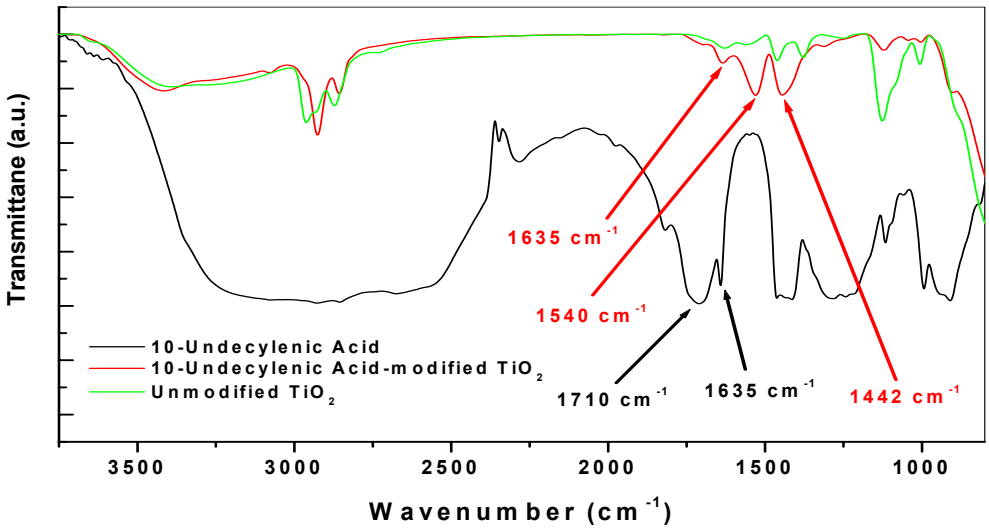


**Figure 42. FT-IR spectrums of the 10-undecylenic acid-modified $TiO_2$ powder, 10-undecylenic acid and unmodified $TiO_2$ powder.**

In the Figure 42, the spectrum of the 10-undecylenic acid molecule shows one broad peak at around 1710 $cm^{-1}$ belongs to carbonyl stretch [258-260] and one peak at around 1635 $cm^{-1}$ belongs to double bond. But, the spectrum of the unmodified-$TiO_2$ nanoparticles does not show these peaks in the same area. After modification of $TiO_2$ nanoparticles with the 10-undecylenic acid, the peak at 1710 $cm^{-1}$ belongs to carbonyl stretch of the 10-undecylenic acid disappeared and two peaks at around 1540 $cm^{-1}$ and 1442 $cm^{-1}$ in the spectrum of the 10-undecylenic acid-modified $TiO_2$ nanoparticles occurred and they are ascribed to $\nu(COO)_{asym}$ and $\nu(COO)_{sym}$ respectively [258-260]. Also, these two peaks are not observed in the spectrum of the unmodified $TiO_2$ particles. Furthermore, one peak at around 1635 $cm^{-1}$ is ascribed to absorption of double bond in the spectrum of the 10-undecylenic acid-modified $TiO_2$ nanoparticles. Also, $-CH_2-$ and $-CH_3$ absorption bands at around 2800-3000 $cm^{-1}$ increased a little as compared to those of the unmodified $TiO_2$ nanoparticles because of linking 10-undecylenic acid molecules to $TiO_2$ nanoparticles. Consequently, it is concluded that $TiO_2$ nanoparticles were modified with 10-undecylenic acid molecules.

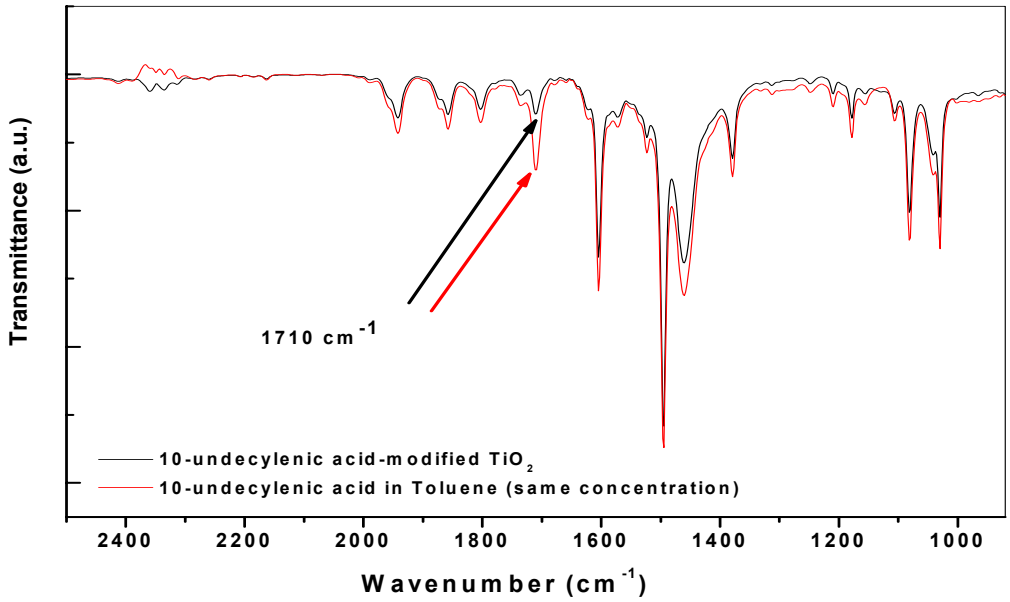


**Figure 43. FT-IR spectrums of the 10-undecylenic acid-modified $TiO_2$ and 10-undecylenic acid in toluene (same concentration).**

According to the Figure 43, it is observed that the intensity of the peak at 1710 $cm^{-1}$ that belongs to the carbonyl stretch of 10-undecylenic acid decreased by 52,1 % after modification. It is concluded that the modification of $TiO_2$ nanoparticles with 10-undecylenic acid molecules was achieved and the conversion of 10-undecylenic acid was detected to be 52,1 %.

### 5.2.7. Modification with stearic acid

After $TiO_2$ nanoparticles were modified with 10-undecylenic acid containing double bond, they were also modified with stearic acid with higher molecular weight for the complexation reaction on the surface (according to section 4.4.1.7., page 51) and then, the stearic acid-modified $TiO_2$ nanoparticles were characterized by elemental analysis and FT-IR. The results are shown in the following.

#### 5.2.7.1. Elemental analysis result

After the stearic acid-modified $TiO_2$ powder was dried, it was characterized by elemental analysis. The result is shown in the following.

| Powder | C% | H% | N% |
|---|---|---|---|
| Stearic acid-modified $TiO_2$ powder | 26,98 | 4,73 | 0,0 |
| Unmodified $TiO_2$ powder | 8,38 | 2,13 | 0,0 |

According to this result, the increase in the carbon and hydrogen percentages as compared to the unmodified nanoparticles indicates that $TiO_2$ nanoparticles were modified with stearic acid.

#### 5.2.7.2. FT-IR analysis result

After the stearic acid-modified $TiO_2$ powder was dried, it was characterized by FT-IR. The result is shown in the following.

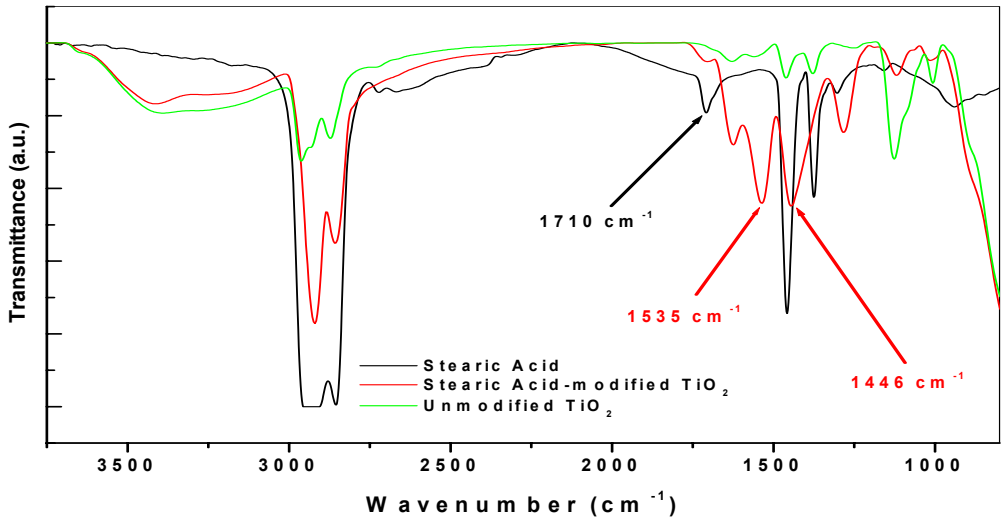


**Figure 44. FT-IR spectrums of the stearic acid-modified $TiO_2$ powder, stearic acid and unmodified $TiO_2$ powder.**

In the Figure 44, the spectrum of the stearic acid molecule shows one peak at around 1710 $cm^{-1}$ belongs to carbonyl stretch of stearic acid and the spectrum of the unmodified-$TiO_2$ nanoparticles does not show these peaks in the same area. After modification of $TiO_2$ nanoparticles with the stearic acid, the peak at around 1710 $cm^{-1}$ that belongs to carbonyl stretch of the stearic acid disappeared and two peaks at around 1535 $cm^{-1}$ and 1446 $cm^{-1}$ in the spectrum of the stearic acid-modified $TiO_2$ nanoparticles occurred and they are ascribed to $\nu(COO)_{asym}$ and $\nu(COO)_{sym}$ respectively [258-260]. Also, these two peaks are not observed in the spectrum of the unmodified $TiO_2$ nanoparticles. Furthermore, -$CH_2$- and -$CH_3$ absorption bands at around 2800-3000 $cm^{-1}$ increased as compared to those of the unmodified $TiO_2$ nanoparticles because of linking stearic acid molecules to $TiO_2$ nanoparticles. Thus, it is concluded that $TiO_2$ nanoparticles were modified with stearic acid molecules.

### 5.2.8. Modification with oleic acid

After the modifications of $TiO_2$ nanoparticles with 10-undecylenic acid and stearic acid, $TiO_2$ nanoparticles were also modified with oleic acid containing double bond (according to section 4.4.1.8. page 52) and then, the oleic acid-modified $TiO_2$ nanoparticles were characterized by elemental analysis and FT-IR. The results are shown in the following.

#### 5.2.8.1. Elemental analysis result

After the oleic acid-modified $TiO_2$ powder was dried, it was characterized by elemental analysis. The result is shown in the following.

| Powder | C% | H% | N% |
|---|---|---|---|
| Oleic acid-modified $TiO_2$ powder | 22,15 | 3,75 | 0,0 |
| Unmodified $TiO_2$ powder | 8,38 | 2,13 | 0,0 |

According to this result, the increase in the carbon and hydrogen percentages as compared to the unmodified nanoparticles indicates that $TiO_2$ nanoparticles were modified with oleic acid molecules.

#### 5.2.8.2. FT-IR analysis result

After the oleic acid-modified $TiO_2$ powder was dried, it was characterized by FT-IR. The result is shown in the following.

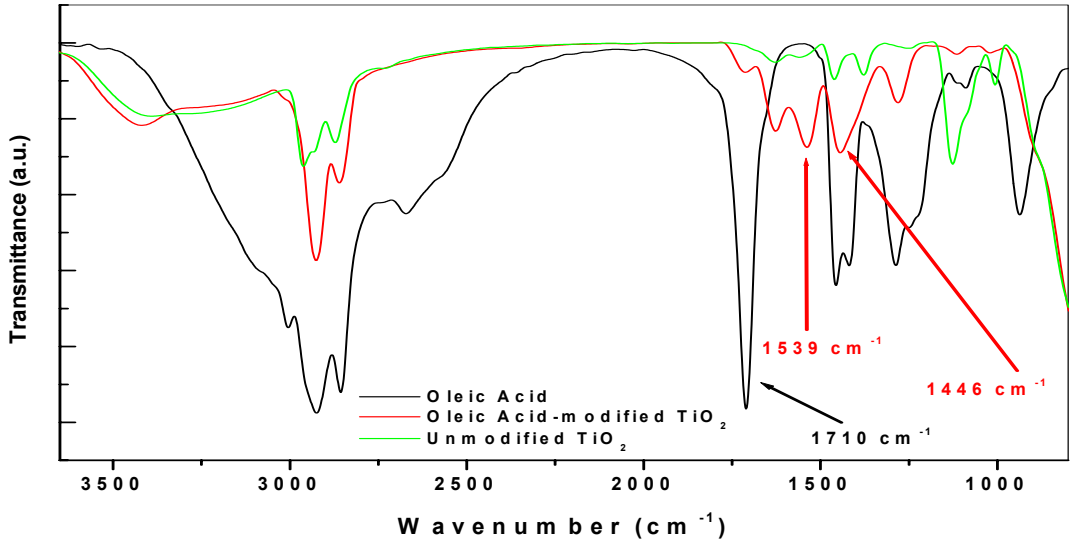


**Figure 45. FT-IR spectrums of the oleic acid-modified $TiO_2$ powder, oleic acid and unmodified $TiO_2$ powder**.

In the Figure 45, the spectrum of the oleic acid molecule shows one peak at around 1710 $cm^{-1}$ belongs to carbonyl stretch of oleic acid and the spectrum of the unmodified-$TiO_2$ nanoparticles does not show these peaks in the same area. After modification of $TiO_2$ nanoparticles with the oleic acid, the peak at around 1710 $cm^{-1}$ belongs to carbonyl stretch of the stearic acid disappeared and two peaks at around 1539 $cm^{-1}$ and 1446 $cm^{-1}$ in the spectrum of the oleic acid-modified $TiO_2$ nanoparticles occurred and they are ascribed to $\nu(COO)_{asym}$ and $\nu(COO)_{sym}$ respectively [258-260]. Also, these two peaks are not observed in the spectrum of the unmodified $TiO_2$ nanoparticles. Furthermore, $-CH_2-$ and $-CH_3$ absorption bands at around 2800-3000 $cm^{-1}$ increased as compared to those of the unmodified $TiO_2$ nanoparticles because of linking oleic acid molecules to $TiO_2$ nanoparticles. Thus, it is concluded that $TiO_2$ nanoparticles were modified with oleic acid molecules.

### 5.2.8.3. Short evaluation on the modification of $TiO_2$ nanoparticles with carboxylic acids

After $TiO_2$ nanoparticles were modified with carboxylic acids, 1-propanol molecules were liberated from $TiO_2$ nanoparticle surface by means of complexation reaction of $-OC_3H_7$ groups on the surface with carboxylic acid groups. Thus, the complex formation on the surface of $TiO_2$ nanoparticles is carried out as one possibility of the linking organic groups to inorganic backbones. Furthermore, according to the elemental analysis results, the amount of carbon and hydrogen in all carboxylic acid-modified powders increased as compared to the unmodified $TiO_2$ nanoparticles as expected. Also, carbon amount of the carboxylic acid-

modified $TiO_2$ nanoparticles were more than those of the silane-modified nanoparticles. For example; although the number of carbon atoms in the HDTMS molecule is close to that in the stearic acid molecule, it is observed that the increase in carbon amount of the stearic acid-modified $TiO_2$ nanoparticles is much more that that of the HDTMS-modified $TiO_2$ nanoparticles. Its reason might be because of reaction difference of silanes and carboxylic acids with surfaces. Namely, silanes react with –OH groups on $TiO_2$ nanoparticles but the carboxylic acids react with $–OC_3H_7$ groups on $TiO_2$ nanoparticles. Although one carboxylic acid molecule reacts with one $–OC_3H_7$ group, one silane can react with three –OH groups on the surface. In addition, for the modification of $TiO_2$ nanoparticles with 10-undecylenic acid, the conversion of 10-undecylenic acid was detected to be 52,1 % by means of FT-IR measurements. In this work, anatase $TiO_2$ nanoparticles, which have both $–OC_3H_7$ and –OH groups, were firstly synthesized and then the $–OC_3H_7$ groups on the surface were complexed with carboxylic acid molecules. On the contrary, in the literature titanium alkoxides were firstly modified with carboxylic acids and then the carboxylic acid-modified $TiO_2$ nanoparticles were synthesized [261]. There are several works related to modifications of metal alkoxides with carboxylic acids [48, 53, 54, 261].

### 5.2.9. Modification with AAA

After $TiO_2$ nanoparticles were modified with silanes, carboxylic acids, they were modified with a β-ketoester molecule, with AAA (according to section 4.4.1.9., page 52). This modification is a typical complexation reaction. It is known that 1-propanol molecules are liberated from the surface of $TiO_2$ nanoparticle with this complexation reaction. Then, the AAA-modified $TiO_2$ nanoparticles were characterized by elemental analysis and FT-IR. The results are shown in the following.

#### 5.2.9.1. Elemental analysis result

After the AAA-modified $TiO_2$ powder was dried, it was characterized by elemental analysis. The result is shown in the following.

| Powder | C% | H% | N% |
|---|---|---|---|
| AAA-modified $TiO_2$ powder | 14,66 | 2,58 | 0,0 |
| Unmodified $TiO_2$ powder | 8,38 | 2,13 | 0,0 |

According to this result, the increase in the carbon and hydrogen percentages as compared to the unmodified nanoparticles indicates that $TiO_2$ nanoparticles were modified with AAA molecules.

### 5.2.9.2. FT-IR analysis result

After the AAA-modified $TiO_2$ powder was dried, it was characterized by FT-IR. The result is shown in the following.

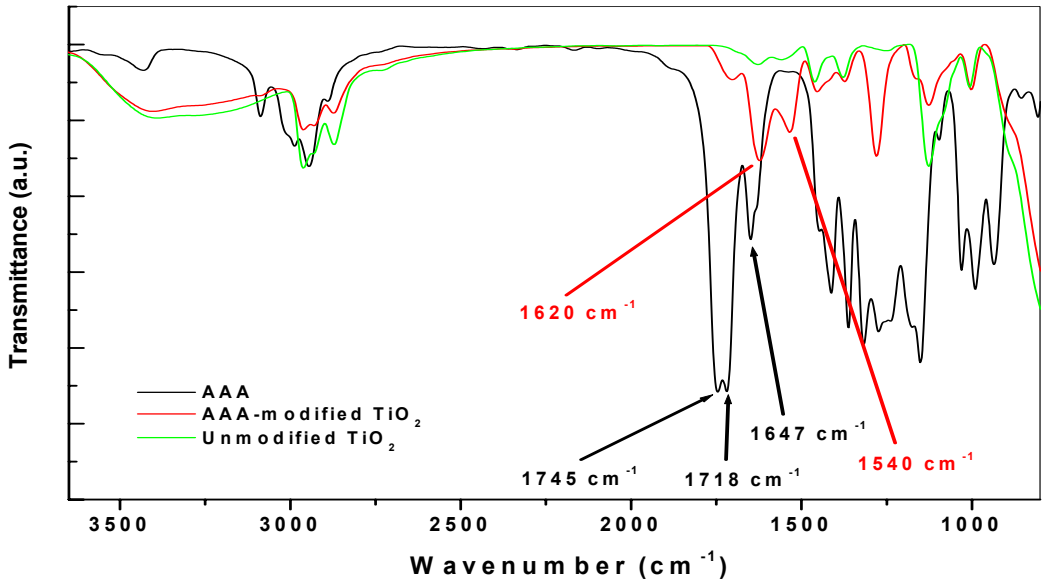


**Figure 46. FT-IR spectrums of the AAA-modified $TiO_2$ powder, AAA and unmodified $TiO_2$ powder.**

In the Figure 46, the spectrum of the AAA molecule shows two peaks at around 1745 $cm^{-1}$ and 1718 $cm^{-1}$ that belongs to carbonyl stretches of AAA and one peak at 1647 $cm^{-1}$ that belongs to double bond of AAA. But, the spectrum of the unmodified-$TiO_2$ nanoparticles does not show these peaks in the same area. After modification of $TiO_2$ nanoparticles with the AAA, the peaks at around 1745 $cm^{-1}$ and 1718 $cm^{-1}$ belongs to carbonyl stretches of the AAA disappeared and two peaks at around 1620 $cm^{-1}$ and 1540 $cm^{-1}$ in the spectrum of the AAA-modified $TiO_2$ nanoparticles occurred and they are ascribed to the bands of the stretching vibrations $\nu$(C=O) and $\nu$(C=C) of the enolic forms of the β-ketoesters respectively according to the literature [76]. Also, these two peaks are not observed in the spectrum of the unmodified $TiO_2$ nanoparticles. Thus, it is concluded that the complexation reaction of $TiO_2$ nanoparticles with AAA molecules was proved by FT-IR measurements on the basis of the literature.

### 5.2.9.3. Short evaluation on the complexation of $TiO_2$ nanoparticles with β-ketoester

It is known that organic groups can be linked to inorganic backbone by means of three different ways. One of them is the formation of complex structures on the surface of the nanoparticle surface. For this reason, one β-ketoester molecule, AAA was chosen for this modification. After $TiO_2$ nanoparticles were modified with AAA, 1-propanol molecules were liberated from the nanoparticle surface by means of the complexation reaction of $–OC_3H_7$ groups on the surface with AAA. Furthermore, according to the elemental analysis results, the amount of carbon and hydrogen on the surface increased as expected. Also, the amount of carbon of the AAA-modified nanoparticles was almost more than those of all silane-modified nanoparticles except for that of the HDTMS-modified nanoparticles. It is known that silanes react with –OH groups on $TiO_2$ nanoparticles but AAA molecules reacts with $–OC_3H_7$ groups on $TiO_2$ nanoparticles. Although β-ketoester molecules react with one $–OC_3H_7$ group on $TiO_2$ nanoparticle, silanes can react with three –OH groups. In this work, anatase $TiO_2$ nanoparticles, which have both $–OC_3H_7$ and –OH groups, were firstly synthesized and then the $–OC_3H_7$ groups on the surface were complexed with β-ketoester molecules. On the contrary, in the literature, titanium alkoxides were firstly modified with β-ketoester molecules and then the β-ketoester-modified $TiO_2$ nanoparticles were synthesized [262]. There are several works related to modifications of metal alkoxides with β-ketoester molecules [74, 76, 263].

## 5.3. Characterization of the urea molecules and modifications of $TiO_2$ nanoparticles with the urea molecules

Another section to functionalize $TiO_2$ nanoparticles is the modifications of $TiO_2$ nanoparticles with the molecules containing urea and ethoxysilane groups, named as urea molecules in this work. In this work, the urea molecules were synthesized by means of a coupling reaction between an isocyanate molecule, 3-IPTES and 10 amine molecules: amine molecules containing two amine groups in their molecules: ethylenediamine, 1,6-diaminohexane, 1,8-diaminooctane, 1,12-diaminododecane, DMS-A15, DMS-A21 and amine molecules containing one amine group in their molecules: pentylamine, octylamine, 1-dodecylamine, octadecylamine. After 10 different urea molecules were synthesized, they were characterized by FT-IR. After that, $TiO_2$ nanoparticles were modified with urea molecules by forming Ti-O-Si covalent bonds on $TiO_2$ surface. Afterwards, the modifications of $TiO_2$ nanoparticles with urea molecules were characterized by GC/MS, FT-IR and elemental analysis.

### 5.3.1. Characterization of Ethylenurea

After Ethylenurea molecule was synthesized by means of the coupling reaction between 3-IPTES and ethylenediamine (according to section 4.5.1., page 53), it was characterized by FT-IR. The result is shown in the following.

#### 5.3.1.1. FT-IR result

After Ethylenurea was synthesized, it was characterized by FT-IR. The result is shown in the following.

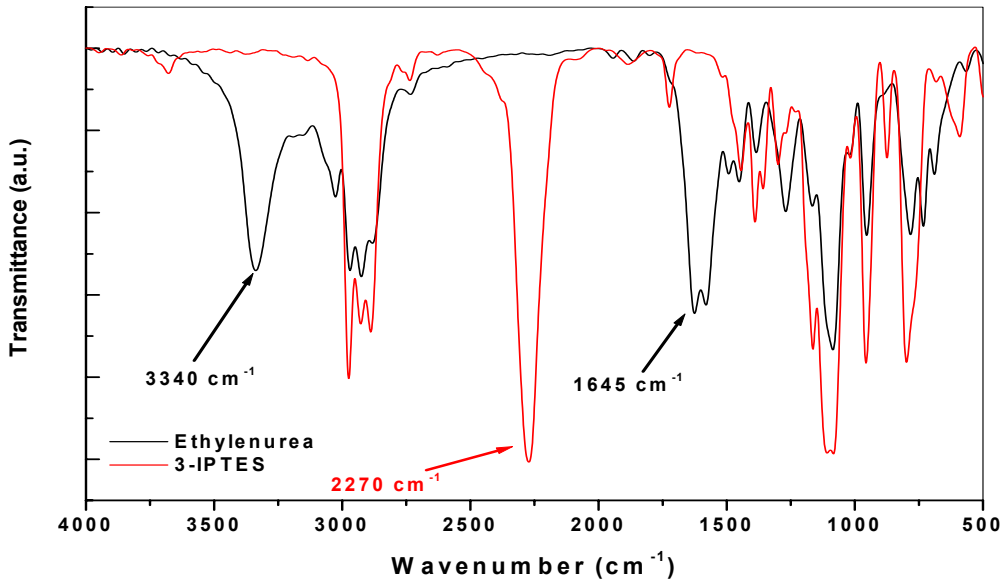


**Figure 47. FT-IR spectrums of Ethylenurea (black line) and 3-IPTES (red line).**

In the Figure 47, the strong absorption bands at around 3340 $cm^{-1}$ (N-H stretch) and at around 1645 $cm^{-1}$ (C=O stretch) for ethylenurea confirm the formation of urea linkages. Also, the absence of a strong absorption band at around 2270 $cm^{-1}$ (due to NCO group) shows that the reaction is completed [241, 258].

#### 5.3.1.2. Characterization of the Ethylenurea-modified $TiO_2$ nanoparticles

After Ethylenurea was synthesized, $TiO_2$ nanoparticles were modified with this molecule (section 4.6.1., page 55). The Ethylenurea-modified $TiO_2$ particles were characterized by GC/MS, FT-IR and elemental analysis. The results are shown in the following.

### 5.3.1.2.1. GC/MS result

After $TiO_2$ nanoparticles were modified with Ethylenurea molecules, the liberated ethanol molecules were detected by GC/MS. The result is shown in the following.

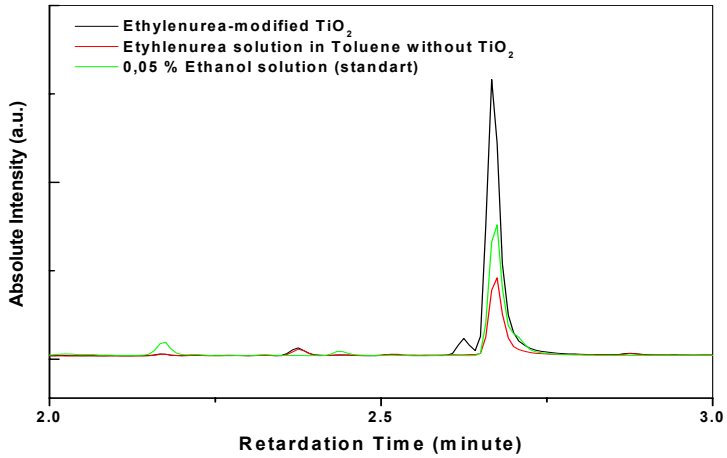


**Figure 48. GC/MS result of the Ethylenurea-modified $TiO_2$ powder.**

In the Figure 48, after modification of $TiO_2$ nanoparticles with Ethylenurea, the liberated ethanol molecules were detected by GC/MS and this result was compared with standart ethanol solution in toluene. Although water-free toluene was always used in the experiments, a little ethanol in the solution of Ethylenurea in toluene was also detected. But, the peak intensity of the Ethylenurea-modified $TiO_2$ nanoparticles is much bigger than that of Ethylenurea solution in toluene. Thus, it is concluded from GC/MS result that $TiO_2$ nanoparticles were modified with Ethylenurea molecules.

### 5.3.1.2.2. FT-IR result

After the Ethylenurea-modified $TiO_2$ powder was dried, it was characterized by FT-IR. The result is shown in the following.

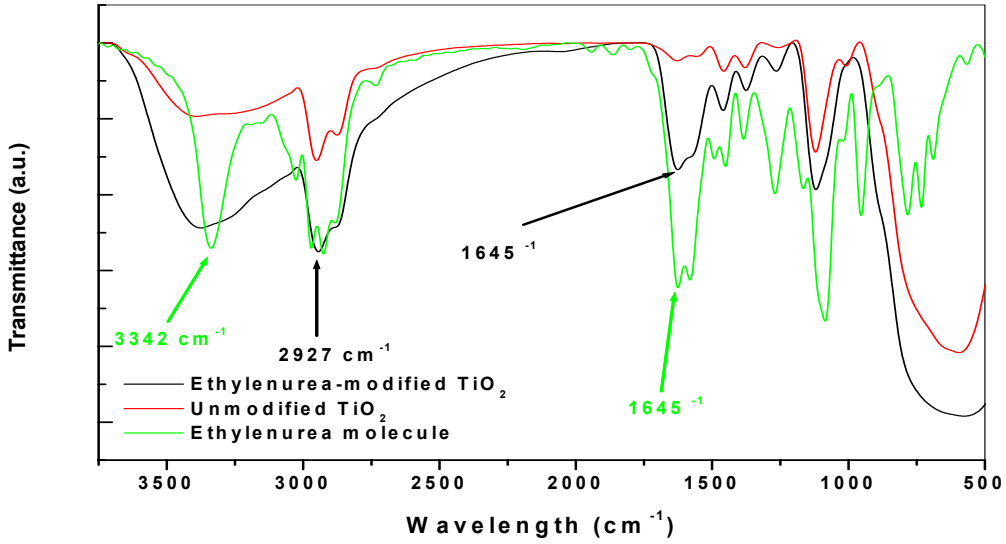


**Figure 49. FT-IR spectrums of the Ethylenurea-modified $TiO_2$ powder, Ethylenurea and unmodified $TiO_2$ powder.**

In the Figure 49, after $TiO_2$ nanoparticles were modified with Ethylenurea molecules, the urea peaks in the spectrum of Ethylenurea-modified nanoparticles seem still at around 1645 $cm^{-1}$ and 3342 $cm^{-1}$. In addition, $CH_3$-, -$CH_2$- absorbsion bands in the spectrum of Ethylenurea-modified $TiO_2$ nanoparticles increased at around 2927 $cm^{-1}$ as compared to the spectrum of unmodified nanoparticles. Thus, it is concluded that the modification of $TiO_2$ nanoparticles with Ethylenurea molecules was succeeded and proved by FT-IR.

### 5.3.1.2.3. Elemental analysis result

After the Ethylenurea-modified $TiO_2$ powder was dried, it was characterized by elemental analysis. The result is shown in the following.

| Powder | C% | H% | N% |
|---|---|---|---|
| Ethylenurea-modified $TiO_2$ powder | 13,26 | 2,92 | 1,53 |
| Unmodified $TiO_2$ powder | 8,38 | 2,13 | 0,0 |

According to this result, the increase in carbon, hydrogen and nitrogen percentages indicates that $TiO_2$ nanoparticles were modified with Ethylenurea molecules.

### 5.3.2. Characterization of 16Hexylurea

After the modification of $TiO_2$ nanoparticles with Ethylenurea, $TiO_2$ nanoparticles were also modified with another urea molecule with higher molecular weight, with 16Hexylurea molecules. After 16Hexylurea molecule was synthesized by means of the coupling reaction between 3-IPTES and 1,6-diaminohexane (according to section 4.5.2., page 53), it was characterized by FT-IR. The result is shown in the following.

#### 5.3.2.1. FT-IR result

After 16Hexylurea was synthesized, it was characterized by FT-IR. The result is shown in the following.

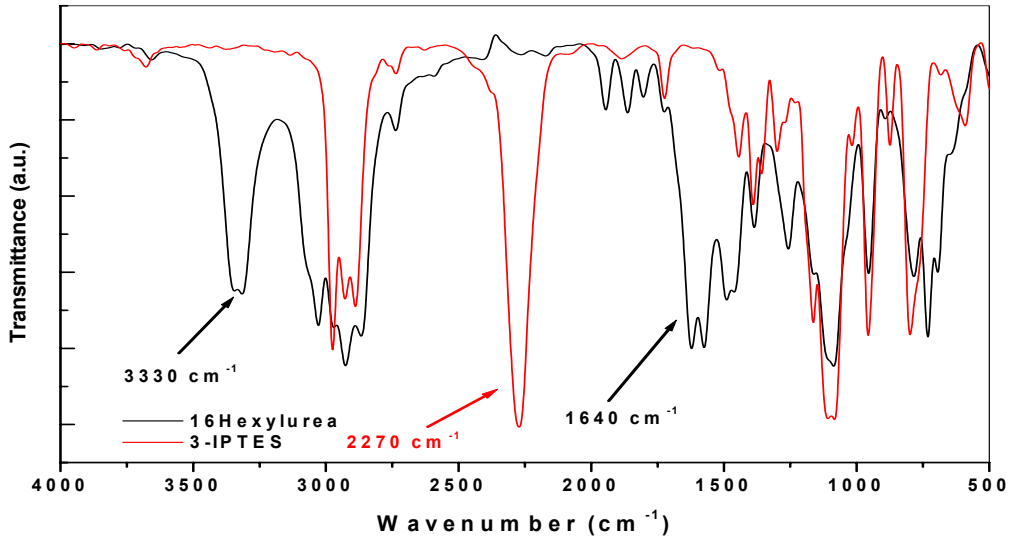


**Figure 50. FT-IR spectrums of 16Hexylurea (black line) and 3-IPTES (red line).**

In the Figure 50, the strong absorption bands at around 3330 $cm^{-1}$ (N-H stretch) and at around 1640 $cm^{-1}$ (C=O stretch) for 16Hexylurea confirm the formation of urea linkages. Also, the absence of a strong absorption band at around 2270 $cm^{-1}$ (due to NCO group) shows that the reaction is completed.

#### 5.3.2.2. Characterization of the 16Hexylurea-modified $TiO_2$ nanoparticles

After 16Hexylurea was synthesized, $TiO_2$ nanoparticles were modified with it (section 4.6.2., page 55). After modification, the 16Hexylurea-modified $TiO_2$ nanoparticles were characterized by GC/MS, FT-IR and elemental analysis.

### 5.3.2.2.1. GC/MS result

After $TiO_2$ nanoparticles were modified with 16Hexylurea molecules, the liberated ethanol molecules were detected by GC/MS. The result is shown in the following.

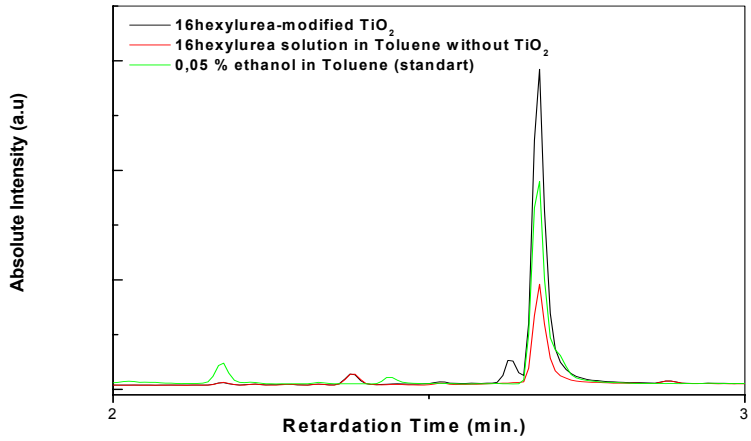


**Figure 51. GC/MS result of the 16Hexylurea-modified $TiO_2$ powder.**

In Figure 51, after modification of $TiO_2$ nanoparticles with 16Hexylurea, the liberated ethanol molecules were detected by GC/MS and this result was compared with standart ethanol solution. Although water-free toluene was always used in the experiments, a little ethanol in the solution of 16Hexylurea in toluene was also detected. But, the peak intensity of the 16Hexyurea-modified $TiO_2$ nanoparticles is much bigger than that of 16Hexyurea solution. Thus, it is concluded from GC/MS result that $TiO_2$ nanoparticles were modified with 16Hexylurea molecules.

### 5.3.2.2.2. FT-IR result

After the 16Hexylurea-modified $TiO_2$ powder was dried, it was characterized by FT-IR. The result is shown in the following.

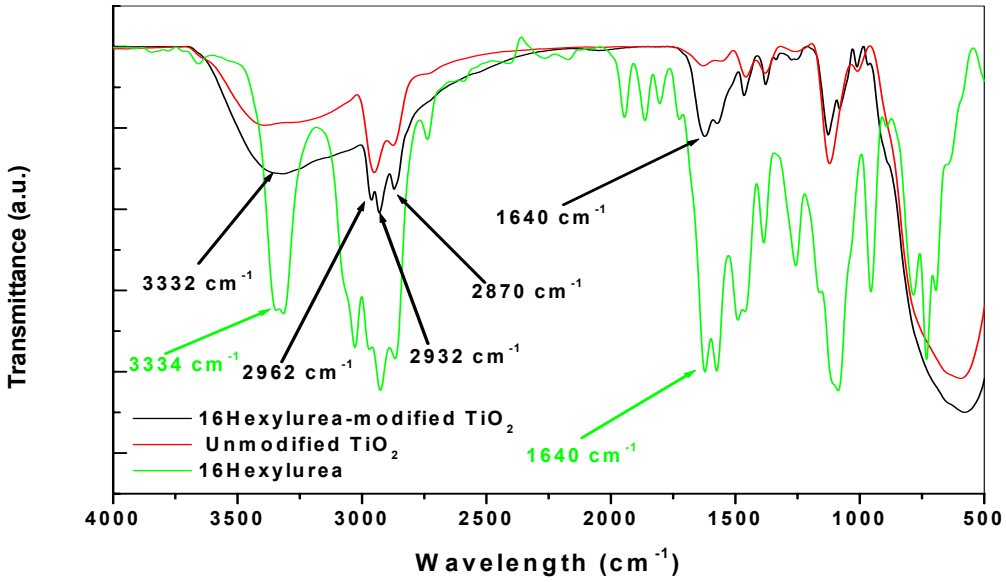


**Figure 52. FT-IR spectrums of the 16Hexylurea-modified $TiO_2$ powder, 16Hexylurea and unmodified $TiO_2$ powder.**

In the Figure 52, after $TiO_2$ nanoparticles were modified with 16Hexylurea molecules, urea peaks in the spectrum of 16Hexylurea-modified nanoparticles seem still at around 1640 $cm^{-1}$ and 3332 $cm^{-1}$. In addition, $CH_3$-, -$CH_2$- absorbsion bands in the spectrum of the 16Hexylurea-modified $TiO_2$ nanoparticles increased at around 2870 $cm^{-1}$, 2962 $cm^{-1}$ and 2932 $cm^{-1}$ as compared to the spectrum of the unmodified nanoparticles. Thus, it is concluded that the modification of $TiO_2$ nanoparticles with 16Hexylurea molecules was succeeded and proved by FT-IR.

### 5.3.2.2.3. Elemental analysis result

After the 16Hexylurea-modified $TiO_2$ powder was dried, it was characterized by elemental analysis. The result is shown in the following.

| Powder | C% | H% | N% |
|---|---|---|---|
| 16Hexylurea-modified $TiO_2$ powder | 14,10 | 3,03 | 1,46 |
| Unmodified $TiO_2$ powder | 8,38 | 2,13 | 0,0 |

According to this result, the increase in carbon, hydrogen and nitrogen percent indicates that $TiO_2$ nanoparticles were modified with 16Hexylurea molecules. Furthermore, the increase in carbon percentage of the 16Hexylurea-modified $TiO_2$ nanoparticles is little more than that of the Ethylenurea-modified $TiO_2$ nanoparticles although the number of carbon atoms in

16Hexyurea molecule is more than that in Ethylenurea molecule. The reason for that finding might be sterical hindrance effects.

### 5.3.3. Characterization of 18Octylurea

After the modifications of $TiO_2$ nanoparticles with Ethylenurea and 16Hexylurea, $TiO_2$ nanoparticles were also modified with another urea molecule with higher molecular weight, with 18Octylurea. After 18Octylurea molecule was synthesized by means of the coupling reaction between 3-IPTES and 1,8-octylamine (according to section 4.5.3., page 53), it was characterized by FT-IR. The result is shown in the following.

#### 5.3.3.1. FT-IR result

After 18Ocytlurea was synthesized, it was characterized by FT-IR. The result is shown in the following.

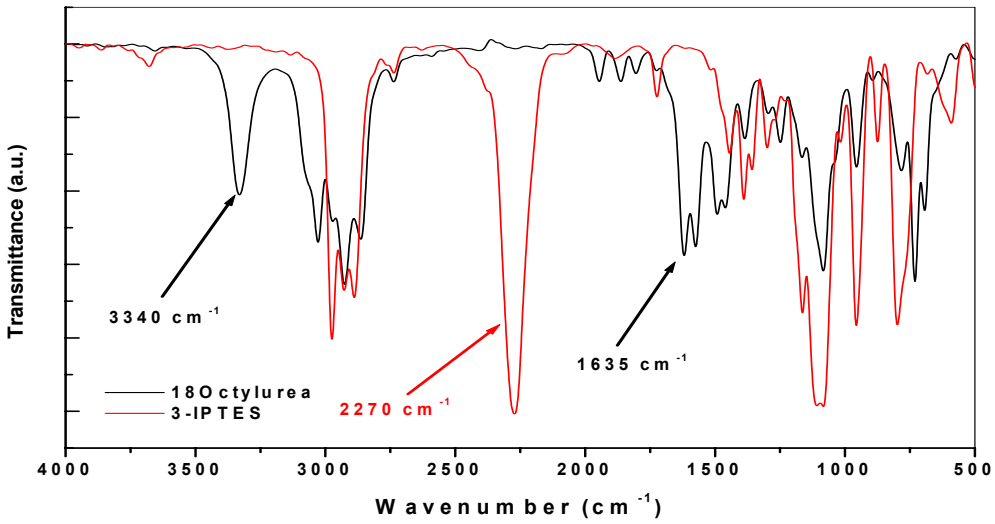


**Figure 53. FT-IR spectrums of 18Octylurea (black line) and 3-IPTES (red line).**

In the Figure 53, the strong absorption bands at around 3340 $cm^{-1}$ (N-H stretch) and at around 1635 $cm^{-1}$ (C=O stretch) for 18Octylurea confirm the formation of urea linkages. Also, the absence of a strong absorption band at around 2270 $cm^{-1}$ (due to NCO group) shows that the reaction is completed.

#### 5.3.3.2. Characterization of the 18Octylurea-modified $TiO_2$ nanoparticles

After 18Octylurea molecule was synthesized, $TiO_2$ nanoparticles were modified with this molecule (section 4.6.3., page 56). After that, the 18Octylurea-modified $TiO_2$ nanoparticles were characterized by GC/MS, FT-IR and elemental analysis.

### 5.3.3.2.1. GC/MS result

After $TiO_2$ nanoparticles were modified with 18Octylurea molecules, the liberated ethanol molecules were detected by GC/MS. The result is shown in the following.

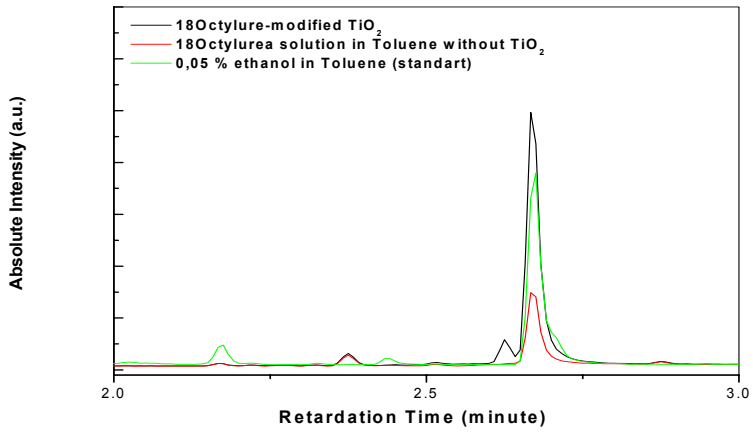


**Figure 54. GC/MS result of the 18Octylurea-modified $TiO_2$ powder.**

In the Figure 54, after the modification of $TiO_2$ nanoparticles with 18Octylurea, the liberated ethanol molecules were detected by GC/MS and this result was compared with standart ethanol solution. Although water-free toluene was always used in the experiments, a little ethanol in the solution of 18Octylurea in toluene was also detected. But, the peak intensity of the 18Octylurea-modified $TiO_2$ nanoparticles is much bigger than that of 18Octylurea solution in toluene. Thus, it is concluded from GC/MS result that $TiO_2$ nanoparticles were modified with 18Octylurea molecules.

### 5.3.3.2.2. FT-IR result

After the 18Octylurea-modified $TiO_2$ powder was dried, it was characterized by FT-IR. The result is shown in the following.

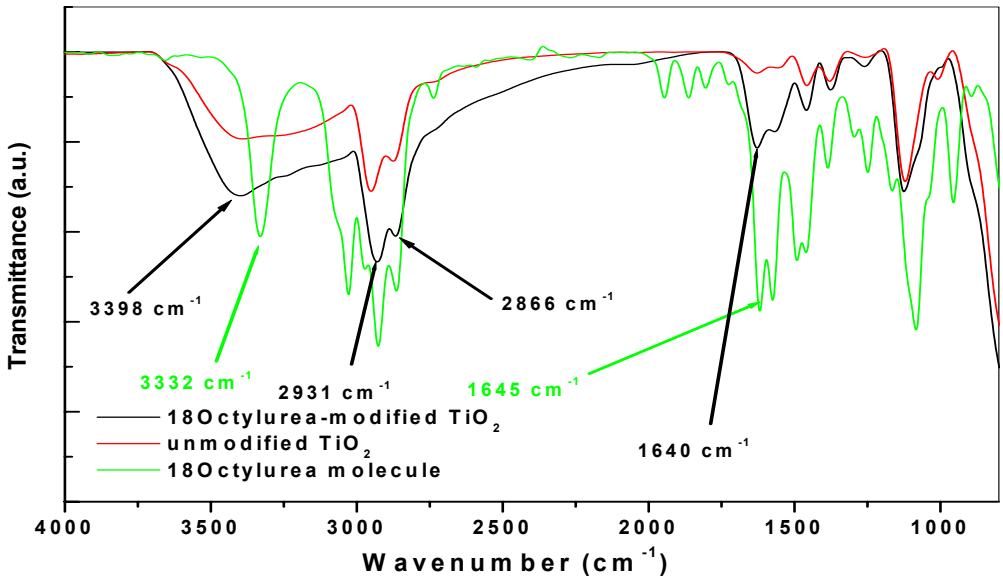


**Figure 55. FT-IR spectrums of the 18Octylurea-modified $TiO_2$ powder, 18Octylurea and unmodified $TiO_2$ powder.**

In the Figure 55, after $TiO_2$ nanoparticles were modified with 18Octylurea, urea peaks in the spectrum of the 18Octylurea-modified nanoparticles seem still at around 1640 $cm^{-1}$ and 3395 $cm^{-1}$. In addition, $CH_3$-, -$CH_2$- absorbsion bands in the spectrum of the 18Octylurea-modified $TiO_2$ nanoparticles increased at around 2866 $cm^{-1}$ and 2931 $cm^{-1}$ as compared to the spectrum of the unmodified nanoparticles. Thus, it is concluded that the modification of $TiO_2$ nanoparticles with 18Octylurea molecules was succeeded and proved by FT-IR.

### 5.3.3.2.3. Elemental analysis result

After the 18Octylurea-modified $TiO_2$ powder was dried, it was characterized by elemental analysis. The result is shown in the following.

| Powder | C% | H% | N% |
|---|---|---|---|
| 18Octylurea-modified $TiO_2$ powder | 15,21 | 3,21 | 1,35 |
| Unmodified $TiO_2$ powder | 8,38 | 2,13 | 0,0 |

According to this result, the increase in carbon, hydrogen and nitrogen percentages indicates that $TiO_2$ nanoparticles were modified with 18Octylurea. Furthermore, the increase in carbon percentage of the 18Octylurea-modified $TiO_2$ nanoparticles is a little more than that of the 16Hexylurea-modified $TiO_2$ nanoparticles because the number of carbon atoms in 18Octylurea molecule is more than that in 16Hexylurea molecule.

### 5.3.4. Characterization of 112Dodecylurea

After the modifications of $TiO_2$ nanoparticles with Ethylenurea, 16Hexylurea, 18Octylurea, $TiO_2$ nanoparticles were also modified with another urea molecule with higher molecular weight, with 112Dodecylurea. After 112Dodecylurea molecule was synthesized by means of the coupling reaction between 3-IPTES and 1,12-diaminododecane (according to section 4.5.4., page 53), it was characterized by FT-IR. The result is shown in the following.

#### 5.3.4.1. FT-IR result

After 112Dodecylurea was synthesized, it was characterized by FT-IR. The result is shown in the following.

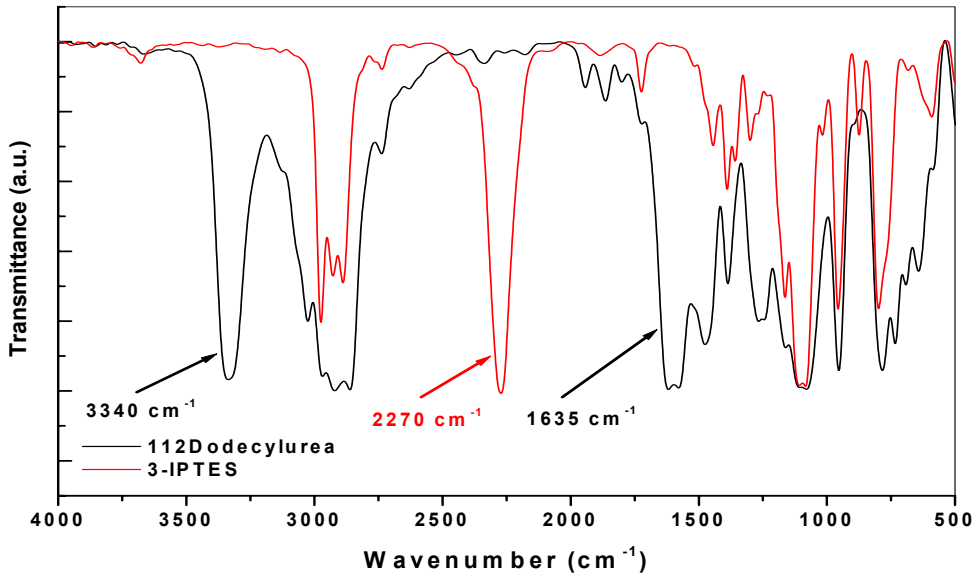


**Figure 56. FT-IR spectrums of 112Dodecylurea (black line) and 3-IPTES (red line).**

In the Figure 56, the strong absorption bands at around 3340 $cm^{-1}$ (N-H stretch) and at around 1635 $cm^{-1}$ (C=O stretch) for 112Dodecylurea confirm the formation of urea linkages. Also, the absence of a strong absorption band at around 2270 $cm^{-1}$ (due to NCO group) shows that the reaction is completed. Thus, this urea molecule was synthesized and characterized by FT-IR.

### 5.3.4.2. Characterization of the 112Dodecylurea-modified $TiO_2$ nanoparticles

After 112Dodecylurea molecule was synthesized, $TiO_2$ nanoparticles were modified with this molecule (section 4.6.4., page 56). After modification, the 112Dodecylurea-modified $TiO_2$ nanoparticles were characterized by GC/MS, FT-IR and elemental analysis.

#### 5.3.4.2.1. GC/MS result

After $TiO_2$ nanoparticles were modified with 112Dodecylurea molecules, the liberated ethanol molecules were detected by GC/MS. The result is shown in the following.

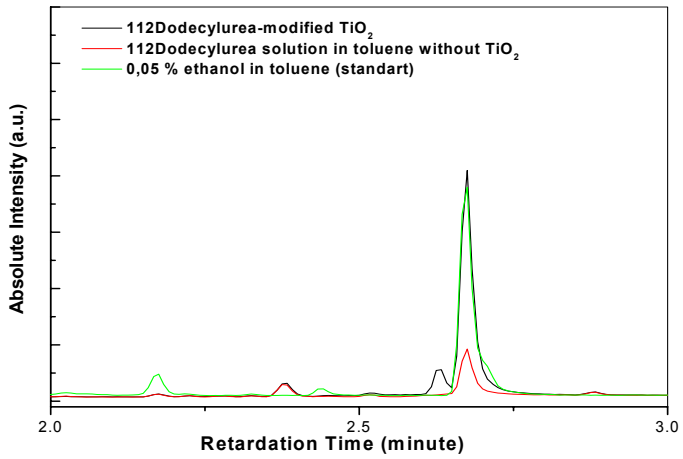


**Figure 57. GC/MS result of the 112Dodecylurea-modified $TiO_2$ powder.**

In Figure 57, after modification of $TiO_2$ nanoparticles with 112Dodecylurea, the liberated ethanol molecules were detected by GC/MS and this result was compared with standart ethanol solution. Although water-free toluene was always used in the experiments, a little ethanol in the solution of 112Dodecylurea in toluene was also detected. But, the peak intensity of the 112Dodecylurea-modified $TiO_2$ nanoparticles is much bigger than that of 112Dodecylurea solution. Thus, it is concluded from GC/MS result that $TiO_2$ nanoparticles were modified with 112Dodecylurea molecules.

#### 5.3.4.2.2. FT-IR result

After the 112Dodecylurea-modified $TiO_2$ powder was dried, it was characterized by FT-IR. The result is shown in the following.

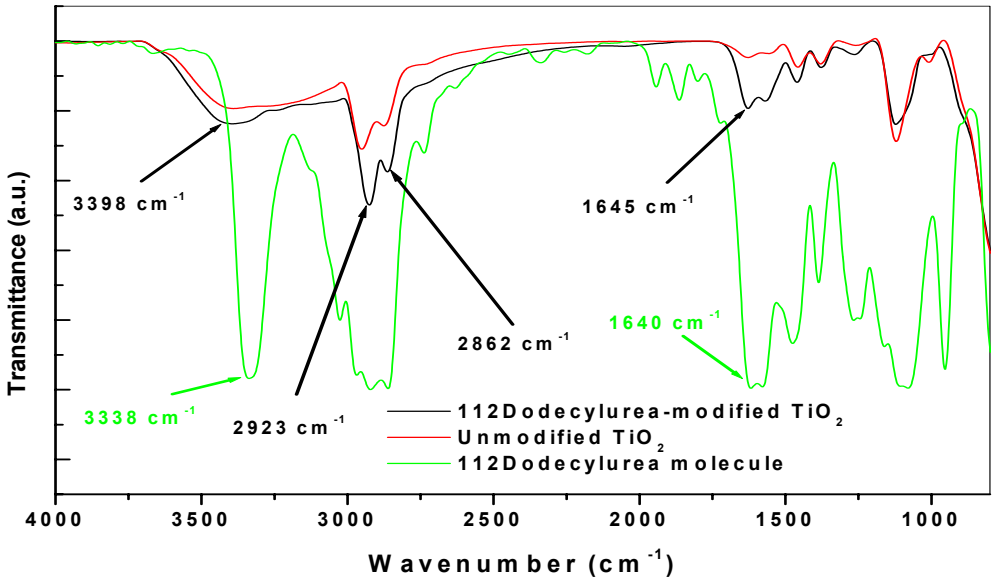


**Figure 58. FT-IR spectrums of the 112Dodecylurea-modified $TiO_2$ powder, 1,12-diamino dodecan and unmodified $TiO_2$ powder.**

In the Figure 58, after $TiO_2$ nanoparticles were modified with 112Dodecylurea molecules, urea peaks in the spectrum of the 112Dodecylurea-modified nanoparticles seem still at around 1645 $cm^{-1}$ and 3398 $cm^{-1}$. In addition, $CH_3$-, -$CH_2$- absorbsion bands in the spectrum of the 112Dodecylurea-modified $TiO_2$ nanoparticles increased at around 2862 $cm^{-1}$ and 2923 $cm^{-1}$ as compared to the spectrum of the unmodified nanoparticles. Thus, it is concluded that the modification of $TiO_2$ nanoparticles with 112Dodecylurea molecules was succeeded and proved by FT-IR.

### 5.3.4.2.3. Elemental analysis result

After the 112Dodecylurea-modified $TiO_2$ powder was dried, it was characterized by elemental analysis. The result is shown in the following.

| Powder | C% | H% | N% |
|---|---|---|---|
| 112Dodecylurea -modified $TiO_2$ powder | 18,64 | 3,75 | 1,57 |
| Unmodified $TiO_2$ powder | 8,38 | 2,13 | 0,0 |

According to this result, the increase in carbon, hydrogen and nitrogen percentages indicates that $TiO_2$ nanoparticles were modified with 112Dodecylurea. Furthermore, the increase in carbon percentage of the 112Dodecylurea-modified $TiO_2$ nanoparticles is more than that of 18Octylurea-modified $TiO_2$ nanoparticles because the number of carbon atoms in 112Dodecylurea molecule is more than that in 18Octylurea molecule.

### 5.3.5. Characterization of DMSA15urea

After the modifications of $TiO_2$ nanoparticles with Ethylenurea, 16Hexylurea, 18Octylurea and 112Dodecylurea, $TiO_2$ nanoparticles were also modified with another urea molecule with very high molecular weight, with DMSA15urea molecules. After DMSA15urea molecule was synthesized by means of the coupling reaction between 3-IPTES and DMS-A15 (according to section 4.5.5., page 54), it was characterized by FT-IR. The result is shown in the following.

#### 5.3.5.1. FT-IR results

After DMSA15urea was synthesized, it was characterized by FT-IR. The result is shown in the following.

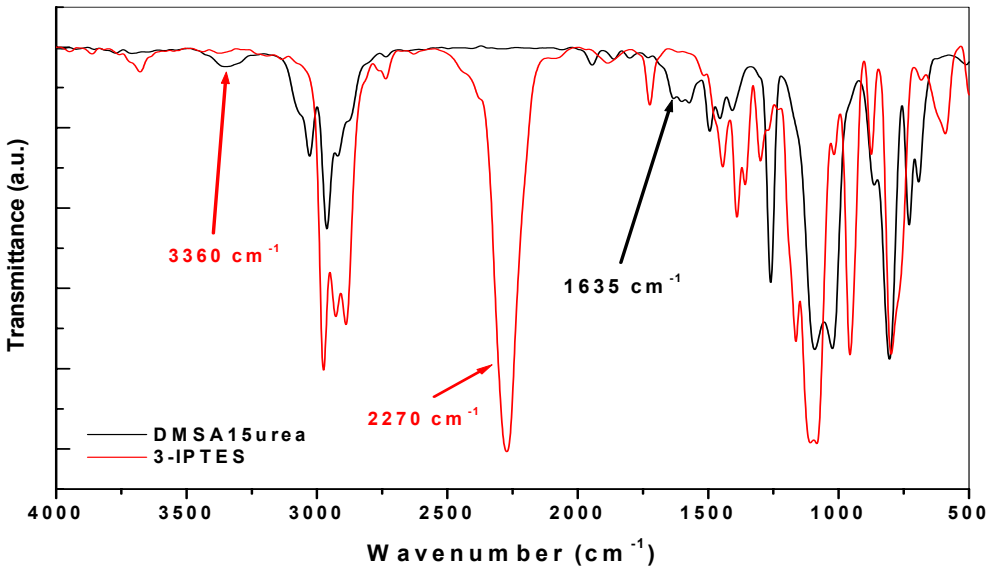


**Figure 59. FT-IR spectrums of DMSA15urea (black line) and 3-IPTES (red line).**

In the Figure 59, the strong absorption bands at around 3360 $cm^{-1}$ (N-H stretch) and at around 1635 $cm^{-1}$ bands (C=O stretch) for DMSA15urea confirm the formation of urea linkages. Also, the absence of a strong absorption band at around 2270 $cm^{-1}$ (due to NCO group) shows that the reaction is completed.

#### 5.3.5.2. Characterization of the DMSA15urea-modified $TiO_2$ nanoparticles

After DMSA15urea molecule was synthesized, $TiO_2$ nanoparticles were modified with this molecule (section 4.6.5., page 57). After modification, the DMSA15urea-modified $TiO_2$ nanoparticles were characterized by GC/MS, FT-IR and elemental analysis.

### 5.3.5.2.1. GC/MS result

After $TiO_2$ nanoparticles were modified with DMSA15urea molecules, the liberated ethanol molecules were detected by GC/MS. The result is shown in the following.

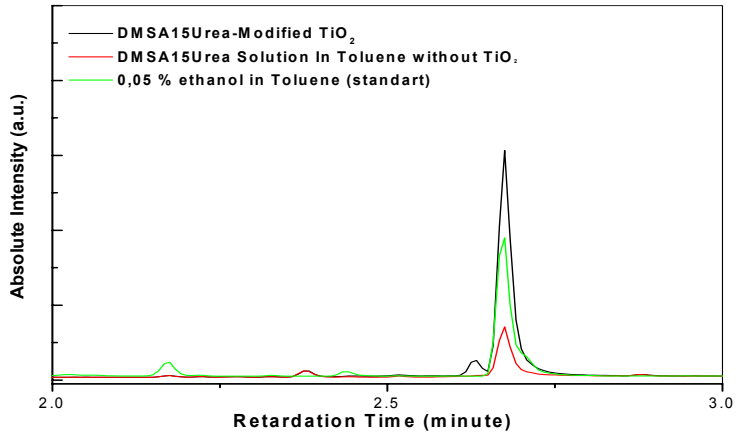


**Figure 60. GC/MS result of the DMSA15urea-modified $TiO_2$ powder.**

In the Figure 60, after the modification of $TiO_2$ nanoparticles with DMSA15urea, the liberated ethanol molecules were detected by GC/MS and this result was compared with standart ethanol solution in toluene. Although water-free toluene was always used in the experiments, a little ethanol in the solution of DMSA15urea in toluene was also detected. But, the peak intensity of the DMSA15urea-modified $TiO_2$ nanoparticles is much bigger than that of DMSA15urea solution in toluene. Thus, it is concluded from GC/MS result that $TiO_2$ nanoparticles were modified with DMSA15urea molecules.

### 5.3.5.2.2. FT-IR result

After the DMSA15urea-modified $TiO_2$ powder was dried, it was characterized by FT-IR. The result is shown in the following.

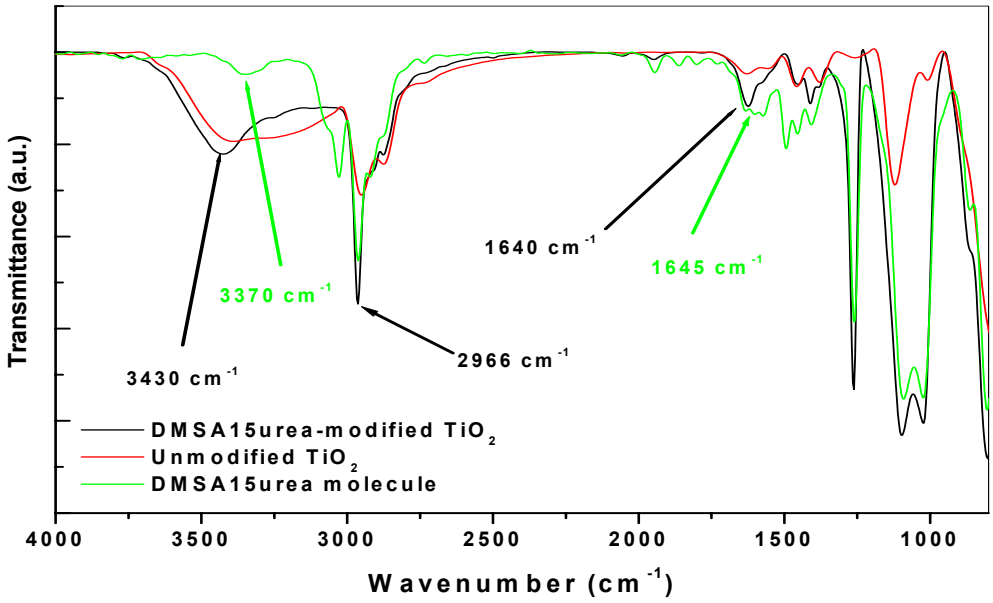


**Figure 61. FT-IR spectrums of the DMSA15urea-modified $TiO_2$ powder, DMSA15urea and unmodified $TiO_2$ powder.**

In the Figure 61, after $TiO_2$ nanoparticles were modified with DMSA15urea molecules, urea peaks in the spectrum of the DMSA15urea-modified nanoparticles seem still at around 1645 $cm^{-1}$ and 3430 $cm^{-1}$. In addition, $CH_3$-, -$CH_2$- absorbsion bands in the spectrum of the DMSA15urea-modified $TiO_2$ nanoparticles increased at around 2966 $cm^{-1}$ as compared to the spectrum of the unmodified nanoparticles. Thus, it is concluded that the modification of $TiO_2$ nanoparticles with DMSA15urea molecules was succeeded and proved by FT-IR.

### 5.3.5.2.3. Elemental analysis result

After the DMSA15urea-modified $TiO_2$ powder was dried, it was also characterized by elemental analysis. The result is shown in the following.

| Powder | C% | H% | N% |
|---|---|---|---|
| DMSA15urea-modified $TiO_2$ powder | 21,36 | 5,11 | 0,50 |
| Unmodified $TiO_2$ powder | 8,38 | 2,13 | 0,0 |

According to this result, the increase in carbon, hydrogen and nitrogen percentages indicates that $TiO_2$ nanoparticles were modified with DMSA15urea. Furthermore, the increase in carbon percent of the DMSA15urea-modified $TiO_2$ nanoparticles is more than that of the 112Dodecylurea-modified $TiO_2$ nanoparticles because the number of carbon atoms in DMSA15urea molecule is much more than that in 112Dodecylurea molecule.

### 5.3.6. Characterization of DMSA21urea

After the modifications of $TiO_2$ nanoparticles with Ethylenurea, 16Hexylurea, 18Octylurea, 112Dodecylurea and DMSA15urea, $TiO_2$ nanoparticles were also modified with another urea molecule with higher molecular weight, with DMSA21urea molecules. After DMSA21urea molecule was synthesized by means of the coupling reaction between 3-IPTES and DMS-A21 (according to section 4.5.6., page 54), it was characterized by FT-IR. The result is shown in the following.

#### 5.3.6.1. FT-IR result

After the DMSA21urea was synthesized, it was characterized by FT-IR. The result is shown in the following.

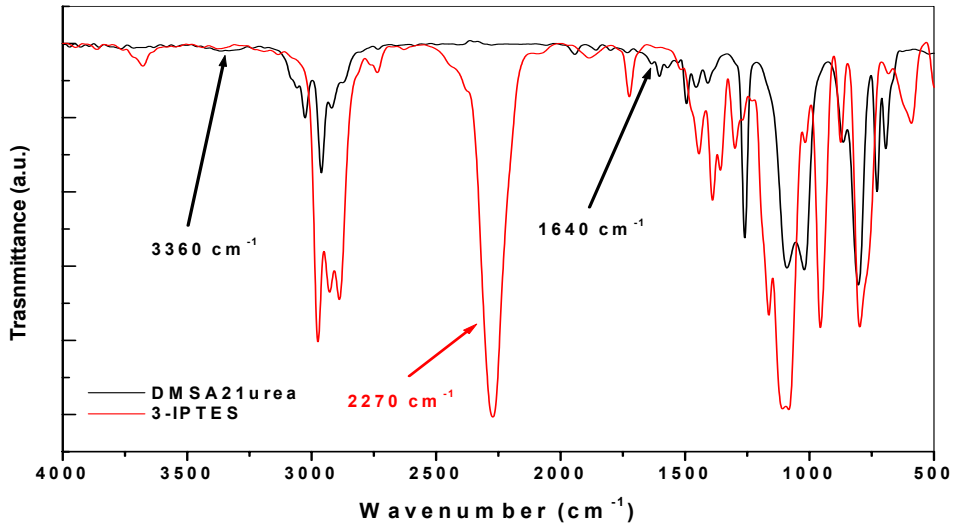


**Figure 62. FT-IR spectrums of DMSA21urea (black line) and 3-IPTES (red line).**

In the Figure 62, the strong absorption bands at around 3360 $cm^{-1}$ (N-H stretch) and at around 1640 $cm^{-1}$ bands (C=O stretch) for DMSA21 confirm the formation of urea linkages. Also, the absence of a strong absorption band at around 2270 $cm^{-1}$ (due to NCO group) shows that the reaction was completed.

#### 5.3.6.2. Characterization of the DMSA21urea-modified $TiO_2$ nanoparticles

After DMSA21urea molecule was synthesized, $TiO_2$ nanoparticles were modified with this molecule (section 4.6.6., page 57). After modification, the DMSA21urea-modified $TiO_2$ nanoparticles were characterized by GC/MS, FT-IR and elemental analysis.

### 5.3.6.2.1. GC/MS result

After $TiO_2$ nanoparticles were modified with DMSA21urea molecules, the liberated ethanol molecules were detected by GC/MS. The result is shown in the following.

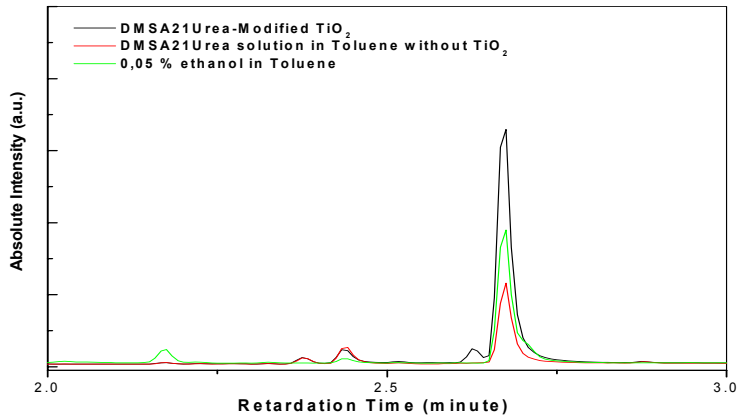


**Figure 63. GC/MS result of the DMSA21urea-modified $TiO_2$ powder.**

In the Figure 63, after the modification of $TiO_2$ nanoparticles with DMSA21urea, the liberated ethanol molecules were detected by GC/MS and this result was compared with standart ethanol solution. Although water-free toluene was always used in the experiments, a little ethanol in the solution of DMSA21urea in toluene was also detected. But, the peak intensity of the DMSA21urea-modified $TiO_2$ nanoparticles is much bigger than that of DMSA21urea solution. Thus, it is concluded from GC/MS result that $TiO_2$ nanoparticles were modified with DMSA21urea molecules.

### 5.3.6.2.2. FT-IR result

After the DMSA21urea-modified $TiO_2$ powder was dried, it was characterized by FT-IR. The result is shown in the following.

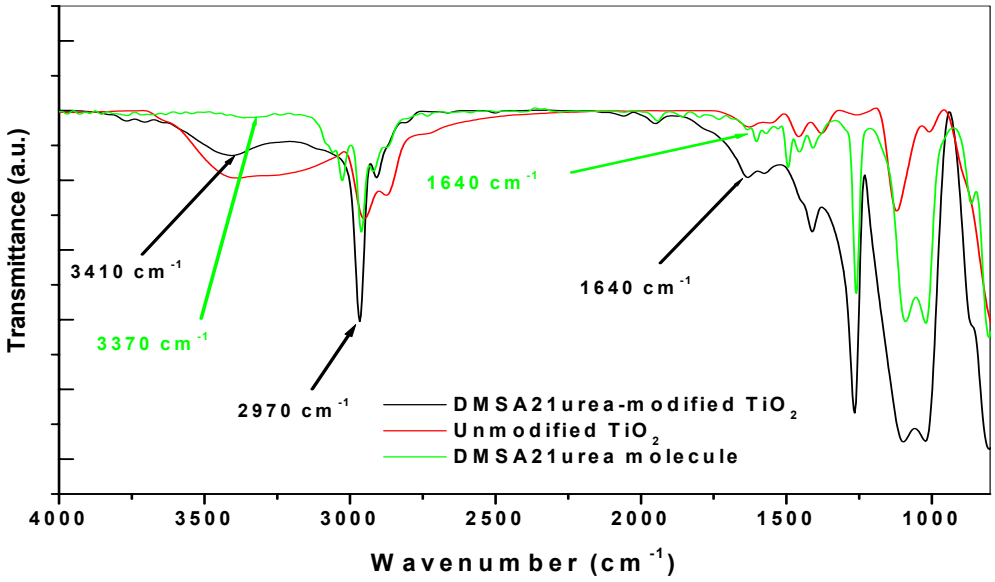


**Figure 64. FT-IR spectrums of the DMSA21urea-modified $TiO_2$ powder, DMSA21urea and unmodified $TiO_2$ powder.**

In the Figure 64, after $TiO_2$ nanoparticles were modified with DMSA21urea molecules, urea peaks in the spectrum of the DMSA21urea-modified nanoparticles seem still at around 1640 $cm^{-1}$ and 3410 $cm^{-1}$. In addition, $CH_3$-, -$CH_2$- absorbsion bands in the spectrum of the DMSA21urea-modified $TiO_2$ nanoparticles increased at around 2970 $cm^{-1}$ as compared to the spectrum of the unmodified nanoparticles. Thus, it is concluded that the modification of $TiO_2$ nanoparticles with the DMSA21urea molecules was succeeded and proved by FT-IR.

### 5.3.6.2.3. Elemental analysis result

After the DMSA21urea-modified $TiO_2$ powder was dried, it was characterized by elemental analysis. The result is shown in the following.

| Powder | C% | H% | N% |
|---|---|---|---|
| DMSA21urea-modified $TiO_2$ powder | 27,66 | 6,92 | 0,49 |
| Unmodified $TiO_2$ powder | 8,38 | 2,13 | 0,0 |

According to this result, the increase in carbon, hydrogen and nitrogen percentages indicates that $TiO_2$ nanoparticles were modified with the DMSA21urea molecules. Furthermore, the increase in carbon percentage of the DMSA21urea-modified $TiO_2$ nanoparticles is more than that of the DMSA15urea-modified $TiO_2$ nanoparticles because the number of carbon atoms in the DMSA21urea molecule is much more than that in the DMSA15urea molecule.

### 5.3.7. Characterization of Pentylurea

After the modifications of $TiO_2$ nanoparticles with amine molecules containing two amine groups in their molecules, namely Ethylenurea, 16Hexylurea, 18Octylurea, 112Dodecylurea, DMSA15urea and DMSA21urea, $TiO_2$ nanoparticles were also modified with other amine molecules containing one amine group in their molecules, namely Pentylurea, Octylurea, 1Dodecylurea and Octadecylurea. Firstly, $TiO_2$ nanoparticles were modified with Pentylurea. After Pentylurea was synthesized by means of the coupling reaction between 3-IPTES and pentylamine (according to section 4.5.7., page 54), it was characterized by FT-IR. The result is shown in the following.

#### 5.3.7.1. FT-IR result

After Pentylurea was synthesized, it was characterized by FT-IR. The result is shown in the following.

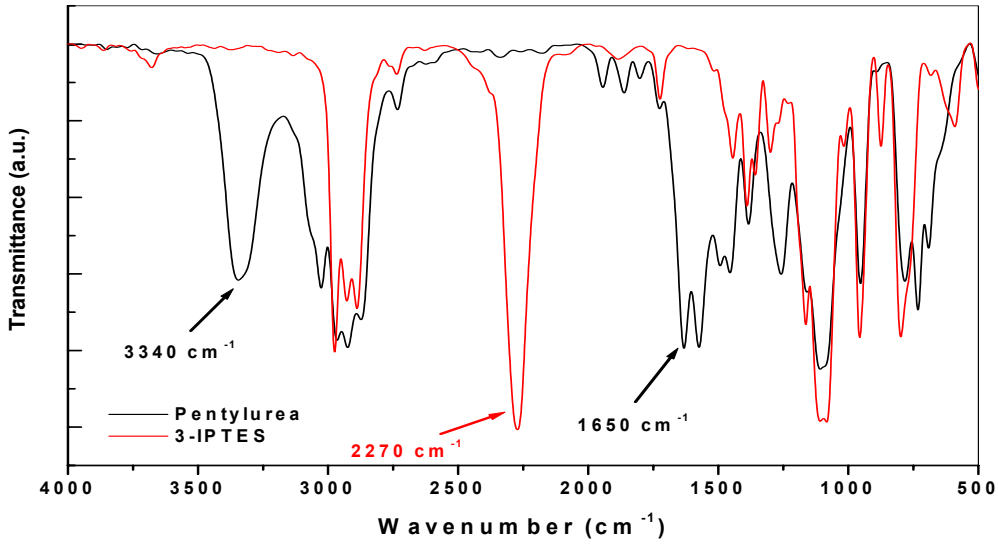


**Figure 65. FT-IR spectrums of Pentylurea (black line) and 3-IPTES (red line).**

In the Figure 65, the strong absorption bands at around 3340 $cm^{-1}$ (N-H stretch) and at around 1650 $cm^{-1}$ (C=O stretch) for pentylurea confirm the formation of urea linkages. Also, the absence of a strong absorption band at around 2270 $cm^{-1}$ (due to NCO group) shows the reaction is completed.

### 5.3.7.2. Characterization of the Pentylurea-modified $TiO_2$ nanoparticles

After Pentylurea was synthesized, $TiO_2$ nanoparticles were modified with this molecule (section 4.6.7., page 58). After modification, the Pentylurea-modified $TiO_2$ nanoparticles were characterized by GC/MS, FT-IR and elemental analysis.

#### 5.3.7.2.1. GC/MS result

After $TiO_2$ nanoparticles were modified with Pentylurea molecules, the liberated ethanol molecules were detected by GC/MS. The result is shown in the following.

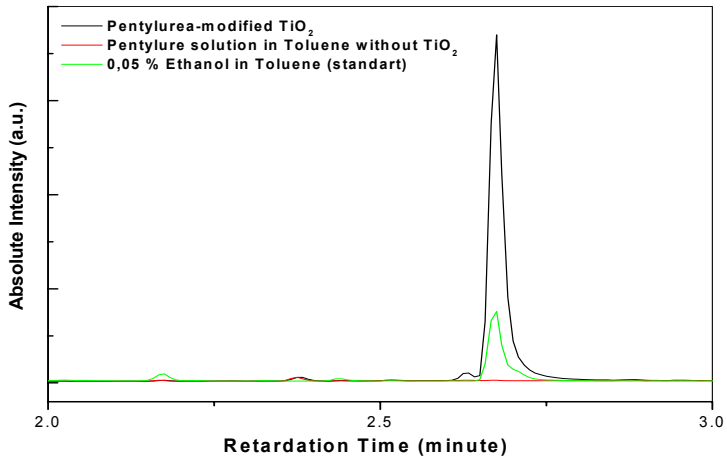


**Figure 66. GC/MS result of the Pentylurea-modified $TiO_2$ powder.**

In the Figure 66, after modification of $TiO_2$ nanoparticles with Pentylurea, the liberated ethanol molecules were detected and this result was compared with standart ethanol solution in toluene. Because it was not detected no ethanol in the solution of Pentylurea in toluene, all ethanol detected by GC/MS was resulted from the modification of $TiO_2$ nanoparticles with Pentylurea. Thus, it is concluded from GC/MS result that $TiO_2$ nanoparticles were modified with Pentylurea molecules.

#### 5.3.7.2.2. FT-IR result

After the Pentylurea-modified $TiO_2$ powder was dried, it was characterized by FT-IR. The result is shown in the following.

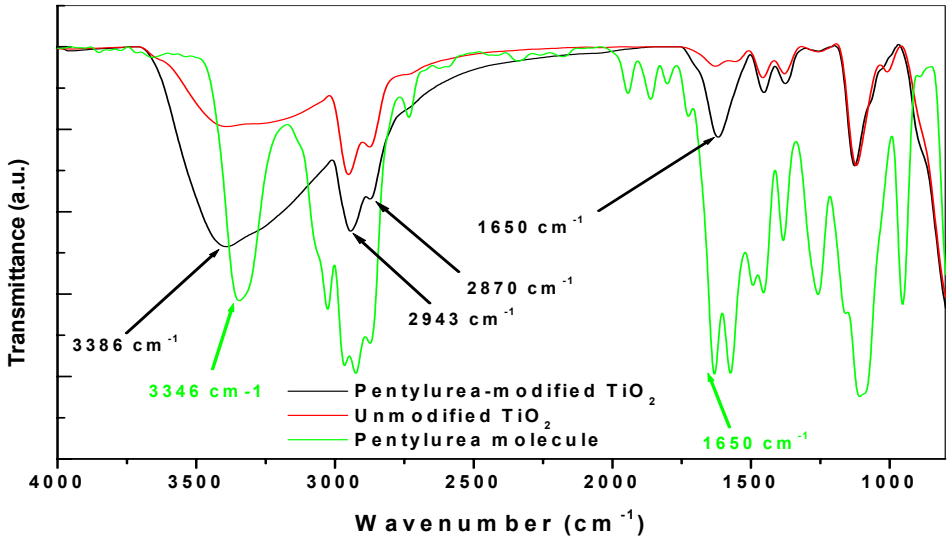


**Figure 67. FT-IR spectrums of the Pentylurea-modified $TiO_2$ powder, pentylurea and unmodified $TiO_2$ powder.**

In the Figure 67, after $TiO_2$ nanoparticles were modified with Pentylurea molecules, the urea peaks in the spectrum of the Pentylurea-modified nanoparticles seem still at around 1650 $cm^{-1}$ and 3386 $cm^{-1}$. In addition, $CH_3$-, -$CH_2$- absorbsion bands in the spectrum of the Pentylurea-modified $TiO_2$ nanoparticles increased at around 2870 $cm^{-1}$ and 2943 $cm^{-1}$ as compared to the spectrum of the unmodified nanoparticles. Thus, it is concluded that the modification of $TiO_2$ nanoparticles with Pentylurea molecules was succeeded and proved by FT-IR.

### 5.3.7.2.3. Elemental analysis result

After the Pentylurea-modified $TiO_2$ powder was dried, it was characterized by elemental analysis. The result is shown in the following.

| Powder | C% | H% | N% |
|---|---|---|---|
| Pentylurea-modified $TiO_2$ powder | 11,75 | 2,60 | 0,36 |
| Unmodified $TiO_2$ powder | 8,38 | 2,13 | 0,0 |

According to this result, the increase in carbon, hydrogen and nitrogen percentages indicates that $TiO_2$ nanoparticles were modified with Pentylurea molecules. Furthermore, it is interesting that the increase in the amount of carbon after modification with Ethylenurea molecules is more than that with Pentylurea although the number of carbon atoms in the Pentylurea molecule is more than that in the Ethylenurea (carbon percent for Ethylenurea-

modified $TiO_2$ powder: 13,26). The reason for that finding might be various interaction types between amino groups and $TiO_2$ surfaces. This is similar to the modification of $TiO_2$ nanoparticles with AMMO molecules (see section 5.2.5, page 85). The interactions between amino group in the Ethylenurea molecule and $TiO_2$ surface are 1) the amine may enter into hydrogen bonding interaction with surface hydroxyl group, 2) the basic amine function may form and ionic bonding with a surface hydroxyl group. This type of interaction is more stable than the former interaction. Because of the mentioned interactions, in this experiment, much more Ethylenurea molecules might interact with $TiO_2$ surface besides covalent bonding to the surface. For this reason, the increase in the carbon amount of the Ethylenurea-modified $TiO_2$ nanoparticles is more than that of the Penytlurea-modified $TiO_2$ nanoparticles although the number of carbon atoms in Pentylurea molecule is more than that in Ethylenurea molecule.

### 5.3.8. Characterization of Octylurea

After the modifications of $TiO_2$ nanoparticles with Pentyurea molecules, $TiO_2$ nanoparticles were also modified with another urea molecule with higher molecular weight, with Octylurea. After Octylurea molecule was synthesized by means of the coupling reaction between 3-IPTES and octylamine (according to section 4.5.8., page 54), it was characterized by FT-IR. The result is shown in the following.

#### 5.3.8.1. FT-IR result

After Octylurea was synthesized, it was characterized by FT-IR. The result is shown in the following.

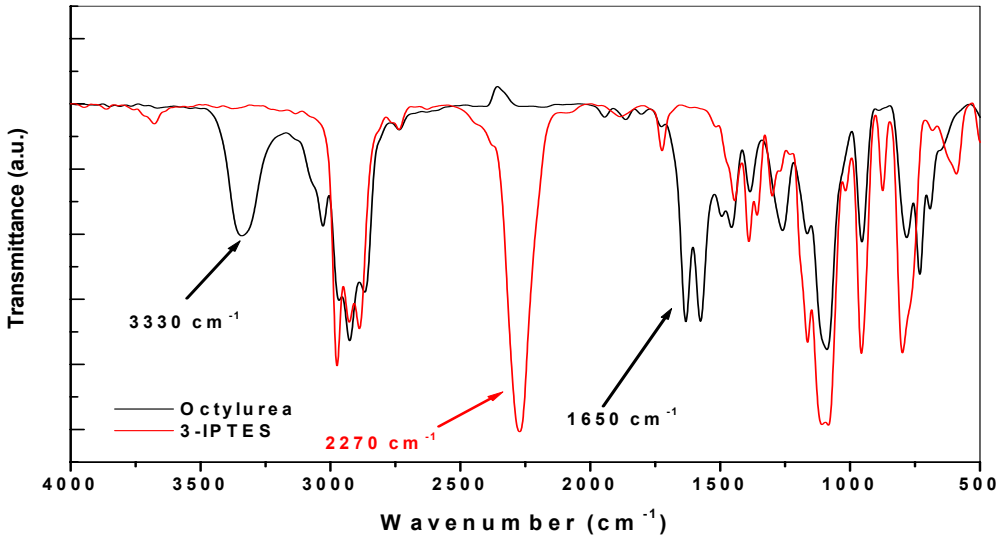


**Figure 68. FT-IR spectrums of Octylurea (black line) and 3-IPTES (red line).**

In the Figure 68, the strong absorption bands at around 3330 $cm^{-1}$ (N-H stretch) and at around 1650 $cm^{-1}$ (C=O stretch) for octylurea confirm the formation of urea linkages. Also, the absence of a strong absorption band at around 2270 $cm^{-1}$ (due to NCO group) shows the reaction is completed.

### 5.3.8.2. Characterization of the Octylurea-modified $TiO_2$ nanoparticles

After Octylurea was synthesized, $TiO_2$ nanoparticles were modified with this molecule (section 4.6.8., page 58). After modification, the Octylurea-modified $TiO_2$ nanoparticles were characterized by GC/MS, FT-IR and elemental analysis.

#### 5.3.8.2.1. GC/MS result

After $TiO_2$ nanoparticles were modified with Octylurea molecules, the liberated ethanol molecules were detected by GC/MS. The result is shown in the following.

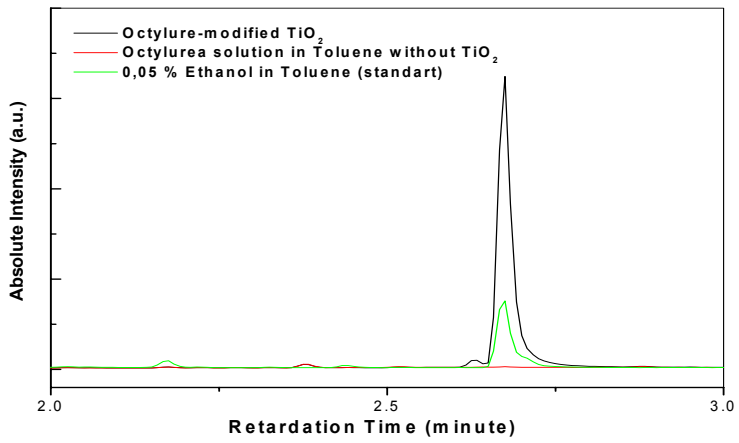


**Figure 69. GC/MS result of the Octylurea-modified $TiO_2$ powder.**

In the Figure 69, after modification of $TiO_2$ nanoparticles with Octylurea, the liberated ethanol molecules were detected and this result was compared with standart ethanol solution in toluene. Because it was not detected any ethanol in the solution of Octylurea in toluene, all ethanol detected by GC/MS was resulted from the modification of $TiO_2$ nanoparticles with Octylurea. Thus, it is concluded from GC/MS result that $TiO_2$ nanoparticles were modified with Octylurea molecules.

#### 5.3.8.2.2. FT-IR result

After the Octylurea-modified $TiO_2$ powder was dried, it was characterized by FT-IR. The result is shown in the following.

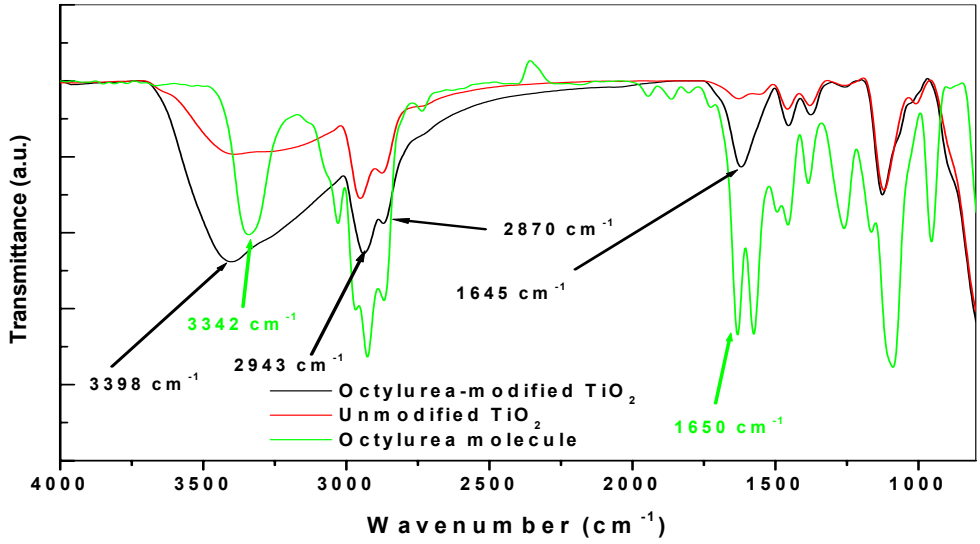


**Figure 70. FT-IR spectrums of the Octylurea-modified $TiO_2$ powder, Octylurea and unmodified $TiO_2$ powder.**

In the Figure 70, after $TiO_2$ nanoparticles were modified with Octylurea molecules, urea peaks in the spectrum of the Octylurea-modified nanoparticles seem still at around 1645 $cm^{-1}$ and 3398 $cm^{-1}$. In addition, $CH_3$-, -$CH_2$- absorbsion bands in the spectrum of the Octylurea-modified $TiO_2$ nanoparticles increased at around 2870 $cm^{-1}$ and 2943 $cm^{-1}$ as compared to the spectrum of unmodified nanoparticles. Thus, it is concluded that the modification of $TiO_2$ nanoparticles with Octylurea molecules was succeeded and proved by FT-IR.

### 5.3.8.2.3. Elemental analysis result

After the Octylurea-modified $TiO_2$ powder was dried, it was characterized by elemental analysis. The result is shown in the following.

| Powder | C% | H% | N% |
|---|---|---|---|
| Octylurea-modified $TiO_2$ powder | 12,53 | 2,74 | 0,39 |
| Unmodified $TiO_2$ powder | 8,38 | 2,13 | 0,0 |

According to this result, the increase in the carbon, hydrogen and nitrogen percentages indicates that $TiO_2$ nanoparticles were modified with Octylurea molecules. Furthermore, it is interesting that the increase in the amount of carbon after modification with 18Octylurea molecules is more than that with Octylurea although the number of carbon atoms in the 18Octylurea molecule is same as the number of carbon atoms in Octylurea molecule (carbon percent for 18Octylurea-modified $TiO_2$ powder: 15,21). The reason for that finding might be

various interaction types between amino groups of the 18Octylurea and $TiO_2$ surfaces. This is similar to the modification of $TiO_2$ nanoparticles with AMMO molecules (see section 5.2.5, page 85). The interactions between amino group in the 18Octylurea molecule and $TiO_2$ surface are 1) the amine may enter into hydrogen bonding interaction with surface hydroxyl group, 2) the basic amine function may form and ionic bonding with a surface hydroxyl group. This type of interaction is more stable than the former interaction. Because of the mentioned interactions, in this experiment, much more 18Octylurea molecules might interact with $TiO_2$ surface besides covalent bonding to the surface. For this reason, the increase in the carbon amount of the 18Octylurea-modified $TiO_2$ nanoparticles is more than that of the Octylurea-modified $TiO_2$ nanoparticles although the number of carbon atoms in the 18Octylurea and Octylurea molecules is same.

### 5.3.9. Characterization of 1Dodecylurea

After the modifications of $TiO_2$ nanoparticles with Pentyurea and Octylurea molecules containing one amine group in their molecules, $TiO_2$ nanoparticles were also modified with another urea molecule with higher molecular weight, with Octylurea. After Octylurea molecule was synthesized by means of the coupling reaction between 3-IPTES and octylamine (according to section 4.5.9., page 54), it was characterized by FT-IR. The result is shown in the following.

#### 5.3.9.1. FT-IR result

After 1Dodecylurea was synthesized, it was characterized by FT-IR. The result is shown in the following.

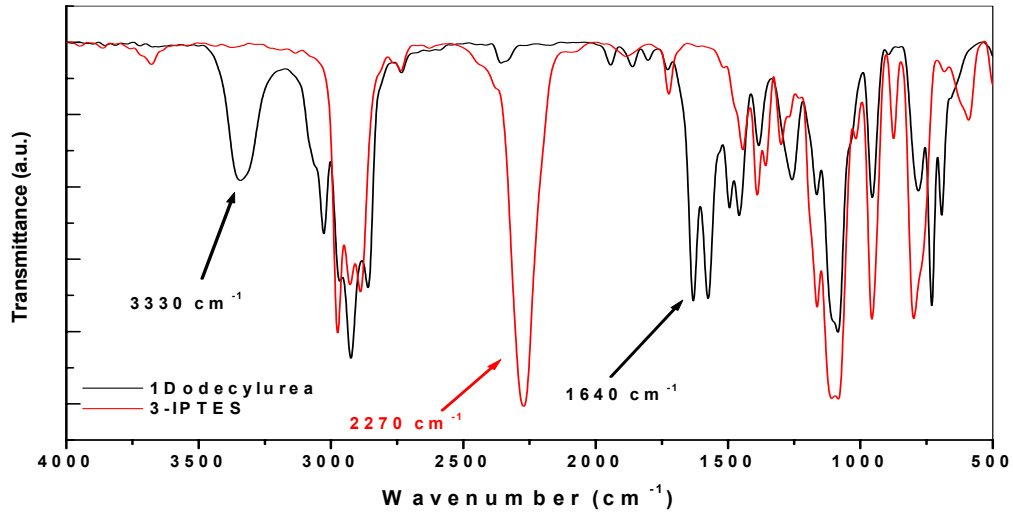


**Figure 71. FT-IR spectrums of the 1Dodecylurea (black line) and 3-IPTES (red line).**

In the Figure 71, the strong absorption bands at around 3330 $cm^{-1}$ (N-H stretch) and at around 1635 $cm^{-1}$ (C=O stretch) for 1Dodecylurea confirm the formation of urea linkages. Also, the absence of a strong absorption band at around 2270 $cm^{-1}$ (due to NCO group) shows that the reaction is completed.

### 5.3.9.2. Characterization of the 1Dodecylurea-modified $TiO_2$ nanoparticles

After 1Dodecylurea molecules were synthesized, $TiO_2$ nanoparticles were modified with this molecule (section 4.6.9., page 59). After modification, the 1Dodecylurea-modified $TiO_2$ nanoparticles were characterized by GC/MS, FT-IR and elemental analysis.

#### 5.3.9.2.1. GC/MS result

After $TiO_2$ nanoparticles were modified with 1Dodecylurea molecules, the liberated ethanol molecules were detected by GC/MS. The result is shown in the following.

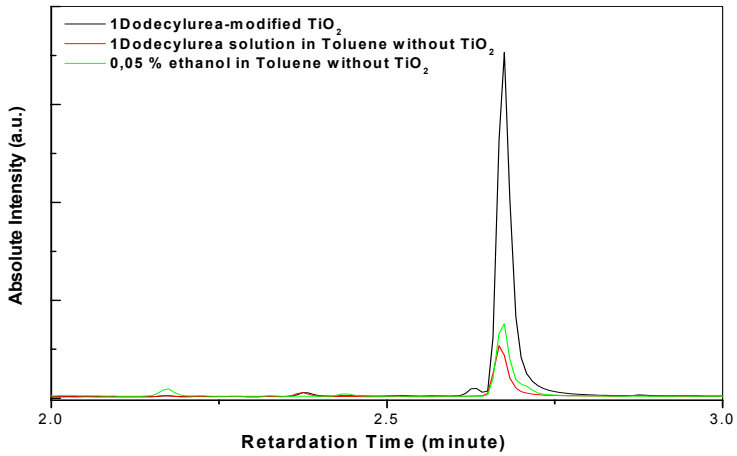


**Figure 72. GC/MS result of the 1Dodecylurea-modified $TiO_2$ powder.**

In the Figure 72, after modification of $TiO_2$ nanoparticles with 1Dodecylurea, the liberated ethanol molecules were detected and this result was compared with standart ethanol solution. Although water-free toluene was always used in the experiments, a little ethanol in the solution of 1Dodecylurea in toluene was also detected. But, the peak intensity of the 1Dodecylurea-modified $TiO_2$ nanoparticles is much bigger than that of 1Dodecylurea solution. Thus, it is concluded from GC/MS result that $TiO_2$ nanoparticles were modified with 1Dodecylurea molecules.

### 5.3.9.2.2. FT-IR result

After the 1Dodecylurea-modified $TiO_2$ powder was dried, it was characterized by FT-IR. The result is shown in the following.

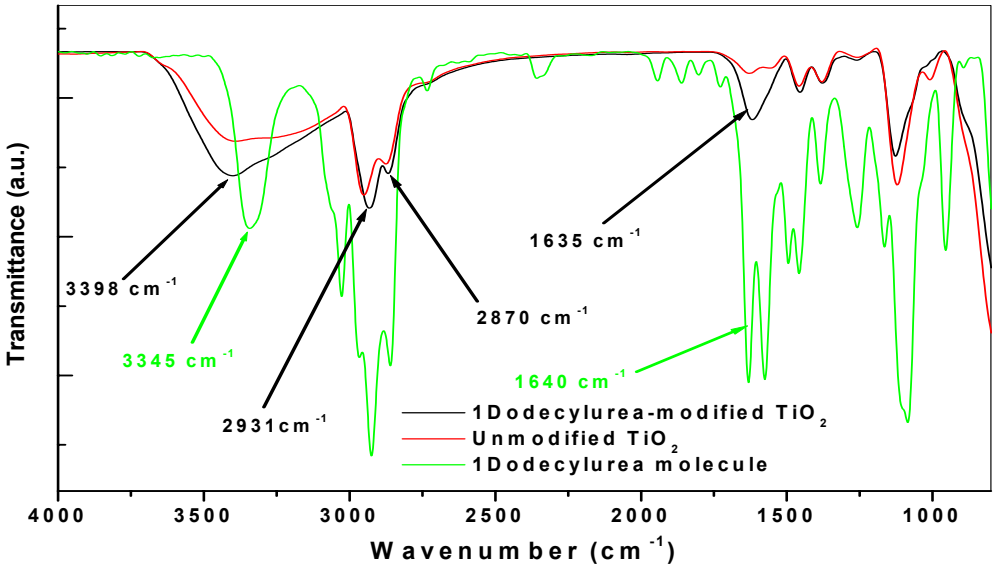


**Figure 73. FT-IR spectrums of the 1Dodecylurea-modified $TiO_2$ powder, 1Dodecylurea and unmodified $TiO_2$ powder.**

In the Figure 73, after $TiO_2$ nanoparticles were modified with 1Dodecylurea molecules, urea peaks in the spectrum of the 1Dodecylurea-modified nanoparticles seem still at around 1635 $cm^{-1}$ and 3398 $cm^{-1}$. In addition, $CH_3$-, -$CH_2$- absorbsion bands in the spectrum of the 1Dodecylurea-modified $TiO_2$ nanoparticles increased at around 2870 $cm^{-1}$ and 2931 $cm^{-1}$ as compared to the spectrum of unmodified nanoparticles. Thus, it is concluded that the modification of $TiO_2$ nanoparticles with 1Dodecylurea molecules was succeeded and proved by FT-IR.

### 5.3.9.2.3. Elemental analysis result

After the 1Dodecylurea-modified $TiO_2$ powder was dried, it was characterized by elemental analysis. The result is shown in the following.

| Powder | C% | H% | N% |
|---|---|---|---|
| 1Dodecylurea-modified $TiO_2$ powder | 14,20 | 3,02 | 0,51 |
| Unmodified $TiO_2$ powder | 8,38 | 2,13 | 0,0 |

According to this result, the increase in the carbon, hydrogen and nitrogen percentages indicates that $TiO_2$ nanoparticles were modified with 1Dodecylurea. Furthermore, it is interesting that the increase in the amount of carbon after modification with 112Dodecylurea molecules is more than that with 1Dodecylurea although the number of carbon atoms in 112Dodecylurea molecule is same as the number of carbon atoms in 1Dodecylurea molecule (carbon percent for the 112Dodecylurea-modified $TiO_2$ powder: 18,64). The reason for that finding might be various interaction types between amino groups of 112Dodecylurea molecules and $TiO_2$ surfaces. This is similar to the modification of $TiO_2$ nanoparticles with AMMO molecules (see section 5.2.5, page 85). The interactions between amino group in the 112Dodecylurea molecule and $TiO_2$ surface are 1) the amine may enter into hydrogen bonding interaction with surface hydroxyl group, 2) the basic amine function may form and ionic bonding with a surface hydroxyl group. This type of interaction is more stable than the former interaction. Because of the mentioned interactions, in this experiment, much more 112Dodecylurea molecules might interact with $TiO_2$ surface besides covalent bonding to the surface. For this reason, the increase in the carbon amount of the 112Dodecylurea-modified $TiO_2$ nanoparticles is more than that of the 1Dodecylurea-modified $TiO_2$ nanoparticles although the numbers of carbon atoms in the 112Dodecylurea and 1Dodecylurea molecules are same.

### 5.3.10. Characterization of Octadecylurea

After the modifications of $TiO_2$ nanoparticles with Pentyurea, Octylurea and 1Dodecylurea containing one amine group in their molecules, $TiO_2$ nanoparticles were also modified with another urea molecule with higher molecular weight, with Octadecylurea. After Octadecylurea molecule was synthesized by means of the coupling reaction between 3-IPTES and octadecylamine (according to section 4.5.10., page 55), it was characterized by FT-IR. The result is shown in the following.

#### 5.3.10.1. FT-IR result

After Octadecylurea was synthesized, it was characterized by FT-IR. The result is shown in the following.

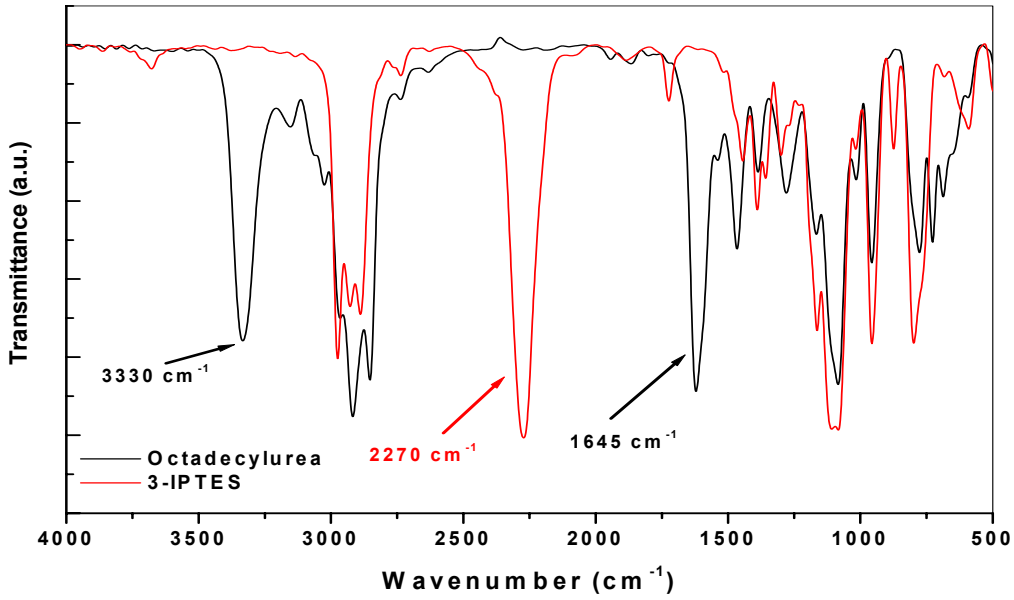


**Figure 74. FT-IR spectrums of the Octadecylurea (black line) and 3-IPTES (red line).**

In the Figure 74, the strong absorption bands at around 3330 $cm^{-1}$ (N-H stretch) and at around 1645 $cm^{-1}$ (C=O stretch) for Octadecylurea confirm the formation of urea linkages. Also, the absence of a strong absorption band at around 2270 $cm^{-1}$ (due to NCO group) shows that the reaction is completed.

### 5.3.10.2. Characterization of the Octadecylurea-modified $TiO_2$ nanoparticles

After Octadecylurea molecule was synthesized, $TiO_2$ nanoparticles were modified with this molecule (section 4.6.10., page 59). After modification, the Octadecylurea-modified $TiO_2$ nanoparticles were characterized by GC/MS, FT-IR and elemental analysis.

#### 5.3.10.2.1. GC/MS result

After $TiO_2$ nanoparticles were modified with Octadecylurea molecules, the liberated ethanol molecules were detected by GC/MS. The result is shown in the following.

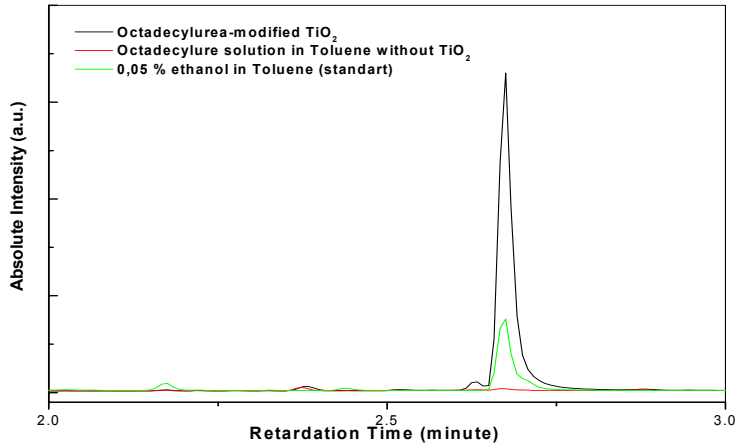


**Figure 75. GC/MS result of the Octadecylurea-modified $TiO_2$ powder.**

In the Figure 75, after modification of $TiO_2$ nanoparticles with Octadecylurea, the liberated ethanol molecules were detected and this result was compared with standart ethanol solution. Because it was not detected no ethanol in the solution of the Octadecylurea in toluene, all ethanol detected by GC/MS was resulted from the modification of $TiO_2$ nanoparticles with Octadecylurea. Thus, it is concluded from GC/MS result that $TiO_2$ nanoparticles were modified with Octadecylurea molecules.

### 5.3.10.2.2. FT-IR result

After the Octadecylurea-modified $TiO_2$ powder was dried, it was characterized by FT-IR. The result is shown in the following.

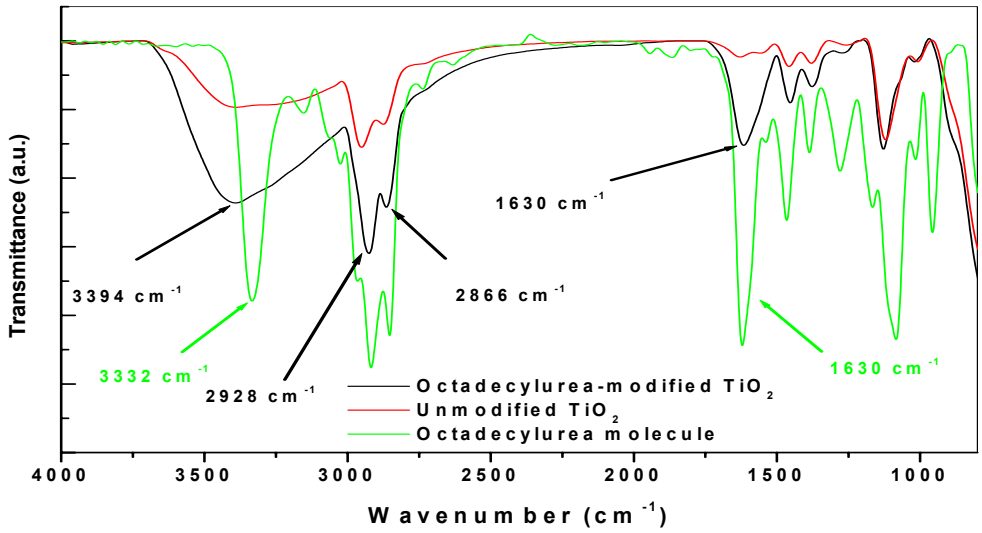


**Figure 76. FT-IR spectrums of the Octadecylurea-modified $TiO_2$ powder, Octadecylurea and unmodified $TiO_2$ powder.**

In the Figure 76, after $TiO_2$ nanoparticles were modified with Octadecylurea molecules, the urea peaks in the spectrum of the Octadecylurea-modified nanoparticles seem still at around 1630 $cm^{-1}$ and 3394 $cm^{-1}$. In addition, $CH_3$-, -$CH_2$- absorbsion bands in the spectrum of the Octadecylurea-modified $TiO_2$ nanoparticles increased at around 2866 $cm^{-1}$ and 2928 $cm^{-1}$ as compared to the spectrum of unmodified nanoparticles. Thus, it is concluded that the modification of $TiO_2$ nanoparticles with Octadecylurea molecules was succeeded and proved by FT-IR.

### 5.3.10.2.3. Elemental analysis result

After the Octadecylurea-modified $TiO_2$ powder was dried, it was characterized by elemental analysis. The result is shown in the following.

| Powder | C% | H% | N% |
|---|---|---|---|
| Octadecylurea-modified $TiO_2$ powder | 16,62 | 3,31 | 0,64 |
| Unmodified $TiO_2$ powder | 8,38 | 2,13 | 0,0 |

According to this result, the increase in the carbon, hydrogen and nitrogen percentages indicates that $TiO_2$ nanoparticles were modified with Octadecylurea molecules. Furthermore, it is interesting that the increase in the amount of carbon after modification with 112Dodecylurea molecules is more than that with Octadecylurea although the number of carbon atoms in Octadecylure molecule is more than that in 112Dodecylurea (carbon percent for the 112Dodecylurea-modified $TiO_2$ powder: 18,64). The reason for that finding might be various interaction types between amino groups of 112Dodecylurea molecules and $TiO_2$ surfaces. This is similar to the modification of $TiO_2$ nanoparticles with AMMO molecules (see section 5.2.5, page 85). The interactions between amino group in the 112Dodecylurea molecule and $TiO_2$ surface are 1) the amine may enter into hydrogen bonding interaction with surface hydroxyl group, 2) the basic amine function may form and ionic bonding with a surface hydroxyl group. This type of interaction is more stable than the former interaction. Because of the mentioned interactions, in this experiment, much more 112Dodecylurea molecules might interact with $TiO_2$ surface besides covalent bonding to the surface. For this reason, the increase in the carbon amount of the 112Dodecylurea-modified $TiO_2$ nanoparticles is more than that of the Octadecylurea-modified $TiO_2$ nanoparticles although the number of carbon atoms in the Octadecylurea molecule is more than that in the 112Dodecylurea.

### 5.3.10.2.4. The evaluation of characterization of the urea molecules and the urea-modified $TiO_2$ nanoparticles

After the urea molecules were synthesized, they were characterized by FT-IR. According to the FT-IR results, new strong absorption bands for all results at around 3300-3400 $cm^{-1}$ and 1600-1700 $cm^{-1}$ confirm the formation of urea linkages. Also, the absence of a strong absorption bands for all results at around 2270 $cm^{-1}$ (due to NCO group) shows that the reaction is completed. Furthermore, after $TiO_2$ nanoparticles were modified with the urea molecules, the urea-modified nanoparticles were characterized by GC/MS, FT-IR and elemental analysis. GC/MS results showed that ethanol molecules were liberated from the reaction between –OH groups of $TiO_2$ nanoparticles and ethoxy groups of the urea molecules with the formation of Ti-O-Si covalent bonds on the surface. Also, after $TiO_2$ nanoparticles were modified with the urea molecules, the urea peaks in the spectrums of the modified $TiO_2$ nanoparticles seemed still at around 1600-1700 $cm^{-1}$ and 3300-3400 $cm^{-1}$. According to the elemental analysis results, the increase in the amount of carbon, hydrogen and nitrogen of the urea-modified $TiO_2$ nanoparticles also confirm the modifications of $TiO_2$ nanoparticles. In the literature, it was not found any work about the modifications of $TiO_2$ nanoparticles (with a diameter of 6 nm, with narrow size distribution and agglomeration-free) with urea molecules.

## 5.4. Calculation of –OH and $–OC_3H_7$ groups reacted with modification agents

After $TiO_2$ nanoparticles were modified with silanes, carboxylic acids, β-ketoester and urea molecules, how many percent –OH or $–OC_3H_7$ groups on the surfaces of $TiO_2$ nanoparticles modified with them were calculated. Also, the moles of –OH and $–OC_3H_7$ groups in 1 g $TiO_2$ powder are $3{,}79.10^{-3}$ and $2{,}33.10^{-3}$ respectively (see section 5.2., page 73). It is known that after the modifications of $TiO_2$ nanoparticles with carboxylic acids, β-ketoesters and β-diketones, the amount of $–OC_3H_7$ groups on the surface of $TiO_2$ nanoparticles is decreased and the carbon and hydrogen on $TiO_2$ surface is increased with respect to the modification agents. Also, by means of the modifications of the silanes and urea molecules, the Ti-O-Si covalent bonds formed on $TiO_2$ surface by means of the reaction between –OH groups on the surface of $TiO_2$ nanoparticles and methoxy groups of silane molecules or ethoxy groups of urea molecules. Consequently, the amount of carbon, hydrogen and nitrogen on the surface of $TiO_2$ nanoparticles increased as compared to the unmodified $TiO_2$ nanoparticles. Thus, it is concluded that the increase in the amount of carbon, hydrogen and nitrogen is resulted from the modifications of $TiO_2$ nanoparticles with the silanes, carboxylic acids, β-ketoester and the urea molecules. The percentages of –OH and $–OC_3H_7$ groups modified with carboxylic acids, β-ketoester, silanes and urea molecules are shown in the following.

**Table 6. Elemental analysis results of the unmodified-$TiO_2$ nanoparticle and modified-$TiO_2$ nanoparticles, the percents of –OH and $–OC_3H_7$ groups modified with modification agents, the number of carbon atoms in the modification agents after modification (it is accepted that three methoxy groups in the silane molecules were reacted with three –OH groups on the surface of $TiO_2$ nanoparticles).**

| Modifications with | The numbers of carbon atoms in the modification agents (after modification) | C % | H % | N % | Modified –OH groups (%) | Modified $–OC_3H_7$ groups (%) |
|---|---|---|---|---|---|---|
| Unmodified $TiO_2$ | - | 8,38 | 2,13 | 0 | - | - |
| HTMS | 6 | 10,7 | 2,48 | 0 | 25,50 | - |
| DTMS | 10 | 13,14 | 2,94 | 0 | 31,40 | - |
| DDTMS | 12 | 13,21 | 2,90 | 0 | 26,54 | - |
| HDTMS | 16 | 14,73 | 3,07 | 0 | 26,18 | - |
| AMMO | 3 | 11,24 | 2,69 | 1,24 | 62,88 | - |
| 10-Undecylenic Acid | 11 | 17,61 | 3,23 | 0 | - | 41,22 |
| Oleic Acid | 18 | 22,15 | 3,75 | 0 | - | 32,81 |
| Stearic Acid | 18 | 26,98 | 4,73 | 0 | - | 44,30 |
| AAA | 7 | 14,66 | 2,58 | 0 | - | 56,08 |

$TiO_2$ nanoparticles were modified with HTMS, DTMS, DDTMS, HDTMS, and AMMO by forming Ti-O-Si covalent bonds on the surface of $TiO_2$ nanoparticles with the reaction between -OH groups on the surface of $TiO_2$ nanoparticles with methoxy groups of the silane molecules. According to the Table 6, the percent of -OH groups changed with AMMO was more than that with other modification agents. Its reason might be various interaction types between AMMO and $TiO_2$ surfaces. All probable reasons for that finding were explained in before sections (see section 5.2.5, page 85). Also, $TiO_2$ nanoparticles were modified with stearic acid, oleic acid, AAA and 10-undecylenic acid molecules by forming the complex structures on the surface. After modifications, it was observed that the percentage of $–OC_3H_7$ groups changed with AAA molecules is the most in all carboxylic acids and β-ketoester molecule. All probable reasons for that finding were explained in before sections (see section 5.2.9.3, page 100).

**Table 7. Elemental analysis results of $TiO_2$ nanoparticles after and before modified with the urea molecules, the modified –OH groups on $TiO_2$ nanoparticle surface, the number of carbon atoms in the urea molecules after modification (it is accepted that three ethoxy groups in the urea molecules were reacted with three –OH groups on the surface of $TiO_2$ nanoparticles).**

| Modification with the urea molecules | The number of carbon atoms in the urea molecules after modification | C % | H % | N % | Modified –OH amount (%) |
|---|---|---|---|---|---|
| Unmodified $TiO_2$ | - | 8,38 | 2,13 | 0 | - |
| Ethylenurea | 6 | 13,26 | 2,92 | 1,53 | 53,65 |
| 16Hexylurea | 10 | 14,10 | 3,03 | 1,46 | 37,73 |
| 18Octylurea | 12 | 15,21 | 3,21 | 1,35 | 37,54 |
| 112Dodecylurea | 16 | 18,64 | 3,75 | 1,57 | 42,30 |
| DMSA15urea | 37 | 21,36 | 5,11 | 0,50 | 10,44 |
| DMSA21urea | 64 | 27,66 | 6,92 | 0,49 | 8,96 |
| Pentylurea | 9 | 11,75 | 2,60 | 0,36 | 24,70 |
| Octylurea | 12 | 12,53 | 2,74 | 0,39 | 22,81 |
| 1Dodecylurea | 16 | 14,20 | 3,02 | 0,51 | 23,99 |
| Octadecylurea | 22 | 16,62 | 3,31 | 0,64 | 24,71 |

$TiO_2$ nanoparticles were also modified with Ethylenurea, Pentylurea, Octylurea, Octadecylurea, 1Dodecylurea, 16Hexylurea, 112Dodecylurea, 18Octylurea, DMSA15urea, DMSA21urea. According to the Table 7, of these urea modifications, the amount of -OH groups changed with Ethylenurea was more than that with other urea modifications. Its reason might be interactions between Ethylenurea and $TiO_2$ surfaces beside covalent bondings. Also, the amount of -OH groups on $TiO_2$ nanoparticles changed with DMSA15urea and DMSA21urea is less than those with the other modification agents. Its reason might be because of their sterical hindrance effects.

## 5.5. PMMA grafting onto $TiO_2$ nanoparticle

After $TiO_2$ nanoparticles were modified with 2AAEM molecules, the grafting of PMMA molecules onto $TiO_2$ nanoparticles were achieved using MMA monomers by means of *the combination of both grafting methods.* After that, the PMMA-grafted $TiO_2$ powders were characterized by TGA/DSC and some of them were also characterized by FT-IR. Also, the percentages of PMMA grafting onto $TiO_2$ nanoparticles were calculated by means of the

following equation. Where A is weight of PMMA grafted (g) and B is weight of $TiO_2$ charged (g) [264-267].

$$\text{Percentage of Grafting}\,(\%) = \frac{A}{B} \text{ x } 100$$

### 5.5.1. Characterization of $TiO_2$-2AAEM-30-1:100-20

In this experiment, PMMA molecules were grafted onto $TiO_2$ surface with modification of 30 % of $-OC_3H_7$ groups with 2AAEM, with a molar ratio of 2AAEM:MMA = 1:100 and 20 % MMA by weight with respect to the total weight (according to section 4.7.2.1., page 61). After that, the PMMA-grafted nanoparticles were characterized by FT-IR and TGA/DSC. The results are shown in the following.

#### 5.5.1.1. FT-IR result

After PMMA molecules were grafted onto $TiO_2$ nanoparticles, the PMMA-grafted powder was dried and characterized by FT-IR. The result is shown in the following.

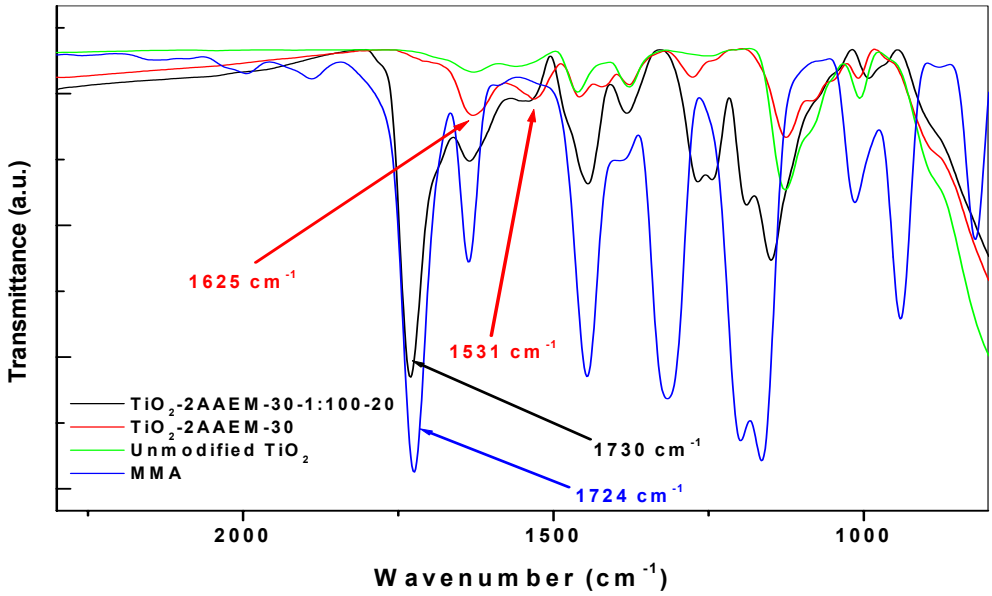


**Figure 77. FT-IR spectrums of the PMMA-grafted $TiO_2$ powder, 2AAEM modified-$TiO_2$ powder, unmodified $TiO_2$ powder and MMA.**

FT-IR spectrums of the unmodified-$TiO_2$ powder, 2AAEM-modified $TiO_2$ powder and PMMA-grafted $TiO_2$ powder are shown in the Figure 77. Although there are no peaks at around 1530 $cm^{-1}$ in the spectrum of the unmodified-$TiO_2$ powder, two peaks occurred at around 1625 $cm^{-1}$ for $\nu$(C=O) and 1531 $cm^{-1}$ for $\nu$(C=C) in the spectrum of the 2AAEM-modified $TiO_2$ powder. According to the literature, the bands of the stretching vibration $\nu$(C=O) and $\nu$(C=C) of the enolic forms of the β-ketoesters at around 1615 $cm^{-1}$ and 1525 $cm^{-1}$ were determined [76]. Thus, it is concluded that $TiO_2$ nanoparticles were modified with 2AAEM molecules. After PMMA molecules were grafted onto the 2AAEM-modified $TiO_2$ nanoparticles using MMA, the PMMA-grafted nanoparticles were characterized by FT-IR. The spectrum of MMA shows a peak at around 1724 $cm^{-1}$ that belongs to carbonyl stretch of the MMA. After PMMA molecules were grafted onto $TiO_2$ nanoparticles, this peak shifted to 1730 $cm^{-1}$ according to the spectrum of the PMMA-grafted nanoparticles, namely in the $TiO_2$-2AAEM-30-1:100-20. Because the peak belongs to carbonyl stretch seems in the same area of the spectrum of the PMMA-grafted nanoparticles in spite of washing of ungrafted PMMA and MMA with solvents and the spectrum of unmodified $TiO_2$ nanoparticles does not show the same peak, it is concluded that PMMA molecules were indeed grafted onto the surface of $TiO_2$ nanoparticles.

### 5.5.1.2. TGA/DSC result

After PMMA molecules were grafted onto $TiO_2$ nanoparticles, the PMMA-grafted powder was dried and characterized by TGA/DSC. TGA/DSC results for the PMMA-grafted $TiO_2$ nanoparticles, ungrafted $TiO_2$ nanoparticles and pure PMMA are shown in the following.

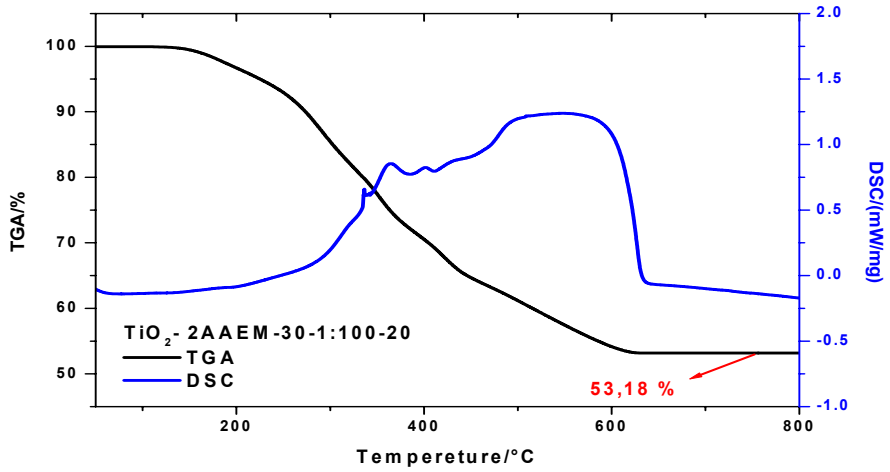


**Figure 78. TGA/DSC result for $TiO_2$-2AAEM-30-1:100-20.**

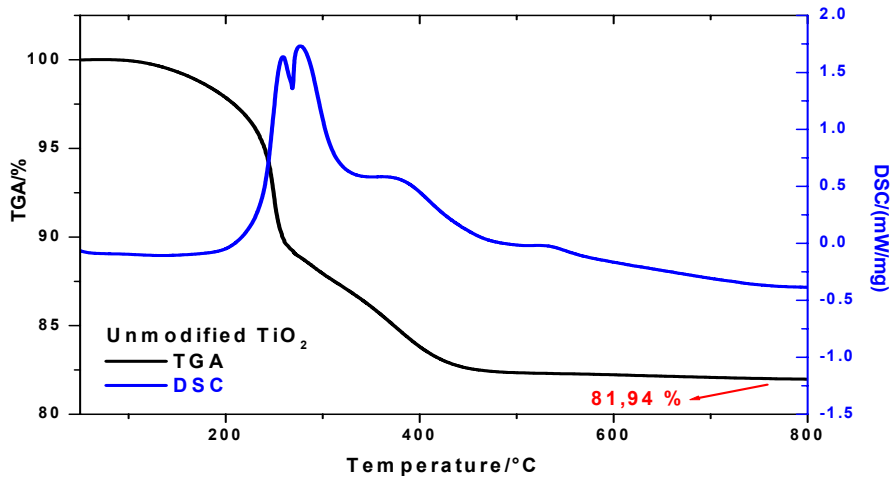


**Figure 79. TGA/DSC result for the unmodified-$TiO_2$ powder.**

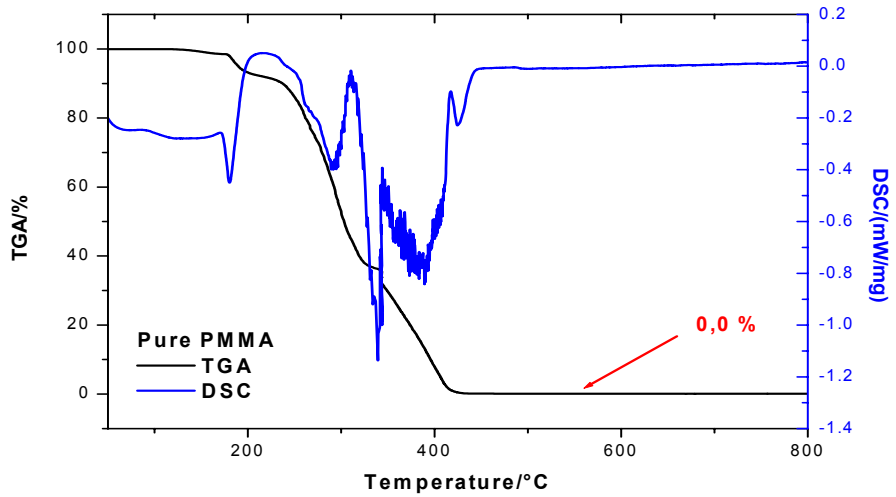


**Figure 80. TGA/DSC result for pure PMMA.**

| Name | Decomposed amount by TGA (%) |
|---|---|
| Unmodified $TiO_2$ powder | 18,06 |
| $TiO_2$-2AAEM-30-1:100-20 | 46,8 |

After the grafting of PMMA onto $TiO_2$ nanoparticles, its thermal behaviour was investigated by TGA/DSC. According to the Figure 78 and 79, the weight loss of the PMMA-grafted nanoparticles is higher than that of the unmodified $TiO_2$ nanoparticles. Of course, this is because of decomposing of PMMA grafted onto the surface of $TiO_2$ nanoparticles at high temperatures. As for DSC result of the PMMA-grafted powder, the peaks between 300-

500 °C could be ascribed to the removal and combustion of the organic groups contained in the product. Furthermore, according to the TGA result for pure PMMA, the whole PMMA was decomposed between 50-440 °C (Figure 80). Consequently, the weight losses of the samples are decreasing in the order: pure PMMA > PMMA-grafted $TiO_2$ nanoparticles > ungrafted $TiO_2$ nanoparticles.

### 5.5.2. Characterization of $TiO_2$-2AAEM-30-1:1000-20

In this experiment, PMMA molecules were grafted onto $TiO_2$ surface with the modification of 30 % of $–OC_3H_7$ groups with 2AAEM, with a molar ratio of 2AAEM:MMA = 1:1000 and 20 % MMA by weight with respect to the total weight (according to section 4.7.2.2., page 61). It is expected that the percentage of PMMA grafting onto $TiO_2$ nanoparticles will increase with the increase in the molar ratio of 2AAEM:MMA from 1:100 to 1:1000. The results are shown in the following.

#### 5.5.2.1. TGA/DSC result

After PMMA molecules were grafted onto $TiO_2$ nanoparticles, the PMMA-grafted powder was dried and characterized by TGA/DSC. The result is shown in the following.

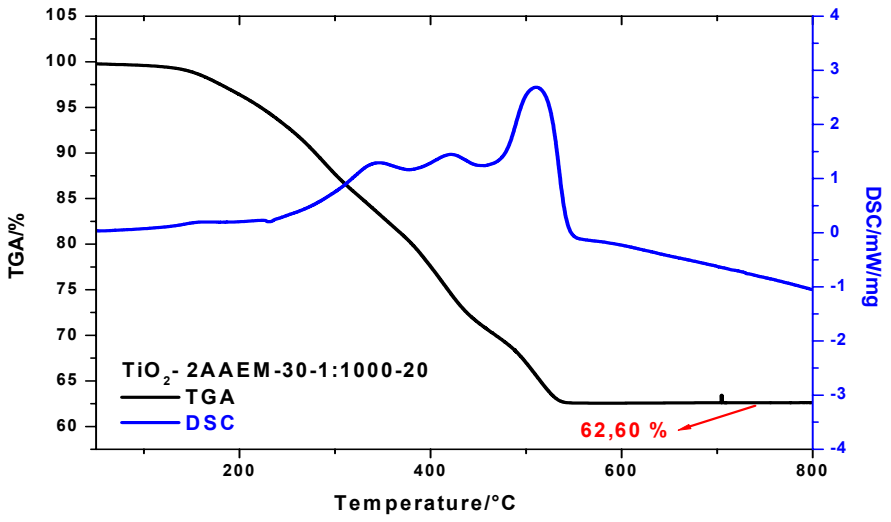


**Figure 81. TGA/DSC result of $TiO_2$-2AAEM-30-1:1000-20.**

| Name | Decomposed amount by TGA (%) |
|---|---|
| Unmodified $TiO_2$ powder | 18,06 |
| $TiO_2$-2AAEM-30-1:1000-20 | 37,4 |

After the grafting of PMMA onto $TiO_2$ nanoparticles, its thermal behaviour was investigated by TGA/DSC. According to the Figure 79 and 81, the weight loss of the PMMA-grafted sample is higher than that of the unmodified $TiO_2$ nanoparticles. This can be explained by decomposing of PMMA on the nanoparticles at high temperatures. Furthermore, according to the DSC result, the peaks between 300-500 °C could be ascribed to the removal and combustion of the organic groups contained in the product. Also, it was expected that the amount of the grafting of PMMA molecules onto $TiO_2$ nanoparticles would increase with the increase in the molar ratio of 2AAEM:MMA from 1:100 to 1:1000 but, it didn't increase. On the contrary, the amount of the grafting onto the nanoparticles decreased by 20 % (see section 5.5.1.2., page 136). The reason for that finding might be because of intermolecular polymerization of MMA molecules for the formation of ungrafted PMMA molecules instead of the grafting onto $TiO_2$ nanoparticles. Because the ungrafted 2AAEM and ungrafted PMMA were removed by washing with solvents, the amount of PMMA grafting onto the surface did not change.

### 5.5.3. Characterization of $TiO_2$-2AAEM-30-1:100-40

In this experiment, PMMA molecules were grafted onto $TiO_2$ surface with the modification of 30 % of $–OC_3H_7$ groups with 2AAEM, with a molar ratio of 2AAEM:MMA = 1:100 and 40 % MMA by weight with respect to the total weight (according to section 4.7.2.3., page 61). It is expected that the percentage of PMMA grafting onto $TiO_2$ nanoparticles will increase with increasing of MMA concentration from 20 % to 40 % [92]. The results are shown in the following.

#### 5.5.3.1. FT-IR result

After PMMA molecules were grafted onto $TiO_2$ nanoparticles, the PMMA-grafted powder was dried and characterized by FT-IR. Also, MMA conversion is calculated by comparing the peak areas of the double bonds after and before polymerization. The results are shown in the following.

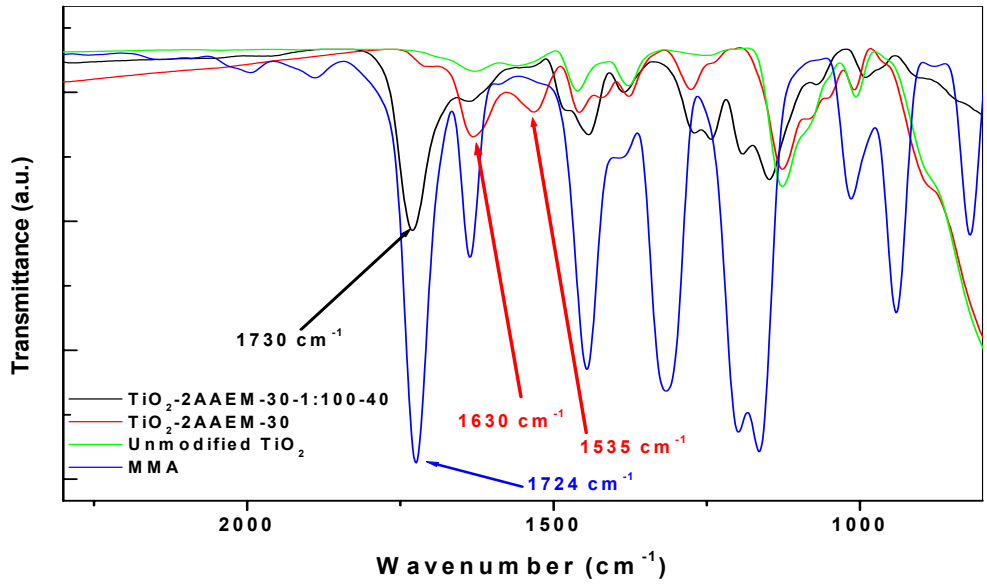


**Figure 82. FT-IR spectrums of the PMMA-grafted $TiO_2$ powder, 2AAEM modified-$TiO_2$ powder, unmodified $TiO_2$ powder and MMA.**

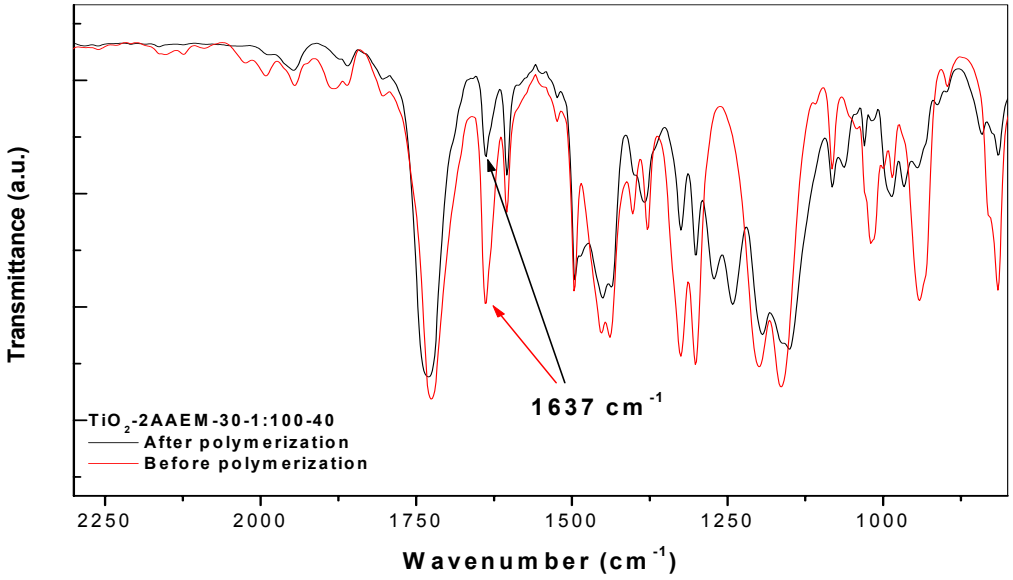


**Figure 83. FT-IR results for the comparison of the peak intensity of double bond after and before polymerization.**

FT-IR spectrums of the unmodified-$TiO_2$ powder, 2AAEM-modified $TiO_2$ powder and PMMA-grafted $TiO_2$ powder are shown in the Figure 82. Although there are no peaks at around 1530 $cm^{-1}$ in the spectrum of the unmodified-$TiO_2$ powder, two peaks occurred at around 1630 $cm^{-1}$

for ν(C=O) and 1535 $cm^{-1}$ for ν(C=C) in the spectrum of the 2AAEM-modified $TiO_2$ powder. This shows that $TiO_2$ nanoparticles were modified with 2AAEM molecules. After PMMA molecules were grafted onto 2AAEM-modified $TiO_2$ nanoparticles using MMA, the PMMA-grafted nanoparticles were characterized by FT-IR. The spectrum of MMA shows a peak at around 1724 $cm^{-1}$ that belongs to carbonyl stretch of the MMA. After PMMA molecules were grafted onto $TiO_2$ nanoparticles, this peak shifted to 1730 $cm^{-1}$ according to the spectrum of the PMMA-grafted nanoparticles, namely in the $TiO_2$-2AAEM-30-1:100-40. Because the peak belongs to carbonyl stretch seems in the same area in the spectrum of the PMMA-grafted nanoparticles in spite of washing of ungrafted PMMA and MMA with solvents and the spectrum of unmodified $TiO_2$ nanoparticles does not show the same peak, it is concluded that PMMA molecules were indeed grafted onto $TiO_2$ surface. Also, according to the Figure 83, when comparing after and before polymerization, it is observed that the peak intensity of the peak at 1637 $cm^{-1}$ that belongs to the double bonds decreased by 66 %. Consequently, it is understood that the polymerization and the PMMA grafting onto the surface were achieved.

### 5.5.3.2. TGA/DSC result

After PMMA molecules were grafted onto $TiO_2$ nanoparticles, the PMMA-grafted powder was dried and characterized by TGA/DSC. The result is shown in the following.

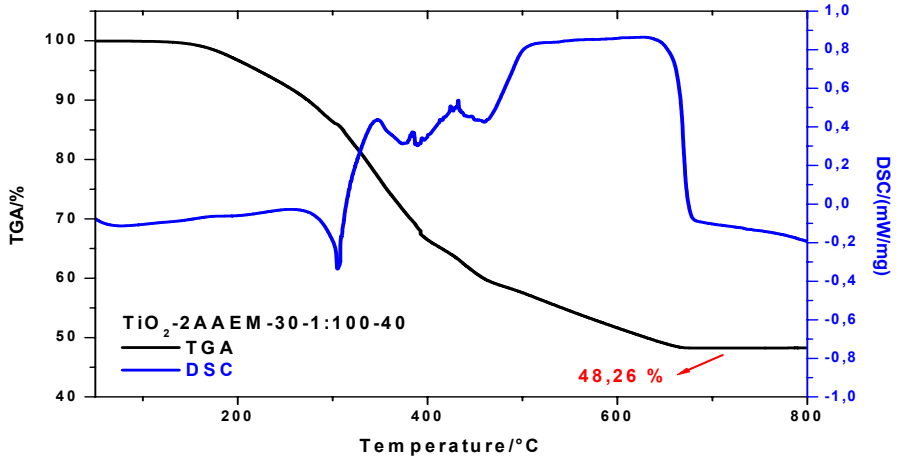


**Figure 84. TGA/DSC result of $TiO_2$-2AAEM-30-1:100-40.**

| Name | Decomposed amount by TGA (%) |
|---|---|
| Unmodified $TiO_2$ | 18,06 |
| $TiO_2$-2AAEM-30-1:100-40 | 51,74 |

After the grafting of PMMA onto $TiO_2$ nanoparticles, its thermal behaviour was investigated by TGA/DSC. According to the Figure 79 and 84, the weight loss of the PMMA-grafted sample is higher than that of the unmodified $TiO_2$ nanoparticles. This can be explained by decomposing of PMMA on the nanoparticles at high temperatures. Furthermore, according to the DSC result of the PMMA-grafted powder, the peaks between 300-500 °C could be ascribed to the removal and combustion of the organic groups contained in the product. Also, it was expected that the percentage of the grafting of PMMA onto $TiO_2$ nanoparticles will increase with increasing of MMA concentration from 20 % to 40 %. Indeed, the percentage of PMMA grafting onto $TiO_2$ nanoparticles increased but only by 10 % (see section 5.5.1.2., page 136). The reason for insufficient increase in the PMMA grafting onto $TiO_2$ nanoparticles might be intermolecular polymerization of MMA molecules for the formation of ungrafted PMMA instead of the grafting onto the surface. Namely, because of intermolecular polymerization of MMA molecules, ungrafted PMMA molecules formed instead of the grafting onto $TiO_2$ nanoparticles. Because ungrafted 2AAEM and ungrafted PMMA were removed by washing with solvents, the amount of PMMA grafting onto the surface did not change.

### 5.5.4. Characterization of $TiO_2$-2AAEM-30-1:1000-40

In this experiment, PMMA molecules were grafted onto $TiO_2$ surface with the modification of 30 % of $–OC_3H_7$ groups with 2AAEM, with a molar ratio of 2AAEM:MMA = 1:1000 and 40 % MMA by weight with respect to the total weight (according to section 4.7.2.4., page 62). It is expected that the percentage of PMMA grafting onto $TiO_2$ nanoparticles will increase with the increase of the molar ratio of 2AAEM:MMA from 1:100 to 1:1000 and with increase of MMA concentration from 20 % to 40 %. The results are shown in the following.

#### 5.5.4.1. FT-IR result

In this section, MMA conversion is calculated by comparing the peak area of the double bonds after and before polymerization. FT-IR result is shown in the following.

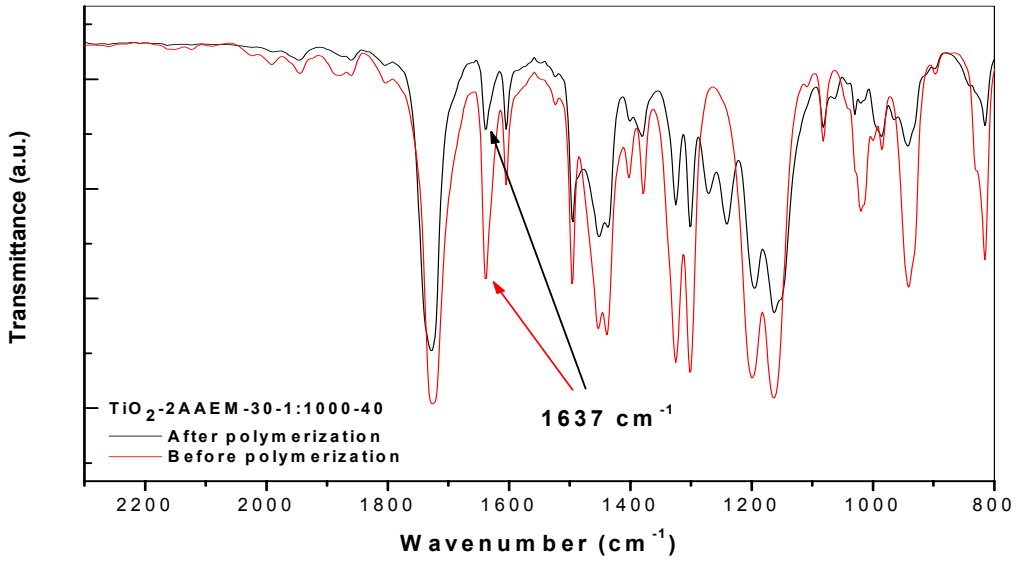


**Figure 85. FT-IR results after and before polymerization for comparison of the peak intensity of double bond.**

According to the Figure 85, it is observed that the intensity of the peak at 1637 $cm^{-1}$ that belongs to the double bond decreased by 69 % after polymerization. Consequently, it is concluded that the polymerization was achieved.

### 5.5.4.2. TGA/DSC result

After PMMA molecules were grafted onto $TiO_2$ nanoparticles, the PMMA-grafted powder was dried and characterized by TGA/DSC. The result is shown in the following.

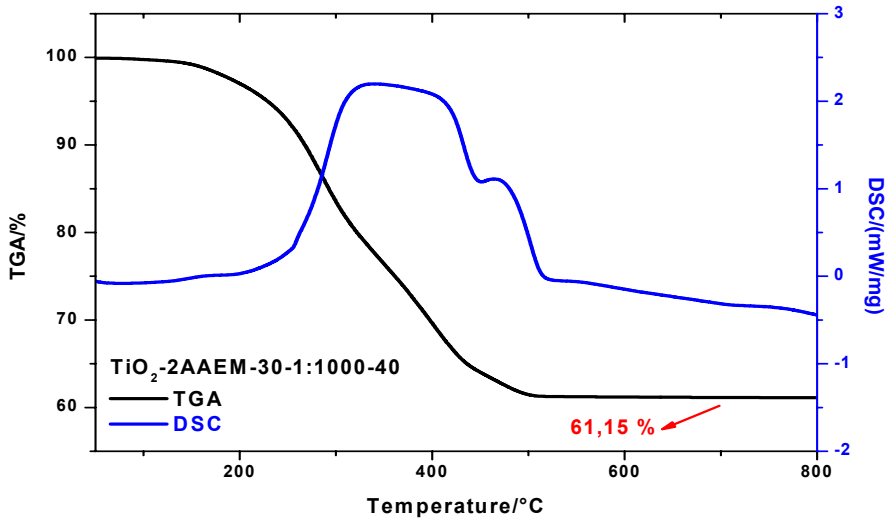


**Figure 86. TGA/DSC result of $TiO_2$-2AAEM-30-1:1000-40.**

| Name | Decomposed amount by TGA (%) |
|---|---|
| Unmodified $TiO_2$ powder | 18,06 |
| $TiO_2$-2AAEM-30-1:1000-40 | 38,85 |

After the grafting of PMMA onto $TiO_2$ nanoparticles, its thermal behaviour was investigated by TGA/DSC. In the Figure 79 and 86, the weight loss of the PMMA-grafted sample is higher than that of the unmodified $TiO_2$ nanoparticles. This can be explained by decomposing of PMMA on the nanoparticles at high temperatures. Furthermore, according to the DSC result of the PMMA-grafted $TiO_2$ nanoparticles, the peaks between 300-500 °C could be ascribed to the removal and combustion of the organic groups contained in the product. Also, it was expected that the percentage of the grafting of PMMA molecules onto $TiO_2$ nanoparticles would increase with the increase of MMA concentration from 20 % to 40 % and with the increase of the molar ratio of 2AAEM:MMA from 1:100 to 1:1000. Indeed, the percentage of grafting of PMMA onto $TiO_2$ nanoparticles increased but only by 4 % with the increase of MMA from 20 % to 40 %(see section 5.5.2, page 138). Also, the amount of grafting of PMMA onto $TiO_2$ nanoparticles with the molar ratio of 2AAEM:MMA from 1:100 to 1:1000 decreased by 25 % as opposed to expected (see section 5.5.3, page 139). Their reasons might be intermolecular polymerization of MMA molecules for the formation of ungrafted PMMA molecules and sterical hindrance effects. Namely, because of intermolecular polymerization of MMA molecules, ungrafted PMMA molecules formed instead of the grafting onto $TiO_2$ nanoparticles. Then, ungrafted PMMA molecules were removed from the mixtures by washing with solvents.

### 5.5.4.3. The evaluation of the PMMA grafting onto 2AAEM-modified $TiO_2$ nanoparticles as 30 % of $–OC_3H_7$ groups on the surface, with the molar ratios of 2AAEM:MMA= 1:100 and 1:1000 and with 20 % and 40 % MMA by weight with respect to the total weight

After $TiO_2$ nanoparticles were modified with 2AAEM molecules as 30 % of $–OC_3H_7$ groups on $TiO_2$ nanoparticles, the 2AAEM-modified $TiO_2$ nanoparticles were dispersed in MMA with a molar ratios of 2AAEM:MMA= 1:100 and 1:1000. Each of these samples was dispersed in toluene with an amount of 20 % and 40 % MMA by weight with respect to the total weight. After that, polymerization was performed. According to the TGA/DSC results, the weight losses of the PMMA-grafted $TiO_2$ nanoparticles were higher than that of the unmodified $TiO_2$ nanoparticles. The summary of the results of PMMA grafting are shown in Table 8. According to the literature, the percentage of the grafting of PMMA onto $TiO_2$ nanoparticles increases

with increasing of MMA concentration from 20 % to 40 % [92]. For this reason, it was expected that because the concentration of MMA was increased from 20 % to 40 %, the percentages of the grafting of PMMA onto $TiO_2$ nanoparticles increased. But, the increases in the grafting percentages were only by 4 % and 10 %. Also, although the molar ratios of 2AAEM:MMA were increased from 1:100 to 1:1000, the percentages of the graftings of PMMA onto $TiO_2$ nanoparticles decreased by 20-25 % as opposed to expected. Its reasons might be intermolecular polymerization of MMA molecules for the formation of ungrafted PMMA molecules and sterical hindrance effects. Namely, because of intermolecular polymerization of MMA molecules, ungrafted PMMA molecules formed instead of the grafting onto $TiO_2$ nanoparticles and after washing of ungrafted PMMA molecules with solvents, they were removed from the mixtures. Furthermore, PMMA grafting onto $TiO_2$ nanoparticles was also proved by FT-IR.

**Table 8. The summary of PMMA grafting results onto $TiO_2$ surface after 30 % modification of $–OC_3H_7$ groups with 2AAEM**

| 2AAEM/ MMA | The percentage of the modified $–OC_3H_7$ groups on the nanoparticles (%) | The concentration of MMA (%) | The percentage of the PMMA grafting onto $TiO_2$ nanoparticle by TGA (%) |
|---|---|---|---|
| Unmodified $TiO_2$ powder | | | 18,06 |
| 1 :100 | 30 | 20 | 46,80 |
| 1:1000 | 30 | 20 | 37,40 |
| 1 :100 | 30 | 40 | 51,74 |
| 1:1000 | 30 | 40 | 38,85 |

### 5.5.5. Characterization of $TiO_2$-2AAEM-50-1:100-20

In this experiment, PMMA molecules were grafted onto $TiO_2$ surface with the modification of 50 % of $–OC_3H_7$ groups with 2AAEM, with a molar ratio of 2AAEM:MMA = 1:100 and 20 % MMA by weight with respect to the total weight (according to section 4.7.3.1., page 63). It is expected that the percentage of PMMA grafting onto $TiO_2$ nanoparticles will increase directly proportional to the amount of $–OC_3H_7$ groups with 2AAEM, namely with the increase from 30 % to 50 % of $–OC_3H_7$ groups on the surface. The results are shown in the following.

### 5.5.5.1. FT-IR result

After PMMA molecules were grafted onto $TiO_2$ nanoparticles, the PMMA-grafted powder was dried and characterized by FT-IR. The result is shown in the following.

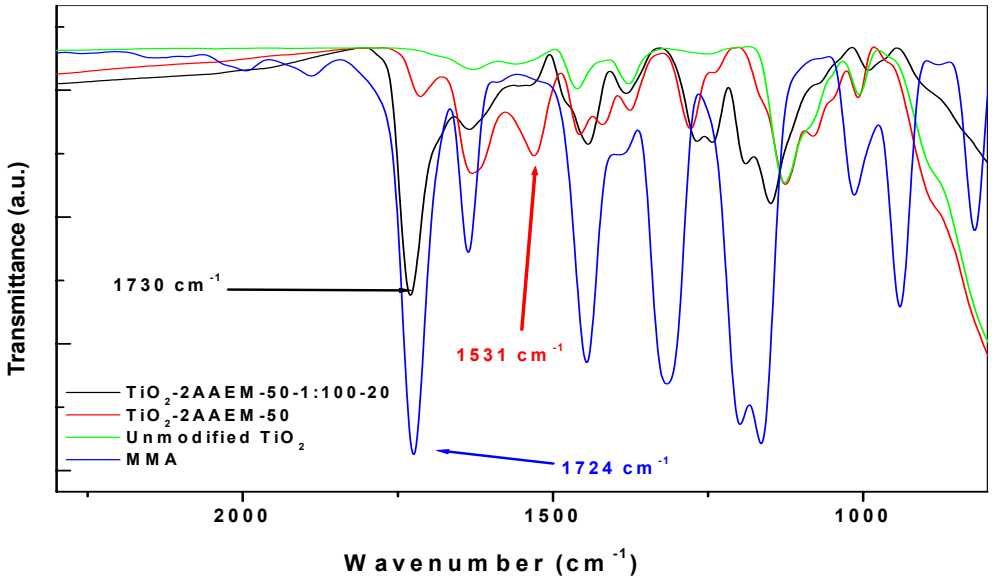


**Figure 87. FT-IR spectrums of the PMMA-grafted $TiO_2$ powder, 2AAEM modified-$TiO_2$ powder (before polymerization), unmodified $TiO_2$ powder and MMA.**

FT-IR spectrums of the unmodified-$TiO_2$ powder, 2AAEM-modified $TiO_2$ powder and PMMA-grafted $TiO_2$ powder are shown in the Figure 87. Although there are no peaks at around 1530 $cm^{-1}$ in the spectrum of the unmodified-$TiO_2$ powder, two peaks occurred at around 1625 $cm^{-1}$ for $\nu$(C=O) and 1531 $cm^{-1}$ for $\nu$(C=C) in the spectrum of the 2AAEM-modified $TiO_2$ powder. This shows that $TiO_2$ nanoparticles were modified with 2AAEM molecules. After PMMA molecules were grafted onto the 2AAEM-modified $TiO_2$ nanoparticles using MMA, the PMMA-grafted nanoparticles were characterized by FT-IR. The spectrum of MMA shows a peak at around 1724 $cm^{-1}$ that belongs to carbonyl stretch of the MMA. After PMMA molecules were grafted onto $TiO_2$ nanoparticles, this peak shifted to 1730 $cm^{-1}$ according to the spectrum of the PMMA-grafted nanoparticles, namely in the $TiO_2$-2AAEM-50-1:100-20. Because the peak belongs to carbonyl stretch seems in the same area in the spectrum of the PMMA-grafted nanoparticles in spite of washing of ungrafted PMMA and MMA with solvents and the spectrum of unmodified $TiO_2$ nanoparticles does not show the same peak, it is concluded that PMMA molecules were indeed grafted onto $TiO_2$ surface.

### 5.5.5.2. TGA/DSC result

After PMMA molecules were grafted onto $TiO_2$ nanoparticles, the PMMA-grafted powder was dried and characterized by TGA/DSC. The result is shown in the following.

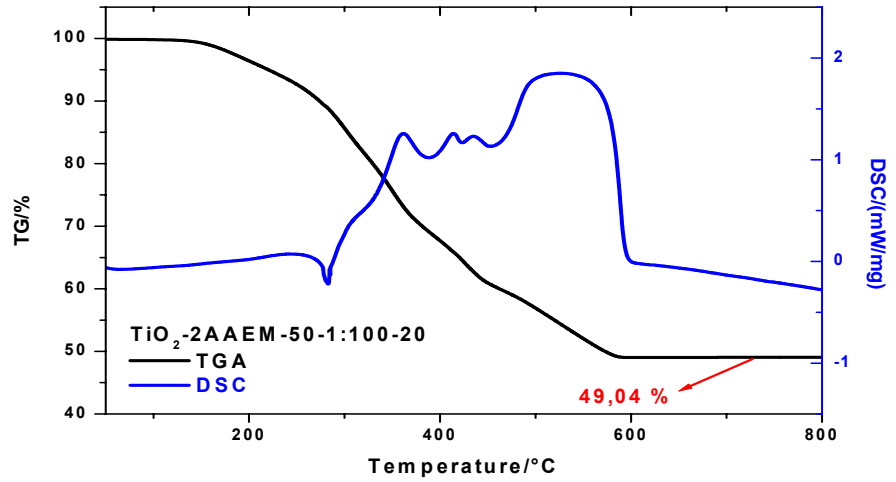


**Figure 88. TGA/DSC result of $TiO_2$-2AAEM-50-1:100-20.**

| Name | Decomposed amount by TGA (%) |
|---|---|
| Unmodified $TiO_2$ powder | 18,06 |
| $TiO_2$-2AAEM-50-1:100-20 | 50,96 |

After the grafting of PMMA onto $TiO_2$ nanoparticles, its thermal behaviour was investigated by TGA/DSC. According to the Figure 79 and 88, the weight loss of the PMMA-grafted sample is higher than that of the unmodified $TiO_2$ nanoparticles. This can be explained by decomposing of PMMA onto $TiO_2$ nanoparticles at high temperatures. Furthermore, according to the DSC result, the peaks between 300-500 °C could be ascribed to the removal and combustion of the organic groups contained in the product. Also, it was expected that the amount of the grafting of PMMA molecules onto $TiO_2$ nanoparticles would increase directly proportional to the amount of $–OC_3H_7$ groups modified with 2AAEM, namely from 30 % to 50 %. As expected, the amount of PMMA grafting onto $TiO_2$ nanoparticles increased but only by 9 % (see section 5.5.1.2., page 136). The reason for that finding might be an insufficient modification of the $–OC_3H_7$ groups. Namely, it was expected that 50 % of $–OC_3H_7$ groups on the surface of $TiO_2$ nanoparticles were modified with 2AAEM molecules but this goal could not be achieved. This might be because of sterical hindrance effects of 2AAEM molecules already attached to the surface. Therefore, after ungrafted 2AAEM and

ungrafted PMMA were removed by washing, the amount of PMMA grafting onto $TiO_2$ nanoparticles did not change.

### 5.5.6. Characterization of $TiO_2$-2AAEM-50-1:1000-20

In this experiment, PMMA molecules were grafted onto $TiO_2$ surface with the modification of 50 % of $–OC_3H_7$ groups with 2AAEM, with the molar ratio of 2AAEM:MMA = 1:1000 and 20 % MMA by weight with respect to the total weight (according to section 4.7.3.2., page 63). It is expected that the percentage of PMMA grafting onto $TiO_2$ nanoparticles will increase directly proportional to the amount of $–OC_3H_7$ groups with 2AAEM, namely with the increase from 30 % to 50 % of $–OC_3H_7$ groups on the surface. Also, it is expected that the percentage of PMMA grafting onto $TiO_2$ nanoparticles will increase with the increase of the molar ratio of 2AAEM:MMA from 1:100 to 1:1000. The results are shown in the following.

#### 5.5.6.1. TGA/DSC result

After PMMA were grafted onto $TiO_2$ nanoparticles, the PMMA-grafted powder was dried and characterized by TGA/DSC. The result is shown in the following.

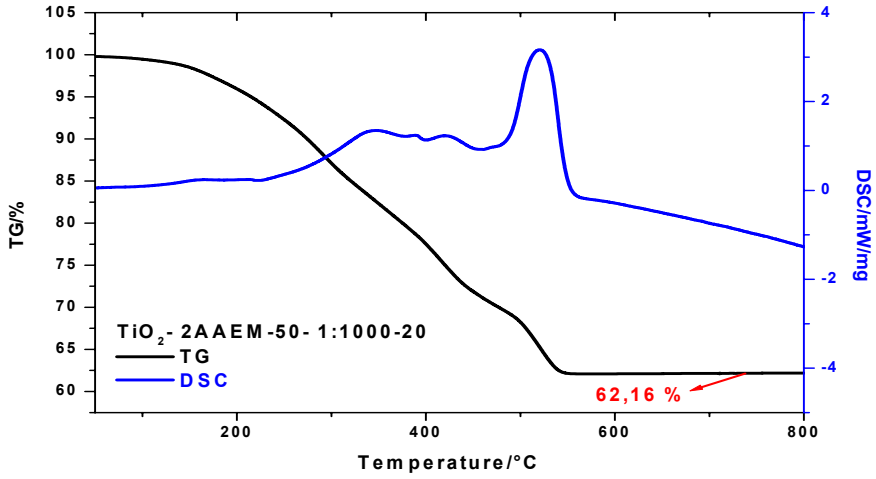


**Figure 89. TGA/DSC result of $TiO_2$-2AAEM-50-1:1000-20.**

| Name | Decomposed amount by TGA (%) |
|---|---|
| Unmodified $TiO_2$ powder | 18,06 |
| $TiO_2$-2AAEM-50-1:1000-20 | 37,80 |

After the grafting of PMMA onto $TiO_2$ nanoparticles, its thermal behaviour was investigated by TGA/DSC. According to the Figure 79 and 89, the weight loss of the PMMA-grafted sample is higher than that of the unmodified $TiO_2$ nanoparticles. This can be explained by decomposing of PMMA onto $TiO_2$ nanoparticles at high temperatures. Furthermore, according to the DSC result, the peaks between 300-500 °C could be ascribed to the removal and combustion of the organic groups contained in the product. Also, it was expected that the amount of the grafting of PMMA molecules onto $TiO_2$ nanoparticles would increase directly proportional to the amount of $–OC_3H_7$ groups modified with 2AAEM, namely from 30 % to 50 %. As expected, the amount of PMMA grafting onto $TiO_2$ nanoparticles increased but only by 1 % (see section 5.5.2, page 138). The reason for that finding might be an insufficient modification of the $–OC_3H_7$ groups. Namely, it was expected that 50 % of $–OC_3H_7$ groups on the surface were modified with 2AAEM molecules but this goal could not be achieved. This might be because of sterical hindrance effects of 2AAEM molecules already attached to the surface and intermolecular polymerization of MMA molecules for the formation of ungrafted PMMA instead of the grafting onto the surface. Therefore, after ungrafted 2AAEM and ungrafted PMMA were removed by washing, the percentage of PMMA grafting onto $TiO_2$ nanoparticles did not change.

### 5.5.7. Characterization of $TiO_2$-2AAEM-50-1:100-40

In this experiment, PMMA molecules were grafted onto $TiO_2$ surface with the modification of 50 % of $–OC_3H_7$ groups with 2AAEM, with the molar ratio of 2AAEM:MMA = 1:100 and 40 % MMA by weight with respect to the total weight (according to section 4.7.3.3., page 63). It is expected that the percentage of PMMA grafting onto $TiO_2$ nanoparticles will increase directly proportional to the amount of $–OC_3H_7$ groups with 2AAEM, namely with the increase from 30 % to 50 % of $–OC_3H_7$ groups on the surface. Also, it is expected that the percentage of PMMA grafting onto $TiO_2$ nanoparticles will increase with increasing of MMA concentration from 20 % to 40 %. The results are shown in the following.

#### 5.5.7.1. FT-IR result

After PMMA molecules were grafted onto $TiO_2$ nanoparticles, the PMMA-grafted powder was dried and characterized by FT-IR. The result is shown in the following.

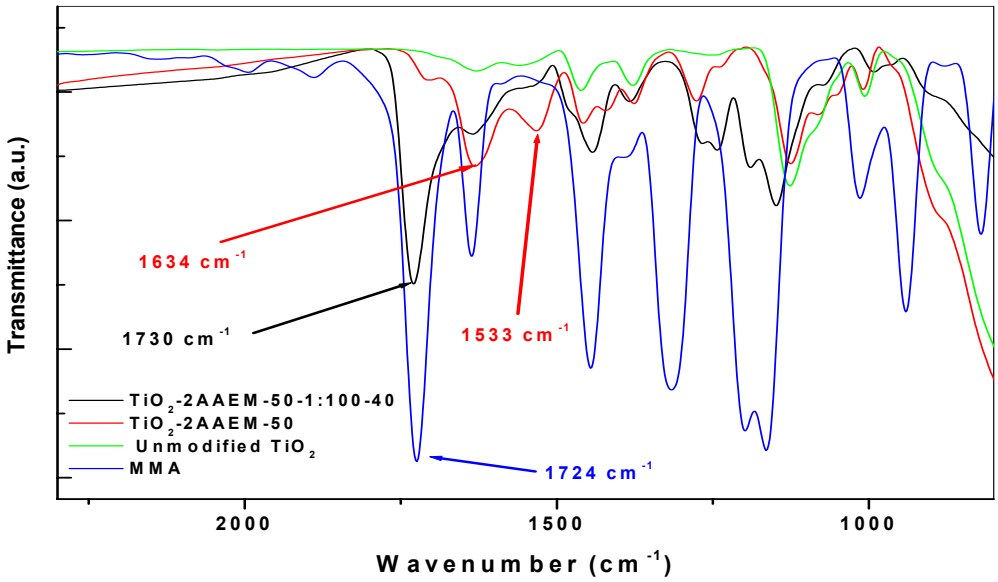


**Figure 90. FT-IR spectrums of the PMMA-grafted $TiO_2$ powder, 2AAEM modified-$TiO_2$ powder (before polymerization), unmodified $TiO_2$ powder and MMA.**

FT-IR spectrums of the unmodified-$TiO_2$ powder, 2AAEM-modified $TiO_2$ powder and PMMA-grafted $TiO_2$ powder are shown in the Figure 90. Although there are no peaks at around 1530 $cm^{-1}$ in the spectrum of unmodified-$TiO_2$ powder, two peaks occurred at around 1634 $cm^{-1}$ for $\nu$(C=O) and 1533 $cm^{-1}$ for $\nu$(C=C) in the spectrum of the 2AAEM-modified $TiO_2$ powder. This shows that $TiO_2$ nanoparticles were modified with 2AAEM molecules. After PMMA molecules were grafted onto the 2AAEM-modified $TiO_2$ nanoparticles using MMA, the PMMA-grafted nanoparticles were characterized by FT-IR. The spectrum of MMA shows a peak at around 1724 $cm^{-1}$ that belongs to carbonyl stretch of the MMA. After PMMA molecules were grafted onto $TiO_2$ nanoparticles, this peak shifted to 1730 $cm^{-1}$ according to the spectrum of the PMMA-grafted nanoparticles, namely in the $TiO_2$-2AAEM-50-1:100-40. Because the peak belongs to carbonyl stretch seems in the same area in the spectrum of the PMMA-grafted nanoparticles in spite of washing of the ungrafted PMMA and MMA with solvents and the spectrum of unmodified $TiO_2$ nanoparticles does not show the same peak, it is concluded that PMMA molecules were indeed grafted on the surface of $TiO_2$ nanoparticles.

### 5.5.7.2. TGA/DSC result

After PMMA were grafted onto $TiO_2$ nanoparticles, the PMMA-grafted powder was dried and characterized by TGA/DSC. The result is shown in the following.

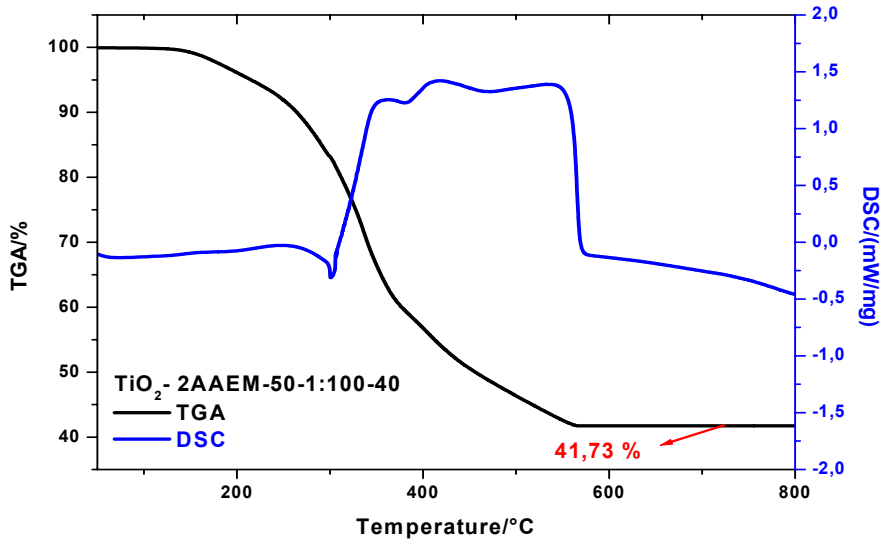


**Figure 91. TGA/DSC result of $TiO_2$-2AAEM-50-1:100-40.**

| Name | Decomposed amount by TGA (%) |
|---|---|
| Unmodified $TiO_2$ powder | 18,06 |
| $TiO_2$-2AAEM-50-1:100-40 | 58,27 |

After the grafting of PMMA onto $TiO_2$ nanoparticles, its thermal behaviour was investigated by TGA/DSC. According to the Figure 79 and 91, the weight loss of the PMMA-grafted sample is higher than that of the unmodified $TiO_2$ nanoparticles. This can be explained by decomposing of PMMA onto $TiO_2$ nanoparticles at high temperatures. Furthermore, according to the DSC result, the peaks between 300-500 °C could be ascribed to the removal and combustion of the organic groups contained in the product. Also, it was expected that the amount of the grafting of PMMA molecules onto $TiO_2$ nanoparticles would increase directly proportional to the amount of $–OC_3H_7$ groups modified with 2AAEM, namely from 30 % to 50 %. As expected, the amount of PMMA grafting onto $TiO_2$ nanoparticles increased but only by 13 % (see section 5.5.3, page 139). The reason for that finding might be an insufficient modification of the $–OC_3H_7$ groups. Namely, it was expected that 50 % of $–OC_3H_7$ groups on the surface were modified with 2AAEM molecules but this goal could not be achieved. This might be because of sterical hindrance effects of 2AAEM molecules already attached to the surface. Therefore, after ungrafted 2AAEM and ungrafted PMMA were removed by washing, the amount of PMMA grafting onto $TiO_2$ nanoparticles did not change. Also, it was expected that the amount of the grafting of PMMA molecules onto $TiO_2$ nanoparticles would change with the increase in the concentration of MMA from 20 % to

40 %. Indeed, the amounts of grafting of PMMA onto $TiO_2$ nanoparticles increased but only by 14 % (see section 5.5.5, page 145). The reason for insufficient increase in the PMMA grafting onto $TiO_2$ nanoparticles might be intermolecular polymerization of MMA molecules for the formation of ungrafted PMMA instead of the grafting onto the surface.

### 5.5.8. Characterization of $TiO_2$-2AAEM-50-1:1000-40

In this experiment, PMMA molecules were grafted onto $TiO_2$ surface with the modification of 50 % of $–OC_3H_7$ groups with 2AAEM, with the molar ratio of 2AAEM:MMA = 1:1000 and 40 % MMA by weight with respect to the total weight (according to section 4.7.3.4., page 64). It is expected that the percentage of PMMA grafting onto $TiO_2$ nanoparticles will increase directly proportional to the amount of $–OC_3H_7$ groups with 2AAEM, namely with the increase from 30 % to 50 % of $–OC_3H_7$ groups on the surface. Also, it is expected that the percentage of PMMA grafting onto $TiO_2$ nanoparticles will increase with increasing of MMA concentration from 20 % to 40 % and will increase with the increase of the molar ratio of 2AAEM:MMA from 1:100 to 1:1000. The results are shown in the following.

#### 5.5.8.1. TGA/DSC result

After PMMA were grafted onto $TiO_2$ nanoparticles, the PMMA-grafted powder was dried and characterized by TGA/DSC. The result is shown in the following.

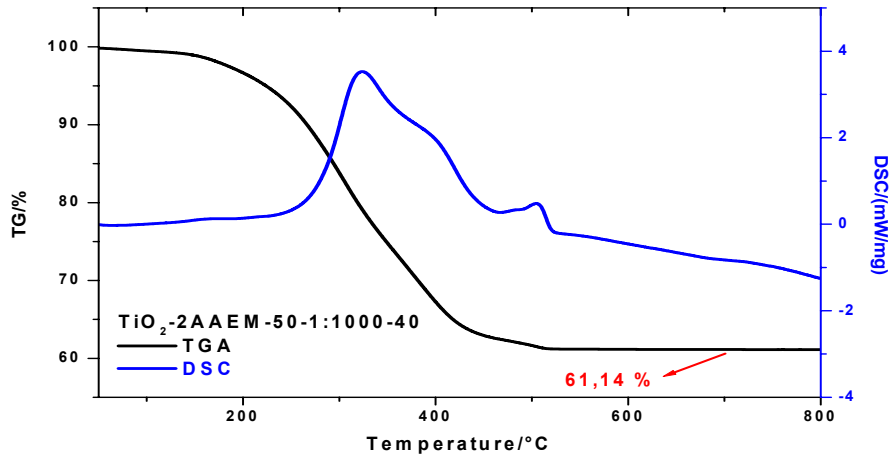


**Figure 92. TGA/DSC result of $TiO_2$-2AAEM-50-1:1000-40.**

| Name | Decomposed amount by TGA (%) |
|---|---|
| Unmodified $TiO_2$ powder | 18,06 |
| $TiO_2$-2AAEM-50-1:1000-40 | 38,86 |

After the grafting of PMMA onto $TiO_2$ nanoparticles, its thermal behaviour was investigated by TGA/DSC. According to the Figure 79 and 92, the weight loss of the PMMA-grafted sample is higher than that of the unmodified $TiO_2$ nanoparticles. This can be explained by decomposing of PMMA onto $TiO_2$ nanoparticles at high temperatures. Furthermore, according to the DSC result, the peaks between 300-500 °C could be ascribed to the removal and combustion of the organic groups contained in the product. Also, it was expected that the amount of the grafting of PMMA molecules onto $TiO_2$ nanoparticles would increase directly proportional to the amount of $–OC_3H_7$ groups modified with 2AAEM, namely from 30 % to 50 %. But, the amount of PMMA grafting onto $TiO_2$ nanoparticles did not increase (see section 5.5.4, page 142). The reason for that finding might be an insufficient modification of the $–OC_3H_7$ groups. Namely, it was expected that 50 % of $–OC_3H_7$ groups on the surface were modified with 2AAEM molecules but this goal could not be achieved. This might be because of sterical hindrance effects of 2AAEM molecules already attached to the surface. Therefore, after ungrafted 2AAEM and ungrafted PMMA were removed by washing, the amount of PMMA grafting onto $TiO_2$ nanoparticles did not change. Also, it was expected that the amount of the grafting of PMMA molecules onto $TiO_2$ nanoparticles would change with the increase in the concentration of MMA from 20 % to 40 %. Indeed, the amount PMMA grafting onto $TiO_2$ nanoparticles increased but only by 3 % (see section 5.5.6, page 148). Furthermore, it was expected that the amount of the grafting of PMMA molecules onto $TiO_2$ nanoparticles will increase with the increase of the molar ratio of 2AAEM:MMA from 1:100 to 1:1000. But, it didn't increase. On the contrary, the amount of the grafting onto the nanoparticles decreased by 33 %. The reason for that finding might be because of intermolecular polymerization of MMA molecules for the formation of ungrafted PMMA molecules instead of the grafting onto $TiO_2$ nanoparticles. Because ungrafted 2AAEM and ungrafted PMMA were removed by washing with solvents, the amount of PMMA grafting onto the surface did not change.

### 5.5.8.2. The evaluation of the PMMA grafting onto the 2AAEM-modified $TiO_2$ nanoparticles as 50 % of $–OC_3H_7$ groups on the surface, with the molar ratios of 2AAEM:MMA= 1:100 and 1:1000 and with 20 % and 40 % MMA by weight with respect to the total weight

After $TiO_2$ nanoparticles were modified with 2AAEM molecules as 50 % of $–OC_3H_7$ groups on $TiO_2$ nanoparticles, the 2AAEM-modified $TiO_2$ nanoparticles were dispersed in MMA with a molar ratios of 2AAEM:MMA= 1:100 and 1:1000. Each of these samples was dispersed in toluene with an amount of 20 % and 40 % MMA by weight with respect to the total weight. After that, polymerization was performed. According to the TGA/DSC result, the weight losses of the PMMA-grafted $TiO_2$ nanoparticles were higher than that of the unmodified $TiO_2$ nanoparticles. The summary of the results of PMMA grafting are shown in Table 9. It was expected that the amount of the grafting of PMMA molecules onto $TiO_2$ nanoparticles would increase directly proportional to the amount of $–OC_3H_7$ groups modified with 2AAEM, namely from 30 % to 50 %. Indeed, the amount of PMMA grafting onto $TiO_2$ nanoparticles increased but only between by 1-13. The reason for insufficient grafting onto the surface might be an insufficient modification of the $–OC_3H_7$ groups. Namely, it was expected that 50 % of $–OC_3H_7$ groups on the surface were modified with 2AAEM molecules but this goal could not be achieved. This might be because of sterical hindrance effects of 2AAEM molecules already attached to the surface. Therefore, after ungrafted 2AAEM and ungrafted PMMA were removed by washing with solvents, the amount of PMMA grafting onto $TiO_2$ nanoparticles did not change. Also, although the concentrations of MMA in the mixtures were increased from 20 % to 40 %, the amount of PMMA grafting onto $TiO_2$ nanoparticles did not increase as expected. The increases in the grafting amounts were only 3 % and 14 %. Also, although the molar ratio of 2AAEM:MMA was increased from 1:100 to 1:1000, the amount of PMMA grafting onto $TiO_2$ nanoparticles were decreased by 25-30 % as opposed to expected. The reason for these findings might be because of intermolecular polymerization of MMA molecules for the formation of ungrafted PMMA molecules instead of the grafting onto $TiO_2$ nanoparticles. Because the ungrafted 2AAEM and ungrafted PMMA were removed by washing with solvents, the amount of PMMA grafting onto the surface did not change as expected. Furthermore, the grafting onto $TiO_2$ nanoparticles was also proved by FT-IR.

**Table 9. The summary of PMMA grafting results onto $TiO_2$ surface after 50 % modification of $–OC_3H_7$ groups with 2AAEM**

| 2AAEM/ MMA | The percentage of the modified $–OC_3H_7$ groups on the nanoparticles (%) | The concentration of MMA (%) | The amount of the grafting of PMMA onto nanoparticle according to TGA results (%) |
|---|---|---|---|
| Unmodified $TiO_2$ powder | | | 18,06 |
| 1 :100 | 50 | 20 | 50,96 |
| 1:1000 | 50 | 20 | 37,80 |
| 1 :100 | 50 | 40 | 58,27 |
| 1:1000 | 50 | 40 | 38,86 |

### 5.5.9. Characterization of $TiO_2$-2AAEM-80-1:100-20

In this experiment, PMMA molecules were grafted onto $TiO_2$ surface with the modification of 80 % of $–OC_3H_7$ groups with 2AAEM, with a molar ratio of 2AAEM:MMA = 1:100 and 20 % MMA by weight with respect to the total weight (according to section 4.7.4.1., page 64). It is expected that the percentage of PMMA grafting onto $TiO_2$ nanoparticles will increase directly proportional to the amount of $–OC_3H_7$ groups with 2AAEM, namely with the increase from 30 % to 80 % of $–OC_3H_7$ groups on the surface. The results are shown in the following.

#### 5.5.9.1. FT-IR result

After PMMA molecules were grafted onto $TiO_2$ nanoparticles, the PMMA-grafted powder was dried and characterized by FT-IR. The result is shown in the following.

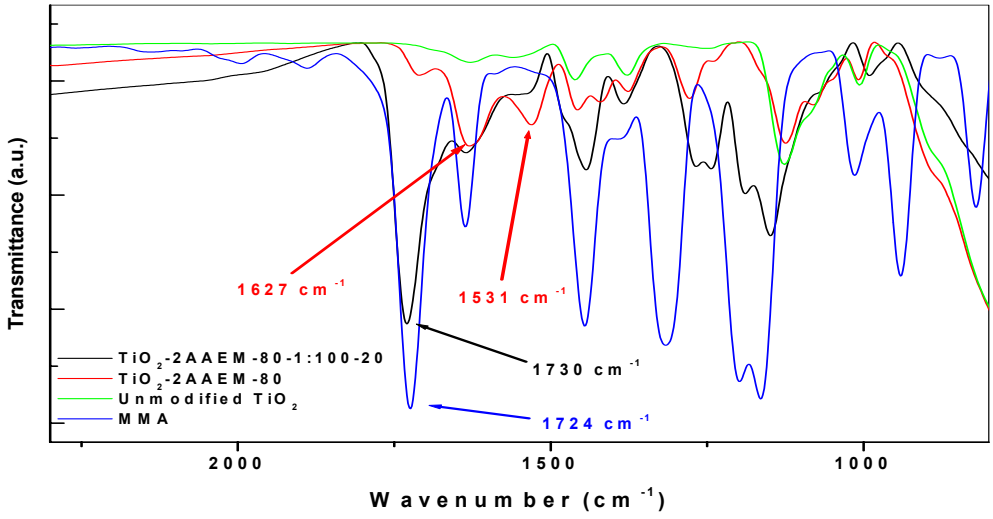

**Figure 93. FT-IR spectrums of the PMMA-grafted $TiO_2$ powder, 2AAEM-modified $TiO_2$ powder (before polymerization), unmodified $TiO_2$ powder and MMA.**

FT-IR spectrums of the unmodified-$TiO_2$ powder, 2AAEM-modified $TiO_2$ powder and PMMA-grafted $TiO_2$ powder are shown in the Figure 93. Although there are no peaks at around 1530 $cm^{-1}$ in the spectrum of the unmodified $TiO_2$ powder, two peaks occurred at around 1627 $cm^{-1}$ for $\nu$(C=O) and 1531 $cm^{-1}$ for $\nu$(C=C) in the spectrum of the 2AAEM-modified $TiO_2$ powder. This shows that $TiO_2$ nanoparticles were modified with 2AAEM molecules. After PMMA molecules were grafted onto the 2AAEM-modified $TiO_2$ nanoparticles using MMA, the PMMA-grafted nanoparticles were characterized by FT-IR. The spectrum of MMA shows a peak at around 1724 $cm^{-1}$ that belongs to carbonyl stretch of the MMA. After PMMA molecules were grafted onto $TiO_2$ nanoparticles, this peak shifted to 1730 $cm^{-1}$ according to the spectrum of the PMMA-grafted nanoparticles, namely in the $TiO_2$-2AAEM-80-1:100-20. Because the peak belongs to carbonyl stretch seems in the same area in the spectrum of the PMMA-grafted nanoparticles in spite of washing of ungrafted PMMA and MMA with solvents and the spectrum of unmodified $TiO_2$ nanoparticles does not show the same peak, it is concluded that PMMA molecules were indeed grafted onto $TiO_2$ surface.

### 5.5.9.2. TGA/DSC result

After PMMA were grafted onto $TiO_2$ nanoparticles, the PMMA-grafted powder was d ried and characterized by TGA/DSC. The result is shown in the following.

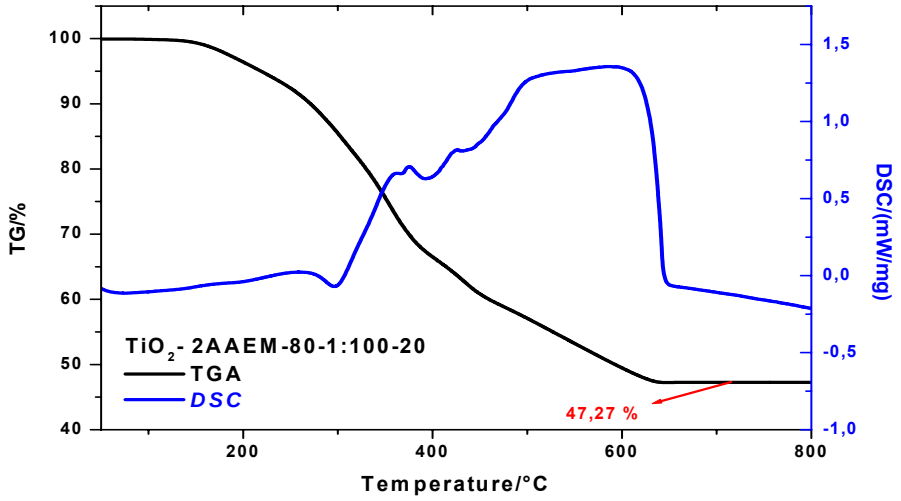


**Figure 94. TGA/DSC result of $TiO_2$-2AAEM-80-1:100-20.**

| Name | Decomposed amount by TGA (%) |
|---|---|
| Unmodified $TiO_2$ powder | 18,06 |
| $TiO_2$-2AAEM-80-1:100-20 | 52,70 |

After the grafting of PMMA onto $TiO_2$ nanoparticles, its thermal behaviour was investigated by TGA/DSC. According to the Figure 79 and 94, the weight loss of the PMMA-grafted sample is higher than that of the unmodified $TiO_2$ nanoparticles. This can be explained by decomposing of PMMA onto $TiO_2$ nanoparticles at high temperatures. Furthermore, according to the DSC result, the peaks between 300-500 °C could be ascribed to the removal and combustion of the organic groups contained in the product. It was expected that the amount of the grafting of PMMA molecules onto $TiO_2$ nanoparticles would increase directly proportional to the amount of $–OC_3H_7$ groups modified with 2AAEM, namely from 30 % to 80 %. Indeed, the amount of PMMA grafting onto $TiO_2$ nanoparticles increased but only by 13 % (see section 5.5.1.2., page 136). The reason for insufficient grafting onto the surface might be an insufficient modification of the $-OC_3H_7$ groups. Namely, it was expected that 80 % of $–OC_3H_7$ groups on the surface were modified with 2AAEM molecules but this goal could not be achieved. This might be because of sterical hindrance effects of 2AAEM molecules already attached to the surface. Therefore, after ungrafted 2AAEM and ungrafted PMMA were removed by washing with solvents, the amount of PMMA grafting onto $TiO_2$ nanoparticles did not change.

### 5.5.10. Characterization of $TiO_2$-2AAEM-80-1:1000-20

In this experiment, PMMA molecules were grafted onto $TiO_2$ surface with the modification of 80 % of $–OC_3H_7$ groups with 2AAEM, with a molar ratio of 2AAEM:MMA = 1:1000 and 20 % MMA by weight with respect to the total weight (according to section 4.7.4.2., page 65). It is expected that the percentage of PMMA grafting onto $TiO_2$ nanoparticles will increase directly proportional to the amount of $–OC_3H_7$ groups with 2AAEM, namely with the increase from 30 % to 80 % of $–OC_3H_7$ groups on the surface and will increase with the increase of the molar ratio of 2AAEM:MMA from 1:100 to 1:1000. The results are shown in the following.

#### 5.5.10.1. TGA/DSC result

After PMMA were grafted onto $TiO_2$ nanoparticles, the PMMA-grafted powder was dried and characterized by TGA/DSC. The result is shown in the following.

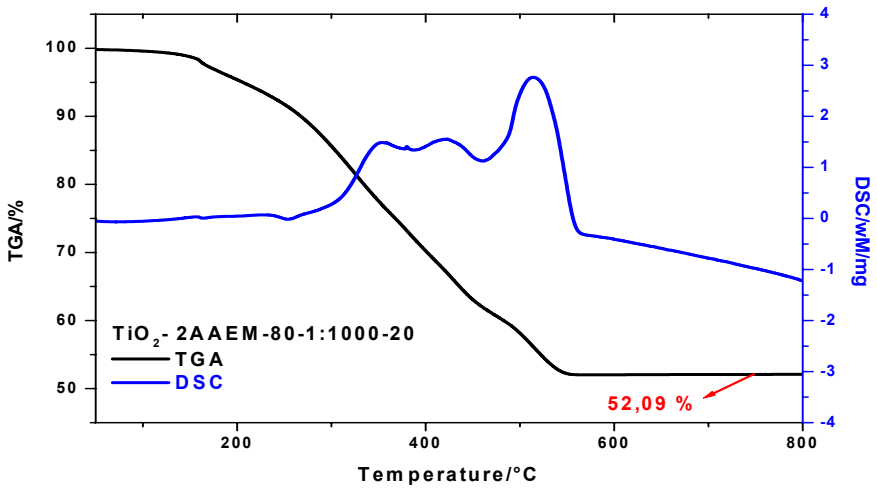


**Figure 95. TGA/DSC result of $TiO_2$-2AAEM-80-1:1000-20.**

| Name | Decomposed amount by TGA (%) |
|---|---|
| Unmodified $TiO_2$ powder | 18,06 |
| $TiO_2$-2AAEM-80-1:1000-20 | 47,91 |

After the grafting of PMMA onto $TiO_2$ nanoparticles, its thermal behaviour was investigated by TGA/DSC. According to the Figure 79 and 95, the weight loss of the PMMA-grafted sample is higher than that of the unmodified $TiO_2$ nanoparticles. This can be explained by decomposing of PMMA on $TiO_2$ nanoparticles at high temperatures. Furthermore, according to the DSC result, the peaks between 300-500 °C could be ascribed to the removal and combustion of the organic groups contained in the product. Also, it was expected that the amount of the grafting of PMMA molecules onto $TiO_2$ nanoparticles would increase directly proportional to the amount of $–OC_3H_7$ groups modified with 2AAEM, namely 80 % of $–OC_3H_7$ groups on the surface. Indeed, the amount of PMMA grafting onto $TiO_2$ nanoparticles increased but only 28 % (see section 5.5.2, page 138). The reason for insufficient grafting onto the surface might be an insufficient modification of the $-OC_3H_7$ groups with 2AAEM molecules. Namely, it was expected that 80 % of $–OC_3H_7$ groups on the surface were modified with 2AAEM molecules but this goal could not be achieved. This might be because of sterical hindrance effects of 2AAEM molecules already attached to the surface. Also, it was expected that the amount of the grafting of PMMA molecules onto $TiO_2$ nanoparticles would increase with the increase in the molar ratio of 2AAEM:MMA from 1:100 to 1:1000 but, it didn't increase. On the contrary, the amount of the grafting onto the nanoparticles decreased by 9 % (see section 5.5.9, page 155). The reason for that finding might be

because of intermolecular polymerization of MMA molecules for the formation of ungrafted PMMA molecules instead of the grafting onto $TiO_2$ nanoparticles. Because the ungrafted 2AAEM and ungrafted PMMA were removed by washing with solvents, the amount of PMMA grafting onto the surface did not change.

### 5.5.11. Characterization of $TiO_2$-2AAEM-80-1:100-40

In this experiment, PMMA molecules were grafted onto $TiO_2$ surface with the modification of 80 % of $–OC_3H_7$ groups with 2AAEM, with a molar ratio of 2AAEM:MMA = 1:100 and 40 % MMA by weight with respect to the total weight (according to section 4.7.4.3., page 65). It is expected that the percentage of PMMA grafting onto $TiO_2$ nanoparticles will increase directly proportional to the amount of $–OC_3H_7$ groups with 2AAEM, namely with the increase from 30 % to 80 % of $–OC_3H_7$ groups on the surface and will increase with increasing of MMA concentration from 20 % to 40 %. Also, the appearance of the PMMA-grafted $TiO_2$ nanoparticles is investigated by TEM. The results are shown in the following.

#### 5.5.11.1. FT-IR result

After PMMA were grafted onto $TiO_2$ nanoparticles, the PMMA-grafted powder was dried and characterized by FT-IR. The result is shown in the following.

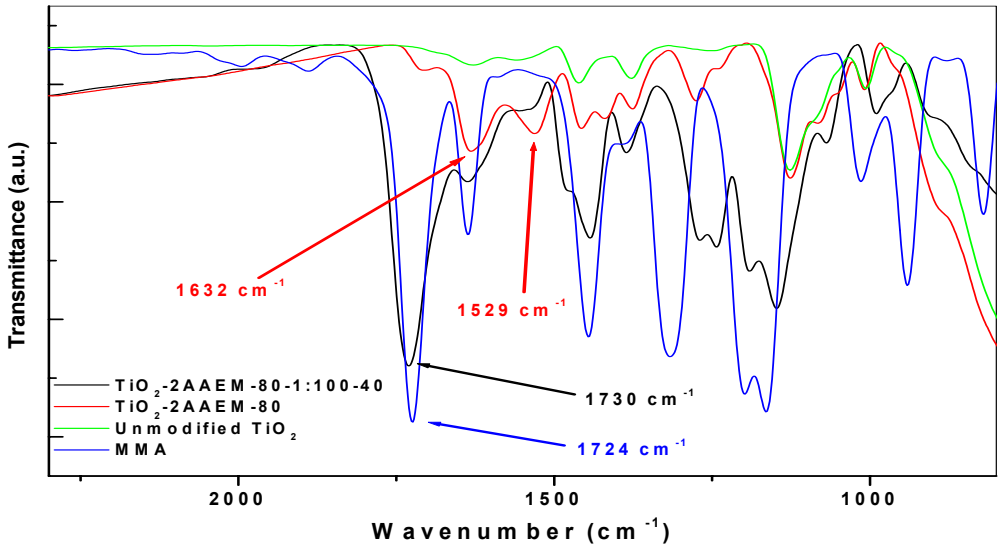


**Figure 96. FT-IR spectrums of the PMMA-grafted $TiO_2$ powder, 2AAEM modified-$TiO_2$ powder (before polymerization), unmodified $TiO_2$ powder and MMA.**

FT-IR spectrums of the unmodified-$TiO_2$ powder, 2AAEM-modified $TiO_2$ powder and PMMA-grafted $TiO_2$ powder are shown in the Figure 96. Although there are no peaks at around 1530 $cm^{-1}$ in the spectrum of unmodified-$TiO_2$ powder, two peaks occurred at around 1632 $cm^{-1}$ for $\nu$(C=O) and 1529 $cm^{-1}$ for $\nu$(C=C) in the spectrum of the 2AAEM-modified $TiO_2$ powder. This shows that $TiO_2$ nanoparticles were modified with 2AAEM molecules. After PMMA molecules were grafted onto the 2AAEM-modified $TiO_2$ nanoparticles using MMA, the PMMA-grafted nanoparticles were characterized by FT-IR. The spectrum of MMA shows a peak at around 1724 $cm^{-1}$ that belongs to carbonyl stretch of the MMA. After PMMA molecules were grafted onto $TiO_2$ nanoparticles, this peak shifted to 1730 $cm^{-1}$ according to the spectrum of the PMMA-grafted nanoparticles, namely in the $TiO_2$-2AAEM-80-1:100-40. Because the peak belongs to carbonyl stretch seems in the same area in the spectrum of the PMMA-grafted nanoparticles in spite of washing of ungrafted PMMA and MMA with solvents and the spectrum of unmodified $TiO_2$ nanoparticles does not show the same peak, it is concluded that PMMA molecules were indeed grafted onto $TiO_2$ surface.

### 5.5.11.2. TGA/DSC result

After PMMA were grafted onto $TiO_2$ nanoparticles, the PMMA-grafted powder was dried and characterized by TGA/DSC. The result is shown in the following.

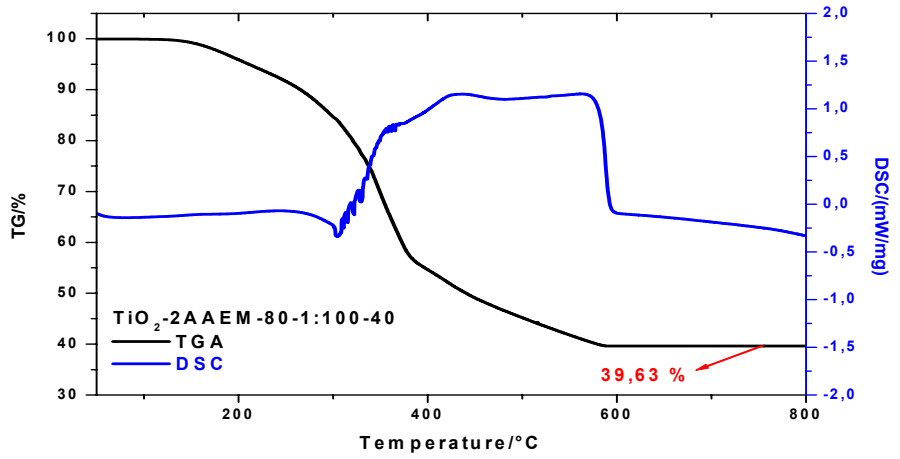


**Figure 97. TGA/DSC result of $TiO_2$-2AAEM-80-1:100-40.**

| Name | Decomposed amount by TGA (%) |
|---|---|
| Unmodified $TiO_2$ powder | 18,06 |
| $TiO_2$-2AAEM-80-1:100-40 | 60,37 |

After the grafting of PMMA onto $TiO_2$ nanoparticles, its thermal behaviour was investigated by TGA/DSC. According to the Figure the 79 and 97, the weight loss of the PMMA-grafted sample is higher than that of the unmodified $TiO_2$ nanoparticles. This can be explained by decomposing of PMMA onto $TiO_2$ nanoparticles at high temperatures. Furthermore, according to the DSC result, the peaks between 300-500 °C could be ascribed to the removal and combustion of the organic groups contained in the product. Also, it was expected that the amount of the grafting of PMMA molecules onto $TiO_2$ nanoparticles would increase directly proportional to the amount of $–OC_3H_7$ groups modified with 2AAEM, namely 80 % of $–OC_3H_7$ groups on the surface. Indeed, the amount of PMMA grafting onto $TiO_2$ nanoparticles increased but only 17 % (see section 5.5.3, page 139). The reason for insufficient grafting onto the surface might be an insufficient modification of the $-OC_3H_7$ groups with 2AAEM molecules. Namely, it was expected that 80 % of $–OC_3H_7$ groups on the surface were modified with 2AAEM molecules but this goal could not be achieved. This might be because of sterical hindrance effects of 2AAEM molecules already attached to the surface. Also, it was expected that the amount of the grafting of PMMA molecules onto $TiO_2$ nanoparticles would increase with the increase in the concentration of MMA from 20 % to 40 %. Indeed, the amounts of grafting of PMMA onto $TiO_2$ nanoparticles increased but only by 15 % (see section 5.5.9, page 155). The reason for insufficient grafting onto the surface might be intermolecular polymerization of MMA molecules. Because of intermolecular polymerization of MMA molecules, the ungrafted PMMA molecules formed instead of the grafting onto $TiO_2$ nanoparticles. After that, because the ungrafted 2AAEM and ungrafted PMMA were removed by washing with solvents, the amount of PMMA grafting onto $TiO_2$ nanoparticles did not change.

### 5.5.11.3. TEM results of the $TiO_2$-2AAEM-80-1:1000-40

After grafting of PMMA molecules by means of the modification of 80 % of $–OC_3H_7$ groups with 2AAEM, with a molar ratio of 2AAEM:MMA = 1:100 and 40 % MMA by weight with respect to the total weight, the appearance of the PMMA-grafted $TiO_2$ nanoparticles was investigated by TEM. The results are shown in the following Figure 98, 99, 100, 101.

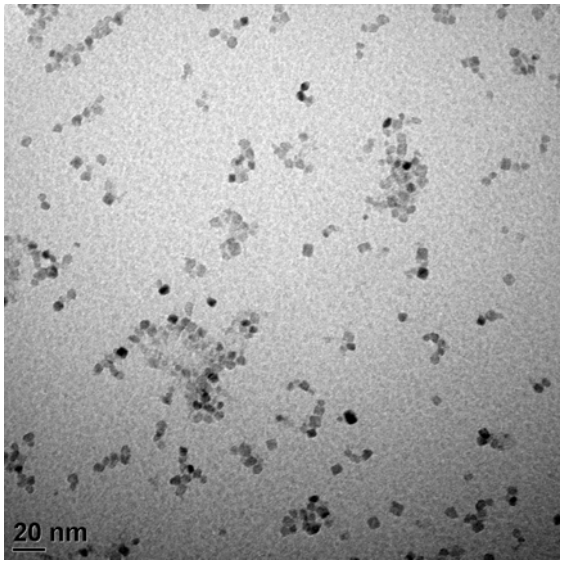


**Figure 98. TEM picture of the $TiO_2$-2AAEM-80-1:100-40.**

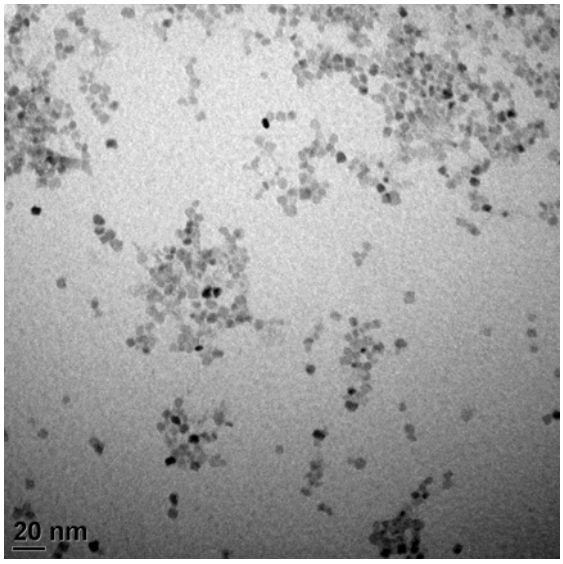


**Figure 99. TEM picture of the $TiO_2$-2AAEM-80-1:100-40.**

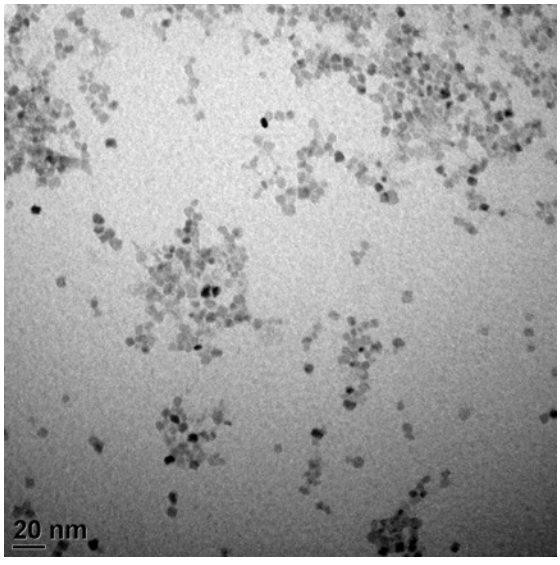


**Figure 100. TEM picture of the $TiO_2$-2AAEM-80-1:100-40.**

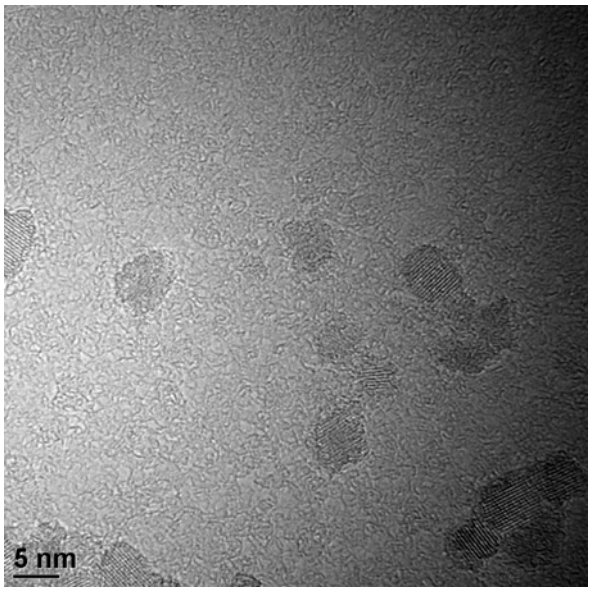


**Figure 101. TEM picture of the $TiO_2$-2AAEM-80-1:100-40.**

According to the TEM results, it seems that after grafting of $TiO_2$ nanoparticles with PMMA molecules, $TiO_2$ particles are very good separated, dispersed. Namely, it is observed agglomeration-free $TiO_2$ nanoparticles. It is of course because of the PMMA molecules on the surface of the $TiO_2$ nanoparticles. But, according to these pictures, any layer on the surface of $TiO_2$ nanoparticles was not seen. Its reason can be because of insufficient resolution of organic groups on the surface of $TiO_2$ nanoparticles. Also, the size of $TiO_2$ nanoparticles synthesized in this work is nearly 6 nm. Small size of $TiO_2$ nanoparticles might also hinder to see the layer of organic groups. In addition, according to the literature, it is also not found any work that they determined the layer of organic groups on inorganic nanoparticles. Namely, it is also not exist in the literature.

### 5.5.12. Characterization of $TiO_2$-2AAEM-80-1:1000-40

In this experiment, PMMA molecules were grafted onto $TiO_2$ surface with the modification of 80 % of $–OC_3H_7$ groups with 2AAEM, with a molar ratio of 2AAEM:MMA = 1:1000 and 40 % MMA by weight with respect to the total weight (according to section 4.7.4.4., page 66). It is expected that the percentage of PMMA grafting onto $TiO_2$ nanoparticles will increase directly proportional to the amount of $–OC_3H_7$ groups with 2AAEM, namely with the increase from 30 % to 80 % of $–OC_3H_7$ groups on the surface. Also, it is expected that the percentage of PMMA grafting onto $TiO_2$ nanoparticles will increase with increasing of MMA concentration from 20 % to 40 % and will increase with the increase of the molar ratio of 2AAEM:MMA from 1:100 to 1:1000. The results are shown in the following.

### 5.5.12.1. TGA/DSC result

After PMMA were grafted onto $TiO_2$ nanoparticles, the PMMA-grafted powder was dried and characterized by TGA/DSC. The result is shown in the following.

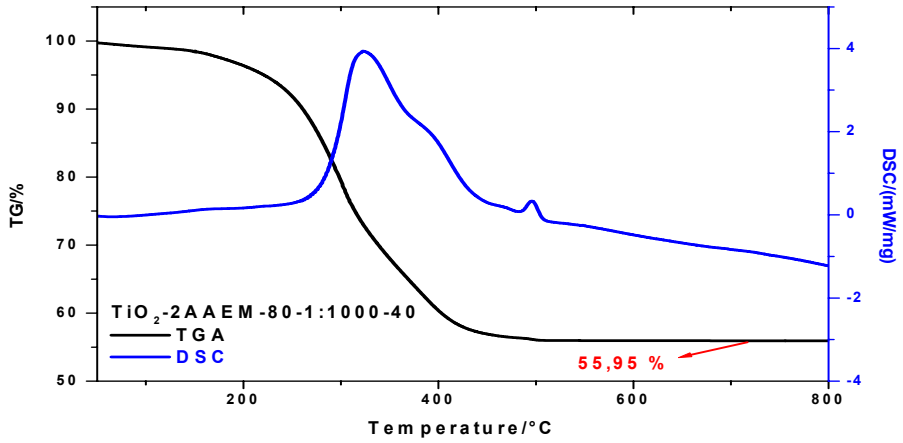


**Figure 102. TGA/DSC result of $TiO_2$-2AAEM-80-1:1000-40.**

| Name | Decomposed amount by TGA (%) |
|---|---|
| Unmodified $TiO_2$ powder | 18,06 |
| $TiO_2$-2AAEM-80-1:1000-40 | 44,05 |

After the grafting of PMMA onto $TiO_2$ nanoparticles, its thermal behaviour was investigated by TGA/DSC. According to the Figure 79 and 102, the weight loss of the PMMA-grafted sample is higher than that of the unmodified $TiO_2$ nanoparticles. This can be explained by decomposing of PMMA grafted onto $TiO_2$ nanoparticles at high temperatures. Furthermore, according to the DSC result, the peaks between 300-500 °C could be ascribed to the removal and combustion of the organic groups contained in the product. Also, it was expected that the amount of PMMA grafting onto $TiO_2$ nanoparticles would increase directly proportional to the amount of $-OC_3H_7$ groups modified with 2AAEM, namely 80 % of $-OC_3H_7$ groups on the surface. Indeed, the amount of PMMA grafting onto $TiO_2$ nanoparticles increased only by 13 % (see section 5.5.4, page 142). The reason for insufficient grafting onto the surface might be an insufficient modification of the $-OC_3H_7$ groups. Namely, it was expected that 80 % of $-OC_3H_7$ groups on the surface were modified with 2AAEM molecules but this goal could not be achieved. This might be because of sterical hindrance effects of 2AAEM molecules already attached to the surface. Also, it was expected that the amount of the grafting of PMMA molecules onto $TiO_2$ nanoparticles would increase with the increase in the concentration of MMA from 20 % to 40 %. But, the amount of grafting of PMMA onto $TiO_2$

nanoparticles decreased by 8 % (see section 5.5.10, page 157). Also, it was expected that the amount of the grafting of PMMA molecules onto $TiO_2$ nanoparticles would increase with the increase in the molar ratio of 2AAEM:MMA from 1:100 to 1:1000 but, it didn't increase. On the contrary, the amount of the grafting onto the nanoparticles decreased by 27 % (see section 5.5.11, page 159). The reason for these findings might be intermolecular polymerization of MMA molecules for the formation of ungrafted PMMA molecules instead of the grafting onto $TiO_2$ nanoparticles. Because the ungrafted 2AAEM and ungrafted PMMA were removed by washing with solvents, the amount of PMMA grafting onto the surface did not increase as expected.

#### 5.5.12.2. The evaluation of PMMA grafting onto 2AAEM-modified $TiO_2$ nanoparticles as 80 % of $–OC_3H_7$ groups on the surface, with the molar ratios of 2AAEM:MMA= 1:100 and 1:1000 and with 20 % and 40 % MMA by weight with respect to the total weight

After $TiO_2$ nanoparticles were modified with 2AAEM molecules as 80 % of $–OC_3H_7$ groups on $TiO_2$ nanoparticles, the 2AAEM-modified $TiO_2$ nanoparticles were dispersed in MMA with molar ratios of 2AAEM:MMA= 1:100 and 1:1000. Each of these samples was dispersed in toluene with an amount of 20 % and 40 % MMA by weight with respect to the total weight. After that, polymerization was performed. According to the TGA/DSC results, the weight losses of the PMMA-grafted $TiO_2$ nanoparticles were higher than that of the unmodified $TiO_2$ nanoparticles. The summary of the results of PMMA grafting are shown in Table 10. It was expected that the amount of the grafting of PMMA molecules onto $TiO_2$ nanoparticles would increase directly proportional to the amount of $–OC_3H_7$ groups modified with 2AAEM, namely from 30 % to 80 %. Indeed, the amount of PMMA grafting onto $TiO_2$ nanoparticles increased by 13-28 % when comparing $TiO_2$ nanoparticles modified with 30 % of $–OC_3H_7$ groups on the surface and with 80 % of $–OC_3H_7$ groups respectively. Of course, this is much less than expected. The reason for that finding might be because of sterical hindrance effects of 2AAEM molecules already attached to the surface. Also, although the concentrations of MMA in the mixtures were changed from 20 % to 40 %, the amount of PMMA grafting onto $TiO_2$ nanoparticles did not change as expected. Furthermore, although the molar ratio of 2AAEM:MMA was increased from 1:100 to 1:1000, the amount of PMMA grafting onto $TiO_2$ nanoparticles decreased by 9-27 % as opposed to expected. After the ungrafted 2AAEM and ungrafted PMMA were removed by washing with solvents, the amount of PMMA grafting onto $TiO_2$ nanoparticles did not increase as expected. Furthermore, PMMA grafting onto $TiO_2$ nanoparticles was also proved by FT-IR. According to the TEM results of the $TiO_2$-2AAEM-80-1:100-40, it seems that after grafting of $TiO_2$ nanoparticles with PMMA molecules, the

particles are good dispersed and it is of course because of the PMMA molecules on the surface.

**Table 10. TGA/DSC results for the grafting of PMMA onto $TiO_2$ surface after 80 % modification of $–OC_3H_7$ groups with 2AAEM**

| 2AAEM/ MMA | The percentage of the modified $–OC_3H_7$ groups on the nanoparticles (%) | The concentration of MMA (%) | The amount of the grafting of PMMA onto nanoparticle according to TGA results (%) |
|---|---|---|---|
| Unmodified $TiO_2$ powder | | | 18,06 |
| 1 :100 | 80 | 20 | 52,70 |
| 1:1000 | 80 | 20 | 47,91 |
| 1 :100 | 80 | 40 | 60,37 |
| 1:1000 | 80 | 40 | 44,05 |

## 5.6. The summary of TGA results and weight calculation results of the PMMA-grafted $TiO_2$ nanoparticles

In addition to TGA results, the percentage of PMMA grafting onto $TiO_2$ surface was calculated using the equation in the following. Where A is weight of PMMA grafted (g) and B is weight of $TiO_2$ charged (g). All calculations made by using this equation are shown in Table 11.

$$\text{Percentage of Grafting}\,(\%) = \frac{A}{B}\,x\,100$$

**Table 11. The general summary of PMMA grafting onto the surface.**

| No | 2AAEM/ MMA | The percentage of the modified $-OC_3H_7$ groups on the nanoparticles (%) | The concentration of MMA (%) | The amount of PMMA grafting onto the nanoparticle according to TGA results (%) | The amount of PMMA grafting onto the nanoparticle according to weight calculations (%) |
|---|---|---|---|---|---|
| 1 | Unmodified $TiO_2$ powder | | | 18,06 | 0 |
| 2 | 1 :100 | 30 | 20 | 46,80 | 49,30 |
| 3 | 1:1000 | 30 | 20 | 37,40 | 16,96 |
| 4 | 1 :100 | 30 | 40 | 51,74 | 106,80 |
| 5 | 1:1000 | 30 | 40 | 38,85 | 53,52 |
| 6 | 1 :100 | 50 | 20 | 50,96 | 75,39 |
| 7 | 1:1000 | 50 | 20 | 37,80 | 18,06 |
| 8 | 1 :100 | 50 | 40 | 58,27 | 55,50 |
| 9 | 1:1000 | 50 | 40 | 38,86 | 10,95 |
| 10 | 1 :100 | 80 | 20 | 52,70 | 44,40 |
| 11 | 1:1000 | 80 | 20 | 47,91 | 40,10 |
| 12 | 1 :100 | 80 | 40 | 60,37 | 88,15 |
| 13 | 1:1000 | 80 | 40 | 44,05 | 12,07 |

After $TiO_2$ nanoparticles were modified with 2AAEM molecules as 30 %, 50 % and 80 % of $–OC_3H_7$ groups on $TiO_2$ nanoparticles, the 2AAEM-modified $TiO_2$ nanoparticles were dispersed in MMA with a molar ratios of 2AAEM:MMA= 1:100 and 1:1000. Each of these samples was dispersed in toluene with an amount of 20 % and 40 % MMA by weight with respect to the total weight. After that, polymerization was performed. The summary of the results of PMMA grafting are shown in Table 11. According to TGA results, the weight losses of the PMMA-grafted $TiO_2$ nanoparticles were higher than that of unmodified $TiO_2$ nanoparticles. It was expected that the amount of the grafting of PMMA molecules onto $TiO_2$ nanoparticles would increase directly proportional to the amount of $–OC_3H_7$ groups modified with 2AAEM, namely from 30 % to 50 % and from 30 % to 80 %. Indeed, the amount of PMMA grafting onto $TiO_2$ nanoparticles increased by between 13-28 % when comparing $TiO_2$ nanoparticles modified with 30 % of $–OC_3H_7$ groups on the surface and with 80 % of $–OC_3H_7$ groups respectively and by between 1-13 % when comparing $TiO_2$ nanoparticles modified with 30 % of $–OC_3H_7$ groups on the surface and with 50 % of $–OC_3H_7$ groups respectively. Of course, the increase is less than expected. The reason for the insufficient increase might be because of sterical hindrance effects of 2AAEM molecules already attached to the surface. Also, according to the literature, the percentage of the grafting of PMMA onto the nanoparticles can be increased with increasing of monomer concentration. But, although the concentrations of MMA in the mixtures were increased from 20 % to 40 %, the amount of PMMA grafting onto $TiO_2$ nanoparticles increased only between by 3-14 % for all results. Furthermore, although the molar ratio of 2AAEM:MMA was increased from 1:100 to 1:1000, the amount of PMMA grafting onto $TiO_2$ nanoparticles decreased by 9-33 % as opposed to expected. The reasons for these findings might be intermolecular polymerization of MMA molecules for the formation of ungrafted PMMA molecules instead of the grafting onto $TiO_2$ nanoparticles. After ungrafted 2AAEM and ungrafted PMMA were removed by washing with solvents, the amount of PMMA grafting onto $TiO_2$ nanoparticles did not increase efficiently. In addition, if the results of TGA and weight calculation are compared, it is seen high difference among the results. When TGA results are more reliable than weight calculation results, the weight calculation results were not taken into account. As for the DSC results, the peaks between 300-500 °C could be ascribed to the removal and combustion of the organic groups. Furthermore, the grafting onto $TiO_2$ nanoparticles was also proved by FT-IR. Because the peak belongs to carbonyl stretch of MMA at around 1730 $cm^{-1}$ seems still in the spectrum of the PMMA-grafted nanoparticles in spite of washing of the ungrafted PMMA and MMA with solvents and the spectrum of unmodified $TiO_2$ nanoparticles does not show the same peak, it is concluded that PMMA molecules were indeed grafted onto $TiO_2$ surface by means of *"the combination of both grafting methods".*

## 6. Conclusions

The nanoparticles are attracting in lots of areas ranging from biotechnology to optic because of their new properties. But sometimes the use of nanoparticles is restricted because of their incompatibility within organic mediums. Namely, sometimes the presence of nanoparticles leads to miscibility problems. To overcome this problem, they need to be chemically modified to change their surface properties, namely their surfaces need to be functionalized with the modification agents. Of course, the main reason of the modifications of the particle surface is not only their dispersion in a desired medium but also gaining them other important properties such as hydrophobic/hydrophilic properties, biocompatibility, direct chemical bonding to organic matrix via nanoparticles, providing sensibility against certain substances, etc. It is understood that the functionalization of the nanoparticles opens new countless probabilities for the use of the nanoparticles in industry and the academic areas. In this connecting, interest to the synthesis and characterization of the nanoparticles and their modifications has been also increased recently.

Organic groups can be linked to inorganic backbone by means of three different ways. One of them is the formation of covalent bonds, for instance; the modification of $SiO_2$ nanoparticles with silanes (for example; 3-methacryloxypropyl trimethxoysilane) to occur covalent bonds (Si-O-Si covalent bonds). Another one is the formation of complex structures with β-ketoesters, β-diketones or carboxylic acids, for instance; the complexation reaction of $Ti(OPr)_4$ molecules with acetylacetone molecules. The other one is the formation of ionic bond to an organic acid (salt formation). In this work, nanostars were named for all modifications of the nanoparticles. Nanostars described in this work that they have the nanoparticles in their center as core and have some different branches on their surface as shell (core-shell structures). Their synthesis and characterization were investigated in this thesis. For this reason, $TiO_2$ nanoparticles were chosen for the core of nanostars because of the fact that $TiO_2$ has been used in lots of areas such as photocatalytic coatings, dyes as a white pigment, remediation of wastewater, etc. Also, $TiO_2$ has high refractive index and colour of $TiO_2$ make it an excellent for reflective optical coatings. This pigment is also used extensively in plastics and other applications for its UV resistant. Firstly, monodisperse anatase $TiO_2$ nanoparticles with a diameter of nearly 6 nm were synthesized by hydrothermal process because of lots of advances of hydrothermal method (see section 2.5.2. and 2.5.3., page 31-32). According to the TEM results of the unmodified $TiO_2$ nanoparticles, $TiO_2$ nanoparticles were much agglomerated in toluene, it is difficult to see single particles and difficult to calculate the size of particles and difficult to speak about their shapes (section 5.1.2., page 67-68). For this reason, $TiO_2$ nanoparticles were modified with stearic acid molecules to see single particles. After modification with stearic acid molecules, $TiO_2$

nanoparticles were agglomeration-free, their particle size was determined easily to be nearly 6 nm and their shape is nearly spherical (section 5.1.2., page 69-70). As for EDX result, the elemental combination of the unmodified $TiO_2$ nanoparticles was detected from the place of having a lot of $TiO_2$ nanoparticles. According to the result, the peaks of belonging to the ***Ti, O*** and ***C*** were exactly determined (section 5.1.3., page 71). As for the XRD result, it is determined that $TiO_2$ nanoparticles were crystalline (section 5.1.4, page 71). Moreover, C % on $TiO_2$ nanoparticles was determined to be 8,38 % by elemental analysis and the surface area of nanoparticles was calculated to be 258 $g/m^2$ and the amount of $–OC_3H_7$ and –OH on the nanoparticles were calculated to be $2{,}33.10^{-3}$ and $3{,}79.10^{-3}$ respectively (it is assumed that the surface density for fully hydroxylated anatase $TiO_2$ nanoparticles are 14 -OH groups/100 $Å^2$) . Namely, 38 % of the surface area of $TiO_2$ nanoparticles was covered with $–OC_3H_7$ groups and 62 % of the surface area of $TiO_2$ nanoparticles was covered with –OH groups. Thus, it is concluded that the synthesized $TiO_2$ nanoparticles have both –OH groups and $–OC_3H_7$ groups on their surface (see section 5.2., page 73).

To synthesize nanostars, $TiO_2$ nanoparticles were modified with three ways. One of them was the modification of the nanoparticles with silanes, carboxylic acids and β-ketoester, another one was the modification of $TiO_2$ nanoparticles with the synthesized urea molecules and the other one was the PMMA grafting onto $TiO_2$ nanoparticle surface by means of *"the combination of both grafting methods".* In the modifications of $TiO_2$ nanoparticles with silanes, after $TiO_2$ nanoparticles were modified with silanes with different molecular weights, methanol molecules were liberated from the surfaces of $TiO_2$ nanoparticles by means of the reaction of –OH groups on the surface with methoxysilane groups of the silane molecules by forming Si-O-Ti covalent bonds. By means of GC/MS, methanol molecules were detected and it is concluded that methanol molecules resulted from only the silane modifications. The silane-modified $TiO_2$ nanoparticles were characterized by elemental analysis, GC/MS and FT-IR. According to the elemental analysis results, the amount of carbon and hydrogen on the surface of $TiO_2$ nanoparticles increased as expected. As the number of carbon atoms in HDTMS molecule is more than that in the other alkylsilanes, the carbon amount of the HDTMS-modified $TiO_2$ nanoparticles increased more than that of the other silanes-modified $TiO_2$ nanoparticles. It is interesting that the increase in the amount of carbon amount after modification with AMMO molecules is more than that with HTMS. It is thought that its reason might be various interaction types between AMMO with $TiO_2$ surfaces (see section 5.2.5, page 85). Because of these mentioned interactions, much more AMMO molecules could have interacted with $TiO_2$ surface besides the covalent bonding to the surface of $TiO_2$ nanoparticles. For this reason, the increase in the amount of carbon in the AMMO-modified $TiO_2$ nanoparticles is more than that in the HTMS-modified $TiO_2$ nanoparticles although the

number of carbon atoms in the HTMS molecule is twice more than that in AMMO molecule. As for FT-IR results, all modifications weren't proved by FT-IR measurements, for example; AMMO and HTMS modifications. It reason might be low concentration of the modification agents in the modified-$TiO_2$ nanoparticles. Furthermore, of all silanes, aminosilanes were chiefly used in the surface modifications. The majority of the works related to the aminosilane modifications are generally relevant to $SiO_2$ nanoparticles [255-257] while only a few consider the modification of other metal alkoxides [63, 268] in the literature and the modifications of $TiO_2$ nanoparticles with the other silanes used in this work were not worked in the literature.

As for TEM results of the AMMO-modified $TiO_2$ nanoparticles, the AMMO-modified $TiO_2$ nanoparticles were not separated because of the structure of the AMMO molecules. AMMO is small molecule and has $–NH_2$ group in the end of its structure. Because of the reasons, the AMMO-modified $TiO_2$ nanoparticles can interact among themselves, so they can be easily agglomerated. But for the modification with big HDTMS molecules, this case is very different. Because HDTMS molecules are big molecules, they form an apolar layer on the surface of $TiO_2$ nanoparticles. Consequently this is resulted in a situation of the repelling to $TiO_2$ nanoparticles each other. Finally, good separated $TiO_2$ nanoparticles are observed. As for EDX results, Silicon was detected for both modifications. But, because the amount of the –OH groups reacted with AMMO molecules is much more than that with HDTMS molecules, of course the amount of the Silicon on the surface of $TiO_2$ nanoparticles is much more in the the modification with AMMO molecules. It is also exactly proved by elemental analysis results. According to the elemental results of the AMMO and HDTMS-modified $TiO_2$ nanoparticles, after modification of $TiO_2$ nanoparticles with AMMO molecules, 62,88 % -OH groups on the surface was modified with AMMO molecules, whereas after modification of $TiO_2$ nanoparticles with HDTMS molecules, only 26,18 % -OH groups on the surface was modified with HDTMS molecules (section 5.4., page 133, Table 6). These results also support the results of the EDX.

$TiO_2$ nanoparticles were also modified with carboxylic acids; stearic acid, oleic acid and 10-undecylenic acid with different molecular weights and with a β-ketoester; AAA. Then, 1-propanol molecules were liberated from $TiO_2$ nanoparticle surface by means of the complexation reaction of $–OC_3H_7$ groups on the surface with the carboxylic acid molecules and the β-ketoester molecule. The carboxylic acid and β-ketoester-modified $TiO_2$ nanoparticles were characterized by elemental analysis and FT-IR. According to the elemental analysis results, the amount of carbon and hydrogen in all carboxylic acid-modified powders increased as expected. Also, carbon amount of the carboxylic acid modified-

nanoparticles were more than those of the silane-modified nanoparticles. For example; although the number of carbon atoms in HDTMS molecule is close to that in stearic acid molecule, it is observed that the increase in carbon amount in the stearic acid-modified $TiO_2$ nanoparticles is much more that that in the HDTMS-modified $TiO_2$ nanoparticles (see sections 5.2.4. and 5.2.7, pages 81 and 95). Its reason might be because of the modification differences between silanes and carboxylic acids with the surfaces. Namely, silanes react with –OH groups on $TiO_2$ nanoparticles but carboxylic acids react with $–OC_3H_7$ groups on $TiO_2$ nanoparticles. Although one carboxylic acid molecule reacts with one $–OC_3H_7$ group on $TiO_2$ nanoparticle, one silane can react with three –OH groups on the surface. Although the literature was searched for the modifications of $TiO_2$ nanoparticles with stearic acid, oleic acid, 10-undecylenic acid and AAA, it was not found any work. But, there are several works only related to metal alkoxides modifications with carboxylic acid and β-ketoester and β-diketone molecules [48, 53, 54, 74, 76, 262, 263, 269-276].

$TiO_2$ nanoparticles were also modified with urea molecules (from section 5.3., page 100). Firstly, the urea molecules were synthesized and characterized by FT-IR. According to the FT-IR results, new strong absorption bands for all results at around 3300-3400 $cm^{-1}$ and 1600-1700 $cm^{-1}$ confirm the formation of urea linkages. Also, the absence of a strong absorption bands for all results at around 2270 $cm^{-1}$ (due to isocyanate group) shows that the reaction is completed. Furthermore, after $TiO_2$ nanoparticles were modified with the urea molecules, the urea-modified nanoparticles were characterized by GC/MS, FT-IR and elemental analysis. GC/MS results showed that ethanol molecules were liberated from the surface by means of the reaction between –OH groups of $TiO_2$ nanoparticles and ethoxysilane groups of the urea molecules by forming Ti-O-Si covalent bonds. Also, after $TiO_2$ nanoparticles were modified with the urea molecules, the urea peaks in the spectrums of the modified $TiO_2$ nanoparticles seemed still at around 1600-1700 $cm^{-1}$ and 3300-3400 $cm^{-1}$. According to the elemental analysis results, the increase in the carbon, hydrogen and nitrogen amount of the urea-modified $TiO_2$ nanoparticles also confirm the modifications of $TiO_2$ nanoparticles (section 5.4., Table 7, page 134). Also, although the literature was searched for the modification of $TiO_2$ nanoparticles with the urea molecules, it was not found any works.

PMMA molecules were also grafted onto the surface of $TiO_2$ nanoparticles (from section 5.5., page 134). After $TiO_2$ nanoparticles were modified with 2AAEM molecules as 30 %, 50 % and 80 % of $–OC_3H_7$ groups on $TiO_2$ nanoparticles, the 2AAEM-modified $TiO_2$ nanoparticles were dispersed in MMA with molar ratios of 2AAEM:MMA= 1:100 and 1:1000. Each of these samples was dispersed in toluene with an amount of 20 % and 40 % MMA by weight with

respect to the total weight. After that, polymerization was performed. According to the TGA results, the weight losses of the PMMA-grafted $TiO_2$ nanoparticles were higher than that of the unmodified $TiO_2$ nanoparticles. Its reason is the decomposing of PMMA on the $TiO_2$ nanoparticles at high temperatures. It was expected that the amount of the grafting of PMMA molecules onto $TiO_2$ nanoparticles would increase directly proportional to the amount of $–OC_3H_7$ groups modified with 2AAEM, namely from 30 % to 50 % and from 30 % to 80 %. Indeed, the amount of PMMA grafting onto $TiO_2$ nanoparticles increased by between 13-28 % when comparing $TiO_2$ nanoparticles modified with 30 % of $–OC_3H_7$ groups on the surface and with 80 % of $–OC_3H_7$ groups respectively and by between 1-13 % when comparing $TiO_2$ nanoparticles modified with 30 % of $–OC_3H_7$ groups on the surface and with 50 % of $–OC_3H_7$ groups respectively. Of course, the increase is less than expected. The reason for that finding might be because of sterical hindrance effects of 2AAEM molecules already attached to the surface. According to the literature, the percentage of the grafting of PMMA onto the nanoparticles is increased with increasing of monomer concentration. But, although the concentrations of MMA in the mixtures were increased from 20 % to 40 %, the amount of PMMA grafting onto $TiO_2$ nanoparticles increased only between by 3-14 % for all results. Furthermore, although the molar ratio of 2AAEM:MMA was increased from 1:100 to 1:1000, the amount of PMMA grafting onto $TiO_2$ nanoparticles decreased by 9-33 % as opposed to expected (see section 5.6., page 167, Table 11). The reason for these findings might be intermolecular polymerization of MMA molecules for the formation of ungrafted PMMA molecules instead of the grafting onto $TiO_2$ nanoparticles. In addition, if the TGA and weight calculation results are compared, it is seen high difference among the results. Because TGA results are more reliable than the weight calculation results, the weight calculation results were not taken into account. As for the DSC results, the peaks between 300-500 °C could be ascribed to the removal and combustion of the organic groups. Also, according to the TGA results, the weight losses of the samples are decreasing in the order: pure PMMA > PMMA-grafted $TiO_2$ nanoparticles > ungrafted $TiO_2$ nanoparticles. In addition, although the monomer conversions were calculated to be 66 % and 69 % for the $TiO_2$-2AAEM-30-1:100-40 and $TiO_2$-2AAEM-30-1:1000-40 by FT-IR respectively (see section 5.5.3.1-Figure 83-page 140 and 5.5.4.1-Figure 85-page 143), the ungrafted PMMA molecules were occurred instead of the grafting onto $TiO_2$ nanoparticles. Namely, although the MMA conversions were very high in the polymerization, the PMMA chains could not be grafted on the surface of the $TiO_2$ nanoparticles. Moreover, the PMMA grafting onto $TiO_2$ nanoparticles was also proved by FT-IR. Because the peak belongs to carbonyl stretch of MMA at around 1730 $cm^{-1}$ seems still in the spectrum of the PMMA-grafted nanoparticles in spite of washing of the ungrafted PMMA and MMA with solvents and the spectrum of unmodified $TiO_2$ nanoparticles does not show the same peak, it is concluded that PMMA

molecules were indeed grafted onto $TiO_2$ surface by means of *"the combination of both grafting methods".* Consequently, PMMA grafting onto anatase $TiO_2$ nanoparticles which have both –OH groups and $–OC_3H_7$ groups were achieved by means of the complexed 2AAEM molecules on the surface of $TiO_2$ nanoparticles in contrary to the covalent bonding to the nanoparticles by forming Ti-O-Si covalent bonds. PMMA grafting on the surface of $TiO_2$ nanoparticles via complexation reaction with 2AAEM is not available in the literature. Also, one sample of the PMMA-grafted $TiO_2$ nanoparticles, $TiO_2$-2AAEM-80-1:100-40 was also investigated by TEM. According to these TEM results, it seems that after grafting of $TiO_2$ nanoparticles with PMMA molecules, $TiO_2$ particles are very good separated, dispersed. Namely, agglomeration-free $TiO_2$ nanoparticles were observed. Of course it is because of the PMMA molecules on the surface of the $TiO_2$ nanoparticles.

Consequently, organic-inorganic $TiO_2$ nanostars were synthesized by modifying anatase monodisperse $TiO_2$ nanoparticles with four alkylmethoxysilanes with different molecular weights, with one aminosilane, with one saturated carboxylic acid, with two unsaturated carboxylic acids with different molecular weights, with 10 different urea molecules with different molecular weights and with PMMA molecules.

## 7. References


[1] P. Holister, J.-W. Weener, C. R. Vas, and T. Harper, "Nanoparticles", in *Technology White Papers nr. 3*, Cientifica. p. 1-11, 2003.

[2] R. C. Advincula, "Surface initiated polymerization from nanoparticle surfaces", *Journal of Dispersion Science and Technology*, 24(3-4), p. 343-361, 2003.

[3] H. Gu, K. Xu, C. Xu, and B. Xu, "Biofunctional magnetic nanoparticles for protein separation and pathogen detection", *Chemical Communications*, (941-949), 2006.

[4] S. Santra, D. Dutta, and B. M. Moudgil, "Functional dye-doped silica nanoparticles for bioimaging, diagnostics and therapeutics", *Food and Bioproducts Processing*, 83(C2), p. 136-140, 2005.

[5] A. K. Gupta and M. Gupta, "Synthesis and surface engineering of iron oxide nanoparticles for biomedical applications", *Biomaterials*, 26(18), p. 3995-4021, 2005.

[6] J. Wang, G. Liu, and Y. Lin, "Electroactive Silica Nanoparticles for Biological Labeling", *Small*, 2(10), p. 1134-1138, 2006.

[7] A. Esteban-Cubillo, C. Pecharroman, E. Aguilar, J. Santaran, and J. Moya, "Antibacterial activity of copper monodispersed nanoparticles into sepiolite", *Journal of Materials Science*, 41(16), p. 5208-5212, 2006.

[8] N. Morishita, H. Nakagami, R. Morishita, S. I. Takeda, F. Mishima, B. Terazono, S. Nishijima, Y. Kaneda, and N. Tanaka, "Magnetic nanoparticles with surface

modification enhanced gene delivery of HVJ-E vector", *Biochemical and Biophysical Research Communications*, 334(4), p. 1121-1126, 2005.

[9] Y. Li, Q. Lu, X. Qian, Z. Zhu, and J. Yin, "Preparation of surface bound silver nanoparticles on polyimide by surface modification method and its application on electroless metal deposition", *Applied Surface Science*, 233(1-4), p. 299-306, 2004.

[10] C. Barbe, J. Bartlett, L. G. Kong, K. Finnie, H. Q. Lin, M. Larkin, S. Calleja, A. Bush, and G. Calleja, "Silica particles: A novel drug-delivery system", *Advanced Materials*, 16(21), p. 1959-1966, 2004.

[11] Z. F. Li and E. Ruckenstein, "Water-Soluble Poly(acrylic acid) Grafted Luminescent Silicon Nanoparticles and Their Use as Fluorescent Biological Staining Labels", *Nano Letters*, 4(8), p. 1463-1467, 2004.

[12] G. Ramakrishna and H. N. Ghosh, "Optical and Photochemical Properties of Sodium Dodecylbenzenesulfonate (DBS)-Capped $TiO_2$ Nanoparticles Dispersed in Nonaqueous Solvents", *Langmuir*, 19(3), p. 505 -508, 2003.

[13] A. Usami and H. Ozaki, "Optical Modeling of Nanocrystalline $TiO_2$ Films", *J. Phys. Chem. B*, 109(7), p. 2591-2596, 2005.

[14] D. U. Saenger, G. Jung, and M. Menning, "Optical and Structural Properties of Doped ZnS Nanoparticles Produced by the Sol-Gel Method", *Journal of Sol-Gel Science and Technology*, 13(1 - 3), p. 635-639, 1998.

[15] Y. H. Tong, Y. C. Liu, S. X. Lu, L. Dong, S. J. Chen, and Z. Y. Xiao, "The Optical Properties of ZnO Nanoparticles Capped with Polyvinyl Butyral", *Journal of Sol-Gel Science and Technology*, 30(3), p. 157-161, 2004.

[16] S. Edmondson, V. L. Osborne, and W. T. S. Huck, "Polymer brushes via surface-initiated polymerizations", *Chemical Society Reviews*, 33(1), p. 14-22, 2004.

[17] H. Schmidt, "Preparation, Application and Potential of Ormocers", in *Proceedings of The Winter School On Glasses and Ceramics from Gels, Sol-Gel Science and Technology*, Sao Carlos (SP), Brazil, 1989.

[18] H. Schmidt and H. Wolter, "Organically Modified Ceramics and Their Applications", *Journal of Non-Crystalline Solids*, 121(1-3), p. 428-435, 1990.

[19] G. M. Dykes, "Dendrimers: a review of their appeal and applications", *Journal of Chemical Technology and Biotechnology*, 76(9), p. 903-918, 2001.

[20] H. Lang and B. Lühmann, "Siloxane and carbosiloxane based dendrimers: Synthesis, reaction chemistry and potential applications." *Advanced Materials*, 13(20), p. 1523-1540, 2001.

[21] U. Boas and P. M. H. Heegaard, "Dendrimers in drug research", *Chem. Soc. Rev.*, 33, p. 43-63, 2004.

[22] A. W. Bosman, H. M. Janssen, and E. W. Meijer, "About Dendrimers: Structure, Physical Properties, and Applications", *Chemical Reviews*, 99, p. 1665-1688, 1999.

[23] S. M. Grayson and J. M. J. Frechet, "Convergent Dendrons and Dendrimers: from Synthesis to Applications", *Chemical Reviews*, 101, p. 3819-3867, 2001.

[24] A. Garcia-Bernabé, M. Krämer, B. Olàh, and R. Haag, "Syntheses and Phase-Transfer Properties of Dendritic Nanocarriers That Contain Perfluorinated Shell Structures", *Chemistry - A European Journal*, 10(11), p. 2822-2830, 2004.

[25] W. A. Daoud, J. H. Xin, and G. K. H. Pang, "Microstructural evolution of titania nanocrystallites by a hydrothermal treatment: A HRTEM study", *Journal of the American Ceramic Society*, 88(2), p. 443-446, 2005.

[26] L. Crespo, G. Sanclimens, M. Pons, E. Giralt, M. Royo, and F. Albericio, "Peptide and Amide Bond-Containing Dendrimers", *Chem. Rev.*, 105(5), p. 1663-1681, 2005.

[27] L. J. Twyman, A. S. H. King, and I. K. Martin, "Catalysis inside dendrimers", *Chemical Society Reviews*, 31(2), p. 69-82, 2002.

[28] F. Vogtle, S. Gestermann, R. Hesse, H. Schwierz, and B. Windisch, "Functional dendrimers", *Progress in Polymer Science*, 25(7), p. 987-1041, 2000.

[29] R. M. Versteegen, D. J. M. v. Beek, R. P. Sijbesma, D. Vlassopoulos, G. Fytas, and E. W. Meijer, "Dendrimer-Based Transient Supramolecular Networks", *J. Am. Chem. Soc.*, 127(40), p. 13862-13868, 2005.

[30] J.-P. Majoral, C.-O. Turrin, R. Laurent, and A.-M. Caminade, "Phosphorus Dendrimers: Nano-objects for Nanosciences", *Macromolecular Symposia*, 229(1), p. 1-7, 2005.

[31] A. Juris, "Recent developments in photo- and redox-active dendrimers", *Annual Reports Section C*, 99, p. 177-241, 2003.

[32] D. K. Smith, "Dendritic supermolecules - towards controllable nanomaterials", *Chemical Communications*, 1, p. 34-44, 2006.

[33] D. Onoshima and T. Imae, "Dendritic nano- and microhydrogels fabricated by triethoxysilyl focal dendrons", *Soft Matter*, 2(2), p. 141-148, 2006.

[34] K. Inoue, "Functional dendrimers, hyperbranched and star polymers", *Progress in Polymer Science*, 25(4), p. 453-571, 2000.

[35] M. C. Roco, "Nanoparticles and Nanotechnology Research", in *Journal of Nanoparticle Research*, 1999.

[36] H. Schmidt, "Nanoparticles by chemical synthesis, processing to materials and innovative applications", *Applied Organometallic Chemistry*, 15(5), p. 331-343, 2001.

[37] I. Garcia, N. E. Zafeiropoulos, A. Janke, A. Tercjak, A. Eceiza, M. Stamm, and I. Mondragon, "Functionalization of iron oxide magnetic nanoparticles with poly(methyl

methacrylate) brushes via grafting-from atom transfer radical polymerization", *Journal of Polymer Science Part a-Polymer Chemistry*, 45(5), p. 925-932, 2007.

[38] F. Grasset, N. Saito, D. Li, D. Park, I. Sakaguchi, N. Ohashi, H. Haneda, T. Roisnel, S. Mornet, and E. Duguet, "Surface modification of zinc oxide nanoparticles by aminopropyltriethoxysilane", *Journal of Alloys and Compounds*, 360(1-2), p. 298-311, 2003.

[39] H. Chen, S. X. Zhou, G. X. Gu, and L. M. Wu, "Modification and dispersion of nanosilica", *Journal of Dispersion Science and Technology*, 25(6), p. 837-848, 2004.

[40] C. Kneuer, M. Sameti, E. G. Haltner, T. Schiestel, H. Schirra, H. Schmidt, and C. M. Lehr, "Silica nanoparticles modified with aminosilanes as carriers for plasmid DNA", *International Journal of Pharmaceutics*, 196(2), p. 257-261, 2000.

[41] I. J. Bruce and T. Sen, "Surface modification of magnetic nanoparticles with alkoxysilanes and their application in magnetic bioseparations", *Langmuir*, 21(15), p. 7029-7035, 2005.

[42] R. P. Bagwe, L. R. Hilliard, and W. Tan, "Surface Modification of Silica Nanoparticles to Reduce Aggregation and Nonspecific Binding", *Langmuir*, 22(9), p. 4357-4362, 2006.

[43] Y. S. Chung, S. A. Song, and S. B. Park, "Hydrophobic modification of silica nanoparticle by using aerosol spray reactor", *Colloids and Surfaces a-Physicochemical and Engineering Aspects*, 236(1-3), p. 73-79, 2004.

[44] X.-C. Shen, X.-Z. Fang, Y.-H. Zhou, and H. Liang, "Synthesis and Characterization of 3-Aminopropyltriethoxysilane-Modified Superparamagnetic Magnetite Nanoparticles", *Chemistry Letters*, 33(11), p. 1468, 2004.

[45] X. Li, Z. Cao, Z. Zhang, and H. Dang, "Surface-modification in situ of nano-$SiO_2$ and its structure and tribological properties", *Applied Surface Science*, 252(22), p. 7856-7861, 2006.

[46] F. Bauer, H.-J. Glasel, U. Decker, H. Ernst, A. Freyer, E. Hartmann, V. Sauerland, and R. Mehnert, "Trialkoxysilane grafting onto nanoparticles for the preparation of clear coat polyacrylate systems with excellent scratch performance", *Progress in Organic Coatings*, 47(2), p. 147-153, 2003.

[47] Z. Csogor, M. Nacken, M. Sameti, C. M. Lehr, and H. Schmidt, "Modified silica particles for gene delivery", *Materials Science & Engineering C-Biomimetic and Supramolecular Systems*, 23(1-2), p. 93-97, 2003.

[48] H. Hayashi, H. Suzuki, and S. Kaneko, "Effect of Chemical Modification on Hydrolysis and Condensation Reaction of Zirconium Alkoxide", *Journal of Sol-Gel Science and Technology*, 12(2), p. 87-94, 1998.

[49] C. Sanchez, J. Livage, M. Henry, and F. Babonneau, "Chemical modification of alkoxide precursors", *Journal of Non-Crystalline Solids*, 100(1-3), p. 65-76, 1988.

[50] H. Sayilkan, S. Sener, and E. Arpac, "Zirconium tetra-n-butylate modified with different organic acids: Hydrolysis and polymerization of the products", *Journal of Inorganic and Organometallic Polymers*, 5(4), p. 409-423, 1995.

[51] L. Bonhomme-Coury, F. Babonneau, and J. Livage, "Investigation of the sol-gel chemistry of ethylacetoacetate modified aluminum sec-butoxide", *Journal of Sol-Gel Science and Technology*, 3(3), p. 157-168, 1994.

[52] G. H. Yi and M. Sayer, "An Acetic-Acid Water-Based Sol-Gel PZT Process .1. Modification of Zr and Ti Alkoxides with Acetic-Acid", *Journal of Sol-Gel Science and Technology*, 6(1), p. 65-74, 1996.

[53] K. Velez, J. F. Quinson, and B. Fenet, "Modification Study of Aluminum sec-Butoxide by Acrylic Acid", *Journal of Sol-Gel Science and Technology*, 16(3), p. 201-208, 1999.

[54] F. X. Perrin, V. Nguyen, and J. L. Vernet, "FT-IR Spectroscopy of Acid-Modified Titanium Alkoxides: Investigations on the Nature of Carboxylate Coordination and Degree of Complexation", *Journal of Sol-Gel Science and Technology*, 28(2), p. 205-215, 2003.

[55] Z. Li and Y. Zhu, "Surface-modification of $SiO_2$ nanoparticles with oleic acid", *Applied Surface Science*, 211(1-4), p. 315-320, 2003.

[56] Y. Zhang, N. Kohler, and M. Zhang, "Surface modification of superparamagnetic magnetite nanoparticles and their intracellular uptake", *Biomaterials*, 23(7), p. 1553-1561, 2002.

[57] P. VanderVoort and E. F. Vansant, "Modification of the silica surface with aminosilanes", *Polish Journal of Chemistry*, 71(5), p. 550-567, 1997.

[58] T. Fesionowski, "Modification and characterization of titanium dioxide surface", *Pigment and Resin Technology*, 30(5), p. 287-295, 2001.

[59] B. Mahltig and H. Böttcher, "Modified Silica Sol Coatings for Water-Repellent Textiles", *Journal of Sol-Gel Science and Technology*, 27(1), p. 43-52, 2003.

[60] F. Bauer, V. Sauerland, H. J. Gläsel, H. Ernst, M. Findeisen, E. Hartmann, H. Langguth, B. Marquardt, and R. Mehnert, "Preparation of Scratch and Abrasion Resistant Polymeric Nanocomposites by Monomer Grafting onto Nanoparticles, 3. Effect of Filler Particles and Grafting Agents", *Macromolecular Materials and Engineering*, 287(8), p. 546-552, 2002.

[61] F. Bauer, H. Ernst, D. Hirsch, S. Naumov, M. Pelzing, V. Sauerland, and R. Mehnert, "Preparation of Scratch and Abrasion Resistant Polymeric Nanocomposites by Monomer Grafting onto Nanoparticles, 5", *Macromolecular Chemistry and Physics*, 205(12), p. 1587-1593, 2004.

[62] S. D. Bhagat and A. V. Rao, "Surface chemical modification of TEOS based silica aerogels synthesized by two step (acid-base) sol-gel process", *Applied Surface Science*, 252(12), p. 4289-4297, 2006.

[63] A. Andrzejewska, A. Krysztafkiewicz, and T. Jesionowski, "Adsorption of organic dyes on the aminosilane modified $TiO_2$ surface", *Dyes and Pigments*, 62(2), p. 121-130, 2004.

[64] M. S. W. Vong, N. Bazin, and P. A. Sermon, "Chemical modification of silica gels", *Journal of Sol-Gel Science and Technology*, 8(1-3), p. 499-505, 1997.

[65] M. Z. Rong, M. Q. Zhang, H. B. Wang, and H. M. Zeng, "Surface modification of magnetic metal nanoparticles and its influence on the performance of polymer composites", *Journal of Polymer Science Part B: Polymer Physics*, 41(10), p. 1070-1084, 2003.

[66] E. Barna, B. Bommer, J. Kursteiner, A. Vital, O. von Trzebiatowski, W. Koch, B. Schmid, and T. Graule, "Innovative, scratch proof nanocomposites for clear coatings", *Composites Part a-Applied Science and Manufacturing*, 36(4), p. 473-480, 2005.

[67] F. Bauer, H. J. Glasel, E. Hartmann, E. Bilz, and R. Mehnert, "Surface modification of nanoparticles for radiation curable acrylate clear coatings", *Nuclear Instruments & Methods in Physics Research Section B-Beam Interactions with Materials and Atoms*, 208, p. 267-270, 2003.

[68] K. Sasazawa, J. Kurachi, T. Narumi, H. Nishi, Y. Yamamoto, and H. Sawada, "Preparation and applications of novel fluoroalkyl end-capped sulfonic acid oligomers-silica gel polymer hybrids", *Journal of Applied Polymer Science*, 103(1), p. 110-117, 2007.

[69] Z. Wu, H. Xiang, T. Kim, M.-S. Chun, and K. Lee, "Surface properties of submicrometer silica spheres modified with aminopropyltriethoxysilane and phenyltriethoxysilane", *Journal of Colloid and Interface Science*, 304(1), p. 119-124, 2006.

[70] M. Qhobosheane, S. Santra, P. Zhang, and W. Tan, "Biochemically functionalized silica nanoparticles", *Analyst*, 126(8), p. 1274-1278, 2001.

[71] S. Phadtare, S. Shah, A. Prabhune, P. P. Wadgaonkar, and M. Sastry, "Immobilization of Candida bombicola cells on free-standing organic-gold nanoparticle membranes and their use as enzyme sources in biotransformations", *Biotechnology Progress*, 20(6), p. 1817-1824, 2004.

[72] M. Mikhaylova, D. K. Kim, N. Bobrysheva, M. Osmolowsky, V. Semenov, T. Tsakalakos, and M. Muhammed, "Superparamagnetism of magnetite nanoparticles: Dependence on surface modification", *Langmuir*, 20(6), p. 2472-2477, 2004.

[73] R. N. E. Arpac, H. Schmidt, "Synthesis and Properties of Transparent $ZrO_2$ Containing SiO2 Polymethacrylate Polymers", in *Sol-gel optics, SPIE Proceedings*, Bellingham, 1990.

[74] T. R. D. Hoebbel, K. Endres, H. Schmidt, A. Kayan, E. Arpac, "Synthesis and Reactions of Unsaturated Ligands Containing Al and Zr Alkoxide Precursors", in *IN: European Workshop on Hybrid Organic-Inorganic Materials: Synthesis, properties, applications*, Chateau de Bierville, France, 1993.

[75] U. Schubert, E. Arpac, W. Glaubitt, A. Helmerich, and C. Chau, "Primary Hydrolysis Products of Methacrylate-Modified Titanium and Zirconium Alkoxides", *Chemistry of Materials*, 4(2), p. 291-295, 1992.

[76] D. Hoebbel, T. Reinert, H. Schmidt, and E. Arpac, "On the Hydrolytic Stability of Organic-Ligands in Al-Alkoxide, Ti-Alkoxide and Zr-Alkoxide Complexes", *Journal of Sol-Gel Science and Technology*, 10(2), p. 115-126, 1997.

[77] F. Ribot, P. Toledano, and C. Sanchez, "Hydrolysis-condensation process of beta-diketonates-modified cerium(IV) isopropoxide", *Chemistry of Materials*, 3, p. 759-764, 1991.

[78] F. Babonneau, L. Coury, and J. Livage, "Aluminum sec-butoxide modified with ethylacetoacetate: An attractive precursor for the sol-gel synthesis of ceramics", *Journal of Non-Crystalline Solids*, 121(1-3), p. 153-157, 1990.

[79] R. J. Young, "Introduction to Polymers", Second ed, London, Chapman & Hall, 1991.

[80] H. G. Elias, "Plastics, General Survey", in *Ullmann's Encyclopedia of Industrial Chemistry*, John Wiley & Sons, Inc., 2000.

[81] A. E. Hamielec and H. Tobita, "Polymerization Processes", in *Ullmann's Encyclopedia of Industrial Chemistry*, John Wiley & Sons, Inc., 2000.

[82] B. Radhakrishnan, R. Ranjan, and W. J. Brittain, "Surface initiated polymerizations from silica nanoparticles", *Soft Matter*, 2, p. 386-396, 2006.

[83] N. Tsubokawa, "Surface Grafting of Polymers onto Nanoparticles in a Solvent-Free Dry-System and Applications of Polymer-grafted Nanoparticles as Novel Functional Hybrid Materials", *Polymer Journal*, 39(10), p. 983-1000, 2007.

[84] C. Li and B. C. Benicewicz, "Synthesis of Well-Defined Polymer Brushes Grafted onto Silica Nanoparticles via Surface Reversible Addition-Fragmentation Chain Transfer Polymerization", *Macromolecules*, 38(14), p. 5929-5936, 2005.

[85] G. Zheng and H. D. H. Stover, "Grafting of Polystyrene from Narrow Disperse Polymer Particles by Surface-Initiated Atom Transfer Radical Polymerization", *Macromolecules*, 35(18), p. 6828-6834, 2002.

[86] C. Bartholome, E. Beyou, E. Bourgeat-Lami, P. Chaumont, and N. Zydowicz, "Nitroxide-Mediated Polymerizations from Silica Nanoparticle Surfaces: "Graft from"

Polymerization of Styrene Using a Triethoxysilyl-Terminated Alkoxyamine Initiator", *Macromolecules*, 36(21), p. 7946-7952, 2003.

[87] Rigoberto C. Advincula, William J. Brittain, Kenneth C. Caster, and J. Rühe, "Polymer Brushes", Wiley-VCH Verlag GmbH & Co. KGaA, Weinheim, 2004.

[88] N. Tsubokawa and A. Kogure, "Surface Grafting of Polymers onto Inorganic Ultrafine Particles - Reaction of Functional Polymers with Acid Anhydride Groups Introduced onto Inorganic Ultrafine Particles", *Journal of Polymer Science Part a-Polymer Chemistry*, 29(5), p. 697-702, 1991.

[89] I. Luzinov, D. Julthongpiput, H. Malz, J. Pionteck, and V. V. Tsukruk, "Polystyrene Layers Grafted to Epoxy-Modified Silicon Surfaces", *Macromolecules*, 33(3), p. 1043-1048, 2000.

[90] S. Minko, S. Patil, V. Datsyuk, F. Simon, K. J. Eichhorn, M. Motornov, D. Usov, I. Tokarev, and M. Stamm, "Synthesis of Adaptive Polymer Brushes via "Grafting To" Approach from Melt", *Langmuir*, 18(1), p. 289-296, 2002.

[91] N. Tsubokawa and H. Ishida, "Graft-Polymerization of Methyl Methacrylate from Silica Initiated by Peroxide Groups Introduced onto the Surface", *Journal of Polymer Science Part a-Polymer Chemistry*, 30(10), p. 2241-2246, 1992.

[92] N. Tsubokawa, Y. Shirai, and K. Hashimoto, "Effect of polymerization conditions on the molecular weight of polystyrene grafted onto silica in the radical graft-polymerization initiated by azo or peroxyester groups introduced onto the surface", *Colloid and Polymer Science*, 273(11), p. 1049-1054, 1995.

[93] N. Tsubokawa, Y. Shirai, H. Tsuchida, and S. Handa, "Photografting of Vinyl Polymers onto Ultrafine Inorganic Particles - Photopolymerization of Vinyl Monomers Initiated by Azo Groups Introduced onto These Surfaces", *Journal of Polymer Science Part a-Polymer Chemistry*, 32(12), p. 2327-2332, 1994.

[94] M. Yang and Y. Dan, "Preparation and characterization of poly(methyl methacrylate)/titanium oxide composite particles", *Colloid & Polymer Science*, 284(3), p. 243-250, 2005.

[95] N. Tsubokawa, A. Kogure, K. Maruyama, Y. Sone, and M. Shimomura, "Graft Polymerization of Vinyl Monomers from Inorganic Ultrafine Particles Initiated by Azo Groups Introduced onto the Surface", *Polymer Journal*, 22(9), p. 827-833, 1990.

[96] K. Sill and T. Emrick, "Nitroxide-mediated radical polymerization from CdSe nanoparticles", *Chemistry of Materials*, 16(7), p. 1240-1243, 2004.

[97] K. Matyjaszewski, P. J. Miller, N. Shukla, B. Immaraporn, A. Gelman, B. B. Luokala, T. M. Siclovan, G. Kickelbick, T. Vallant, H. Hoffmann, and T. Pakula, "Polymers at interfaces: Using atom transfer radical polymerization in the controlled growth of

homopolymers and block copolymers from silicon surfaces in the absence of untethered sacrificial initiator", *Macromolecules*, 32(26), p. 8716-8724, 1999.

[98] J. B. Kim, M. L. Bruening, and G. L. Baker, "Surface-initiated atom transfer radical polymerization on gold at ambient temperature", *Journal of the American Chemical Society*, 122(31), p. 7616-7617, 2000.

[99] H. Mori, D. C. Seng, M. F. Zhang, and A. H. E. Muller, "Hybrid nanoparticles with hyperbranched polymer shells via self-condensing atom transfer radical polymerization from silica surfaces", *Langmuir*, 18(9), p. 3682-3693, 2002.

[100] X. Y. Chen, S. P. Armes, S. J. Greaves, and J. F. Watts, "Synthesis of hydrophilic polymer-grafted ultrafine inorganic oxide particles in protic media at ambient temperature via atom transfer radical polymerization: use of an electrostatically adsorbed polyelectrolytic macroinitiator", *Langmuir*, 20(3), p. 587-595, 2004.

[101] Y. Tsujii, K. Ohno, S. Yamamoto, A. Goto, and T. Fukuda, "Structure and properties of high-density polymer brushes prepared by surface-initiated living radical polymerization", in *Surface-Initiated Polymerization I*, p. 1-45, 2006.

[102] X. Y. Huang, L. J. Doneski, and M. J. Wirth, "Surface-confined living radical polymerization for coatings in capillary electrophoresis", *Analytical Chemistry*, 70(19), p. 4023-4029, 1998.

[103] X. Y. Huang and M. J. Wirth, "Surface-initiated radical polymerization on porous silica", *Analytical Chemistry*, 69(22), p. 4577-4580, 1997.

[104] J. Ok and K. Matyjaszewski, "Synthesis of Magnesium Dihydroxide Hybrid Nanocomposites via ATRP", *Journal of Inorganic and Organometallic Polymers and Materials*, 16(2), p. 129-137, 2006.

[105] Y. Rong, H. Z. Chen, G. Wu, and M. Wang, "Preparation and characterization of titanium dioxide nanoparticle/polystyrene composites via radical polymerization", *Materials Chemistry and Physics*, 91(2-3), p. 370-374, 2005.

[106] M. J. Yang and Y. Dan, "Preparation of poly(methyl methacrylate)/titanium oxide composite particles via in-situ emulsion polymerization", *Journal of Applied Polymer Science*, 101(6), p. 4056-4063, 2006.

[107] M. Z. Rong, M. Q. Zhang, G. Shi, Q. L. Ji, B. Wetzel, and K. Friedrich, "Graft polymerization onto inorganic nanoparticles and its effect on tribological performance improvement of polymer composites", *Tribology International*, 36(9), p. 697-707, 2003.

[108] P. Dallas, V. Georgakilas, D. Niarchos, P. Komninou, T. Kehagias, and D. Petridis, "Synthesis, characterization and thermal properties of polymer/magnetite nanocomposites", *Nanotechnology*, 17(8), p. 2046-2053, 2006.

[109] N. Tsubokawa, T. Kimoto, and K. Koyama, "Polymerization of Vinyl Monomers in the Presence of Silica Having Surface Functional-Groups", *Colloid and Polymer Science*, 271(10), p. 940-946, 1993.

[110] M. Z. Rong, Q. L. Ji, M. Q. Zhang, and K. Friedrich, "Graft polymerization of vinyl monomers onto nanosized alumina particles", *European Polymer Journal*, 38(8), p. 1573-1582, 2002.

[111] N. Tsubokawa, K. Fujiki, and Y. Sone, "Radical Grafting from Carbon-Black - Graft-Polymerization of Vinyl Monomers Initiated by Peroxyester Groups Introduced onto Carbon-Black Surface", *Polymer Journal*, 20(3), p. 213-220, 1988.

[112] D. A. Savin, J. Pyun, G. D. Patterson, T. Kowalewski, and K. Matyjaszewski, "Synthesis and characterization of silica-graft-polystyrene hybrid nanoparticles: Effect of constraint on the glass-transition temperature of spherical polymer brushes", *Journal of Polymer Science Part B-Polymer Physics*, 40(23), p. 2667-2676, 2002.

[113] X. H. Liu, J. Yang, L. Wang, X. J. Yang, L. D. Lu, and X. Wang, "An improvement on sol-gel method for preparing ultrafine and crystallized titania powder", *Materials Science and Engineering a-Structural Materials Properties Microstructure and Processing*, 289(1-2), p. 241-245, 2000.

[114] J. W. Li, J. M. Tian, and L. M. Dong, "Synthesis of SiC precursors by a two-step sol-gel process and their conversion to SiC powders", *Journal of the European Ceramic Society*, 20(11), p. 1853-1857, 2000.

[115] J. Li, Y. B. Pan, C. S. Xiang, Q. M. Ge, and J. K. Guo, "Low temperature synthesis of ultrafine alpha-Al2O3 powder by a simple aqueous sol-gel process", *Ceramics International*, 32(5), p. 587-591, 2006.

[116] C.-C. Wang and J. Y. Ying, "Sol-gel synthesis and hydrothermal processing of anatase and rutile titania nanocrystals", *Chemistry of Materials*, 11(11), p. 3113-3120, 1999.

[117] M. Epifani, C. Giannini, L. Tapfer, and L. Vasanelli, "Sol-Gel Synthesis and Characterization of Ag and Au Nanoparticles in $SiO_2$, $TiO_2$, and $ZrO_2$ Thin-Films", *Journal of the American Ceramic Society*, 83(10), p. 2385-2393, 2000.

[118] Y. C.-D. Kobayashi, M. A.; Liz-Marzán, L. M., "Sol-Gel Processing of Silica-Coated Gold Nanoparticles", *Langmuir*, 17(20), p. 6375 - 6379, 2001.

[119] R. J. P. Corriu, D. Leclercq, P. Lefevre, P. H. Mutin, and A. Vioux, "Preparation of Monolithic Metal-Oxide Gels by a Non-Hydrolytic Sol-Gel Process." *Journal of Materials Chemistry*, 2(6), p. 673-674, 1992.

[120] Y. Lirong and Y. Guoxing, "$TiO_2$-$SiO_2$ monolithic glass formation from sol-gel", *Journal of Non-Crystalline Solids*, 100(1-3), p. 309-315, 1988.

[121] Y. Hu, "Preparation of Lead Zirconate Titanate Ceramic Fibers by Sol-Gel Method", *Journal of Sol-Gel Science and Technology*, 18(3), p. 235-247, 2000.

[122] A. Karout, P. Buisson, A. Perrard, and A. Pierre, "Shaping and Mechanical Reinforcement of Silica Aerogel Biocatalysts with Ceramic Fiber Felts", *Journal of Sol-Gel Science and Technology*, 36(2), p. 163-171, 2005.

[123] C. G. Guizard, A. C. Julbe, and A. Ayral, "Design of nanosized structures in sol-gel derived porous solids. Applications in catalyst and inorganic membrane preparation", *Journal of Materials Chemistry*, 9(1), p. 55-65, 1999.

[124] S. Dire, E. Pagani, F. Babonneau, R. Ceccato, and G. Carturan, "Unsupported $SiO_2$-based organic-inorganic membranes .1. Synthesis and structural characterization", *Journal of Materials Chemistry*, 7(1), p. 67-73, 1997.

[125] S. Dire, E. Pagani, R. Ceccato, and G. Carturan, "Unsupported $SiO_2$-based organic-inorganic membranes .2. Surface features and gas permeation", *Journal of Materials Chemistry*, 7(6), p. 919-922, 1997.

[126] C. Guizard, C. Mouchet, R. Vacassy, A. Julbe, and A. Larbot, "Sol-gel processing of inorganic membranes", *Journal of Sol-Gel Science and Technology*, 2(1 - 3), p. 483-487, 1994.

[127] P. Etienne, J. Denape, J. Y. Paris, J. Phalippou, and R. Sempere, "Tribological properties of ormosil coatings", *Journal of Sol-Gel Science and Technology*, 6, p. 287-297, 1996.

[128] M. S. W. Vong, P. A. Sermon, Y. Sun, and D. Spriggs, "Sol-gel processing of zirconia high-index coatings", *Proc. SPIE-Int. Soc. Opt. Eng.*, p. 446-56, 1995.

[129] K.-C. Song, J.-K. Park, H.-U. Kang, and S.-H. Kim, "Synthesis of Hydrophilic Coating Solution for Polymer Substrate Using Glycidoxypropyltrimethoxysilane", *Journal of Sol-Gel Science and Technology*, 27(1), p. 53-59, 2003.

[130] R. A. Caruso and M. Antonietti, "Sol-gel nanocoating: An approach to the preparation of structured materials", *Chemistry of Materials*, 13(10), p. 3272-3282, 2001.

[131] H. Bottcher, "Bioactive sol-gel coatings", *Journal Für Praktische Chemie-Practical Applications and Applied Chemistry*, 342(5), p. 427-436, 2000.

[132] B. Mahltig, D. Fiedler, A. Thron, and H. Böttcher, "Biocidal coatings based on silica nanosols", *VDI-Berichte*, 1803, p. 291, 2003.

[133] J. Livage and D. Ganguli, "Sol-gel electrochromic coatings and devices: A review", *Solar Energy Materials and Solar Cells*, 68(3-4), p. 365-381, 2001.

[134] J. Puetz, M. A. Aegerter, and G. Guzman, "Sol-gel coating of thin display glasses - Problems and remedy", *Journal of Sol-Gel Science and Technology*, 32(1-3), p. 125-129, 2004.

[135] B. C. Dave, X. K. Hu, Y. Devaraj, and S. K. Dhali, "Sol-gel-derived corrosion-protection coatings", *Journal of Sol-Gel Science and Technology*, 32(1-3), p. 143-147, 2004.

[136] Y. Chen, L. Jin, and Y. Xie, "Sol-Gel Processing of Organic-Inorganic Nanocomposite Protective Coatings", *Journal of Sol-Gel Science and Technology*, 13(1 - 3), p. 735-738, 1998.

[137] M. L. Zheludkevich, I. M. Salvado, and M. G. S. Ferreira, "Sol-gel coatings for corrosion protection of metals", *Journal of Materials Chemistry*, 15(48), p. 5099-5111, 2005.

[138] D. R. Uhlmann, T. Suratwala, K. Davidson, J. M. Boulton, and G. Teowee, "Sol-gel derived coatings on glass", *Journal of Non-Crystalline Solids*, 218, p. 113-122, 1997.

[139] N. Sanz, A. C. Gaillot, Y. Usson, P. L. Baldeck, and A. Ibanez, "Organic nanocrystals grown in sol-gel coatings", *Journal of Materials Chemistry*, 10(12), p. 2723-2726, 2000.

[140] S. Hofacker, M. Mechtel, M. Mager, and H. Kraus, "Sol-gel - A new tool for coatings chemistry", *Progress in Organic Coatings*, 45(2-3), p. 159-164, 2002.

[141] C. J. Brinker and M. S. Harrington, "Sol-Gel Derived Antireflective Coatings for Silicon", *Solar Energy Materials*, 5(2), p. 159-172, 1981.

[142] B. Samuneva, V. Kozhukharov, C. Trapalis, and R. Kranold, "Sol-gel processing of titanium-containing thin coatings Part 1 Preparation and structure", *Journal of Materials Science*, 28(9), p. 2353-2360, 1993.

[143] C. Trapalis, V. Kozhukharov, B. Samuneva, and P. Stefanov, "Sol-gel processing of titanium-containing thin coatings Part 2 XPS Studies", *Journal of Materials Science*, 28(5), p. 1276-1282, 1993.

[144] V. Kozhukharov, C. Trapalis, and B. Samuneva, "Sol-gel processing of titanium-containing thin coatings Part 3 Properties", *Journal of Materials Science*, 28(5), p. 1283-1288, 1993.

[145] M. Shane and M. L. Mecartney, "Sol-gel synthesis of zirconia barrier coatings", *Journal of Materials Science*, 25(3), p. 1537-1544, 1990.

[146] P. Lima Neto, M. Atik, L. A. Avaca, and M. A. Aegerter, "Sol-gel $ZrO_2$ coatings for chemical protection of stainless steel", *Journal of Sol-Gel Science and Technology*, 1(2), p. 177-184, 1994.

[147] D. B. Haddow, P. F. James, and R. Van Noort, "Sol-Gel Derived Calcium Phosphate Coatings for Biomedical Applications", *Journal of Sol-Gel Science and Technology*, 13(1 - 3), p. 261-265, 1998.

[148] O. A. Shilova, S. V. Hashkovsky, and L. A. Kuznetsova, "Sol-Gel Preparation of Ceramic Coatings for Electrical, Laser, Space Engineering and Power", *Journal of Sol-Gel Science and Technology*, 26(1 - 3), p. 687-691, 2003.

[149] T. P. Chou, C. Chandrasekaran, and G. Z. Cao, "Sol-Gel-Derived Hybrid Coatings for Corrosion Protection", *Journal of Sol-Gel Science and Technology*, 26(1 - 3), p. 321-327, 2003.

[150] M. Zaharescu, M. Crisan, L. Predoana, M. Gartner, D. Cristea, S. Degeratu, and E. Manea, "Hybrid Inorganic-Organic Sol-Gel Coatings in the $SiO_2$-$TiO_2$ System", *Journal of Sol-Gel Science and Technology*, 32(1 - 3), p. 173-177, 2004.

[151] S. Pellice, P. Galliano, Y. Castro, and A. Duran, "Hybrid Sol-Gel Coatings Produced from TEOS and MPS", *Journal of Sol-Gel Science and Technology*, 28(1), p. 81-86, 2003.

[152] B. Mahltig, F. Audenaert, and H. Böttcher, "Hydrophobic Silica Sol Coatings on Textiles-the Influence of Solvent and Sol Concentration", *Journal of Sol-Gel Science and Technology*, 34(2), p. 103-109, 2005.

[153] R. L. Goswamee, F. Bosc, D. Cot, A. E. Mansouri, M. Lopez, F. Morato, and A. Ayral, "Sol-Gel Derived Nanocomposites and Nanoporous Oxide Powders and Related Coatings for the Reversible Chemisorption of Hydrogen Sulfide", *Journal of Sol-Gel Science and Technology*, 29(2), p. 97-105, 2004.

[154] M. Crisan, M. Gartner, L. Predoana, R. Scurtu, M. Zaharescu, and R. Gavrila, "Sol-Gel $SiO_2$-$ZrO_2$ Coatings for Optical Applications", *Journal of Sol-Gel Science and Technology*, 32(1 - 3), p. 167-172, 2004.

[155] A. C. Ristschkoff, R. Mahlberg, M. Loija, M. Kallio, J. Mannila, and A. Vesa, "Sol-gel hybrid coatings for wood products with improved surface durability and repellence properties", *Paint and Coatings Industry*, 21(7), p. 96-101, 2005.

[156] A. N. Khramov, V. N. Balbyshev, N. N. Voevodin, and M. S. Donley, "Nanostructured sol-gel derived conversion coatings based on epoxy- and amino-silanes", *Progress in Organic Coatings*, 47(3-4), p. 207-213, 2003.

[157] S. Hofacker, M. Mechtel, M. Mager, and H. Kraus, "Sol-gel: a new tool for coatings chemistry", *Progress in Organic Coatings*, 45(2-3), p. 159-164, 2002.

[158] N. Carmona, M. A. Villegas, and J. M. Fernandez Navarro, "Sol-gel coatings in the ZrO2-SiO2 system for protection of historical works of glass", *Thin Solid Films*, 515(4), p. 1320-1326, 2006.

[159] D. J. Suh and T. J. Park, "Sol-gel strategies for pore size control of high-surface-area transition-metal oxide aerogels", *Chemistry of Materials*, 8(2), p. 509-513, 1996.

[160] A. V. Rao and S. D. Bhagat, "Synthesis and physical properties of TEOS-based silica aerogels prepared by two step (acid-base) sol-gel process", *Solid State Sciences*, 6(9), p. 945-952, 2004.

[161] M. Moner-Girona, A. Roig, E. Molins, and J. Llibre, "Sol-Gel Route to Direct Formation of Silica Aerogel Microparticles Using Supercritical Solvents", *Journal of Sol-Gel Science and Technology*, 26(1 - 3), p. 645-649, 2003.

[162] C. Stöcker and A. Baiker, "Zirconia Aerogels: Effect of the Use of Mono- and Dicarboxylic Acids in the Sol-Gel Process on Structural Properties", *Journal of Sol-Gel Science and Technology*, 10(3), p. 269-282, 1997.

[163] J. Livage, M. Henry, and C. Sanchez, "Sol-gel Chemistry of Transition Metal Oxides", *Prog. Solid Satate Chem.*, 18(4), p. 259-341, 1989.

[164] J. Y. Wen and G. L. Wilkes, "Organic/inorganic hybrid network materials by the sol-gel approach", *Chemistry of Materials*, 8(8), p. 1667-1681, 1996.

[165] L. L. Hench and J. K. West, "The Sol-Gel Process", *Chemical Reviews*, 90(1), p. 33-72, 1990.

[166] H. Schmidt, "Chemistry of Material Preparation by the Sol-Gel Process", *Journal of Non-Crystalline Solids*, 100(1-3), p. 51-64, 1988.

[167] J. Livage and J. Lemerle, "Transition metal oxide gels and colloids", in *Annual Review of Materials Science*, 1982.

[168] A. C. Pierre, "Introduction to Sol-gel Processing", Kluwer Academic Publishers, 1-4, 1998.

[169] H. Dislich, "Glassy and Crystalline Systems from Gels - Chemical Basis and Technical Application", *Journal of Non-Crystalline Solids*, 57(3), p. 371-388, 1983.

[170] D. R. Uhlmann and G. Teowee, "Sol-gel science and technology: Current state and future prospects", *Journal of Sol-Gel Science and Technology*, 13(1-3), p. 153-162, 1998.

[171] S. Bhandarkar, "Sol-Gel Processing for Optical Communication Technology", *Journal of the American Ceramic Society*, 87(7), p. 1180-1199, 2004.

[172] S. M. Attia, J. Wang, G. Wu, J. Shen, and J. Ma, "Review on sol-gel derived coatings process, techniques and optical applications", *Journal of Materials Science and Technology*, 18(3), p. 211, 2002.

[173] Y. Haruvy, I. Gilath, M. Maniewictz, and N. Eisenberg, "Sol-Gel Prepared Glass for Refractive and Diffractive Micro-Optical Elements and Arrays", *Journal of Sol-Gel Science and Technology*, 13(1 - 3), p. 547-551, 1998.

[174] B. Dunn and J. I. Zink, "Optical-Properties of Sol-Gel Glasses Doped with Organic-Molecules", *Journal of Materials Chemistry*, 1(6), p. 903-913, 1991.

[175] H. G. Floch and P. F. Belleville, "Damage-resistant sol-gel optical coatings for advanced lasers at CEL-V", *Journal of Sol-Gel Science and Technology*, 2(1 - 3), p. 695-705, 1994.

[176] N. Tohge, G. S. Moore, and J. D. Mackenzie, "Structural Developments During the Gel to Glass-Transition", *Journal of Non-Crystalline Solids*, 63(1-2), p. 95-103, 1984.

[177] E. J. A. Pope, "Sol-gel optical nanocomposites: Design and applications", *Journal of Sol-Gel Science and Technology*, 2(1 - 3), p. 717-722, 1994.

[178] B.-S. Bae, "High Photosensitive Sol-Gel Hybrid Materials for Direct Photo-Imprinting of Micro-Optics", *Journal of Sol-Gel Science and Technology*, 31(1 - 3), p. 309-315, 2004.

[179] L. C. Klein, "Sol-gel optical materials", *Annual Review of Materials Science*, 23(1), p. 437-452, 1993.

[180] X. J. Wang, L. Xu, D. X. Li, L. Y. Liu, and W. C. Wang, "Thermo-optic properties of sol-gel-fabricated organic-inorganic hybrid waveguides", *Journal of Applied Physics*, 94(6), p. 4228-4230, 2003.

[181] M. Feuillade, C. Croutxe-Barghorn, L. Mager, C. Carre, and A. Fort, "Photopatterning of hybrid sol-gel glasses for optical and non-linear optical applications", in *Proceedings of SPIE - The International Society for Optical Engineering*, 2004.

[182] M. Serwadczak, M. W. Ubbenhorst, and S. Kucharski, "Optical and dielectric characteristics of photochromic hybrid sol-gel materials", *Journal of Sol-Gel Science and Technology*, 40(1), p. 39-44, 2006.

[183] H. M. Cheng, J. M. Ma, Z. G. Zhao, and L. M. Qi, "Hydrothermal Preparation of Uniform Nanosize Rutile and Anatase Particles", *Chemistry of Materials*, 7(4), p. 663-671, 1995.

[184] S. Somiya and R. Roy, "Hydrothermal synthesis of fine oxide powders", *Bulletin of Materials Science*, 23(6), p. 453-460, 2000.

[185] A. Somiya, K. Hishinuma, and T. Akiba, "A New Materials Processing - Hydrothermal Processing", *Bulletin of Materials Science*, 18(6), p. 811-818, 1995.

[186] D. Qin and H. L. Chen, "The influence of alcohol additives on the crystallization of ZrO2 under hydrothermal conditions", *Journal of Materials Science*, 41(21), p. 7059-7063, 2006.

[187] M. Yoshimura and S. Somiya, "Hydrothermal synthesis of crystallized nano-particles of rare earth-doped zirconia and hafnia", *Materials Chemistry and Physics*, 61(1), p. 1-8, 1999.

[188] Y. V. Kolen'ko, V. D. Maximov, A. A. Burukhin, V. A. Muhanov, and B. R. Churagulov, "Synthesis of ZrO2 and TiO2 nanocrystalline powders by hydrothermal process",

*Materials Science & Engineering C-Biomimetic and Supramolecular Systems*, 23(6-8), p. 1033-1038, 2003.

[189] E. Delgado, A. Bohorquez, G. P. Alcazar, and A. Bolanos, "Study of the evolution in the iron oxide synthesis by hydrothermal process", *Hyperfine Interactions*, 148(1-4), p. 129-134, 2003.

[190] J. Yang, S. Mei, and J. M. F. Ferreira, "Hydrothermal synthesis of well-dispersed TiO2 nano-crystals", *Journal of Materials Research*, 17(9), p. 2197-2200, 2002.

[191] S. T. Aruna, S. Tirosh, and A. Zaban, "Nanosize rutile titania particle synthesis via a hydrothermal method without mineralizers", *Journal of Materials Chemistry*, 10(10), p. 2388-2391, 2000.

[192] K. M. Reddy, D. Guin, S. V. Manorama, and A. R. Reddy, "Selective synthesis of nanosized $TiO_2$ by hydrothermal route: Characterization, structure property relation, and photochemical application", *Journal of Materials Research*, 19(9), p. 2567, 2004.

[193] M. M. Wu, G. Lin, D. H. Chen, G. G. Wang, D. He, S. H. Feng, and R. R. Xu, "Sol-hydrothermal synthesis and hydrothermally structural evolution of nanocrystal titanium dioxide", *Chemistry of Materials*, 14(5), p. 1974-1980, 2002.

[194] K. Yanagisawa and J. Ovenstone, "Crystallization of anatase from amorphous titania using the hydrothermal technique: Effects of starting material and temperature", *Journal of Physical Chemistry B*, 103(37), p. 7781-7787, 1999.

[195] J. Yang, S. Mei, and J. M. F. Ferreira, "Hydrothermal Synthesis of Nanosized Titania Powders: Influence of Peptization and Peptizing Agents on the Crystalline Phases and Phase Transitions", *Journal of the American Ceramic Society*, 83(6), p. 1361-1368, 2000.

[196] Y. Q. Zheng, E. W. Shi, S. X. Cui, W. J. Li, and X. F. Hu, "Hydrothermal preparation of nanosized brookite powders", *Journal of the American Ceramic Society*, 83(10), p. 2634-2636, 2000.

[197] J.-G. Li, C. Tang, D. Li, H. Haneda, and T. Ishigaki, "Monodispersed Spherical Particles of Brookite-Type $TiO_2$: Synthesis, Characterization, and Photocatalytic Property", *Journal of the American Ceramic Society*, 87(7), p. 1358-1361, 2004.

[198] J. Ovenstone, "Preparation of novel titania photocatalysts with high activity." *Journal of Materials Science*, 36, p. 1325-1329, 2001.

[199] G. Li, L. Li, J. Boerio-Goates, and B. F. Woodfield, "Grain-growth kinetics of rutile $TiO_2$ nanocrystals under hydrothermal conditions", *Journal of Materials Research*, 18(11), p. 2664-2669, 2003.

[200] E. L. Crepaldi, G. J. d. A. A. Soler-Illia, D. Grosso, F. Cagnol, F. Ribot, and C. Sanchez, "Controlled Formation of Highly Organized Mesoporous Titania Thin Films:

From Mesostructured Hybrids to Mesoporous Nanoanatase $TiO_2$", *Journal of American Chemical Society*, 125, p. 9770-9786, 2003.

[201] N. I. Alsalim, S. A. Bagshaw, A. Bittar, T. Kemmitt, A. J. Mcquillan, A. M. Mills, and M. J. Ryan, "Characterization and Activity of Sol-Gel-Prepared $TiO_2$ Photocatalysts Modified with Ca, Sr or Ba Ion Additives", *Journal of Materials Chemistry*, 10(10), p. 2358-2363, 2000.

[202] P. Lobmann, R. Jahn, S. Seifert, and D. Sporn, "Inorganic Thin-Films Prepared from Soluble Powders and Their Applications", *Journal of Sol-Gel Science and Technology*, 19(1-3), p. 473-477, 2000.

[203] J. C. Yu, H. Y. Tang, J. G. Yu, H. C. Chan, L. Z. Zhang, Y. D. Xie, H. Wang, and S. P. Wong, "Bactericidal and Photocatalytic Activities of $TiO_2$ Thin-Films Prepared by Sol-Gel and Reverse Micelle Methods", *Journal of Photochemistry and Photobiology A: Chemistry*, 153(1-3), p. 211-219, 2002.

[204] W. A. Daoud, J. H. Xin, and W. A. Daoud, "Low Temperature Sol-Gel Processed Photocatalytic Titania Coating", *Journal of Sol-Gel Science and Technology*, 29(1), p. 25-29, 2004.

[205] T. Lopez, R. Gomez, E. Sanchez, F. Tzompantzi, and L. Vera, "Photocatalytic activity in the 2,4-dinitroaniline decomposition over $TiO_2$ sol-gel derived catalysts." *Journal of Sol-Gel Science and Technology*, 22, p. 99-107, 2001.

[206] S. Eiden-Assmann, J. Widoniak, and G. Maret, "Synthesis and Characterization of Porous and Nonporous Monodisperse Colloidal $TiO_2$ Particles", *Chemistry of Materials*, 16(1), p. 6 -11, 2004.

[207] M. Hashizume and T. Kunitake, "Preparation of Self-Supporting Ultrathin Films of Titania by Spin Coating", *Langmuir*, 19, p. 10172-10178, 2003.

[208] G. Oskam, A. Nellore, R. L. Penn, and P. C. Searson, "The Growth Kinetics of $TiO_2$ Nanoparticles from Titanium(IV) Alkoxide at High Water/Titanium Ratio", *J. Phys. Chem. B*, 107, p. 1734-1738, 2003.

[209] W. W. So, S. B. Park, K. J. Kim, C. H. Shin, and S. J. Moon, "The crystalline phase stability of titania particles prepared at room temperature by the sol-gel method." *Journal of Materials Science*, 36, p. 4299-4305, 2001.

[210] S. Y. Chae, M. K. Park, S. K. Lee, T. Y. Kim, S. K. Kim, and W. I. Lee, "Preparation of size-controlled $TiO_2$ nanoparticles and derivation of optically transparent photocatalytic films", *Chemistry of Materials*, 15(17), p. 3326-3331, 2003.

[211] C. Guillard, B. Beaugiraud, C. Dutriez, J. M. Herrmann, H. Jaffrezic, N. Jaffrezicrenault, and M. Lacroix, "Physicochemical Properties and Photocatalytic Activities of $TiO_2$-Films Prepared by Sol-Gel Methods", *Applied Catalysis B: Environmental*, 39(4), p. 331-342, 2002.

[212] B. L. Bischoff and M. A. Anderson, "Peptization process in the sol-gel preparation of porous anatase ($TiO_2$)", *Chemistry of Materials*, 7, p. 1772-1778, 1995.

[213] M. Addamo, V. Augugliaro, A. D. Paola, E. Garcia-Lopez, V. Loddo, G. Marci, R. Molinari, L. Palmisano, and M. Schiavello, "Preparation, Characterization, and Photoactivity of Polycrystalline Nanostructured $TiO_2$ Catalysts", *J. Phys. Chem. B*, 108, p. 3303-3310, 2004.

[214] H. Yin, Y. Wada, T. Kitamura, S. Kambe, S. Murasawa, H. Mori, T. Sakata, and S. Yanagida, "Hydrothermal synthesis of nanosized anatase and rutile $TiO_2$ using amorphous phase $TiO_2$." *Journal of Materials Chemistry*, 11, p. 1694-1703, 2001.

[215] X. Jiang, T. Herricks, and Y. Xia, "Monodispersed Spherical Colloids of Titania: Synthesis, Characterization, and Crystallization", *Advanced Materials*, 15(14), p. 1205-1209, 2003.

[216] H.-s. Yun, K. c. Miyazawa, H. Zhou, I. Honma, and M. Kuwabara, "Synthesis of mesoporous thin $TiO_2$ films with hexagonal pore structures using triblock copolymer templates." *Advanced Materials*, 13(18), p. 1377-1380, 2001.

[217] M. Bialk, O. Prucker, and J. Ruhe, "Grafting of polymers to solid surfaces by using immobilized methacrylates", *Colloids and Surfaces a-Physicochemical and Engineering Aspects*, 198, p. 543-549, 2002.

[218] Y. H. Yang and Y. Dan, "Preparation of PMMA/SiO2 composite particles via emulsion polymerization", *Colloid and Polymer Science*, 281(8), p. 794-799, 2003.

[219] N. Tsubokawa, A. Kogure, K. Maruyama, Y. Sone, and M. Shimomura, "Graft-Polymerization of Vinyl Monomers from Inorganic Ultrafine Particles Initiated by Azo Groups Introduced onto the Surface", *Polymer Journal*, 22(9), p. 827-833, 1990.

[220] O. Prucker and J. Ruhe, "Mechanism of radical chain polymerizations initiated by azo compounds covalently bound to the surface of spherical particles", *Macromolecules*, 31(3), p. 602-613, 1998.

[221] M. Sartor, "Dynamic Light Scattering", http://physics.ucsd.edu/neurophysics/ courses/ physics_173_273/dynamic_light_scattering_03.pdf, 2003.

[222] G. Tölg, H. Günzler, and A. Williams, "Analytical Chemistry: Purpose and Procedures", in *Ullmann's Encyclopedia of Industrial Chemistry*, Wiley-VCH Verlag GmbH & Co. KGaA, 2003.

[223] R. L. S. Ron Jenkins, "Introduction to X-ray Powder Diffractometry", John Wiley & Sons, Inc., 1, 1996.

[224] Z. Guo, "Electrotransport studies of the anomalous semimetal ground state in CeRu4Sn6", 2006.

[225] P. W. Stephens, "X-Ray Powder Diffraction", in *Characterization of Materials*, John Wiley & Sons Inc., 2003.

[226] P. Moeck, "X-ray Diffraction (XRD)", http://physics.pdx.edu/~pmoeck/ phy381/ Topic5a-XRD.pdf, 2004.

[227] P. Scherrer, "Bestimmung der Grösse und der inneren Struktur von Kolloidteilchen mittels Röntgenstrahlen", *Gött. Nachrichten*, 2, p. 98-100, 1918.

[228] A. Kriete, H. Gundlach, S. Amelinckx, and L. Reimer, "Microscopy", in *Ullmann's Encyclopedia of Industrial Chemistry* Wiley-VCH Verlag, 2005.

[229] D. Shindo and T. Oikawa, "Analytical Electron Microscopy for Materials Science", Springer-Verlag, Tokyo, 1998.

[230] B. Fultz and J. M. Howe, "Transmission Electron Microscopy and Diffractometry of Materials", Second Edition ed, Springer-Verlag, 2004.

[231] D. B. Williams and C. B. Carter, "Transmission Electron Microscopy, Spectrometry IV", Vol. 4, Plenum Publishing Corporation, 1996.

[232] P. J. F. Sandra, "Gas Chromatography", in *Ullmann's Encyclopedia of Industrial Chemistry*, Wiley-VCH Verlag GmbH & Co. KGaA, 2001.

[233] M. Linscheid, "Mass Spectrometry", in *Ullmann's Encyclopedia of Industrial Chemistry*, Wiley-VCH Verlag GmbH & Co. KGaA, 2001.

[234] L. E. Amand and C. J. Tullin (1999) *The Theory Behind FTIR Analysis*, DOI: http://www.entek.chalmers.se/~leam/ftir/ftir_pdf/own_pub/theory_ftir.pdf

[235] G. W. H. H. Stephen B. Warrington, "Thermal Analysis and Calorimetry", in *Ullmann's Encyclopedia of Industrial Chemistry*, Wiley-VCH Verlag GmbH & Co. KGaA, 2007.

[236] H. K. D. H. Bhadeshia (2002) *Differential Scanning Calorimetry*, http://www.msm. cam.ac.uk/phase-trans/2002/Thermal2.pdf

[237] S. M. Lee, C. Y. Chen, and C. C. Wang, "Conductivity and characterization of polyurea electrolytes with carboxylic acid", *Journal of Polymer Science Part a-Polymer Chemistry*, 41(24), p. 4007-4016, 2003.

[238] Z. F. Li, G. H. Yang, and C. M. Xu, "Effect of the crosslink density on the morphology and properties of reaction-injection-molding poly(urethane urea) elastomers", *Journal of Polymer Science Part a-Polymer Chemistry*, 42(5), p. 1126-1131, 2004.

[239] E. Yilgor, G. E. Atilla, A. Ekin, P. Kurt, and I. Yilgor, "Isopropyl alcohol: an unusual, powerful, 'green' solvent for the preparation of silicone-urea copolymers with high urea contents", *Polymer*, 44(26), p. 7787-7793, 2003.

[240] D. J. Liaw and H. C. Sang, "Radical polymerization of new functional monomers derived from methacryloyl isocyanate and urea", *Journal of Polymer Science Part a-Polymer Chemistry*, 37(12), p. 1789-1796, 1999.

[241] I. Yilgör, J. S. Riffle, G. L. Wilkes, and J. E. McGrath, "Siloxane-urea segmented copolymers 1. Synthesis and characterization of model polymers from MDI and

bis(aminopropyl)polydimethylsiloxane", *Polymer Bulletin*, 8(11 - 12), p. 535-542, 1982.

[242] D. Tyagi, G. L. Wilkes, I. Yilgör, and J. E. McGrath, "Siloxane-urea segmented copolymers 2. Investigation of mechanical behavior", *Polymer Bulletin*, 8(11 - 12), p. 543-550, 1982.

[243] H. Pasch, I. S. Dairanieh, and B. Altahou, "Investigations of the Chemical-Structure of Sulfonated Amino-Formaldehyde Resins .1. C-13-Nmr Analysis of Sulfonated Urea-Formaldehyde Resins", *Journal of Polymer Science Part a-Polymer Chemistry*, 28(8), p. 2049-2062, 1990.

[244] A. Katti, N. Shimpi, S. Roy, H. Lu, E. F. Fabrizio, A. Dass, L. A. Capadona, and N. Leventis, "Chemical, Physical, and Mechanical Characterization of Isocyanate Cross-linked Amine-Modified Silica Aerogels", *Chem. Mater.*, 18(2), p. 285-296, 2006.

[245] D. Y. Chao, "The Role of Surfactants in Synthesizing Polyurea Microcapsule", *Journal of Applied Polymer Science*, 47(4), p. 645-651, 1993.

[246] W. L. F. Armarego and C. L. L. Chai, "Purification of Laboratory Chemicals", Fifth Edition ed, Elsevier, 2003.

[247] M. H. H. P. Boehm, "Über die Chemie der Oberfläche des Titandioxids. I. Bestimmung des aktiven Wasserstoffs, thermische Entwässerung und Rehydroxylierung", *Zeitschrift für anorganische und allgemeine Chemie*, 352(3-4), p. 156-167, 1967.

[248] R. Mueller, H. K. Kammler, K. Wegner, and S. E. Pratsinis, "OH Surface Density of $SiO_2$ and $TiO_2$ by Thermogravimetric Analysis", *Langmuir*, 19(1), p. 160-165, 2003.

[249] L. Téllez, J. Rubio, F. Rubio, E. Morales, and J. L. Oteo, "FT-IR Study of the Hydrolysis and Polymerization of Tetraethyl Orthosilicate and Polydimethyl Siloxane in the Presence of Tetrabutyl Orthotitanate", *Spectroscopy Letters*, 37(1), p. 11-31, 2004.

[250] R. Pena-Alonso, L. Tellez, J. Rubio, and F. Rubio, "Surface chemical and physical properties of TEOS-TBOT-PDMS hybrid materials", *Journal of Sol-Gel Science and Technology*, 38(2), p. 133-145, 2006.

[251] L. Tellez, J. Rubio, F. Rubio, E. Morales, and J. L. Oteo, "Synthesis of inorganic-organic hybrid materials from TEOS, TBT and PDMS", *Journal of Materials Science*, 38(8), p. 1773-1780, 2003.

[252] E. Ukaji, T. Furusawa, M. Sato, and N. Suzuki, "The effect of surface modification with silane coupling agent on suppressing the photo-catalytic activity of fine $TiO_2$ particles as inorganic UV filter", *Applied Surface Science*, 254(2), p. 563-569, 2007.

[253] G. S. Caravajal, D. E. Leyden, G. R. Quinting, and G. E. Maciel, "Structural characterization of (3-aminopropyl)triethoxysilane-modified silicas by silicon-29 and carbon-13 nuclear magnetic resonance", *Anal. Chem.*, 60(17), p. 1776-1786, 1988.

[254] P. Van der Voort and E. F. Vansant, "Modification of the silica surface with aminosilanes", *Polish Journal of Chemistry*, 71(5), p. 550-567, 1997.

[255] S. R. Culler, H. Ishida, and J. L. Koenig, "Structure of silane coupling agents adsorbed on silicon powder", *Journal of Colloid and Interface Science*, 106(2), p. 334-346, 1985.

[256] E. T. Vandenberg, L. Bertilsson, B. Liedberg, K. Uvdal, R. Erlandsson, H. Elwing, and I. Lundstrom, "Structure of 3-aminopropyl triethoxy silane on silicon oxide", *Journal of Colloid and Interface Science*, 147(1), p. 103-118, 1991.

[257] K. N. Pham, D. Fullston, and K. Sagoe-Crentsil, "Surface modification for stability of nano-sized silica colloids", *Journal of Colloid and Interface Science*, 315(1), p. 123-127, 2007.

[258] J. A. Dean, "Lange's Handbook of Chemistry", 15. ed, McGraw Hill, 1999.

[259] R. M. S. F. X. Webster, "Spectrometric Identification of Organic Compounds", Sixth ed, John Wiley & Sons, Inc. , 1997.

[260] H. U. Gremlich, "Infrared and Raman Spectroscopy ", in *Ullmann's Encyclopedia of Industrial Chemistry*, Wiley-VCH Verlag GmbH & Co. KGaA, 2000.

[261] Y. Gao, G. Chen, Y. Oli, Z. Zhang, and Q. Xue, "Study on tribological properties of oleic acid-modified $TiO_2$ nanoparticle in water", *Wear*, 252(5-6), p. 454-458, 2002.

[262] A. Leaustic, F. Babonneau, and J. Livage, "Structural investigation of the hydrolysis-condensation process of titanium alkoxides $Ti(OR)_4$ (OR = OPr-iso, OEt) modified by acetylacetone. 2. From the modified precursor to the colloids", *Chem. Mater.*, 1(2), p. 248-252, 1989.

[263] A. Kayan, "Solvent Effect on Complexation of Titanium Tetraethoxide with Allylacetoacetate", *Journal of Inorganic and Organometallic Polymers and Materials*, 15(3), p. 361-365, 2005.

[264] L. Z. Z. S. Peng Liu, "Core/shell SiOx@PAM nanospheres from UV-assisted surface-initiated free radical polymerization", *Journal of Applied Polymer Science*, 100(5), p. 3433-3438, 2006.

[265] H. I. Norio Tsubokawa, "Graft polymerization of methyl methacrylate from silica initiated by peroxide groups introduced onto the surface", *Journal of Polymer Science Part A: Polymer Chemistry*, 30(10), p. 2241-2246, 1992.

[266] P. Xu, H. Wang, R. Tong, Q. Du, and W. Zhong, "Preparation and morphology of $SiO_2$/PMMA nanohybrids by microemulsion polymerization", *Colloid & Polymer Science*, 284(7), p. 755-762, 2006.

[267] N. Nishizawa, J. i. Nishimura, H. Saitoh, K. Fujiki, and N. Tsubokawa, "Grafting of branched polymers onto nano-sized silica surface: Postgrafting of polymers with pendant isocyanate groups of polymer chain grafted onto nano-sized silica surface", *Progress in Organic Coatings*, 53(4), p. 306-311, 2005.

[268] W. Posthumus, P. C. M. M. Magusin, J. C. M. Brokken-Zijp, A. H. A. Tinnemans, and R. van der Linde, "Surface modification of oxidic nanoparticles using 3-methacryloxypropyltrimethoxysilane", *Journal of Colloid and Interface Science*, 269(1), p. 109-116, 2004.

[269] U. Schubert, "Chemical modification of titanium alkoxides for sol-gel processing", *Journal of Materials Chemistry*, 15(35-36), p. 3701-3715, 2005.

[270] H. Sayilkan, E. Arpac, and E. Sener, "The Modification of Aluminium Tri-sec-butoxide with Different Alcohols and Chelating Ligands: Hydrolysis and Condensation of the Products", *Synthesis and Reactivity in Inorganic, Metal-Organic, and Nano-Metal Chemistry*, 27(10), p. 1437 - 1452, 1997.

[271] T. Kiyoharu, I. Tomoaki, T. Noboru, and M. Tsutomu, "Precursor structure and hydrolysis-gelation process of Al(O-sec-Bu)3 modified with ethylacetoacetate", *Journal of Sol-Gel Science and Technology*, 3(1), p. 5-10, 1994.

[272] G. Bulut, E. Mercanci, and A. Kayan, "Complexation of zirconium alkoxides with 3-pentenoic acid and hydrolytic stability of their products", *Journal of Inorganic and Organometallic Polymers*, 14(3), p. 191-200, 2004.

[273] A. Kayan, D. Hoebbel, and H. Schmidt, "Complexation of titanium alkoxides with pentenoic acid and allylacetoacetate and their hydrolysis and addition reactions with H-silanes", *Journal of Applied Polymer Science*, 95(4), p. 790-796, 2005.

[274] M. Puchberger, W. Rupp, U. Bauer, and U. Schubert, "Reaction of metal alkoxides with 3-alkyl-substituted acetylacetone derivatives - coordination vs. hydrodeacylation", *New Journal of Chemistry*, 28(11), p. 1289-1294, 2004.

[275] M. J. Percy, J. R. Bartlett, L. Spiccia, B. O. West, and J. L. Woolfrey, "The Influence of Diketones on the Hydrolysis and Growth of Particles from Zirconium(IV) n-Propoxide", *Journal of Sol-Gel Science and Technology*, 19(1 - 3), p. 315-319, 2000.

[276] M. J. Percy, J. R. Bartlett, J. L. Woolfrey, L. Spiccia, and B. O. West, "The influence of β-diketones on the induction times for hydrolysis of zirconium(IV) alkoxides", *Journal of Materials Chemistry*, 9(2), p. 499-505, 1999.